BEHAVIOR OF REINFORCED CONCRETE FLOOR SYSTEMS UNDER LATERAL LOADS

by

Milind Ramchandra Joglekar, B.E., M.A.Sc.

DISSERTATION

Presented to the Faculty of the Graduate School of
The University of Texas at Austin
in Partial Fulfillment
of the Requirements
for the Degree of

DOCTOR OF PHILOSOPHY

THE UNIVERSITY OF TEXAS AT AUSTIN

December 1984

BEHAVIOR OF REINFORCED CONCRETE FLOOR SYSTEMS UNDER LATERAL LOADS

APPROVED BY SUPERVISORY COMMITTEE:

James O Jirsa

Richard Klingner

John E Breen

Jose M. Roesset

Stelios Kyriakides

To my parents

ACKNOWLEDGMENTS

The author wishes to express his gratitude to Dr. James O. Jirsa for his guidance and assistance in making this research project possible. The author is indebted to Dr. Richard E. Klingner for his advice and encouragement during the analytical phase of this research project and to Dr. John E. Breen for his critical review of this research effort. The author also wishes to thank Dr. Jose Roesset and Dr. S. Kyriakides for serving on the supervisory committee.

The financial support of the National Science Foundation under Grant No. PFR-8009039 as part of the U.S.-Japan Cooperative Research Program Utilizing Large-Scale Testing Facilities is gratefully acknowledged.

The author would like to express his personal thanks to Paul Murray for his invaluable help in the early phases of this research project. The assistance, support and friendship provided by the author's fellow graduate students Roberto Leon, Randy Poston, Gregg Reese, Tim Overman, Mary Lou Ralls, and Bart Bett is greatly appreciated.

The help and friendship of the Ferguson Laboratory's staff of George Moden, Blake Stasney, Gorham Hinckley, Dick Marshall, Maxine DeButts, Laurie Golding and Jean Gehrke was invaluable in making this work possible. Typing was provided by Patricia Henderson and her help is gratefully acknowledged. The author would like to extend his personal thanks to Alex Tahmassebi for his assistance in

the data acquisition and reduction phases of the project and especially for his friendship.

The author would like to thank his past roommates Rajan Kapur, Matt Sejnowski, Roberto Leon and Ashok Adiga, who made the author's stay in Austin a pleasure. The friendship and help of Suhas Keetkar and Vincent and Gillian Fernandes was invaluable and is gratefully acknowledged.

The author would like to express his sincere love and gratitude to his wife, Mrinal, for her love, encouragement and patience. The author is deeply indebted to his sister, Bharati, for her encouragement, understanding and love. Finally, the author is forever indebted to his parents, Aie and Nana, for their encouragement, understanding, sacrifice and love, without which this author's education would have been impossible.

M.R.J.
September 1984

BEHAVIOR OF REINFORCED CONCRETE FLOOR SYSTEMS UNDER LATERAL LOADS

Publication No. _______

Milind Ramchandra Joglekar, Ph.D.
The University of Texas at Austin, 1984

Supervising Professor: James O. Jirsa

The behavior of slab-beam-column connections in reinforced concrete floor systems subjected to lateral loads was investigated. Four full-scale reinforced concrete slab-beam-column assemblies were tested under reversed cyclic loads.

The test program included two interior and two exterior joint specimens. The beams and columns of the first two specimens, one interior and one exterior, had low longitudinal reinforcement ratios compared to standard U.S. practice. In the remaining two specimens, the longitudinal reinforcement in the beams and the columns was increased to provide a variation in beam to slab strength. The performance of the slab-beam-column assemblies was evaluated in terms of member behavior, failure modes, shear and anchorage in the beam column joint region and contribution of the slab to flexural resistance.

The behavior of the four specimens under reversed cyclic loads was excellent up to story drift levels of 1-1.5 percent. The

behavior of all four specimens up to this drift level was governed by flexure. No shear distress was observed in the joint region during any stage of testing. The large columns resulted in low shear stresses in the joint.

In addition to the physical tests, a finite element analysis was conducted to examine the behavior of the slab-beam-column assemblies. A finite element program which can model cracking of concrete and nonlinear behavior of reinforced concrete was selected since nonlinear response of the reinforced concrete structure after cracking was of interest.

The influence of the slab on the strength of the floor system under imposed deformations was significantly greater than would be anticipated by the interpretation of the current provisions for effective slab widths acting as a flange in a T-beam analysis. In designing structures to resist seismic loads, underestimation of the flexural strength of the floor system could result in subjecting columns to larger moments than considered in design.

The full width of the slab did not act as an effective flange of the T-beam section. But the reduction in participation of the slab at greater distance from the web was not due to lower stress as predicted by shear lag concept, but due to the change in the location of the neutral axis across the width of the slab. Guidelines based on experimental and analytical results were developed to estimate the influence of the slab in the flexural behavior of the

floor systems. These design guidelines can be used to compute the strength and stiffness of the floor systems.

TABLE OF CONTENTS

Chapter Page

I INTRODUCTION 1

1.1 Introduction 1
1.2 Objectives of the Investigation--Slab-Beam-Column Subassemblages 5
1.3 Background--Role of the Slab 5
1.4 Outline of the Investigation 7
  1.4.1 Experimental Program 7
  1.4.2 Description of the Seven-Story R/C Building 8
  1.4.3 Full Scale Tests of Slab-Beam-Column Subassemblages 11
  1.4.4 Analytical Program 16
  1.4.5 Design Recommendations 17

II DESCRIPTION OF THE EXPERIMENTAL PROGRAM ON FULL-SCALE JOINT ASSEMBLIES 18

2.1 Introduction 18
2.2 Specimen Geometry 18
2.3 Reinforcing Details 22
  2.3.1 Prototype Specimens 22
  2.3.2 Modified Specimens 26
2.4 Fabrication of the Specimens 30
  2.4.1 Formwork 30
  2.4.2 Construction and Assembly of Reinforcing Cages 30
  2.4.3 Reference Inserts 33
  2.4.4 Casting and Curing 37
2.5 Instrumentation 37
  2.5.1 Strain Measurements 37
  2.5.2 Beam Deflections and Beam Load 39
  2.5.3 Beam Rotations 44
  2.5.4 Joint Shear Strain 46
  2.5.5 Slip of Longitudinal Beam Bars 49
  2.5.6 Twist of the Transverse Beam 52
2.6 Experimental Setup 52
  2.6.1 Test Frame 52
  2.6.2 Pin Connections 57
  2.6.3 Loading System 57
2.7 Test Procedure 61
2.8 Data Acquisition and Reduction 61

TABLE OF CONTENTS (continued)

Chapter Page

2.9 Material Strengths 61
  2.9.1 Concrete 61
  2.9.2 Steel Reinforcement 61
2.10 Member Strengths 63
  2.10.1 Column Strength 63
  2.10.2 Beam Flexural Strength 63
  2.10.3 Beam Torsional Strength 65

III TEST RESULTS AND BEHAVIOR 71

3.1 Introduction 71
3.2 Load History 71
  3.2.1 Load Stage Nomenclature 73
3.3 Interior Prototype 73
3.4 Exterior Prototype 85
3.5 Modified Interior 96
3.6 Modified Exterior 105
3.7 General Behavior 112
3.8 Anchorage 116
3.9 Joint Shear 117
3.10 Comparisons of Crack Patterns Between Seven-Story Structure and Slab-Beam-Column Assemblages . 121

IV INFLUENCE OF THE SLAB ON FLOOR SYSTEM STRENGTH 123

4.1 Introduction 123
4.2 Behavior of the Slab 125
  4.2.1 Crack Patterns 126
  4.2.2 Steel Strains 126
4.3 Torsional Rotations of the Transverse Beam 139
4.4 Summary 141
4.5 Comparison of Measured and Predicted Beam Slab Flexural Capacities 141
4.6 Relative Strength of Columns to Beams 147
  4.6.1 Review of Current Code Procedures 147
  4.6.2 Comparison of Measured and Computed Relative Column Capacities 154
4.7 Need for Analytical Studies 154

V COMPARISON OF EXPERIMENTAL AND ANALYTICAL RESULTS 157

5.1 Introduction 157
5.2 Analytical Model 158

TABLE OF CONTENTS (continued)

Chapter Page

5.2.1 Objectives 158
5.2.2 Choice of Finite Element Program 158
5.3 Geometry 159
5.3.1 Boundary Conditions 165
5.3.2 Material Model 165
5.4 Elastic Finite Element Analysis 169
5.4.1 Elastic Stiffness 171
5.4.2 Interior versus Exterior Specimens 172
5.4.3 Distribution of Torsion Along Transverse Beam 173
5.4.4 Effective Width of T-Beams, Elastic Range . 175
5.5 Comparison of Crack Patterns 180
5.6 Nonlinear Finite Element Analysis 182
5.6.1 Stiffness 182
5.6.2 Effective Width of T-Beams, Inelastic Range 188
5.7 Development of Design Guidelines 193
5.7.1 ACI Provisions for Effective Width 193
5.7.2 Stiffness 194
5.7.3 Estimation of Strength 202
5.7.4 Idealized Model Based on Varying Neutral Axis Position 203
5.7.5 Simplified Design Idealization 206
5.8 Further Research Needs 210

VI SUMMARY AND CONCLUSIONS 211

6.1 Summary 211
6.1.1 Experimental Program 211
6.1.2 Analytical Studies 213
6.1.3 Behavior of Slab Systems 214
6.1.4 Proposed Idealized Cross Section for Slab Systems 215
6.1.5 Comparison of Stiffnesses 216
6.1.6 Comparison of Strengths 217
6.2 Conclusions 218
6.2.1 Performance of the Test Specimens 218
6.2.2 Influence of Slab on the Behavior of the Floor System 220

APPENDIX A: PROBLEMS ENCOUNTERED DURING ANALYTICAL STUDY 223

REFERENCES 227

LIST OF TABLES

Table Page

2.1 Average Concrete Strength (in psi) 62

2.2 Average Yield Strength of Steel 64

2.3 Flexural Capacity 66

2.4 Predicted Torsional Capacities 70

3.1 Comparison of Observed and Computed Flexural Capacities, kip-in. 115

3.2 Joint Shear Stresses 120

4.1 Beam Strength—Negative Bending 142

4.2 Beam Strength—Positive Bending 143

4.3 Relative Strength of Column to Beams, Interior Specimens .. 155

5.1 Distribution of Elastic Torsion 176

5.2 Computations for Negative Moment Capacities 207

5.3 Moment Capacity Using Effective Beam 209

LIST OF FIGURES

Figure Page

1.1 Plan of seven-story structure 9

1.2 Elevation of seven-story structure 10

1.3 Comparison of real and idealized loading situations 13

1.4 Lateral drift for seven-story structure 15

1.5 Lateral drift for isolated test specimen 15

2.1 Plan view of test specimens 19

2.2 Elevation view of test specimens 20

2.3 Cross sectional details of test specimens 21

2.4 Interior joint reinforcing detail,
prototype test specimen 24

2.5 Interior joint reinforcing detail, seven-story structure . 24

2.6 Exterior joint reinforcing detail,
prototype test specimen 25

2.7 Exterior joint reinforcing detail, seven-story structure . 25

2.8 Slab reinforcement detail 27

2.9 Cross ties in the joint, exterior modified specimen 29

2.10 Lower column formwork 31

2.11 Slab-beam formwork 31

2.12 Column reinforcement cage, interior prototype specimen ... 32

2.13 Steel sleeve for pin connection 32

2.14 Beam reinforcement cage, interior prototype specimen 34

2.15 Beam reinforcement cage, exterior prototype specimen 34

LIST OF FIGURES (continued)

Figure Page

2.16 Column and beam reinforcement placed in forms 35

2.17 Slab reinforcement placed in forms 35

2.18 Reference inserts and slip wires in the joint 36

2.19 PVC tube inserts to attach loading rams 38

2.20 Upper column formwork 38

2.21 Beam and column bar strain gage locations 40

2.22 Slab bar strain gage locations 41

2.23 Strain gage locations for joint and beam hoops 42

2.24 Load cell and deflection LVDT instrumentation 43

2.25 Beam rotation instrumentation 45

2.26 Beam rotation geometry 45

2.27 Joint shear strain instrumentation and geometry 47

2.28 Bar slip measurement instrumentation 48

2.29 Torsional rotation instrumentation 50

2.30 Details of torsional rotation instrumentation 50

2.31 Torsional rotation measurement geometry 51

2.32 Test setup 53

2.33 Floor fixture 55

2.34 Lower column pin connection detail 55

2.35 Upper column clamping assembly 56

2.36 Hydraulic loading system 58

2.37 Load history, interior prototype specimen 59

LIST OF FIGURES (continued)

Figure Page

2.38 Typical load history for test specimens 60

2.39 Moment-axial force interaction diagrams for columns 67

2.40 Moment-curvature relationships for longitudinal beam, prototype specimens 67

2.41 Moment-curvature relationships for longitudinal beam, modified specimens 68

2.42 Torque-twist relationships for transverse beams 68

3.1 Slip correction 75

3.2 Load versus deflection, interior prototype specimen 76

3.3 Top slab at D0.6, interior prototype 78

3.4 Bottom of slab and longitudinal beam at D0.6, interior prototype 78

3.5 Torsional cracks in transverse beam, interior prototype .. 79

3.6 Beam load versus torsional rotation, interior prototype .. 81

3.7 Cracks around the load point 81

3.8 Bottom of slab at D1.2, interior prototype 82

3.9 Vertical cracks in transverse beam at D2.4, interior prototype 82

3.10 Top of slab at D2.4, interior prototype 84

3.11 Longitudinal beam at D2.4, interior prototype 84

3.12 Joint area at end of test, interior prototype 86

3.13 Load versus deflection, exterior prototype 87

3.14 Top of slab at D0.5, exterior prototype 89

LIST OF FIGURES (continued)

Figure Page

3.15 Torsional cracks in transverse beam at D0.75, exterior prototype 89

3.16 Beam load versus torsional rotation, exterior prototype .. 91

3.17 Longitudinal beam at U1.2, exterior prototype 91

3.18 Transverse beam at D1.2, exterior prototype 92

3.19 Top longitudinal beam bar strain versus deflection, prototype specimens 94

3.20 Top longitudinal beam bar slip versus deflection, prototype specimens 94

3.21 Top of slab at D2.4, exterior prototype 95

3.22 Bottom of slab at D2.4, exterior prototype 95

3.23 Transverse beam at D3.6, exterior prototype 97

3.24 Back of column at end of test, exterior prototype 97

3.25 Load versus deflection, interior modified specimen 98

3.26 Longitudinal beam at U0.75, interior modified 100

3.27 Bottom of slab at D0.75, interior modified 100

3.28 Beam load versus torsional rotations, interior modified .. 102

3.29 View of beams at end of test, interior modified 104

3.30 View of joint region at end of test, interior modified ... 104

3.31 Load versus deflection, exterior modified specimens 106

3.32 Beam load versus torsional rotation, exterior modified ... 108

3.33 Bottom of slab at U1.2, exterior modified 108

3.34 Longitudinal beam at U1.2, exterior modified 109

LIST OF FIGURES (continued)

Figure Page

3.35 Top of slab at D1.2, exterior modified 109

3.36 Transverse beam at D1.2, exterior modified 111

3.37 Transverse beam east face at D1.2, exterior modified 111

3.38 Torsional cracking at D3.6, exterior modified 113

3.39 Joint region at end of test, exterior modified 113

3.40 Joint shear strain versus deflection, interior prototype . 118

3.41 Comparison of crack patterns, seven-story structure versus prototype test specimens 122

4.1 Flexural cracks at top fo slab under negative moment 127

4.2 Flexural cracks at bottom slab under negative moment 127

4.3 Flexural cracks at bottom of slab under positive moment .. 128

4.4 Beam bar strains versus beam deflection, interior prototype 130

4.5 Slab bar strain versus beam deflection, interior prototype 130

4.6 Profiles of top slab steel strain under negative moment, interior prototype 131

4.7 Profiles of bottom slab steel strain under negative moment, interior prototype 131

4.8 Profiles of slab steel strains under negative moment, exterior prototype 132

4.9 Profiles of slab steel strains under negative moment, interior modified 132

4.10 Profiles of slab steel strain under negative moment, exterior modified 133

LIST OF FIGURES (continued)

Figure		Page
4.11	Flexural resistance of slab, flange of T-section, versus shallow slab section	135
4.12	Profiles of top slab steel strain under positive moment, interior prototype	136
4.13	Profiles of bottom slab steel strain under positive moment, interior prototype	136
4.14	Profiles of slab steel strain under positive moment, exterior prototype	137
4.15	Profiles of slab steel strain under positive moment, interior modified	137
4.16	Profiles of slab steel strain under positive moment, exterior modified	138
4.17	Load versus torsional rotation along the length of transverse beam	140
4.18	Influence of slab on floor strength, negative moment	146
4.19	Influence of slab on floor strength, positive moment	148
4.20	Load versus deflection envelopes for test specimens	149
5.1	Finite element model of test specimen	160
5.2	Slab discretization	161
5.3	Longitudinal and end beam sections	163
5.4	Transverse beam discretization	164
5.5	Boundary conditions for the finite element model	166
5.6	Concrete constitutive relationship	168
5.7	Tension stiffening model	168
5.8	Specified concrete stress-strain relationship	170

LIST OF FIGURES (continued)

Figure Page

5.9 Specified reinforcing steel stress-strain relationship ... 170

5.10 Comparison of load-deflection behavior, interior specimens ... 172

5.11 Comparison of load-deflection behavior, exterior specimens ... 172

5.12 Comparison of normalized torsion, interior vs. exterior specimens ... 174

5.13 Effective width of T-beam, theory of elasticity ... 177

5.14 Stress distribution along the slab, elastic analysis ... 179

5.15 Comparison of slab stress variation, finite element analysis theory of elasticity ... 179

5.16 Variation of location of neutral axis across the slab width, elastic analysis ... 181

5.17 Comparison of load-deflection behavior, interior prototype specimen ... 183

5.18 Comparison of total column moment, interior prototype specimen ... 186

5.19 Specified actual tension stiffening relationship ... 187

5.20 Slab steel stress profiles from nonlinear analysis ... 190

5.21 Comparison of slab steel stress profiles, analytical vs. experimental ... 190

5.22 Profiles of location of neutral axis across the slab width, nonlinear analysis ... 191

5.23 Comparison of load-deflection relationship under positive moment, interior prototype ... 196

5.24 Comparison of load-deflection relationship under positive moment, interior modified ... 197

LIST OF FIGURES (continued)

Figure Page

5.25 Comparison of load-deflection relationship under positive moment, exterior modified 198

5.26 Comparison of load-deflection relationship under negative moment, interior prototype 199

5.27 Comparison of load-deflection relationship under negative moment, interior modified 200

5.28 Comparison of load-deflection relationship under negative moment, exterior modified 201

5.29 Idealized model based on varying neutral axis location ... 205

5.30 Proposed idealized section 208

CHAPTER I

INTRODUCTION

1.1 Introduction

The research project described herein was carried out as a portion of the U.S.-Japan Cooperative Program on Large Scale Testing [15]. The U.S.-Japan Cooperative Program was set up with the objective of improving seismic safety practices, by investingating the relationship among full-scale lists, small scale tests, component tests of different scales, and analytical studies.

The Cooperative Program [15] was designed to:

> a) achieve clearly stated scientific objectives; b) represent total building systems as realistically as possible; c) balance the simplicity and economy of the test specimens with the need to test structures representing real situations; d) maintain a balance among small-scale, component, and full scale tests; e) utilize previously performed experiments and studies to the extent practical; f) represent the best design and construction practice in use in both countries; g) check validity of newly developed earthquake-resistant design procedures; h) maintain flexibility to accommodate new knowledge and conditions as successive experiments are completed; and i) ensure practicality of program results.

At the time the Cooperative Program was being formulated, one of the major drawbacks in previous experimental research on the response of reinforced concrete structures to earthquakes was the lack of definitive information correlating the experimental results with the behavior of actual structures. To examine this missing link, it was deemed essential to correlate test results from the full-scale component tests, shake table tests, and small- to medium-scale frame tests, with the results from tests on a full-scale, multibay, multistory structure under controlled testing conditions. The merits and limitations of the data base available from component testing could be established from such correlation studies, and could be used to improve in seismic resistant design practice.

The joint research program included design, construction and testing of a full-scale, multibay, seven-story, reinforced concrete building structure. A series of tests on this structure were carried out at the Large Size Structure Laboratory, Building Research Institute, Tsukuba New Town for Research and Education, Japan. Supporting tests, performed in both the U.S. and Japan, included component beam-column joint assemblies, scale models of full-scale structures, and shake-table models. These coordinated experiments were intended to provide important test data such as force deformation relationships, energy dissipation characteristics, and damage and failure models.

The original intent was to conduct the supporting tests before designing the seven-story structure so that results from the supporting tests could be used in determining the design details, loading, and instrumentation requirements for the seven-story structure. However, it was not possible to conduct the U.S. supporting tests before construction and testing began on the seven-story structure in Japan. Problems arose involving funding and overall scheduling of the different phases of the project. As a result, in most of the supporting tests were conducted after the primary tests on the seven-story structure were completed.

The portion of the U.S.-Japan program carried out at The University of Texas consisted of testing isolated full-scale beam-column-joint assemblages. The original objectives of this portion of the program were (1) to study the problems associated with beam-column joint connections in reinforced concrete structures (shear in the joint, anchorage of reinforcement in the joint); and (2) to correlate the results from the isolated joint specimens with the results for the joints of the seven-story structure. It was also intended that the details of the joints in the seven-story structure be modified if the isolated joint specimens identified any problem areas. However, since the joint tests were actually started after the design and testing procedure of the seven-story structure had been decided upon, results from the isolated joint tests did not influence the design and/or testing of the seven-story structure.

The design of the seven-story structure was based on both the Japanese and U.S. design practices, and hence certain compromises had to be made where the standard design practices in the two countries differed. Initial examination of the design of the joint specimens indicated that due to the column size and low percentages of longitudinal reinforcement in the beams and columns there would probably be no shear distress in the joint. It was also concluded that the isolated joint test specimens would probably not result in any new information regarding beam column joint behavior. However, tests of the seven-story structure indicated that the slab played a more important role in resisting applied deformations than was envisioned in the planning and analysis of the large structure. Therefore, the proposed joint subassemblages provided an excellent opportunity to study the behavior of the slab and its participation with the beams in resisting applied lateral deformations, and the objectives of this part of the program were modified accordingly. The correlation studies originally envisioned between the test results from the isolated and joint specimens and the joints in the seven-story structure could not be undertaken because: (1) the data from the seven-story structure were not available in a form which permitted easy access or processing, (2) the data needed (deformation and strains in the joint region) were not obtained; and (3) the schedule for this project did not permit such correlation. However, these studies are currently being conducted at The University of Texas at Austin in a subsequent project.

The tests on the joint assemblages in this investigation were designed to increase understanding of the behavior of the slab under imposed lateral deformations. Test results revealed that the participation of the slab could not be inferred from experimental results alone. Hence, a finite element analysis was also carried out to further study the factors affecting slab participation, and to aid in the development of design guidelines.

1.2 Objectives of the Investigation--Slab-Beam-Column Subassemblages

The primary objective of this dissertation is to investigate the behavior of slab-beam-column connections in reinforced concrete floor systems subjected to lateral loads. The specific objectives are:

1. to study both experimentally and analytically the path of moment transfer in such a floor system;
2. to determine the influence of the slab in resisting applied lateral deformations;
3. to compare observed and analytical response of the slab in order to determine the adequacy of current design provisions; and
4. to propose guidelines to predict strength and stiffness of such slab systems subjected to lateral loads.

1.3 Background--Role of the Slab

A clear understanding of the behavior of reinforced concrete floor systems subjected to lateral loads is essential in designing such systems to resist wind and earthquake loads. The analysis of floor systems subjected to lateral loads is essential for two primary reasons. First, the lateral drift of the structure must be determined for serviceability reasons. Second, the forces introduced into the columns by the floor elements due to large imposed lateral deformations, as in the case of earthquakes, must be evaluated. Hence, it is essential to study the behavior of the floor systems under both service and ultimate states.

The fundamental difficulty in analyzing a floor system with beams is in determining the distribution of moment between the slab and the beams. A three-dimensional finite element analysis of the whole structure would be extremely expensive and not necessarily accurate. The usual approach is to reduce the three-dimensional structure to a two-dimensional frame for analysis. The major problem in this conversion is how to model the three-dimensional behavior of the columns, the beams, and the effective width of the slabs. The beams and the columns have generally comparable widths, but the width of the slab is typically 10 to 20 times as large. Furthermore, the slab usually frames into transverse beams which transfer moment to the column. The determination of the path of moment transfer thus becomes complex even for an elastic material. For reinforced concrete the problem is aggravated due to the nonlinear response of the material.

Many designers ignore the presence of the slab, and analyze the "bare" beam and column frame. This approach is conservative in determining the resistance to applied loads, but becomes unconservative when determining the forces the floor system can impose on the column under large lateral deformations. When the structure is deformed laterally, the slab may introduce large forces into the transverse beams and the columns. Under these conditions the effect of the slab cannot be ignored.

Some designers use the "Equivalent Frame Method" to analyze floor systems subjected to lateral loads. The "Equivalent Frame Method" [1,2] is based on reducing a 3-D floor system to a 2-D frame and then analyzing the 2-D frame to determine the distribution of moments in the 3-D floor system. The stiffnesses of the various members defined in the "Equivalent Frame Method" are not exact stiffnesses but are based on experimental results and elastic analyses. The experimental results were obtained from structures subjected only to gravity loadings. The method as originally developed was not intended to be applied to slab structures under lateral loads. The method must be modified if it is used for analyzing frames with floor slabs under lateral loads.

Currently, the design engineer has very little guidance for analyzing floor systems subjected to lateral loads. A few approaches to the problem have been suggested [16], but the lack of experimental data makes it difficult to verify the validity of these approaches.

1.4 Outline of the Investigation

The three main phases of the investigation on the behavior of the slab systems under lateral loads were 1) experimental program, 2) analytical program, and 3) development of design guidelines based on the results of the experimental and analytical studies.

1.4.1 Experimental Program.

The slab-beam-column assemblages tested at The University of Texas were governed by the design of the seven-story structure tested in Japan. Therefore, the dimensions, loading and instrumentation for the seven-story structure will be described briefly to help identify the similarities and differences between the large structure and the isolated test specimens.

1.4.2 Description of the Seven-Story R/C Building. The test structure had three spans in the direction of lateral loading and two in the transverse direction. Plan and elevation views of the seven-story structure are shown in Figs. 1.1 and 1.2. In addition to the beam-column frames, the design structure included a structural wall in the middle frame parallel to the direction of loading. Lateral load resistance of the building was provided by the interaction of the frame wall structural system but the wall was the primary element. The columns and beams of the frame were rather large, lightly reinforced sections, characteristic of Japanese seismic design. Some of the reinforcement details differed from standard U.S. practice and will be discussed later. In general, the full-scale seven-story structure was designed as a compromise between the earthquake engineering design practices of both the U.S. and Japan and the physical limitations of the testing facility.

The test program for the seven-story structure consisted of two phases. The first phase consisted of four sub-phases: 1) recording of earthquake response; 2) vibration tests; 3) static tests; and 4) the pseudo-dynamic test. In the second phase, the damage to the structure due to the loadings in the first phase was repaired. A variety of nonstructural elements was installed in the

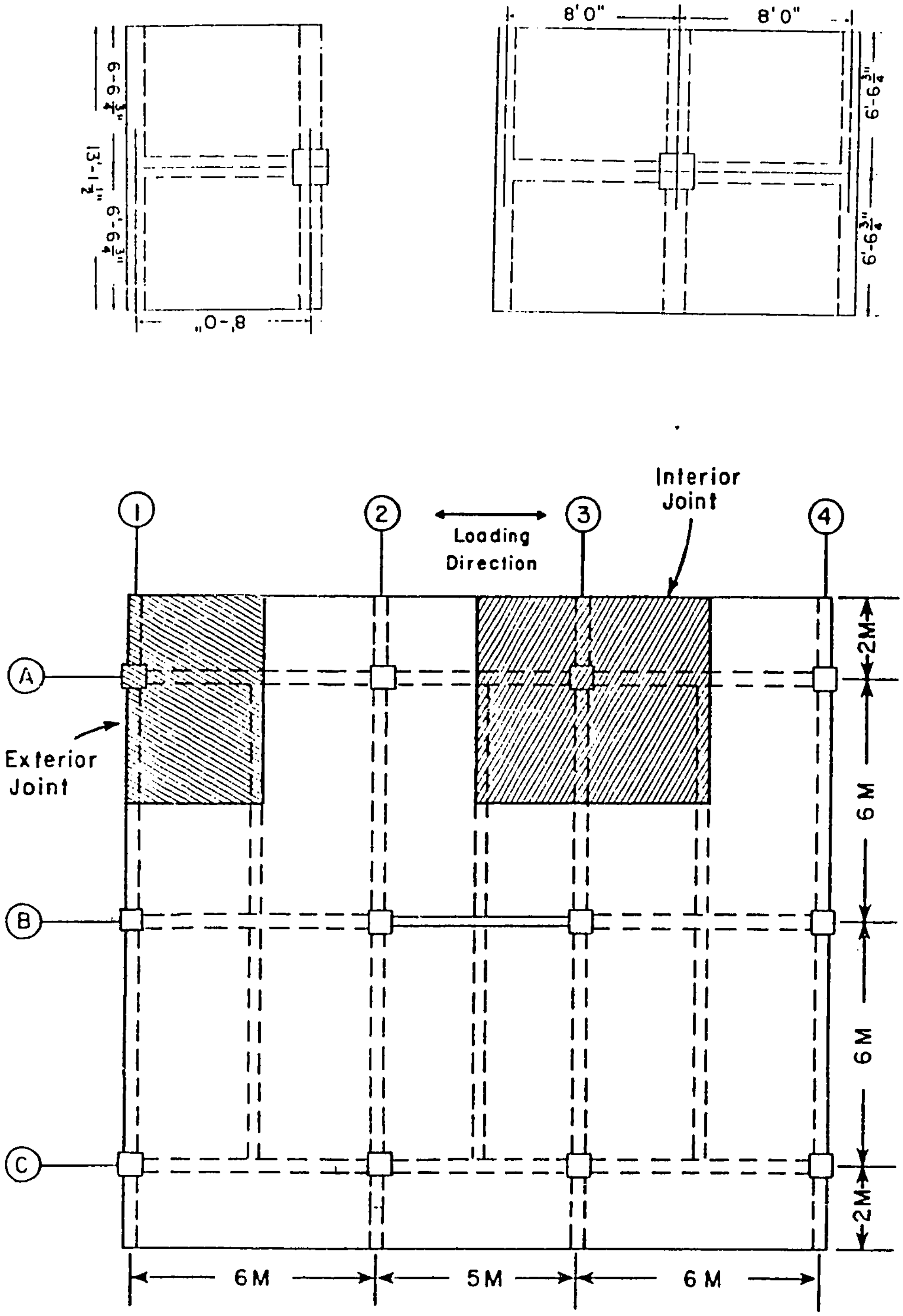

6'-6¾"
13'-1½"
6'-6¾"
8'-0"
8'0"
8'0"
6'-6¾"
6'-6¾"
Interior Joint
①
②
③
④
Loading Direction
Ⓐ
Ⓑ
Ⓒ
Exterior Joint
2M
6 M
6 M
2M
6M
5M
6 M

Fig. 1.1 Plan of seven-story structure

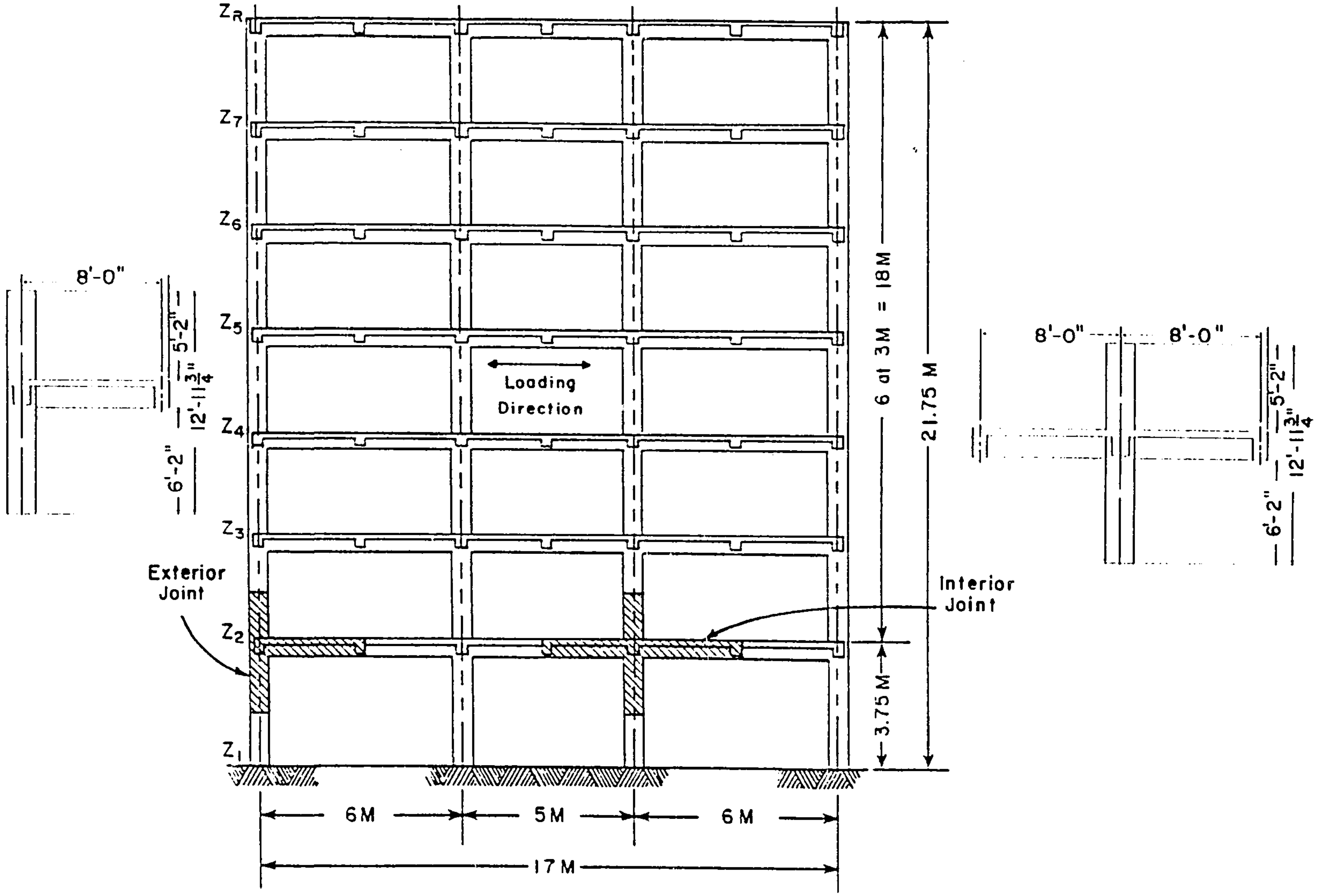
Z_R
Z_7
Z_6
Z_5
Z_4
Z_3
Z_2
Z_1
Loading Direction
Exterior Joint
Interior Joint
6 at 3M = 18M
21.75 M
3.75 M
6M
5M
6M
17M
8'-0"
5'-2"
12'-11 3/4"
6'-2"
8'-0"
8'-0"
5'-2"
12'-11 3/4"
6'-2"

Fig. 1.2 Elevation of seven-story structure

repaired structure. Subsequently, the effectiveness of the repair and the interaction between structural and nonstructural elements was examined. A detailed report on these experiments is documented in Ref. 12.

1.4.3 Full Scale Tests of Slab Beam-Column Subassemblages. The geometry and the boundary and loading conditions for the full-scale joint specimens tested in this investigation were derived assuming that under the action of lateral loads the points of inflection in the seven-story structure were located at the midheights of the columns and at the midspans of the beams and the slab. The portion of the seven-story structure represented by the test specimens is shown in Figs. 1.1 and 1.2. The overall geometry of the test specimens themselves is shown in Figs. 1.1 and 1.2.

To facilitate fabrication and testing of the slab-beam-column assemblages, their geometry was slightly modified from that of the joints regions of the seven story structure. To maintain tranvserve symmetry about the column a slab width of 2m was used on both sides, rather than duplicating the geometry of the seven-story structure with a slab width of 2m on one side and 3m on the other. A 16-ft span was used in the loading direction to facilitate testing in the laboratory, which has bolt groups centered at 4-ft intervals in the structural floor. The difference in column heights between the first story and the others was reproduced by using different top and bottom column heights in the test specimens.

The continuity in a real structure cannot be achieved in component test specimens. Hence, the precise distribution of internal forces in the seven-story structure could not be duplicated in the test specimens. The lateral loading in the seven-story structure was simulated by applying vertical racking loads at the ends of the longitudinal beams, while restraining the column in the horizontal direction by simple supports as shown in Fig. 1.3. In that same figure, the real loading situation is also compared with the loading scheme used in the testing of isolated specimens to facilitate testing and because the dead load on the columns in the seven-story structure was small, no axial load was applied to the column. Due to the lack of axial column load, and because displacements were applied to the beams rather than the columns, P-delta effects were not duplicated in the test specimens. When results from the seven-story structure were evaluted, some problems arose with duplication of loading conditions which were not envisioned at the beginning of the test program were encountered when results from the seven-story structure were evaluated. For instance, it was not foreseen at the beginning of the test program that the rocking and subsequent uplift of the of the wall would introduce forces in the joint region from the transverse direction [15].

The boundary conditions at the exterior joint differed in that the seven-story structure included a spandrel wall along sections 1 and 4 shown in Fig. 1.1. This spandrel wall, which was not planned in the initial stage of the project, altered the torsional

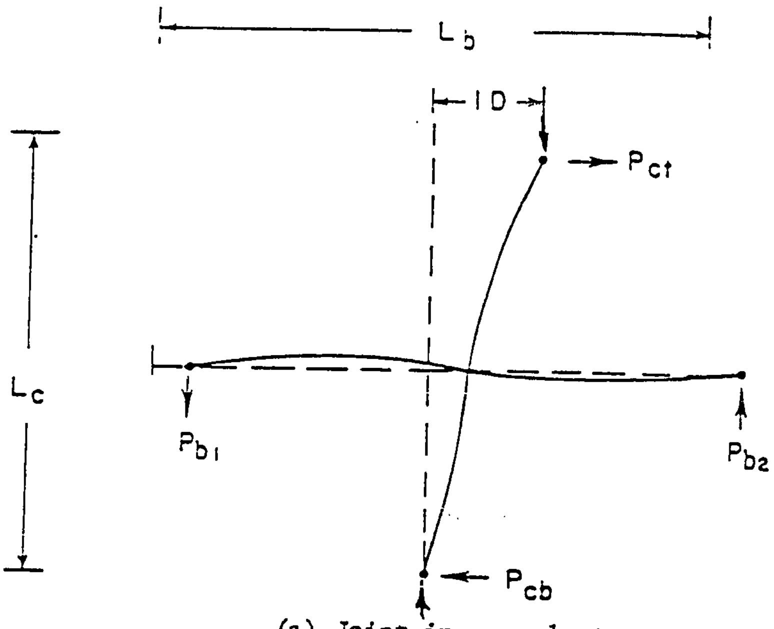
L b
ID
P ct
L c
P b1
P b2
P cb

(a) Joint in a real structure

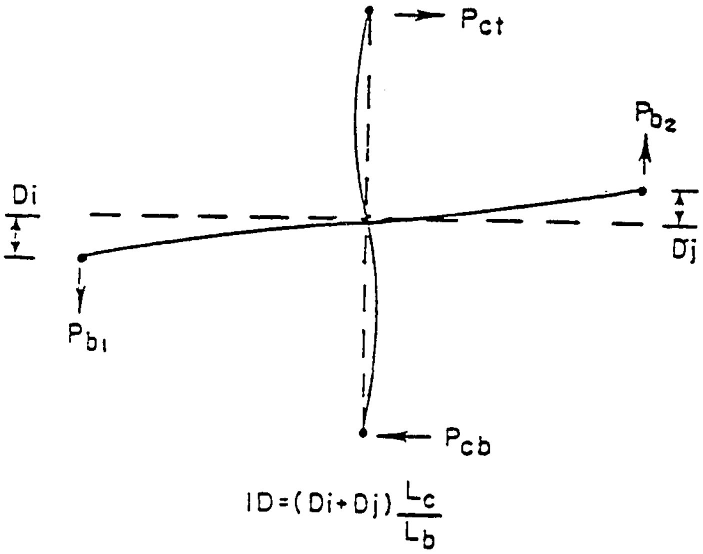
P ct
P b2
Di
Dj
P b1
P cb
ID=(Di+Dj) Lc/Lb

(b) Joint in test setup

Fig. 1.3 Comparison of real and idealized loading situations.

characteristics of the transverse members and precluded direct comparison of the behavior of the exterior joints with the isolated exterior specimens. The load histories for the seven-story structure were based on recorded earthquake motions, modified to excite primarily a first-mode response of the structure. Because of the then-current uncertainties regarding the actual response of the seven-story structure, a displacement record based on such ground motions was judged too difficult to reproduce in the component tets. Therefore, the slab-beam-column subassemblages were subjected to selected displacement histories in which peak deflection levels were increased as testing continued.

Due to the lack of specific data regarding points of inflection in the columns and beams, and local deformations of the slab, beams and columns of the seven-story structure, it was difficult to compare directly the beam end displacements imposed in the test specimens with the deflection levels of the seven-story structure. A reference parameter, drift angle, was used to compare some of the test results. For the seven-story structure, this drift angle was computed using the relative lateral drifts of the second and third levels. An approximate drift angle for the joint at the second level was calculated by averaging the drift angles of the first and second stories, both of which contributed to the rotation of the joint, as shown in Fig. 1.4. To calculate the drift angle for the test specimens, the total beam end deflections were divided by the length between the loading points as shown in Fig. 1.5.

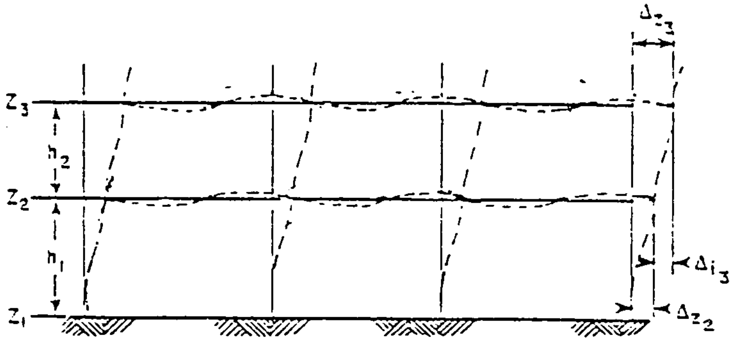
Z_3
Z_2
Z_1
h_2
h_1
Δ_{z_3}
Δ_{i_3}
Δ_{z_2}

Δ_{z_2} = total horizontal displacement at level z_2, cm.
Δ_{z_3} = total horizontal displacement at level z_3, cm.
Δ_{i_3} = interstory drift between levels z_2 and z_3, cm.
h_1 = first story height, cm.
h_2 = second story height, cm.
R = drift-angle index for joint at z_2, rad.
R_1 = drift-angle index for first story, rad.
R_2 = drift-angle index for second story, rad.

$$R_1 = \frac{\Delta_{z_2}}{h_1} \qquad R_2 = \frac{\Delta_{i_3}}{h_2}$$

$$R = \frac{R_1 + R_2}{2}$$

For h_1 = 375 cm. and h_2 = 300 cm.

$$R = \frac{\Delta_{z_2} + 1.25\Delta_{i_3}}{750}$$

Fig. 1.4 Lateral drift for seven-story structure.

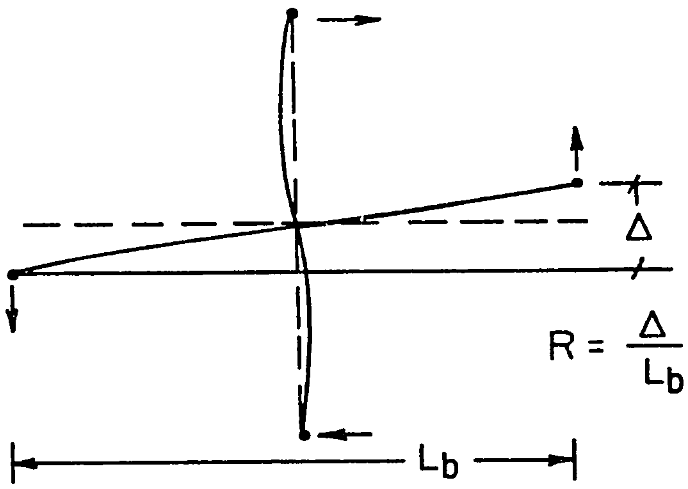
Δ
$R = \frac{\Delta}{L_b}$
L_b

Fig. 1.5 Lateral drift for isolated test specimens.

Four full-scale beam-column-slab assemblies were tested in the Ferguson Structural Engineering Laboratory at The University of Texas as part of the U.S.-Japan Cooperative program on large-scale testing. The test program included two interior and two exterior joint assemblies. The first two specimens (one interior and one exterior, referred to hereafter as PROTOTYPE INTERIOR and PROTOTYPE EXTERIOR) were identical in terms of both geometry and reinforcing details to the beam-column joints in the second story of the full-scale, seven-story structure tested in Japan. Locations of the typical interior and exterior joints in the seven-story structure are indicated in Figs. 1.1 and 1.2. In the remaining two specimens (one interior and one exterior, referred to hereafter as MODIFIED INTERIOR and MODIFIED EXTERIOR), the longitudinal reinforcement in the beams and columns was increased to vary beam-to-slab strength. The geometry of the "modified" specimens was otherwise identical to that of the "prototype" specimens.

It should be mentioned, however, that the proposed research program represents the first opportunity to correlate test results and observations from a continuous real structure subjected to simulated earthquakes with test results from component tests.

1.4.4 Analytical Program. Results obtained from the experimental program showed a need for analytical research to better understand the behavior of slab systems subjected to lateral loads. A finite element analysis of the test specimen was conducted to examine the behavior of the connection. A finite element program

(ABAQUS) [6,7,8] which can model nonlinear behavior of reinforced columns was selected since the nonlinear response of the reinforced concrete structure after cracking was of interest. Results from this analysis are compared with the experimental results. While some problems were encountered in these analyses, the results were encouraging.

1.4.5 Design Recommendations. Some of the observed results showed that the actual behavior of specimens differed considerably from that anticipated in the development of current ACI design recommendations. Use of some current design guidelines [2,9,13], especially those regarding assessment of negative flexural capacity of slab systems, can result in unconservative design solutions. Hence, it was necessary to develop design recommendations to compute flexural capacity of slab systems based on observed and analytical results. These guidelines are compared with current design procedures.

CHAPTER II

DESCRIPTION OF THE EXPERIMENTAL PROGRAM ON FULL-SCALE JOINT ASSEMBLIES

2.1 Introduction

Two interior and two exterior joint assemblies were built using the dimensions of the joints at the second level of the seven-story structure. Since correlation of the results from the seven-story structure and the full-scale specimens was one of the primary objectives of the U.S.-Japan program, the geometry and reinforcement was duplicated from the seven-story structure and no detailed design calculations were required. Since the full-scale structure was designed and built in Japan using metric dimensions, whereas the test specimens were based partly on English units, some dimensions were adjusted slightly and nominal material properties were approximated. Fabrication and testing constraints were also considered in selecting the geometry of the test specimens.

2.2 Specimen Geometry

The dimensions of the test specimen are shown in plan and elevation views in Figs. 2.1 and 2.2. The shaded portion indicates the geometry of the exterior joints. The longitudinal beam refers to the single beam in the long direction of the specimen intersecting the joint, and running parallel to the direction of simulated lateral

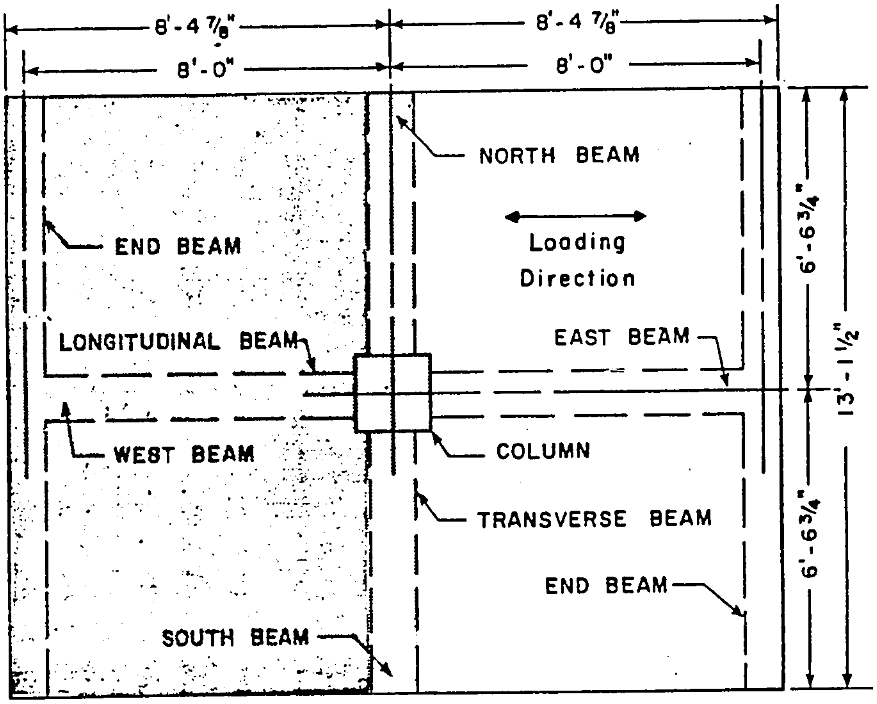
8'-4 7/8"
8'-4 7/8"
8'-0"
8'-0"
NORTH BEAM
END BEAM
Loading Direction
LONGITUDINAL BEAM
EAST BEAM
WEST BEAM
COLUMN
TRANSVERSE BEAM
END BEAM
SOUTH BEAM
6'-6 3/4"
6'-6 3/4"
13'-1 1/2"

Fig. 2.1 Plan view of test specimens

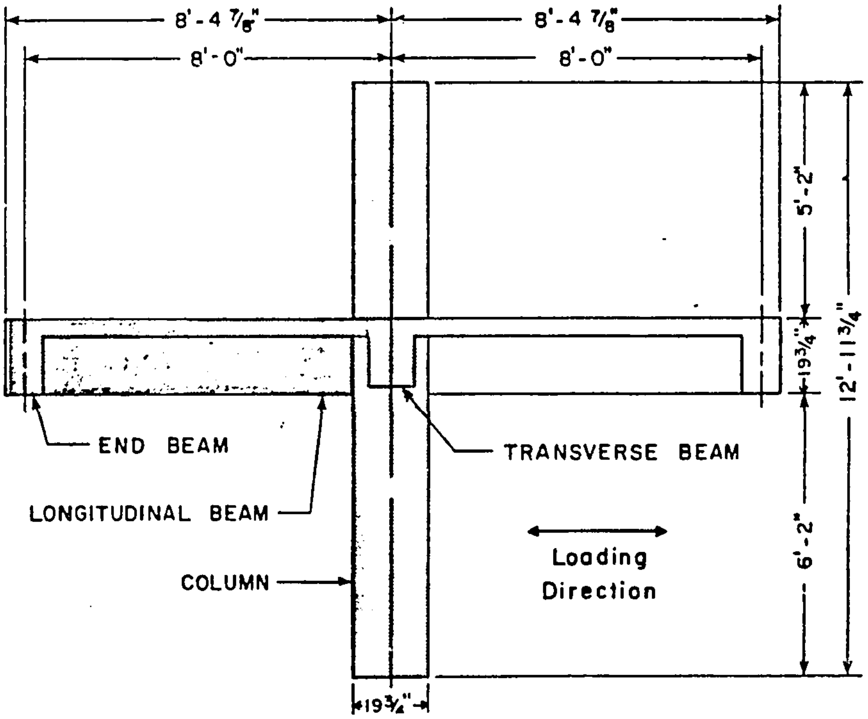
8'-4 7/8"
8'-4 7/8"
8'-0"
8'-0"
5'-2"
19 3/4"
12'-11 3/4"
6'-2"
END BEAM
TRANSVERSE BEAM
LONGITUDINAL BEAM
Loading Direction
COLUMN
19 3/4"

Fig. 2.2 Elevation view of test specimens

loading. The racking loads were applied at the ends of the longitudinal beams. The beams intersecting the joint and orthogonal to the longitudinal beam are referred to as the transverse beams. The beams parallel to the transverse beam at the opposite edges of the specimens are the end beams. The orientation of the joint assemblies, as positioned in the test setup, is shown in Fig. 2.1. The directions (north, etc.) were utilized to locate the instrumentation and to document the crack patterns and the damage to the specimens.

The length of the longitudinal beam, on either side of the column centerline, represents approximately half the span length of the middle bay in the seven-story structure. A half-span length of 8 ft was convenient with regard to layout of the structural floor in the laboratory where bolt groups are centered at 4-ft intervals. The transverse dimension of the specimens, 4 m (13ft 1-1/2 in.), was chosen to duplicate the transverse span length of the seven-story structure, with a 2 m transverse beam on each side of the column.

The column lengths were determined assuming points of contraflexure at the midpoints of the columns. The first-story height in the seven-story structure was 3.75 m (12 ft 4 in.) compared to a 3 m (9 ft 10 in.) height for the top six stories. Therefore, the upper and lower column lengths differed in order to reflect the geometry of the seven-story structure.

The cross-sectional dimensions of the column and the longitudinal and transverse beams are shown in Fig. 2.3. Metric

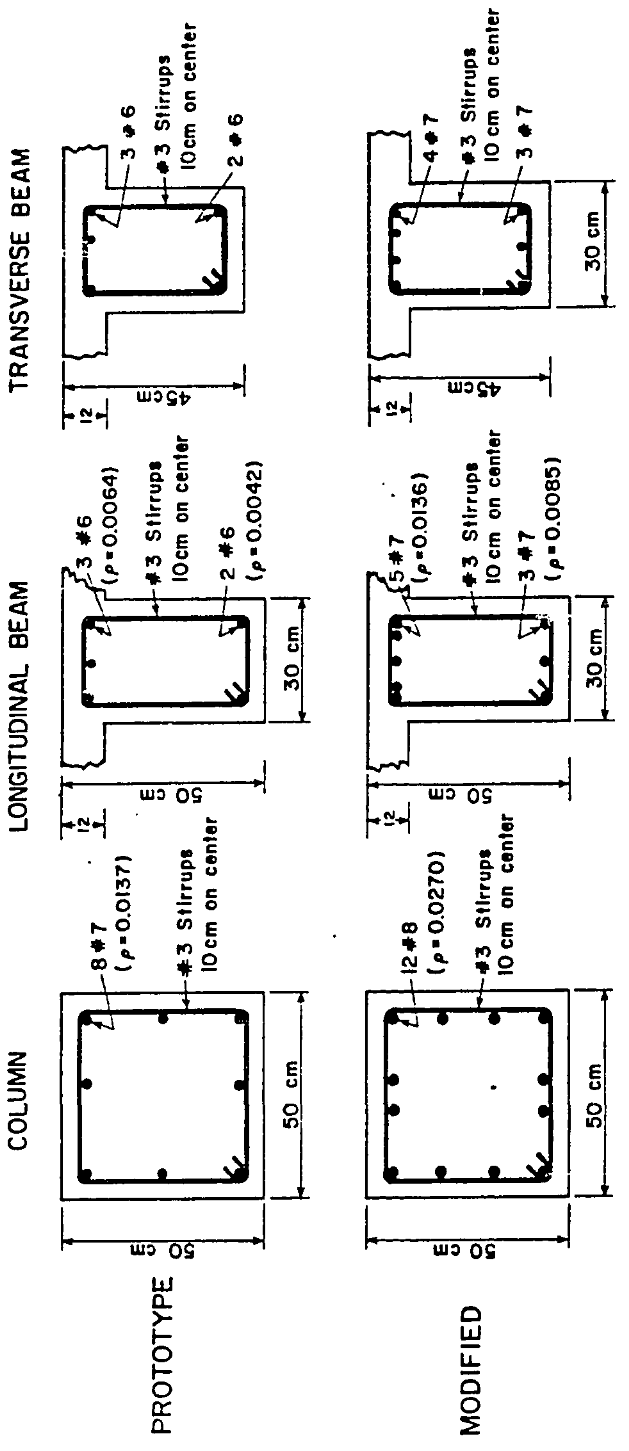
COLUMN
LONGITUDINAL BEAM
TRANSVERSE BEAM
PROTOTYPE
MODIFIED
50 cm
50 cm
8 #7 (ρ=0.0137)
#3 Stirrups 10cm on center
12 #8 (ρ=0.0270)
#3 Stirrups 10 cm on center
12
50 cm
30 cm
3 #6 (ρ=0.0064)
#3 Stirrups 10cm on center
2 #6 (ρ=0.0042)
5 #7 (ρ=0.0136)
#3 Stirrups 10 cm on center
3 #7 (ρ=0.0085)
12
45cm
30 cm
3 #6
#3 Stirrups 10cm on center
2 #6
4 #7
#3 Stirrups 10 cm on center
3 #7

Fig. 2.3 Cross sectional details of test specimens

dimensions were used for fabrication of the test specimens except when compatibility with laboratory floor dimensions was required.

2.3 Reinforcing Details

Reinforcement ratios for the members in the seven-story structure were quite low, particularly by U.S. standards where they approach the minimum recommended values given by ACI 318-83 [2]. However, the large, lightly-reinforced sections are typical of Japanese seismic design practice. The reinforcement details for the prototype specimens, the first interior and exterior joint assemblies, were similar to the details used in the seven-story structure. The steel percentages and bar arrangements in these specimens were duplicated using standard U.S. bar sizes and grades which were essentially equivalent to the metric bars used in the seven-story structure. In the third and fourth (or "modified") specimens the longitudinal reinforcement in the column and the beams was increased to provide variation in beam-to-slab strength. The increase in the longitudinal reinforcement was selected to simulate more closely the details used at the Portland Cement Association Laboratories for the 1/3.5 scale frames.

2.3.1 Prototype Specimens. Cross-sectional details of the prototype specimens are illustrated in Fig. 2.3. The column reinforcement consisted of eight #7 bars ($\delta =$ 1.37 percent), three in each face. The transverse reinforcement in the column consisted of #3 hoops, spaced at 10 cm (3.9 in.). Throughout the length of the column, including the joint region, clear cover was 3.8 cm (1-1/2 in.).

The longitudinal and transverse beams were reinforced with three #6 bars at the top and two #6 bars at the bottom. This resulted in a reinforcement percentage (δ) of 0.64 percent and 0.42 percent for the top and bottom steel, respectively; the reinforcement percentages were computed using the rectangular beam section. Top steel in the longitudinal beam was placed under the top steel in the transverse beam, a detail used in the full-scale structure, as shown in Figs. 2.4 and 2.5. The longitudinal reinforcement was continuous through the joint and anchored at the end of each beam with a standard 90° hook. In the exterior joint the longitudinal beam bars were carried to the far end of the column as is common U.S. practice as shown in Figs. 2.6 and 2.7. Bars are taken only to the center of the joint in typical Japanese practice, but as a compromise the standard U.S. detail was used. The transverse reinforcement in both the longitudinal and transverse beams was provided by #3 hoops at a spacing of 10 cm for the first meter from the column face. (The first stirrup was 5 cm from the column face.) Thereafter, the hoop spacing was increased to 20 cms.

The reinforcement hook details for the beam and columns stirrups differed slightly from the standard U.S. practice. A six bar diameter hook extension, a common Japanese practice, was used as a compromise instead of the 10 bar diameter (10 d_b) hook extension required by Appendix A of ACI 318-83.

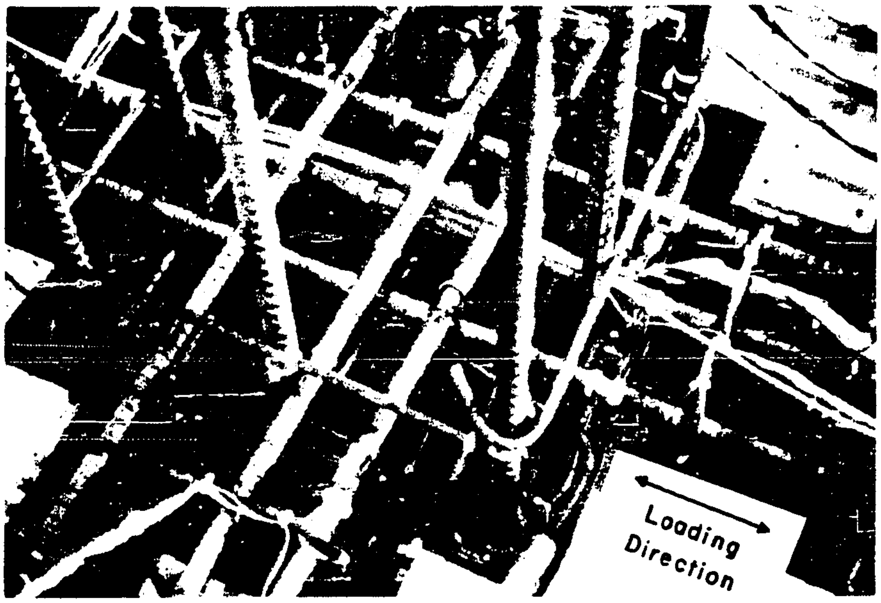
Loading
Direction

Fig. 2.4 Interior joint reinforcing detail, prototype test specimen

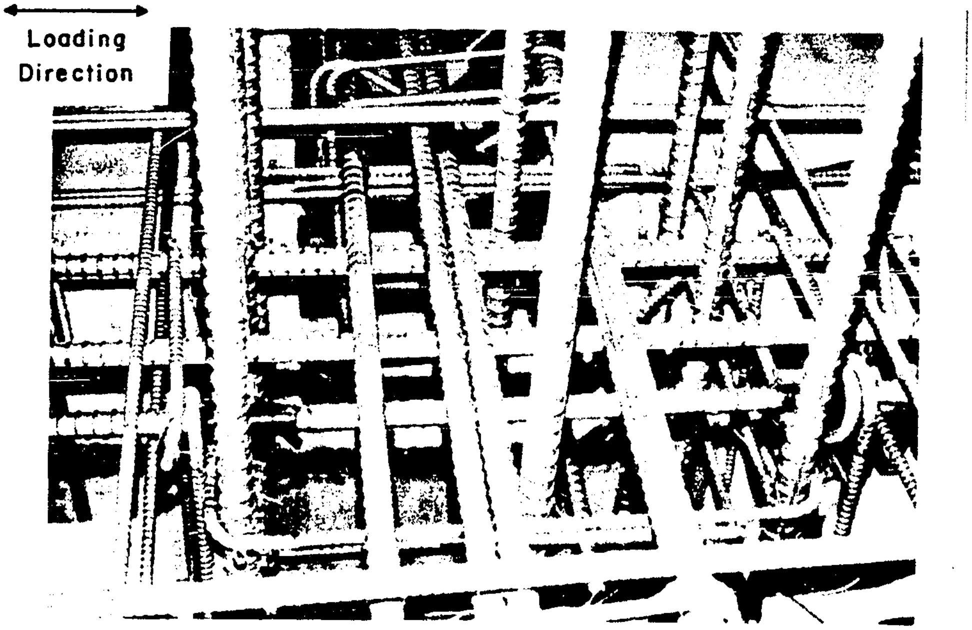
Loading
Direction

Fig. 2.5 Interior joint reinforcing detail, seven-story structure

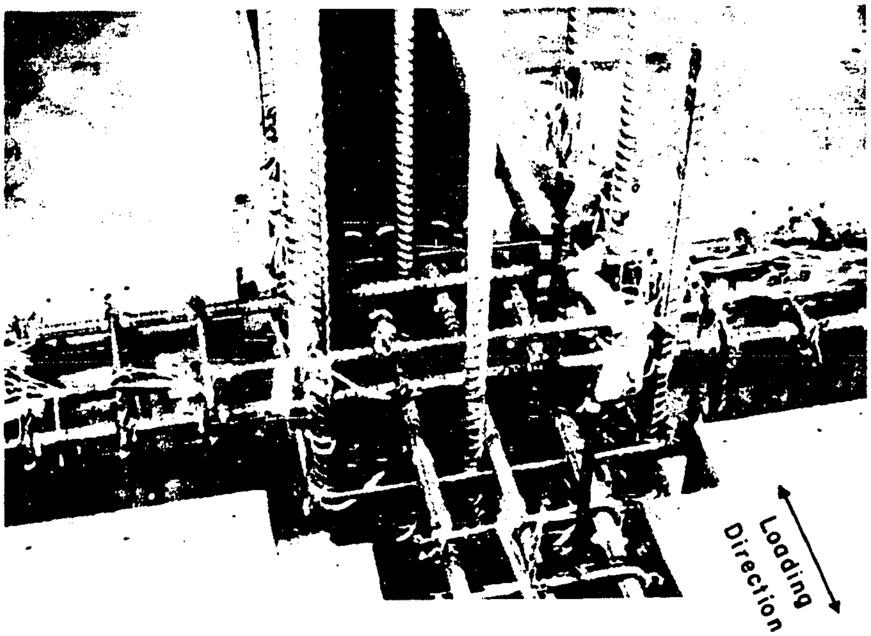
Loading Direction

Fig. 2.6 Exterior joint reinforcing detail, prototype test specimen

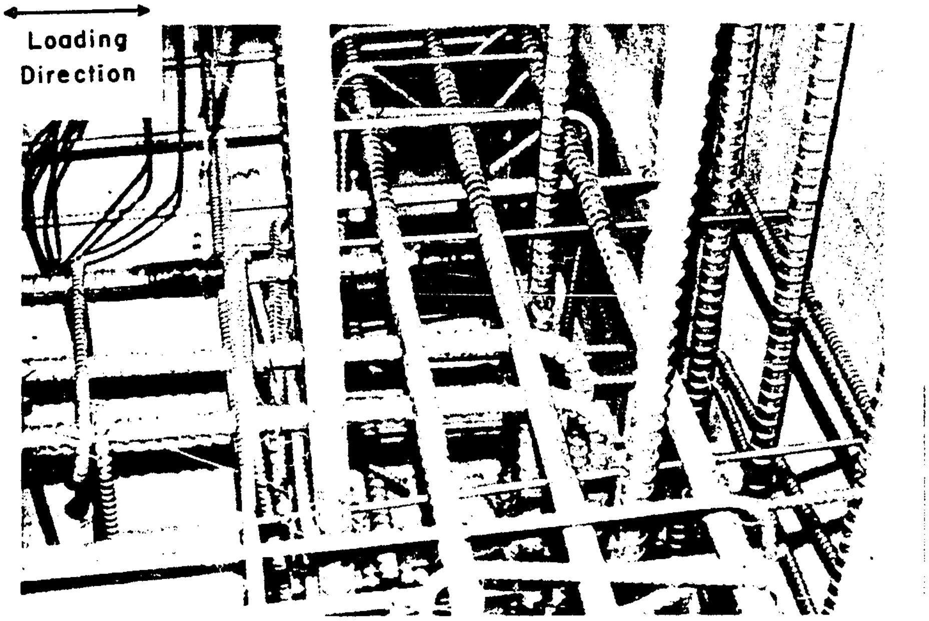
Loading Direction

Fig. 2.7 Exterior joint reinforcing detail, seven-story structure

The end beams were reinforced with two #7 bars top and bottom. The transverse reinforcement in the end beams consisted of #3 stirrups at 20 cm (7.9 in.) throughout the length of the beam.

The slab reinforcement consisted of two mats of #3 bars, with a 2 cm (3/4 in.) clear cover (see Fig. 2.8). The top steel in the longitudinal direction was placed over the top steel in the transverse direction, and the bottom steel in the longitudinal direction was placed under the bottom steel in the transverse direction. The longitudinal reinforcement was placed at 30 cm (11.8 in.) spacing for the first 90 cm (35.4 in.) measured from the beam centerline and then decreased to a 20 cm (7.9 in.) spacing. The bottom layer of the longitudinal slab steel in the interior joints was continuous over the transverse beam, a detail not normally used in U.S. practice. A uniform spacing of 30 cm was used in the transverse direction. The longitudinal slab steel had standard ACI 180° hooks at the ends, whereas the transverse slab steel had no hooks at the ends.

2.3.2 Modified Specimens. The primary difference between the detailing of the modified interior and exterior joint assemblies and that of the corresponding prototype specimens was the increased amount of longitudinal steel in the column and all the beams (see details in Fig. 2.3).

The column reinforcement consisted of twelve #8 bars (δ = 2.7 percent), four on each face. The column transverse reinforcement was identical to that in prototype specimens, #3 hoops at 10 cm (3.9

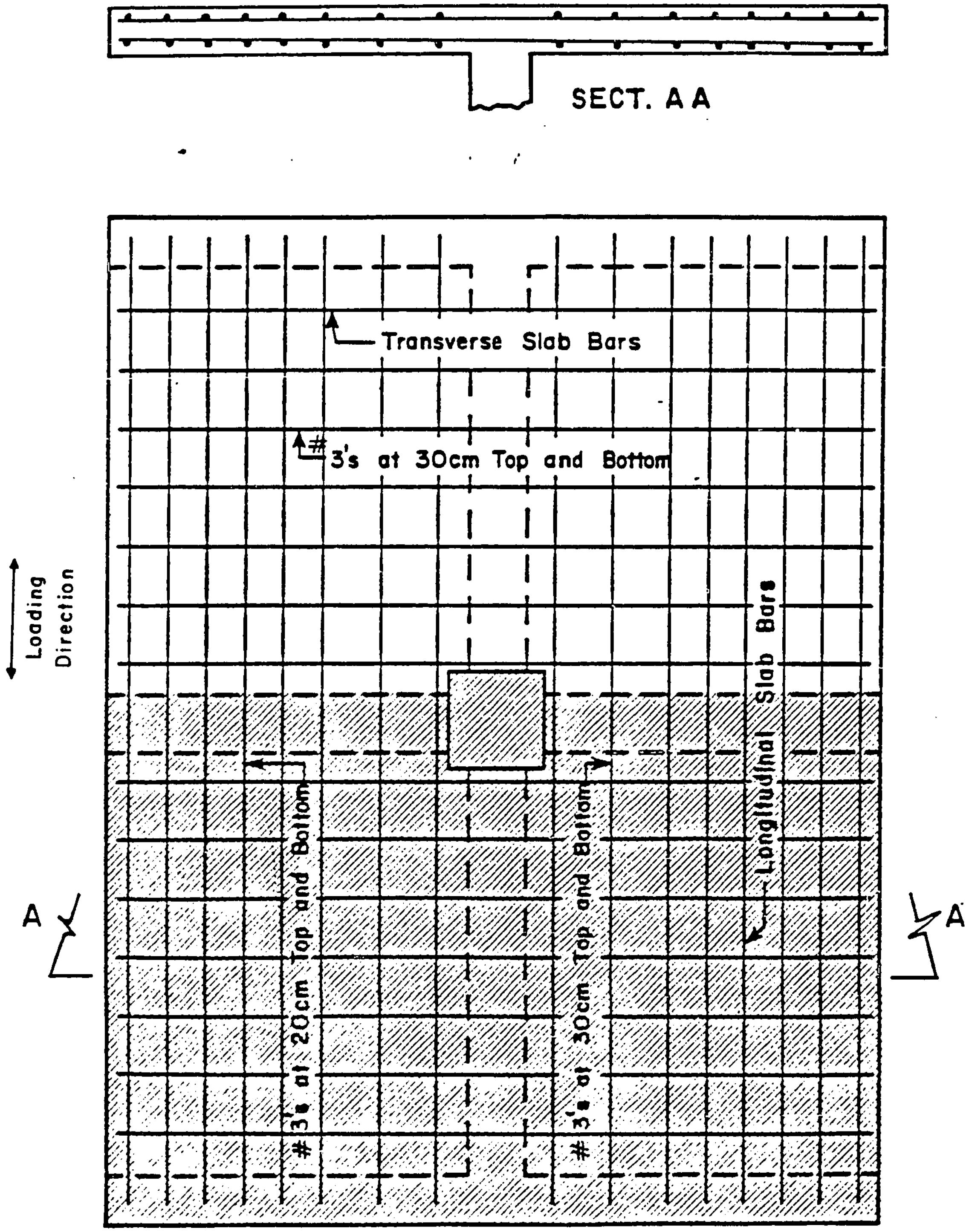
SECT. AA
Transverse Slab Bars
#3's at 30cm Top and Bottom
Loading Direction
Longitudinal Slab Bars
#3's at 20cm Top and Bottom
#3's at 30cm Top and Bottom
A
A

Fig. 2.8 Slab reinforcement detail

in.) along the column and through the joint. The exterior prototype specimen exhibited an anchorage failure due to lack of sufficient transverse confinement. Hence, to provide additional joint transverse confinement, in the case of the exterior modified specimen, cross ties were added in the joint. The cross ties consisted of #3 bars with ACI 135° standard hooks at either end. The hooks were in the vertical plane, as illustrated in Fig. 2.9. One cross tie was placed in the longitudinal direction at the center of each of the four #3 hoops in the joint region.

The longitudinal beam had five #7 bars at the top and three #7 bars at the bottom. The reinforcement percentages were 1.36 and 0.85, respectively, based on the rectangular beam section only. Four of the top five bars were bundled in groups of two bars, and were located at the corners of the hoops. The longitudinal reinforcement in the transverse beam consisted of four #7 bars at the top and three #7 bars at the bottom. The transverse reinforcement in both the longitudinal and transverse beams was identical to that used in the prototype specimen.

Two #8 bars were used at the top and at the bottom to reinforce the end beams. The transverse reinforcement was identical to that in the prototype specimens.

The slab steel in the modified specimens was identical to that of the prototype specimens (see Fig. 2.8).

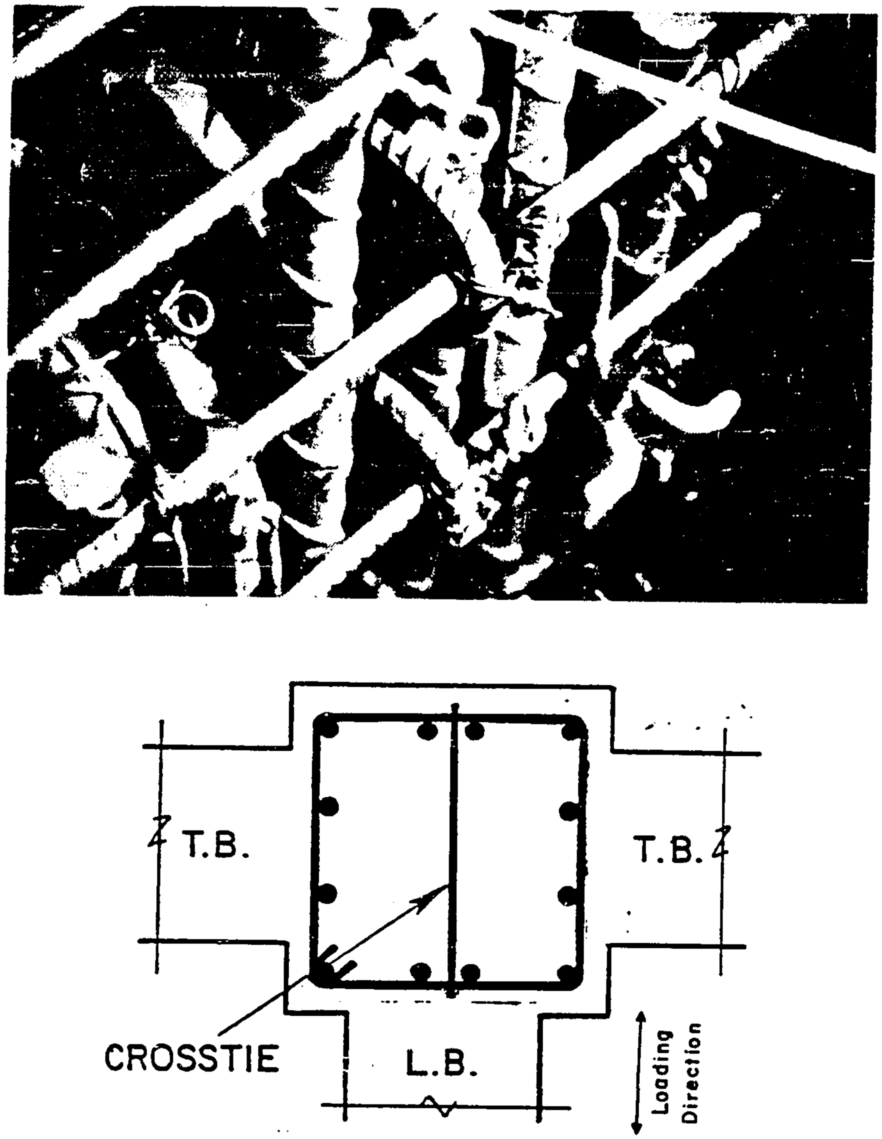
T.B.
T.B.
CROSSTIE
L.B.
Loading Direction

Fig. 2.9 Cross ties in the joint, exterior modified specimen

2.4 Fabrication of the Specimens

2.4.1 Formwork. The formwork included typical lower and upper column forms (see Fig. 2.10) and four rectangular pans with side forms (see Fig. 2.11) used to mold the beams and the slab. To avoid binding of the pan forms between the transverse beam and end beam, each of the four pans was built using two individual units separated by a narrow opening. Once the formwork was assembled the openings were filled with strips of styrofoam and then caulked to prevent loss of water through the opening.

Only one form was built and was used repeatedly to fabricate the four specimens. The formwork was modified slightly for the construction of the exterior specimens. The formwork was lacquered to provide a protective coating as well as a smooth finish for the concrete surface.

2.4.2 Construction and Assembly of Reinforcing Cages. The column cage was fabricated with only the lower column stirrups tied in position (see Fig. 2.12), and was then lowered into the casting platform. A thick-walled pipe, 50 cm (19-3/4 in.) long and 1-1/4 in. inside diameter was carefully aligned and tied in place 4-1/2 in. above the base of the column. This pipe served as a sleeve through which a 1-1/4-in. diameter high strength steel bolt was later inserted to provide a pin connection at the base of the specimen. The area surrounding the pipe was reinforced with extra column hoops and cross ties. In addition, a 1/4 in. spiral 3 in. in diameter at 1-1/2-in. pitch was placed around the pipe to prevent local failure

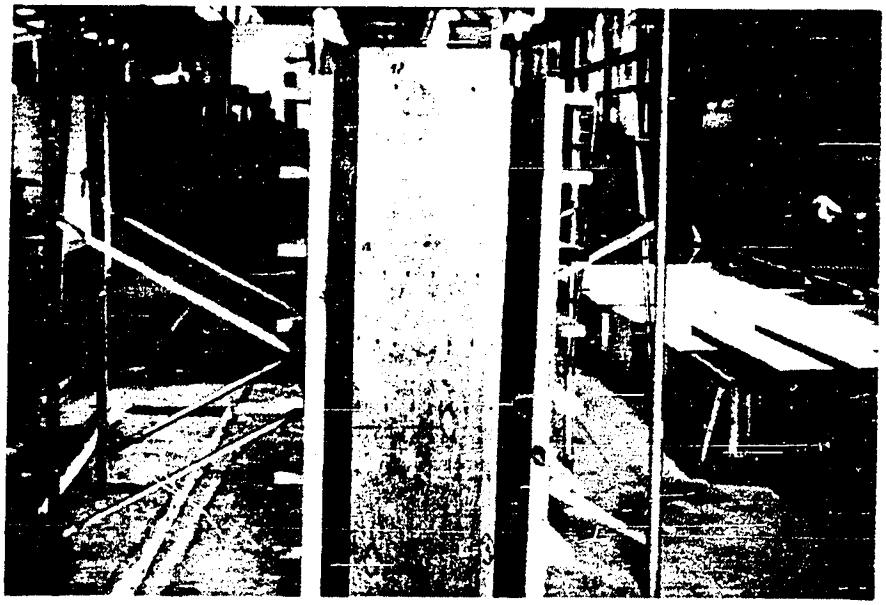

Fig. 2.10 Lower column form work

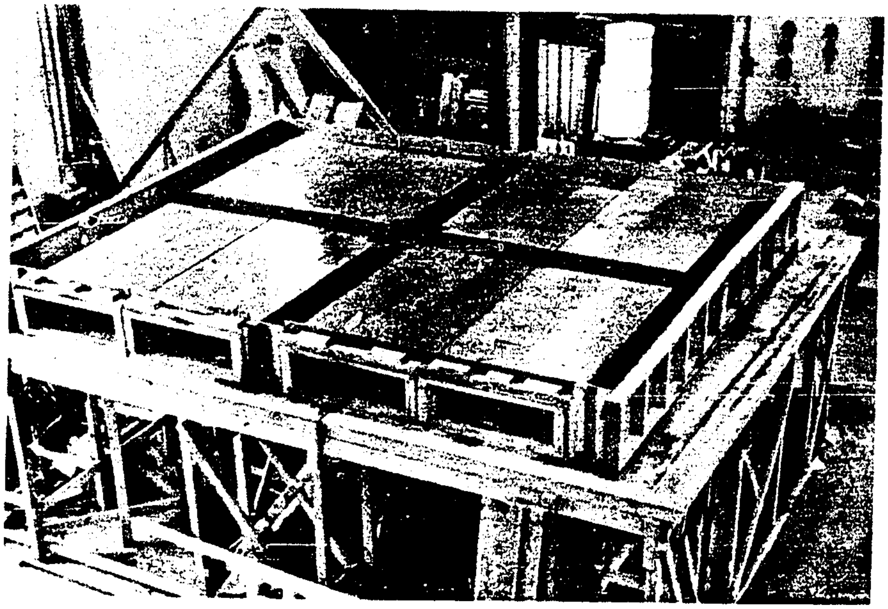

Fig. 2.11 Slab-beam form work

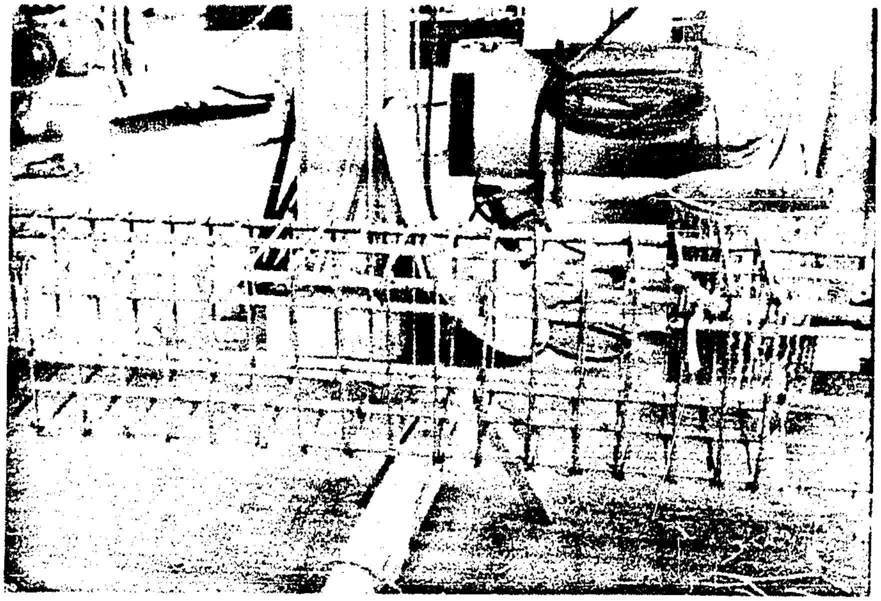

Fig. 2.12 Column reinforcement cage, interior prototype specimen

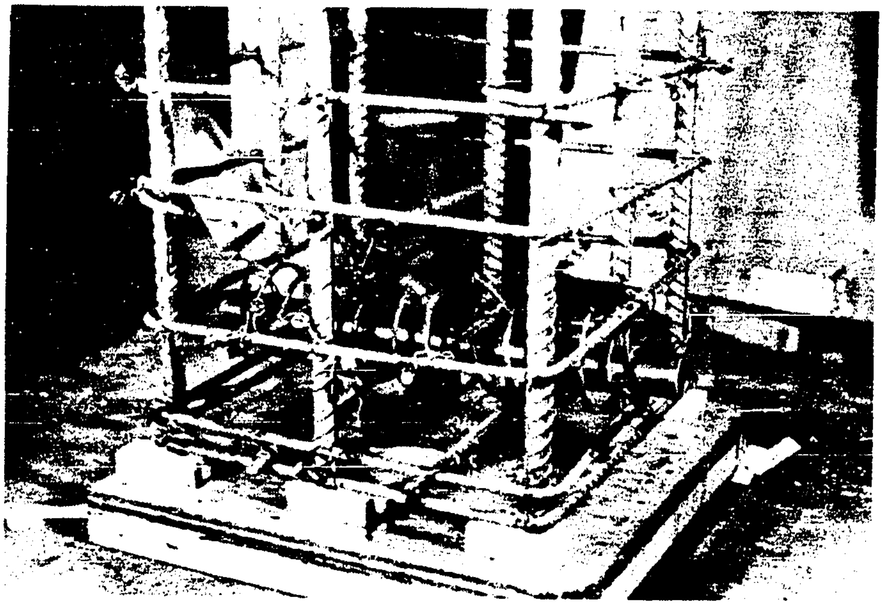

Fig. 2.13 Steel sleeve for pin connection

during testing (see Fig. 2.13). The lower column forms were oiled and secured in place with the column cage aligned within.

The eight pan forms (six in the exterior joint assemblies) were then positioned and secured to the platform with lag bolts (see Fig. 2.11). The longitudinal and transverse beam cages were constructed as one unit (see Figs. 2.14, 2.15). The column hoops in the joint region were loosely tied inside the beam cages. The longitudinal and transverse beam cages and the four joint core ties were threaded simultaneously through the upper column bars and lowered into place (see Fig. 2.16). In the modified exterior joint, four cross ties with 135° hooks at one end were slid into the joint core, and were then bent in place to form a 135° hook on the other side (see Fig. 2.9). The partially fabricated end beam cages were placed and then completely tied. The remaining formwork was oiled and bolted to the platform. The slab steel mats were placed and secured in position as shown in Fig. 2.17. Three top column hoops were placed and tied. A collar to form the lower 3 in. of the upper column was secured around the top column cage. The strain gage lead wires were bundled and tied to the upper column bars.

2.4.3 Reference Inserts. Inserts were secured in selected positions in and near the joint core to serve as reference points for instrumentation used to determine beam and joint deformations (Fig. 2.18). To reduce inaccuracy due to spalling concrete moving the reference points, the inserts were isolated from the cover concrete with foam rubber and tape. Several screw anchors were also provided

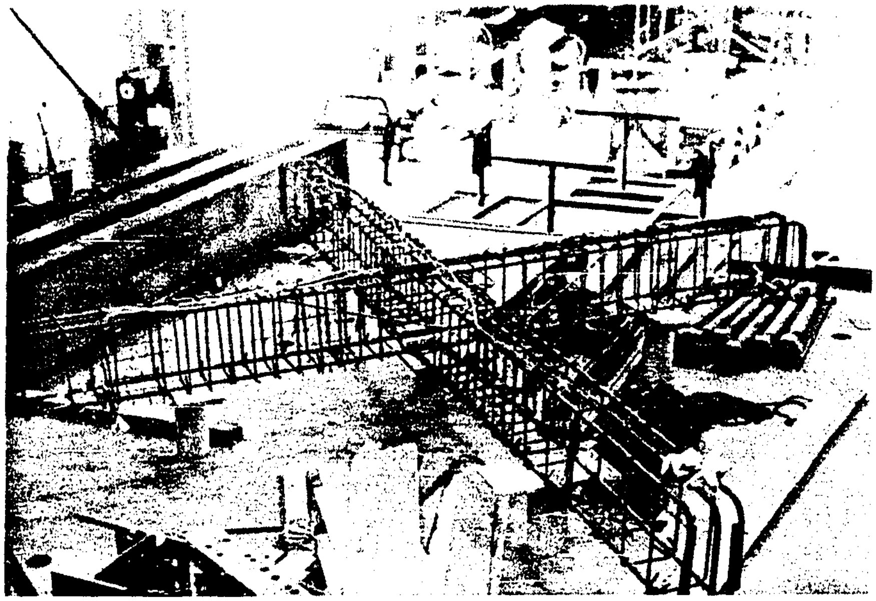

Fig. 2.14 Beam reinforcement cage, interior prototype specimen

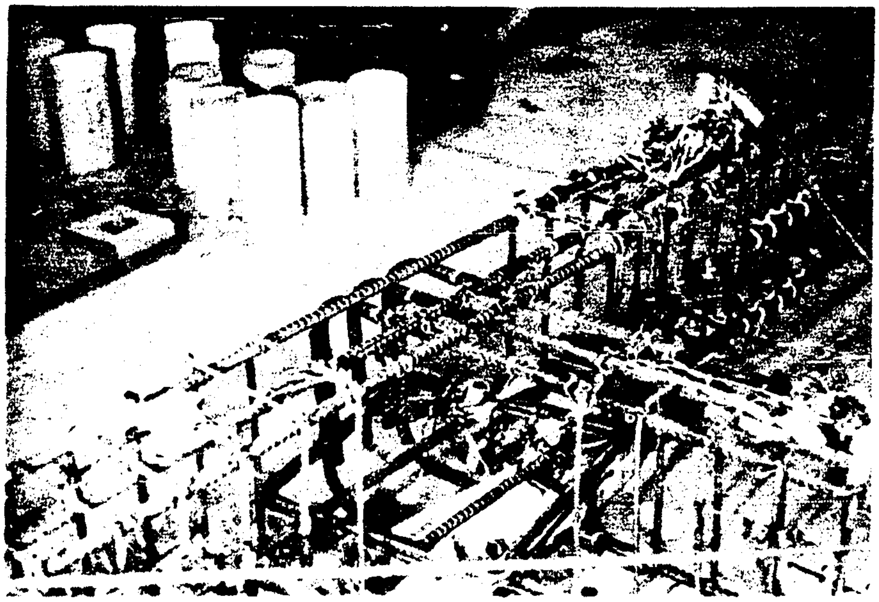

Fig. 2.15 Beam reinforcement cage, exterior prototype specimen

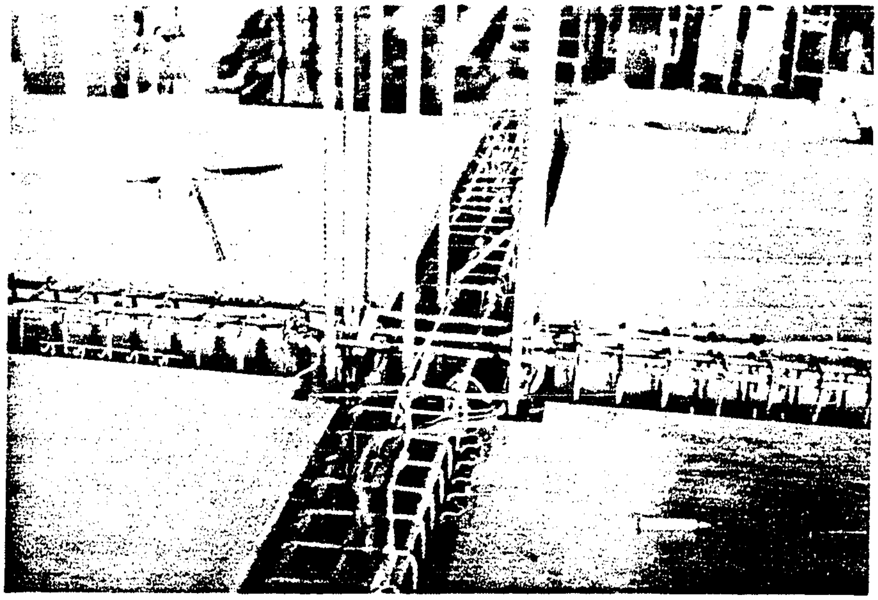

Fig. 2.16 Column and beam reinforcement placed in forms

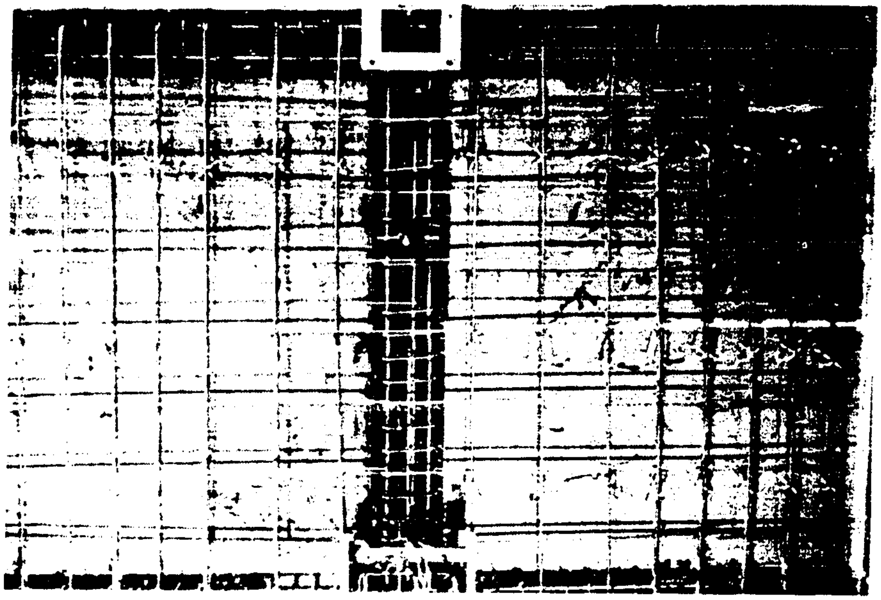

Fig. 2.17 Slab reinforcement placed in forms

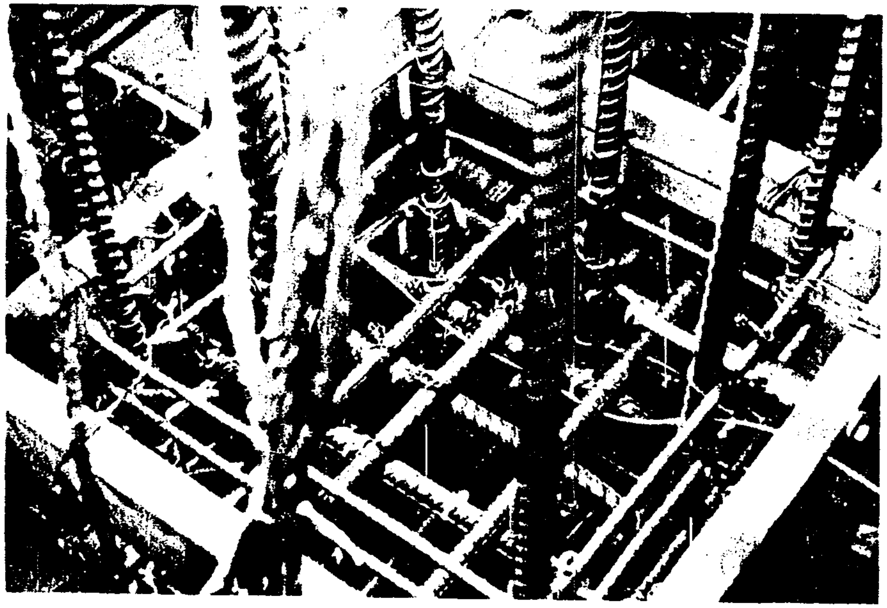

Fig. 2.18 Reference inserts and slip wires in the joint

at various locations to help attach instrumentation. To provide reference points for beam rotations, two straight rods (1/2-in. diameter steel stock) were embedded in the longitudinal beam, on either side of the column, at 6 in. and 24 in. from the column face. At the longitudinal beam-end beam joints, four PVC tubes were placed to correspond with the four holes in the loading plates used to attach the loading rams to the specimen, as shown in Fig. 2.19.

2.4.4 Casting and Curing. Each specimen was cast in two stages. The lower column, the joint region and the slab were cast in the first operation. Following a four-day curing period the forms were stripped. The specimens were lifted from the platform and set on a steel frame prior to casting the upper column. The upper column cage was completed and a pipe was inserted for the upper pin connection. The upper column forms were aligned using the 3-in. projection left in the column during the earlier concrete placement, as shown in Fig. 2.20. The upper column was cast and allowed to cure for several days before the forms were removed.

2.5 Instrumentation

The instrumentation used was identical for all four specimens. Each of the specimens was extensively instrumented to gather sufficient data to monitor behavior during the test and to help in correlating the results with those of the seven-story structure.

2.5.1 Strain Measurements. Strain gages were mounted on beam, column and slab longitudinal bars as well as the beam and

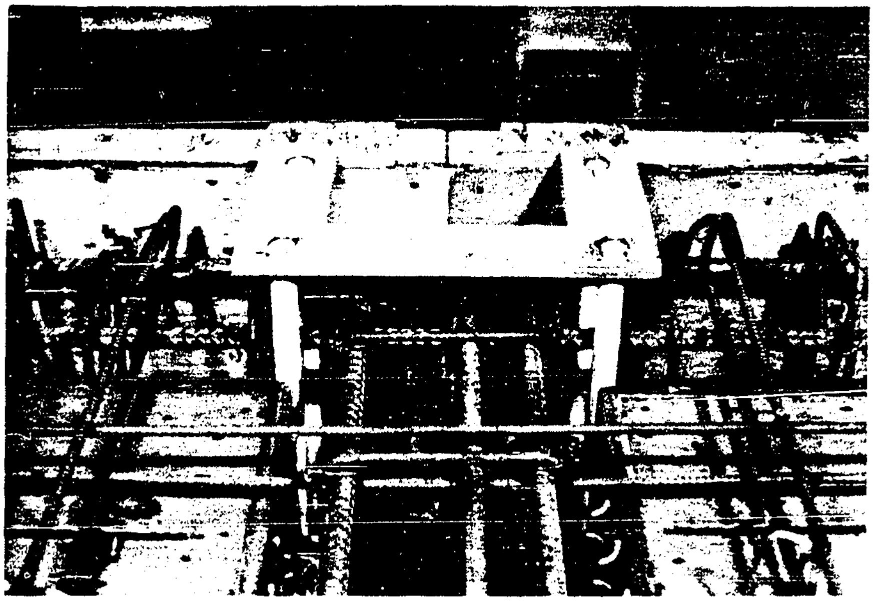

Fig. 2.19 PVC tube inserts to attach loading rams

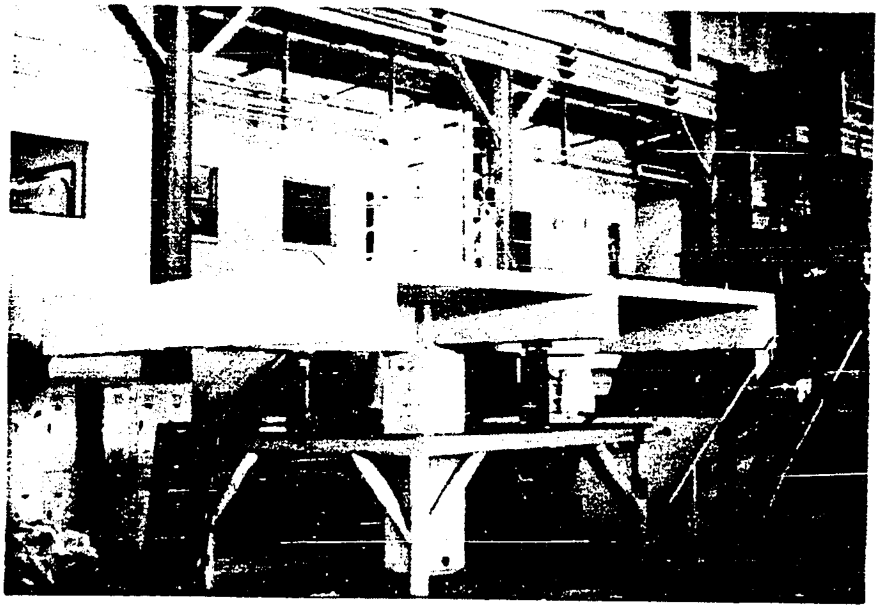

Fig. 2.20 Upper column form work

column transverse reinforcement. Prior to mounting the strain gages on a reinforcing bar, bar lugs were removed by grinding and the surface was sanded and cleaned. The gages were attached with epoxy. The gage and its connection were waterproofed with a moisture barrier and covered with an adhesive rubber compound. The strain gages had a gage length of 0.64 in. on the larger bars (#8, #7, and #6) and a gage length of 0.32 in. on the smaller bars (#3).

The primary strain gage locations in the test specimen were identical to those in the prototype structure. Gages were located on beam and column bars near the critical sections at the beam-column interfaces (see Fig. 2.21), and on longitudinal slab bars at the transverse beam-slab interfaces (see Fig. 2.22). Additional gages were located in the slab (Fig. 2.22), in the joint core column hoops and on the hoops of the transverse beam (Fig. 2.23). The number of strain gages required was reduced by taking advantage of symmetry. The southwest quadrant of each specimen was extensively gaged, and only a few gages were placed in the remaining quadrants to serve as checks.

2.5.2 Beam Deflections and Beam Load. The beam end deflections were measured with a 12-in. LVDT potentiometer attached to the loading actuator (see Fig. 2.24). The displacement of the potentiometer corresponded to the piston displacement. The load applied at the ends of the longitudinal beam was monitored by a load cell attached between the specimen and the hydraulic ram (Fig. 2.24).

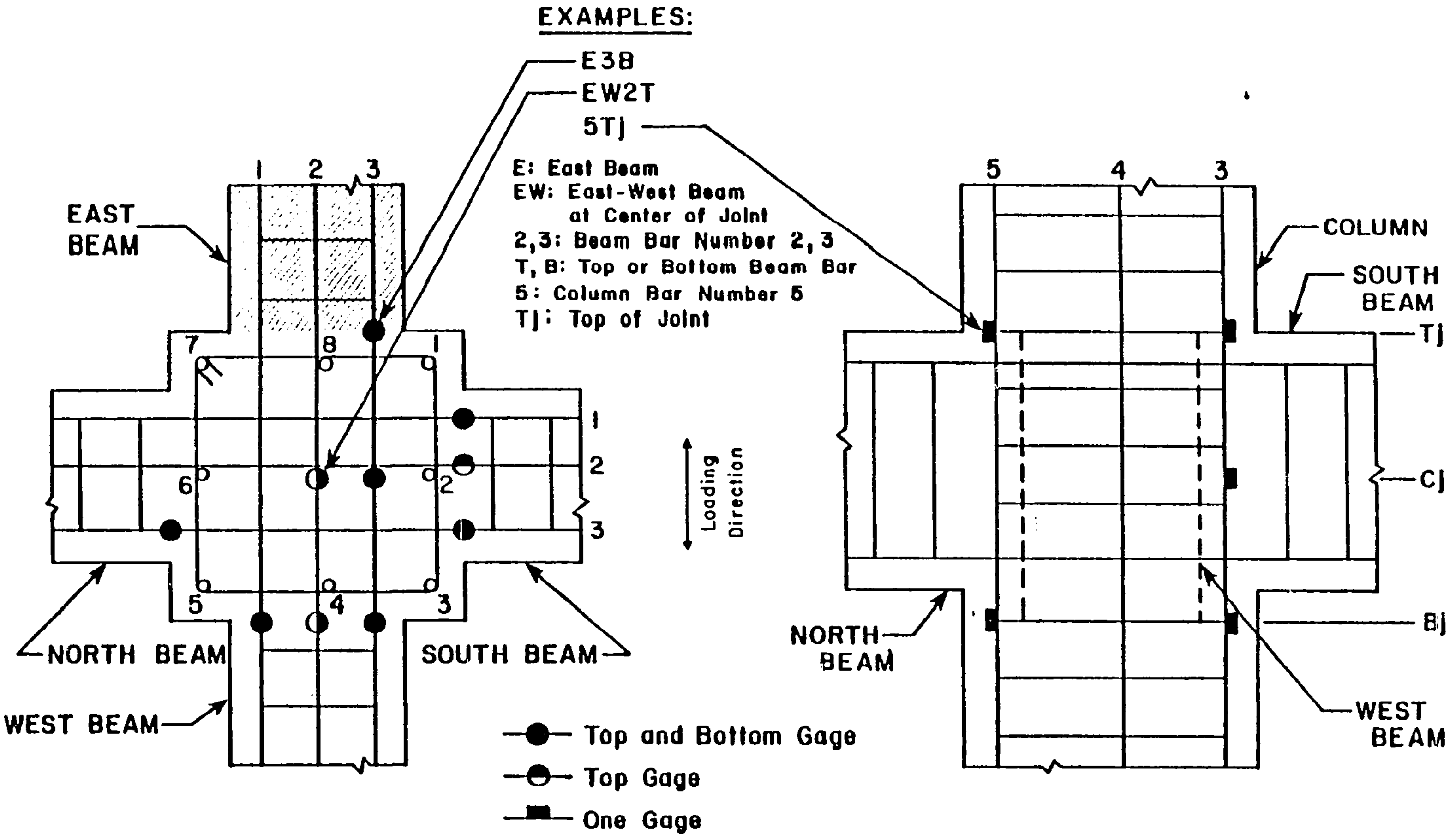
EXAMPLES:
E3B
EW2T
5TJ
E: East Beam
EW: East-West Beam at Center of Joint
2,3: Beam Bar Number 2, 3
T, B: Top or Bottom Beam Bar
5: Column Bar Number 5
TJ: Top of Joint
EAST BEAM
NORTH BEAM
SOUTH BEAM
WEST BEAM
1
2
3
4
5
6
7
8
Loading Direction
Top and Bottom Gage
Top Gage
One Gage
COLUMN
TJ
CJ
BJ

(a) Plan view

(b) Side view

Fig. 2.21 Beam and column bar strain gage locations

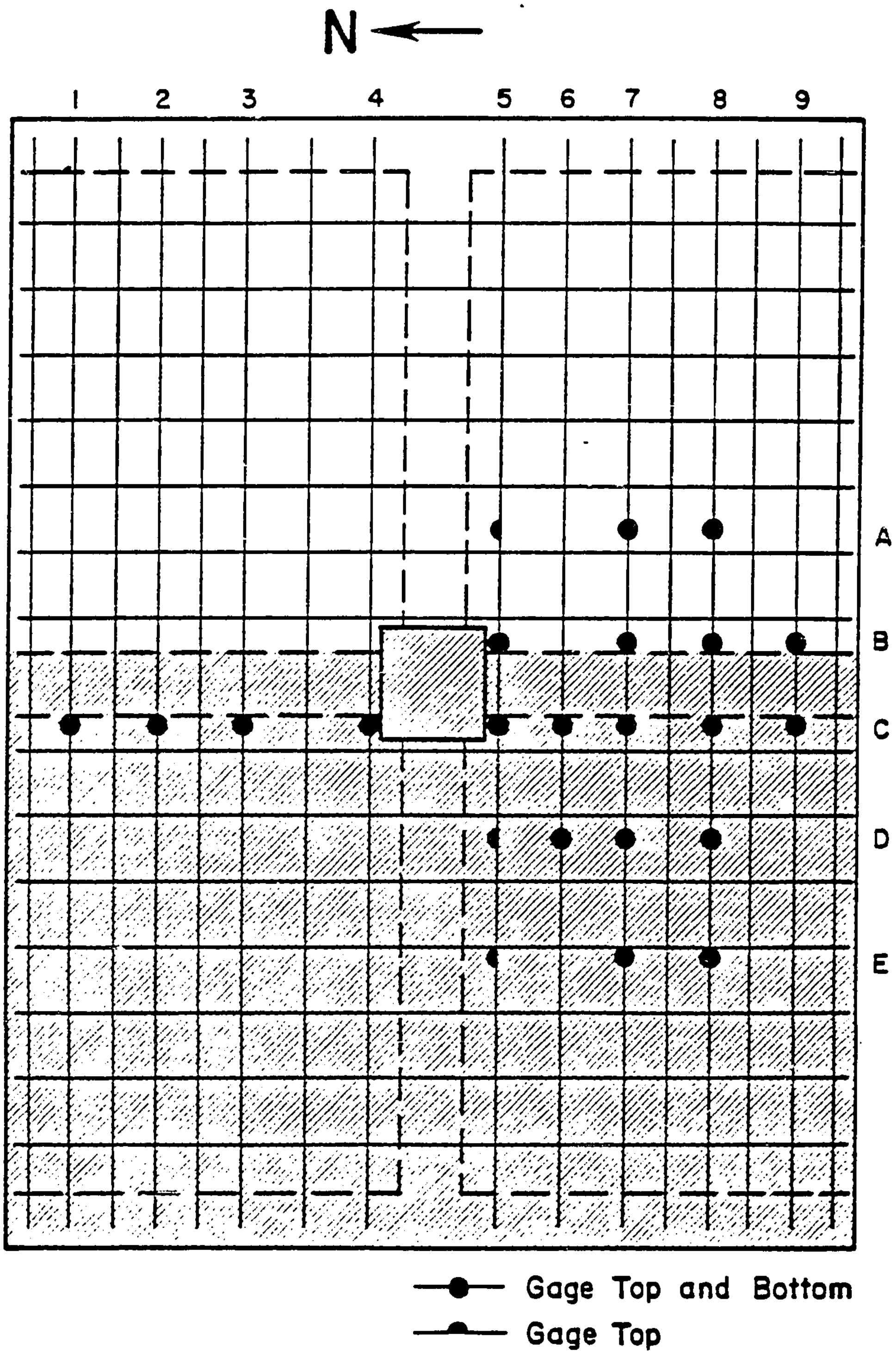
N
1
2
3
4
5
6
7
8
9
A
B
C
D
E
Gage Top and Bottom
Gage Top

Fig. 2.22 Slab bar strain gage locations

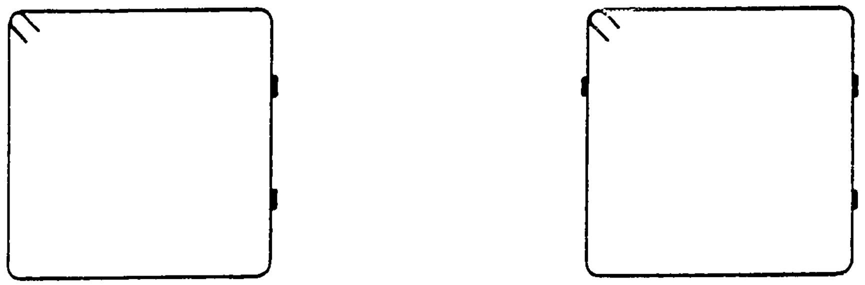

Ties 1,4

Ties 2,3

(a) Joint core ties

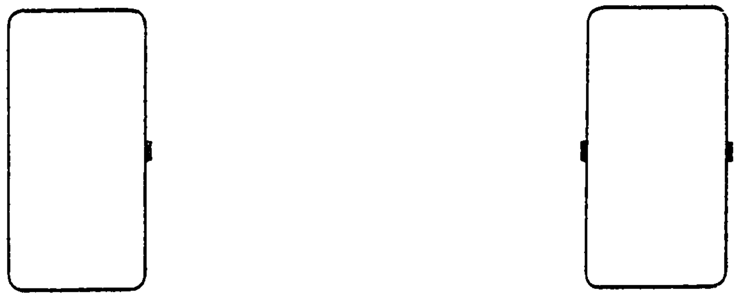

North Beam Hoops 2,3

South Beam Hoops 1-4

(b) Transverse beam hoops

Fig. 2.23 Strain gage locations for joint and beam hoops

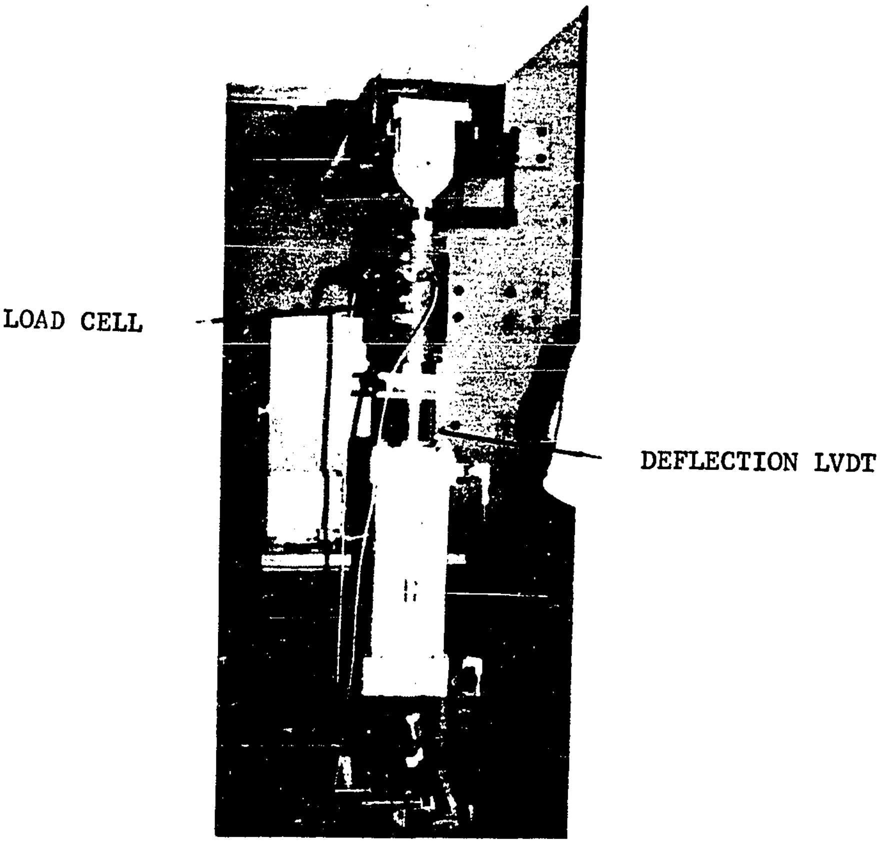
LOAD CELL
DEFLECTION LVDT

Fig. 2.24 Load cell and deflection LVDT instrumentation

2.5.3 Beam Rotations. The longitudinal beam rotations near the column faces (6 in. from the column face) were measured relative to the column using linear potentiometers mounted on the embedded rods above and below the longitudinal beam (see Fig. 2.25). Aluminum plates bolted to the column inserts above and below the joint provided smooth reference surfaces for the potentiometer shafts.

The beam rotations along the longitudinal beam between 6 in. and 24 in. from the column face were also measured. An aluminum plate was soldered at the end of a hollow aluminum tube; this provided a reference surface when attached to the rod embedded 6 in. from the column face (see Fig. 2.25). Two potentiometers, one above and one below the beam, were attached to the rod embedded at a distance of 24 in. from the column face.

The potentiometers measured horizontal displacements over known gage lengths as the beam rotated (see Fig. 2.26). The difference in the readings between the corresponding top and bottom potentiometers was used to determine the angle of beam rotation between the column and the rod embedded in the beam 6 in. from the column face in the first case and between the two rods embedded at 6 in. and 24 in. from the column face in the second case.

The measured rotations include the effects of both elastic and inelastic beam deformations as well as slip of the beam bars through the joints. The calculation for the beam rotations, relative to the column, are based on the approximate geometry and beam deformation shown in Fig. 2.26. The measured rotations do not

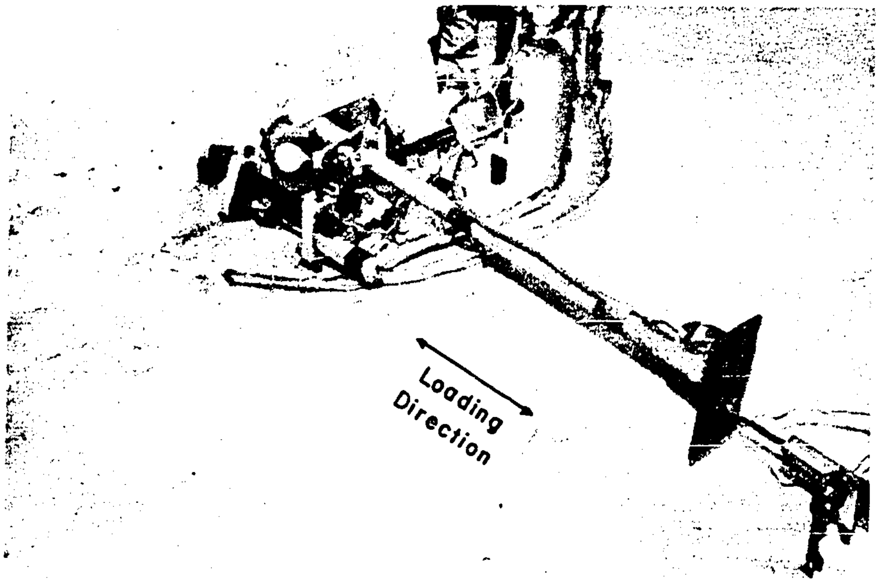
Loading Direction

Fig. 2.25 Beam rotation instrumentation

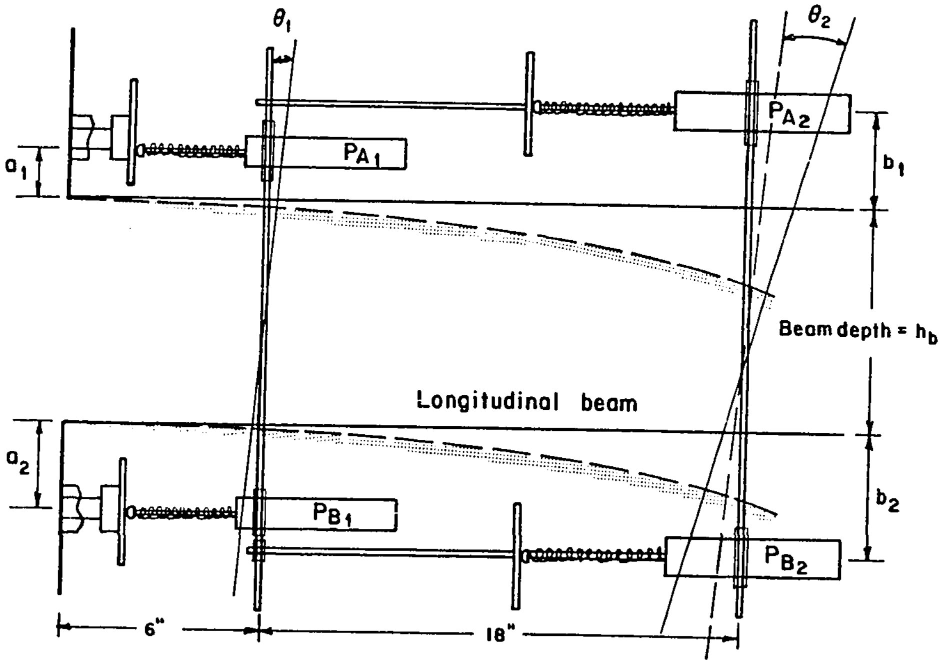
θ_1
θ_2
P_{A_1}
P_{A_2}
a_1
b_1
Beam depth = h_b
Longitudinal beam
a_2
b_2
P_{B_1}
P_{B_2}
6"
18"

$$\theta_1 = \text{Beam rotation @ 6 in.} = \frac{\text{Diff. in readings between } P_{A1} \text{ and } P_{B2}}{a_1 + h_b + a_2}$$

$$\theta_2 = \text{Beam rotation bt. 6 \& 24 in.} = \frac{\text{Diff. in readings between } P_{A2} \text{ and } P_{B2}}{b_1 + h_b + b_2}$$

Fig. 2.26 Beam rotation geometry

correct for the contributions due to joint shear rotations or flexural rotations of the column. The rotations were determined in an identical manner for the seven-story structure over an 8 to 9 in. length from the column face.

2.5.4 Joint Shear Strain. The joint shear strain was measured with the assembly shown in Fig. 2.27. Two sliding arms were attached to three reference inserts embedded in the joint core and located on the north column face below the slab. A linear potentiometer was mounted on the diagonal between the extension of the two sliding arms. Shear deformations of the joint produced movement of the arms relative to each other. The potentiometer measured changes in the length of the third side of the triangle between the arms. The joint shear strain was obtained using the law of cosines as illustrated in Fig. 2.27.

2.5.5 Slip of Longitudinal Beam Bars. The slip of the longitudinal beam bars was monitored by a potentiometer attached to a fixed insert embedded in the joint core (Fig. 2.18). A stiff piano wire was firmly attached to the beam bars by inserting it into a tight-fitting hole drilled in the bar, and a nylon tie further secured the wire to the bar. A plastic tube was then placed on the piano wire. The plastic tube allowed the wire to move relative to the surrounding concrete (see Figs. 2.18 and 2.28). A rod was bolted to the fixed insert in the joint core. A small plate was attached firmly to the end of the wire and a spring was inserted between a fixed plate on the rod and the plate on the wire. A linear

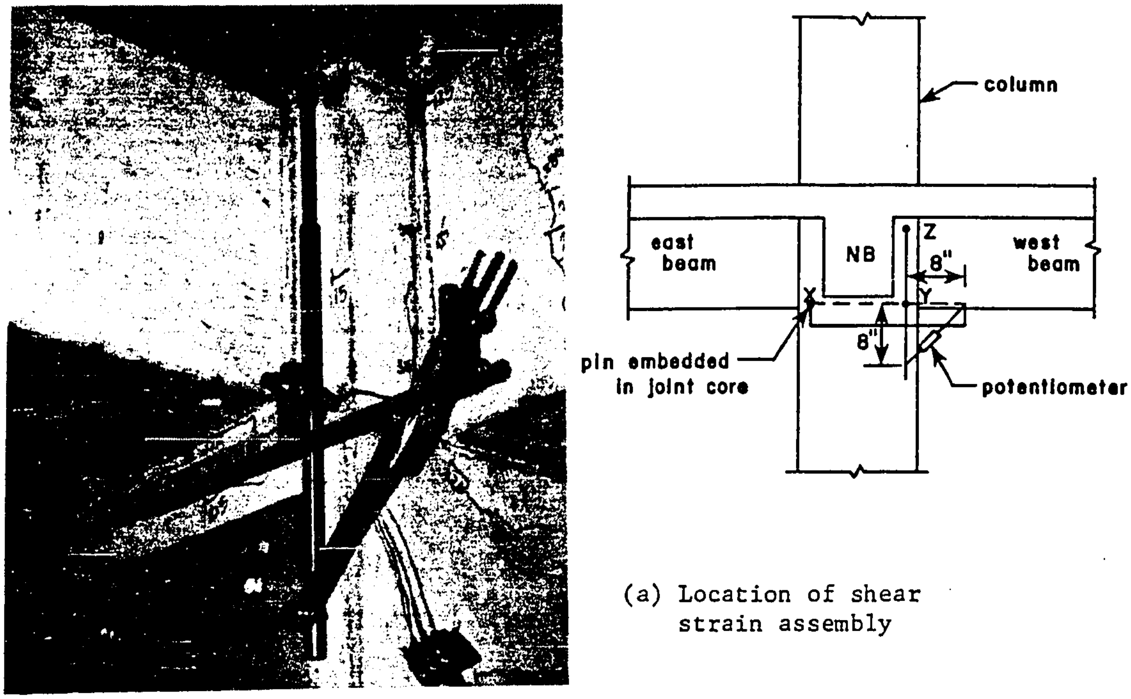
column
east beam
NB
west beam
Z
8"
Y
X
8"
pin embedded in joint core
potentiometer

(a) Location of shear strain assembly

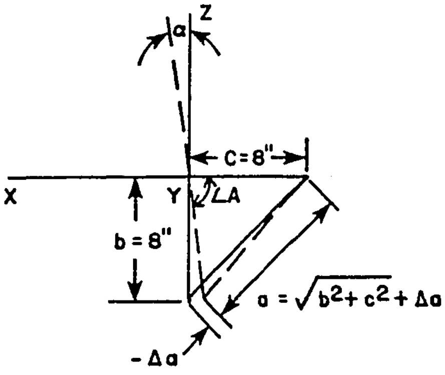
α
Z
C=8"
X
Y
∠A
b=8"
a = √(b²+c²+Δa)
-Δa

(b) shear strain geometry

α = joint shear strain, rad.

Δa = potentiometer measurement, in.

Law of cosines:

$$a^2 = b^2 + c^2 - 2bc \cos \angle A$$

$$\angle A = \cos^{-1}\left(\frac{-a^2 + b^2 + c^2}{2bc}\right)$$

$$= \cos^{-1}\left(\frac{b^2 + c^2 - (\sqrt{b^2 + c^2} + \Delta a)^2}{2bc}\right)$$

$$= \cos^{-1}\left(\frac{128 - (11.31 + \Delta a)^2}{128}\right)$$

$$\alpha = \angle A - \frac{\pi}{2}$$

Fig. 2.27 Joint shear strain instrumentation and geometry

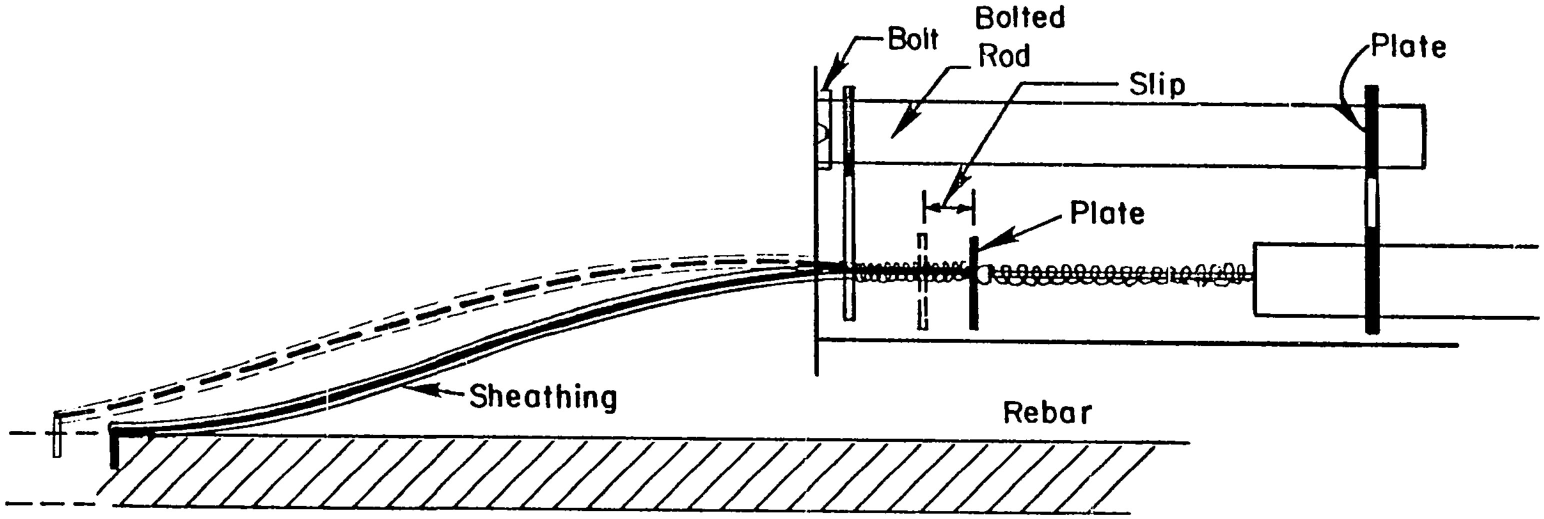
Bolt
Bolted Rod
Slip
Plate
Plate
Sheathing
Rebar

Fig. 2.28 Bar slip measurement instrumentation

potentiometer was mounted on the fixed rod with its plunger bearing against the small plate on the wire.

As the beam bar slipped with respect to the concrete, the piano wire moved inside the plastic sheath. Movement of the bar was monitored by the potentiometer. The slip wire monitored the relative movement of the longitudinal beam bars with respect to the column face (see Fig. 2.28).

2.5.6 Twist of the Transverse Beam. The twist of the transverse beam was measured relative to the column. The twists were determined at 19.5 in. (distance d) and 63.5 in. (near the end of the transverse beam) from the column face on both sides of the column (see Fig. 2.29). A stiff frame, made out of a 2-in. box section and two 1/2-in. steel plates, was bolted to the column. Four 1/2-in. structural tubes were welded to the box section at distances of 19.5 in. and 63.5 in. from the column face on both sides of the column. Two 3/8-in. threaded rods were bolted to the bottom of the transverse beam at each location. A steel angle, with plates attached at the ends to provide a smooth surface for the potentiometer rods to rest against, was secured horizontally to the threaded rods. Potentiometers were mounted on the ends of the steel tubes with the rods bearing against the horizontal plates. See Fig. 2.30 for details.

As the transverse beam twisted with respect to the column (see Fig. 2.31), the steel angle rotated with it. The potentiometers

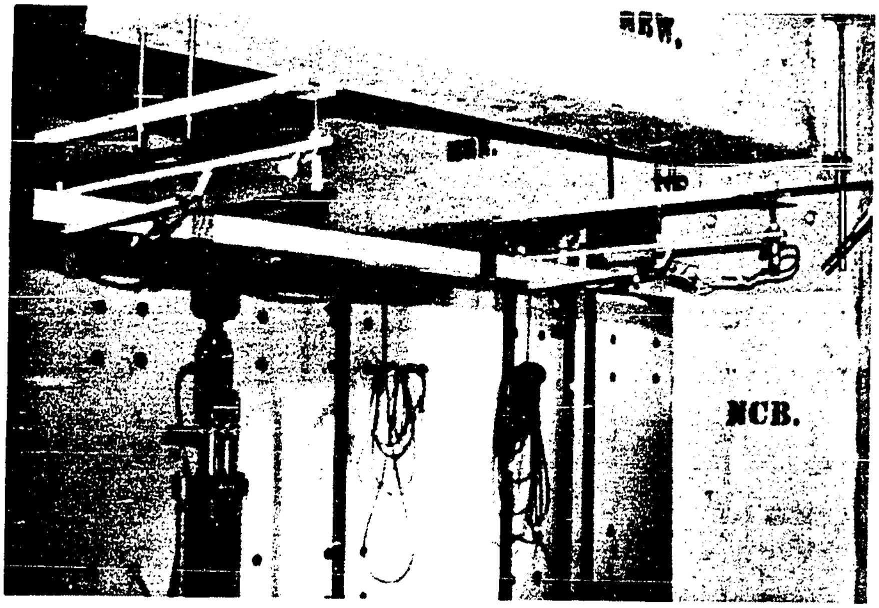

Fig. 2.29 Torsional rotation instrumentation

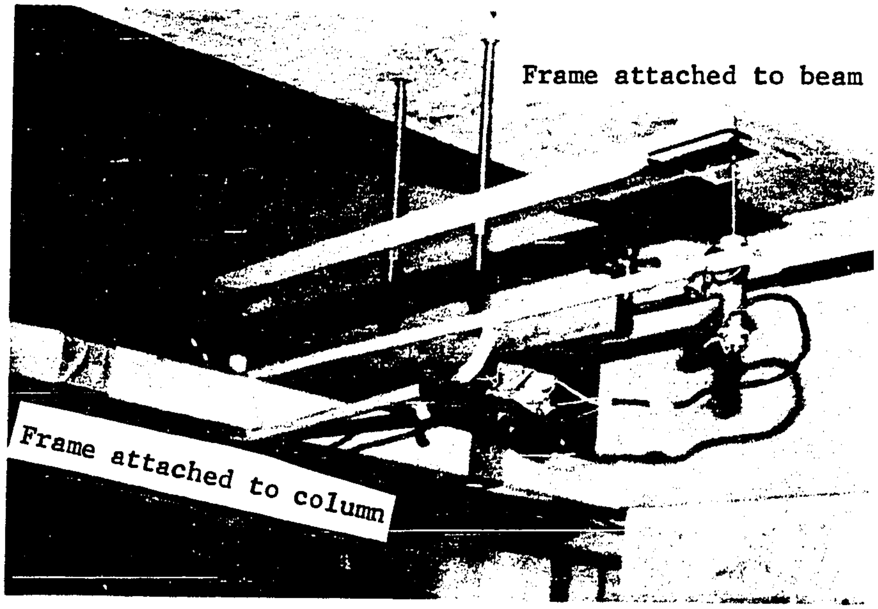
Frame attached to beam
Frame attached to column

Fig. 2.30 Details of torsional rotation instrumentation

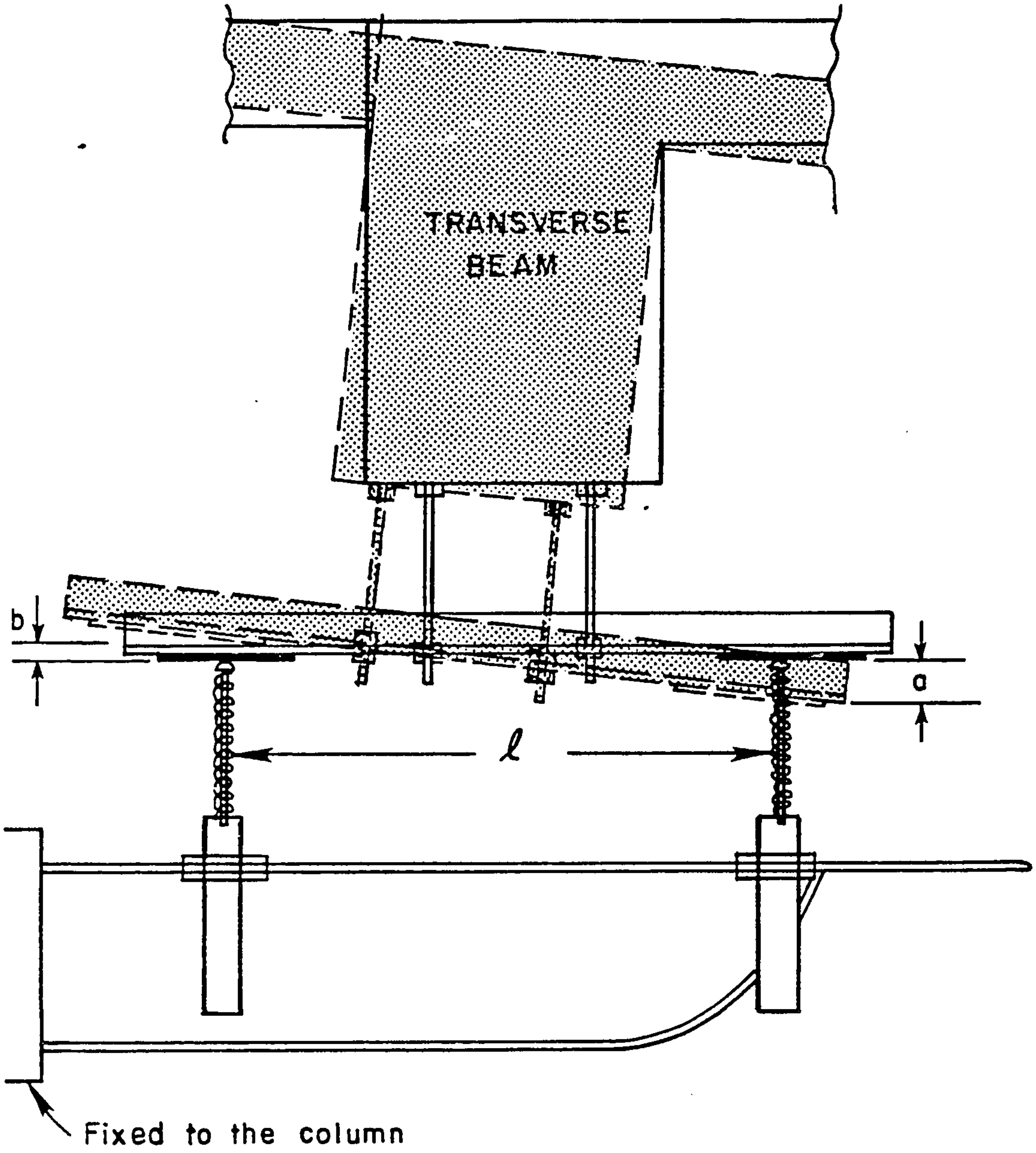
TRANSVERSE BEAM
b
a
ℓ
Fixed to the column

$$\text{TORSIONAL ROTATION} = \frac{a+b}{\ell}$$

Fig. 2.31 Torsional rotation measurement geometry

measured the vertical displacements at each end, from which the torsional rotations were determined as shown in Fig. 2.31.

2.6 Experimental Setup

The experimental setup is shown in Fig. 2.32. The points of inflection for a multistory, multibay structure when subjected to lateral load were assumed to be at the midspan of both the columns and the beams. The specimen was supported at the top and bottom of the column by pin supports, to simulate zero moment condition. Racking loads were applied to both ends of the longitudinal beam to simulate story shear.

2.6.1 Test Frame. The test apparatus (Fig. 2.32) included a floor fixture, a wall bracket, struts extending from the reaction wall, and braces at right angles to the struts. The lower column was pin-connected to the floor fixture which was bolted to the reaction floor. The upper column was pinned to the channel struts which were pin-connected to the wall bracket. Braces attached to the south channel strut supplied lateral bracing to the specimen.

2.6.2 Pin Connections. Similar pin connections were used at both top and bottom. The floor fixture, shown in Fig. 2.33, was fabricated with two 18-in. deep channel sections and a rectangular 1-1/4-in. floor plate. To facilitate positioning of the specimen, one channel was welded to the floor plate, and the other channel was bolted after the specimen was in place. Two clamping plates, one between the column face and the channel and the other on the outside

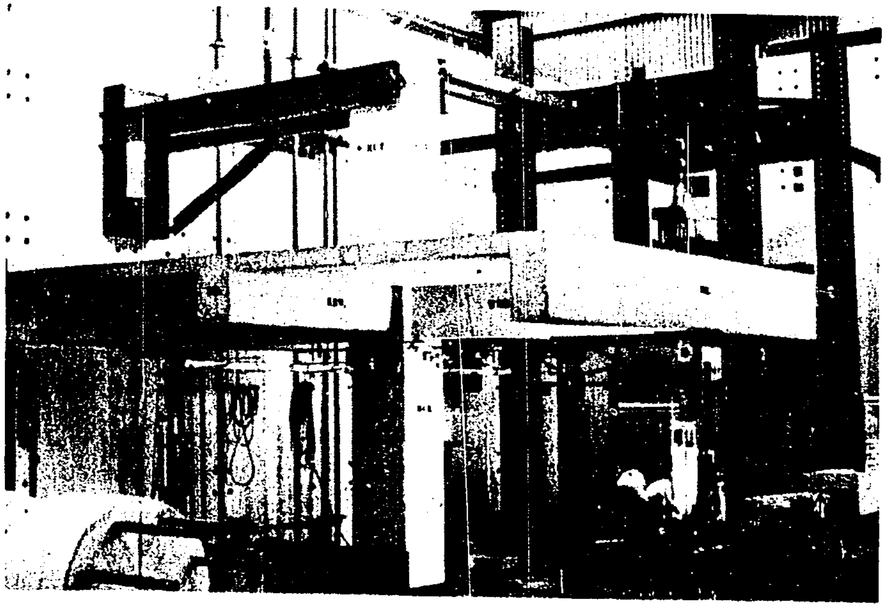

Fig. 2.32 Test setup

of the channel, were bolted to each channel after the pin was inserted through the entire assembly, including the column, to secure the specimen (see Fig. 2.34). Oversized holes for the pin and the four clamping bolts were drilled in each channel section to offset any alignment problems due to fabrication errors.

A minor problem with the pin connections did arise during testing of the first specimen, the prototype interior assembly. Slip of the top and bottom pins in the oversized holes was detected, as the specimen was loaded, up to a particular deflection level; thereafter, the pins seated and deflected very little. A correction determined from the measured displacements or the slip of the lower and upper columns in the pin connections was used to adjust the beam deflections.

For the other three specimens this problem was avoided by modifying the pin connection assembly. Two 1-in. stiffened steel plates were clamped on either side of the channels. High strength bolts, used to clamp the plates, were torqued in order to ensure perfect clamping at all load levels. The column was clamped in the loading direction by three bolts on either side coming from the steel plates. The clamping assembly at the top pin is shown in Fig. 2.35. This allowed the column to rotate at the pin but prevented its movement in the horizontal direction. Slip of the column was monitored throughout all the tests, and none was detected. The upper pin connection was modified in a similar manner.

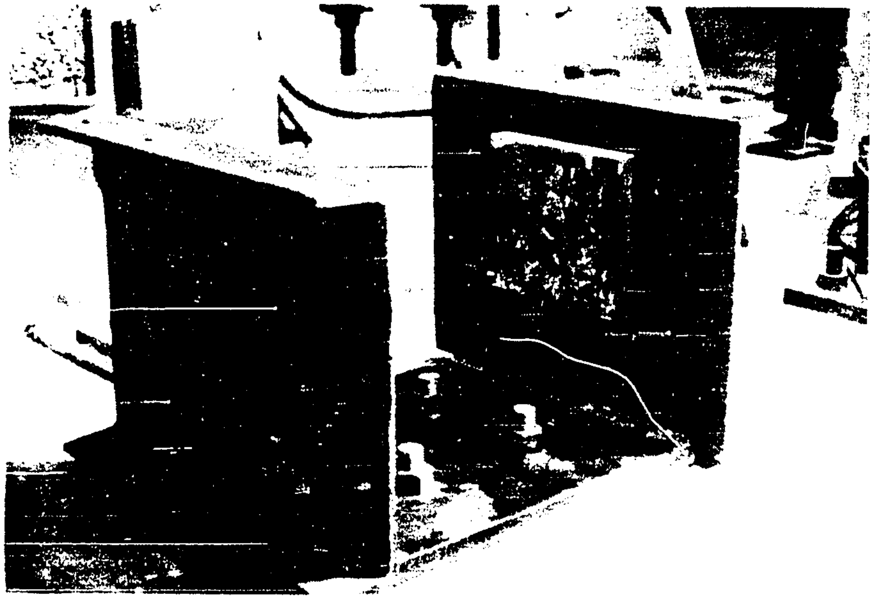

Fig. 2.33 Floor fixture

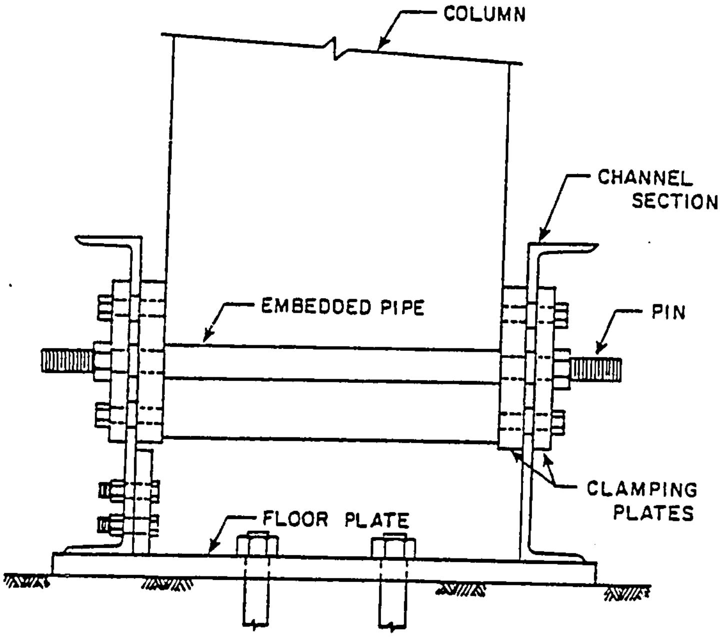
COLUMN
CHANNEL SECTION
EMBEDDED PIPE
PIN
CLAMPING PLATES
FLOOR PLATE

Fig. 2.34 Lower column pin connection detail

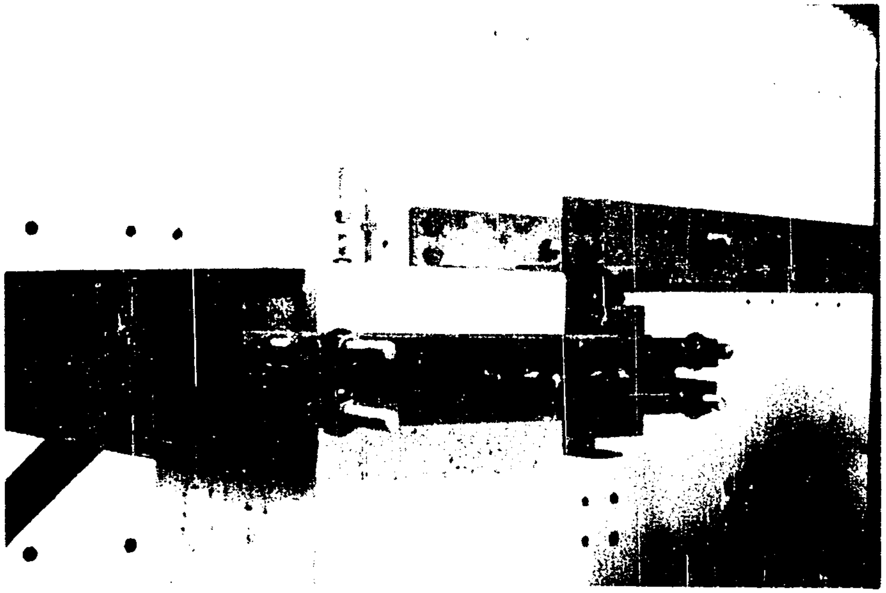

Fig. 2.35 Upper column clamping assembly

2.6.3 Loading System. Racking loads were applied to the longitudinal beams as illustrated in Fig. 2.36. Two double-rodded hydraulic rams, each with a capacity of 100 kips, were used to apply the loads. However, during the initial stages of testing of the first interior prototype specimen, a single hydraulic system was employed to apply the west and east end beam deflections. Due to an error in the hydraulic line connection, the specimen was tested under load control rather than deflection control, and the west and east beam end displacements differed. This problem was corrected for the subsequent testing.

2.7 Test Procedure

The specimens were subjected to predetermined displacement levels typical of the interstory drift levels imposed on the seven-story structure. No loads were applied directly at column ends. Horizontal reactions were induced by the restraint against motion. A series of cycles with increasing magnitude of deflection levels were applied. Between each deflection level, cycles to smaller deflection level were applied. The load history for the interior prototype differed in details from that of the other three specimens. The load history for the interior prototype is shown in Fig. 2.37. A typical load history for the other three specimens is illustrated in Fig. 2.38.

The east and west beam deflections and corresponding beam loads were continuously monitored with X-Y recorders and were used to

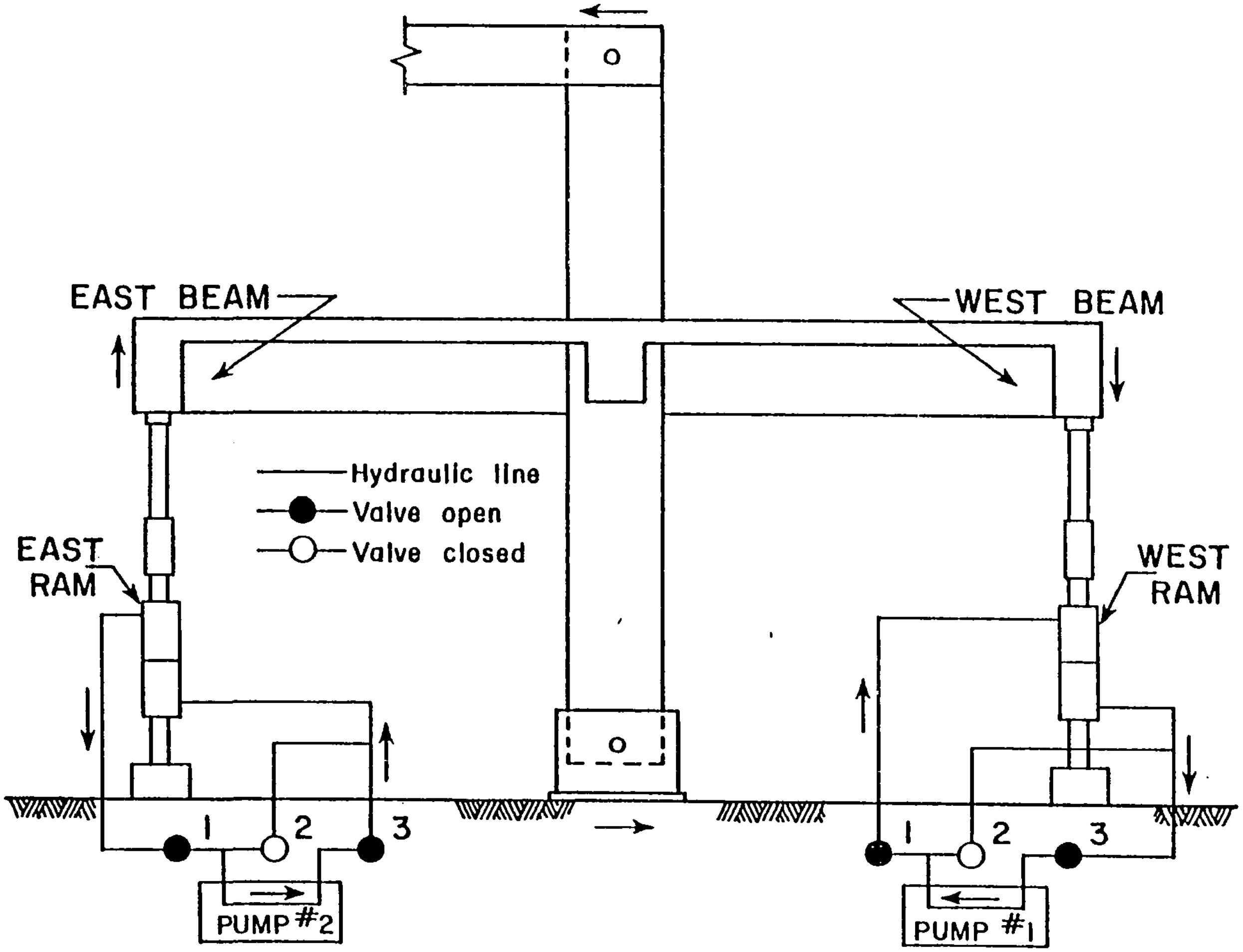
EAST BEAM
WEST BEAM
Hydraulic line
Valve open
Valve closed
EAST RAM
WEST RAM
1
2
3
1
2
3
PUMP #2
PUMP #1

Fig. 2.36 Hydraulic loading system

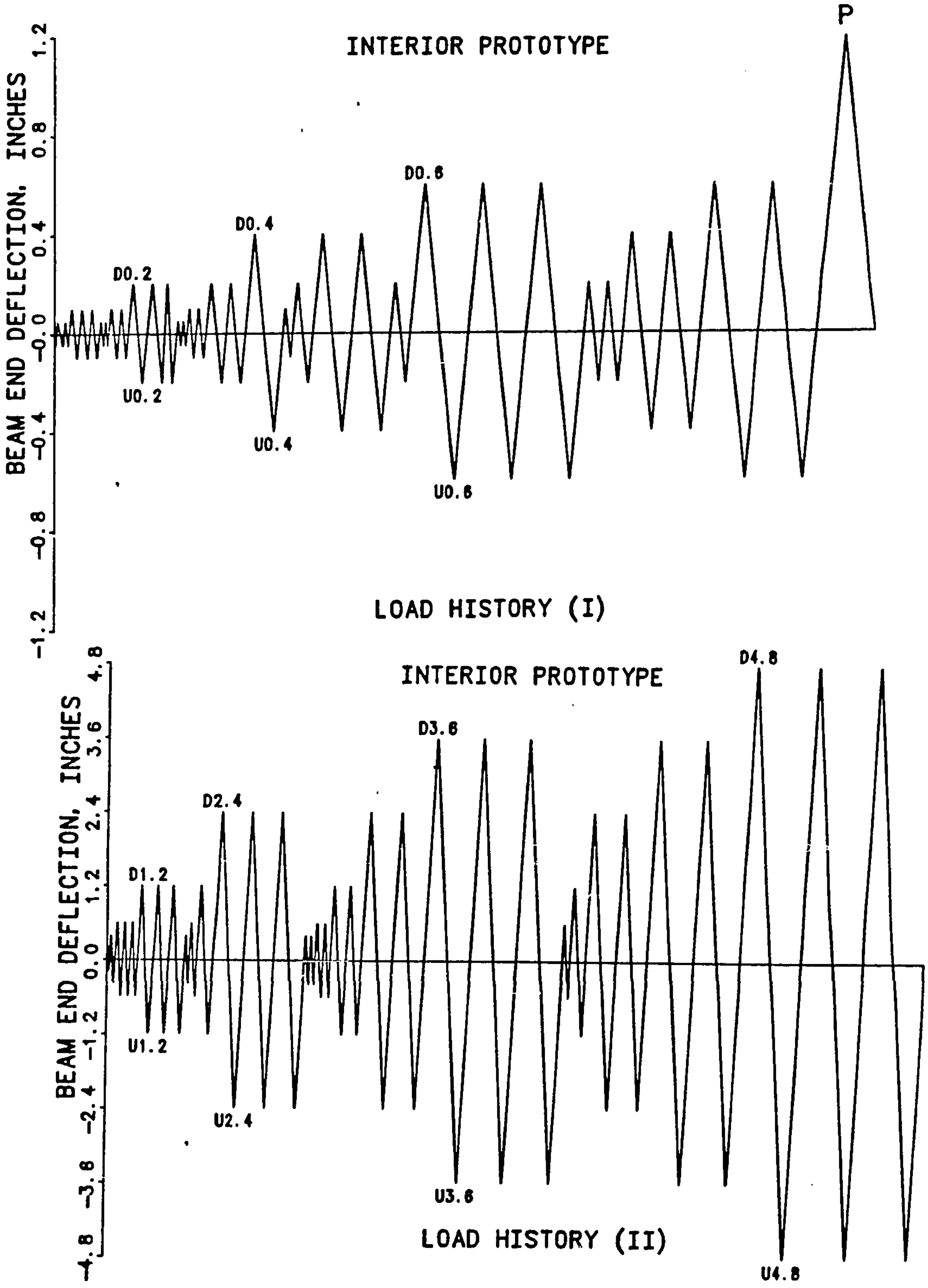

Fig. 2.37 Load history, interior prototype specimen

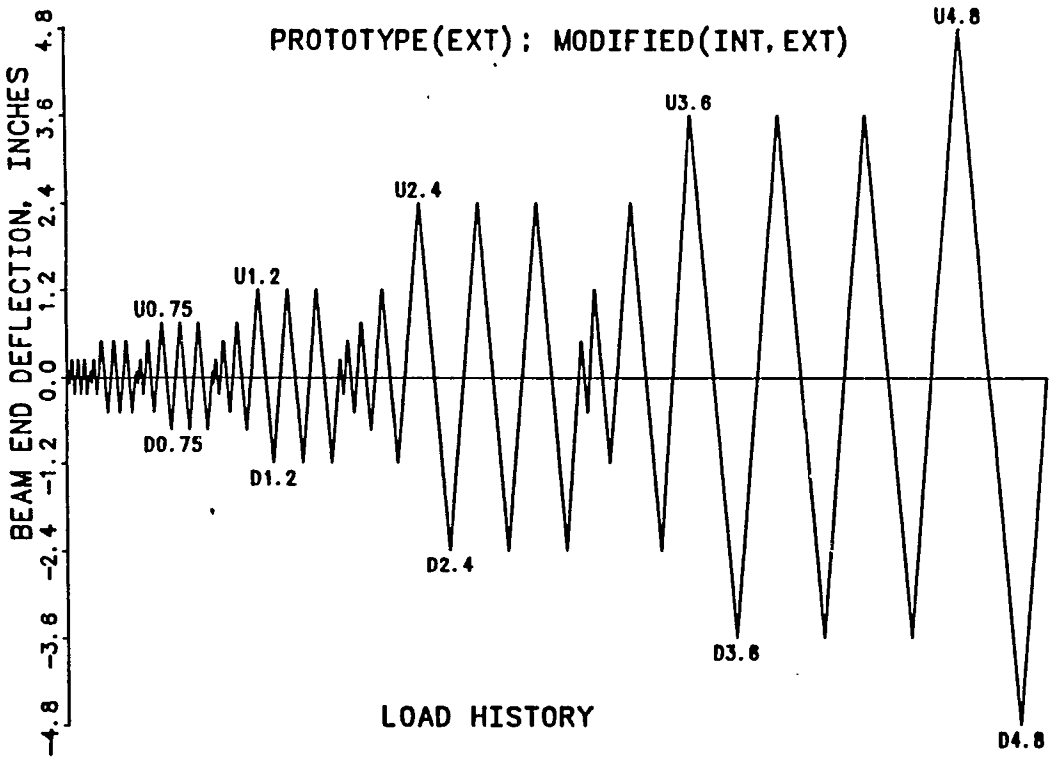

Fig. 2.38 Typical load history for test specimens

control the applied loads. The instrumentation was monitored at several stages within each cycle and at the peak of each cycle. All 125 data channels were scanned at each of the load stages.

2.8 Data Acquisition and Reduction

The test data were recorded on magnetic tape with a digital data acquisition system. A hard copy of the voltage readings was obtained on a line printer near the test setup. The magnetic tape was mounted on a mini-computer tape drive to store the data on a computer disk for future processing.

2.9 Material Strengths

2.9.1 Concrete. The concrete mix design was proportioned according to standard ACI procedures with an adjustment made for the high strength characteristics of Texas cements. The design strength of 4000 psi and a 1-in. maximum aggregate size was specified as in the full-scale structure. Standard 6- x 12-in. cylinders were cast during each operation. The average cylinder strengths at testing are given in Table 2.1. The small difference between the concrete strengths in the lower column and slab, and in the upper column, was not considered a problem, because all of the instrumentation was located within the first cast. Relatively small forces were imposed on the upper column.

2.9.2 Steel Reinforcement. ASTM A615, Gr. 60 reinforcement was used in all four specimens. Since the reinforcing bars were ordered in two batches, their yield strengths differed for the

TABLE 2.1 Average Concrete Strength (in psi)

Specimen	First Cast Lower Column psi	Second Cast Upper Column psi
Interior Prototype	4860	3430
Exterior Prototype	4690	2340
Interior Modified	3950	4940
Exterior Modified	4850	5010

prototype and modified specimens. The average yield strength for the steel used is given in Table 2.2.

2.10 Member Strengths

To understand the behavior of the joint assemblies, the response of the individual members was calculated. The force-deformation curves for flexural response of the longitudinal beam, torsional response of the transverse beam, and moment-axial force interaction diagram for the column were determined using the actual material strengths. The theoretical response characteristics of the individual members provided some insight into the role and interaction of members in the structure and in the assembly tests.

2.10.1 Column Strength. The moment-axial force interaction curves for the columns of the four specimens are shown in Fig. 2.39. The curves were obtained using a program which considers the effects of concrete confinement and strain hardening of steel. Kent and Park stress-strain characteristics for confined concrete were assumed. The interaction curves for the interior and exterior prototype specimen are similar (same steel strength, similar concrete strength). The large difference in the concrete strength between the two modified specimens affects the interaction curves. However, under zero axial load, the capacity of the interior and exterior modified specimens is nearly the same.

2.10.2 Beam Flexural Strength. The moment-curvature relationships were computed for the longitudinal beam using the same

TABLE 2.2 Average Yield Strength of Steel

Location	Bar Size	Yield Strength ksi
Prototype Specimens		
Longitudinal Column Bars	#7 (22.2 mm)	79
Longitudinal Beam Bars	#6 (19.1 mm)	61
Longitudinal Slab Bars	#3 (9.5 mm)	58
Transverse Steel	#3 (9.5 mm)	60
Modified Specimens		
Longitudinal Column Bars	#8 (25.4 mm)	72
Longitudinal Beam Bars	#7 (22.2 mm)	75
Longitudinal Slab Bars	#3 (9.5 mm)	75
Transverse Steel	#3 (9.5 mm)	67

computer program. The flexural capacities were dependent on the assumed effective slab width acting as a flange in the analysis of the T-section. Estimates of the flexural strength were made using only beam rectangular section, the ACI effective width of 59 in. (in compliance with ACI 318-77 Section 8.10.2), and the full slab width of 157.5 in. as the effective flange of the T-section. The flexural capacities are listed in Table 2.3.

The assumed effective slab width had only a small effect on calculated positive moment flexural capacity (slab in compression and bottom steel in tension), which was controlled by area and strength of the bottom longitudinal beam steel. For negative moment (slab in tension), however, the area of the tension steel increased with the assumed effective flange width due to the addition of slab steel in the tension zone. This resulted in a wide range of moment capacities depending on the assumed effective width. The concrete strength did not significantly affect computed flexural behavior, and hence only the representative moment-curvature relationships for the prototype and the modified specimen are given in Figs. 2.40 and 2.41, respectively.

2.10.3 Beam Torsional Strength. Torque-twist relationships, for the transverse beam, shown in Fig. 2.42, were computed using the diagonal compression field theory [11]. In this approach, only the post-cracking response of a reinforced concrete section is determined. Elastic analysis was used to compute the cracking torque and twist. These computations did not consider any contribution from

TABLE 2.3 Flexural Capacity

	M_{yield}, k-in.			M_{ult}, k-in.		
	Beam Only	ACI	Full	Beam Only	ACI	Full
Slab in Tension						
Int Prot[a]	1200	2000	4200	1635	2485	4380
Ext Prot[b]	1195	2000	4150	1615	2460	4320
Int Mod[c]	3200	4120	6040	3535	4380	6490
Ext Mod[d]	3245	4150	6720	3625	4515	6765
Slab in Compression						
Int Prot	850	910	975	1200	1810	2220
Ext Prot	855	915	975	1195	1805	2215
Int Mod	2080	2245	2360	2405	3335	4025
Ext Mod	2100	2260	2380	2465	3480	4100

[a] Interior Prototype
[b] Exterior Prototype
[c] Interior Modified
[d] Exterior Modified

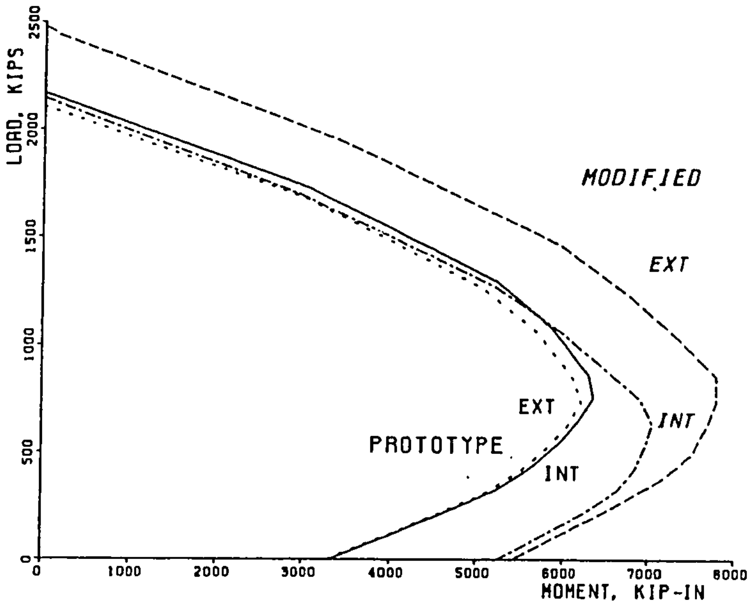

Fig. 2.39 Moment-axial force interaction diagrams for columns

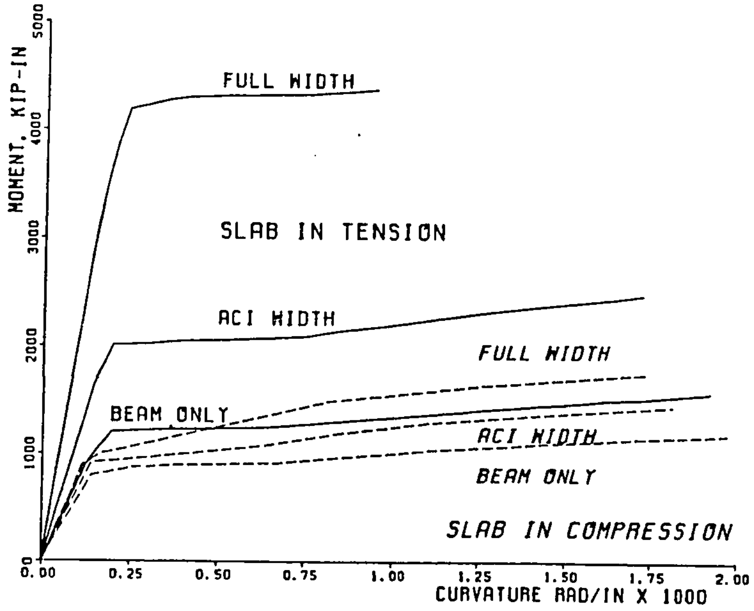

Fig. 2.40 Moment-curvature relationships for longitudinal beam, prototype specimens

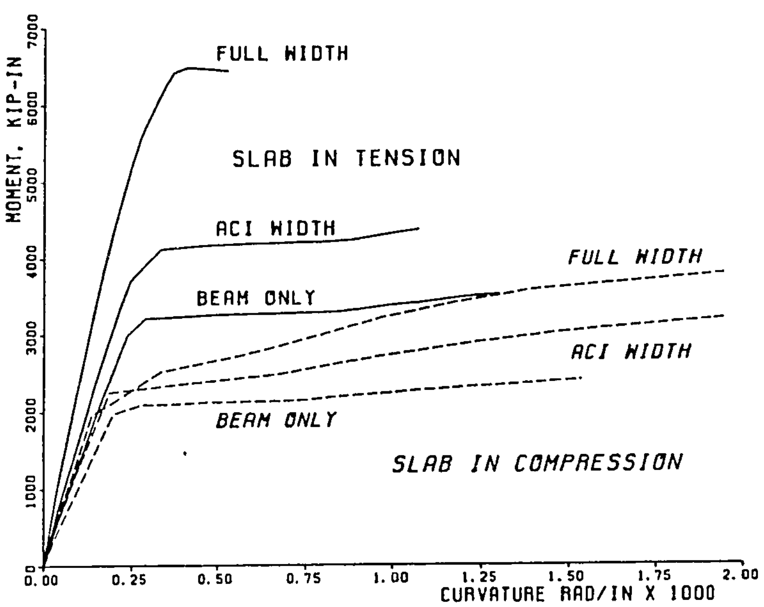

Fig. 2.41 Moment-curvature relationships for longitudinal beam, modified specimens

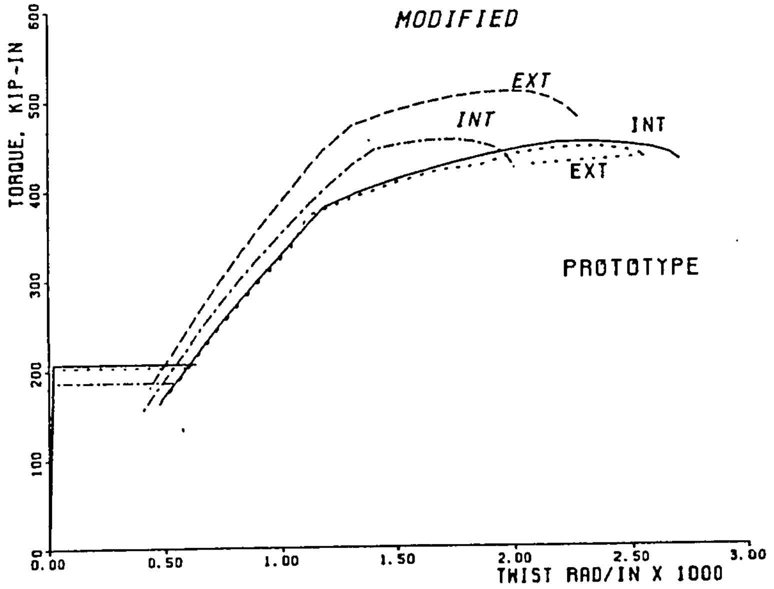

Fig. 2.42 Torque-twist relationships for transverse beams

the slab. The torsional capacities at cracking, yielding of transverse reinforcement, and ultimate are given in Table 2.4.

To facilitate testing it was decided to impose no axial load on the columns. The ratio of nominal column-to-beam flexural capacities, a critical design consideration in seismic zones, was between 2.36 and 1.01 for the prototype interior and between 1.77 and 1.00 for the modified interior. The ratios are much larger, and hence less critical, for the exterior joints. The range of values results from the assumptions made for the width of the slab acting as a flange. Most codes [1,2,9,13] require that the sum of the moment strengths of the column exceed the sum of the moment strengths of the beam. A ratio of column-to-beam ultimate moment capacities greater than unity is required to prevent column hinging and to ensure beam hinging. In seismic-resistant structures, such a behavior is ideal for energy dissipation and prevention of a column sidesway mechanism. Underestimating the effectiveness of the slab would result in overestimating (unconservative) the available ratios of column-to-beam moment capacities. These ratios were computed using the actual material properties. Using nominal material strengths, the values available at design stage, the ratios could be different depending on the difference between the assumed and actual material strengths, especially steel strengths.

TABLE 2.4 Predicted Torsional Capacities

	Prototype: T, in.-k		Modified: T, in.-k	
	Interior	Exterior	Interior	Exterior
Cracking	205	205	205	185
Yielding of stirrips	380	375	430	460
Ultimate	450	450	455	510

CHAPTER III

TEST RESULTS AND BEHAVIOR

3.1 Introduction

Results and observations from the tests on the four specimens are presented and discussed. The specimens were instrumented with strain gages and deformation transducers. Photographs were taken before, during, and after the tests to document the crack patterns and the general behavior of the specimens.

In this chapter, the overall behavior of the specimens will be discussed. Specific attention will be given to load versus deflection behavior, crack patterns, joint shear and anchorage performance. A critical discussion of the influence of the slab on the strength of the floor system and on the joint response will be provided in Chapter IV.

3.2 Load History

Each of the beam-column joint assemblages was subjected to uniaxial, reversed cyclic loads. The selected load histories, deflections applied at the longitudinal beam ends, represented equivalent interstory drifts measured at the second level of the seven-story structure [12]. It was not feasible to duplicate the loading sequence used in the seven-story structure tests. Load histories for the seven-story structure were based on recorded earthquake motions modified to excite primarily a first-mode response of the structure. A displacement record based on ground motion would be difficult to reproduce in component tests. Therefore, selected peak deflection levels, which increased as testing continued, were used. All the specimens were tested to failure. A deflection level of about 1.2 in. at the beam ends to correspond to the maximum deflection level achieved during PSD4 was estimated in the seven-story structure tests based on its overall drift. (PSD4 is the pseudodynamic test performed on the seven-story structure. The pseudodynamic test was actually what is commonly known as the quasi-static test. In this test, the largest lateral displacements were applied to the seven-story structure.) A maximum beam end deflection of 4.8 in., about four times the maximum deflection level in PSD4, was imposed on each of the four specimens. This would correspond to a lateral drift of 5 percent; a very high lateral drift for real structures.

The applied load histories for the specimens were discussed in Chapter II (Figs. 2.37 and 2.38). A number of small deflection level cycles were applied prior to applying a higher peak deflection. At each peak deflection level the specimen was subjected to three full cycles. For the sake of clarity, only the first cycles at each deflection level are plotted and discussed. The first cycles at each higher deflection level are representative of the performance of the specimens.

3.2.1 Load Stage Nomenclature. The critical load stages in the load history are identified by the descriptive symbols shown in Figs. 2.37 and 2.38. The prefix letters D and U indicate the direction downward and upward, respectively, of the displacement of the west end of the longitudinal beam. The magnitude of the displacement in inches is shown by the number following the letter. For example, D1.2 indicates the load stage at which the west end of the longitudinal beam was displaced 1.2 in. downward for the first time in the loading sequence. At load stage U2.4, an upward displacement of 2.4 in. was imposed on the west end of the longitudinal beam for the first time in the loading sequence.

3.3 Interior Prototype

The interior prototype was the first specimen tested. As equal deflections were applied at the ends of the east and the west beam, the behavior of the west portion of the specimen for downward west end deflection was nearly the same as the behavior of the east portion of the specimen when downward east end deflection was applied. Hence, only the behavior of the west portion of the specimen is discussed for the interior joint specimens.

Two minor problems developed during the testing of this specimen. During pilot testing of the specimen, slip, or horizontal movement, of the top and bottom pins in the reaction assembly was detected as the specimen was loaded. The slip nearly stopped when the pins became seated. The slip gradually increased at higher load levels due to the bending of the pin. The movement of the column at the pins was monitored by potentiometers and a correction as calculated in Fig. 3.1 was applied to the deflections. A more sophisticated connection was employed in testing the other three specimens (discussed in Section 2.6.2) and the slip problem was not encountered.

The other problem was regarding the loading system. An improper connection of the hydraulic lines resulted in application of equal loads, rather than the desired equal deflections, at either end of the longitudinal beam. The problem was discovered at load stage P shown in Fig. 2.37, and the specimen was unloaded immediately. The test was then continued with proper loading connections. A substantially large upward displacement of 2.4 in., instead of 1.2 in., was inadvertently applied to the east beam due to this problem. The damage appeared to be minimal and was confined to the tension zone of the east beam. The damage to the specimen was not extensive and was not considered to significantly affect further test results.

The west beam load versus beam end deflection response for the first peak cycles of the interior prototype specimen is shown in Fig. 3.2. The response of the specimen was generally elastic up to a deflection level of 0.2 in., when a few short flexural cracks were observed.

Well-defined flexural cracking of the longitudinal beam was observed at U0.4. Two cracks, extending about 7-8 in. into the beam were located at approximately 6 in. and 20 in. from the column face. The initial flexural cracking in the top of the slab occurred at the

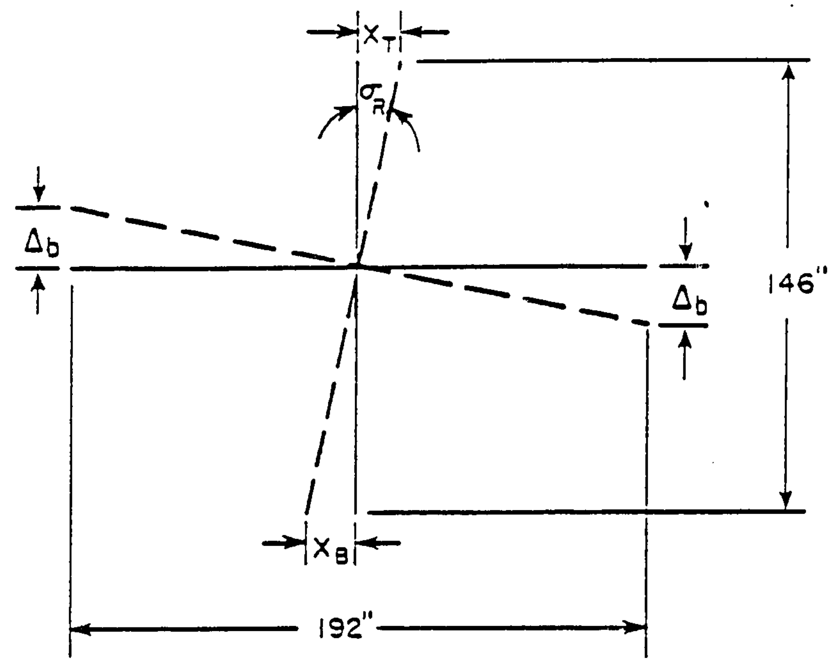

X_T
σ_R
Δ_b
Δ_b
146"
X_B
192"

X_T = measured slip at top, in.
X_B = measured slip at bottom, in.
σ_R = angle of rigid body rotation, rad.
Δ_b = correction for beam deflection, in.

$$\sigma_R = \frac{X_T + X_B}{146}$$

$$\Delta_b = \frac{X_T + X_B}{146}(96) = 0.658(X_T + X_B)$$

Fig. 3.1 Slip correction

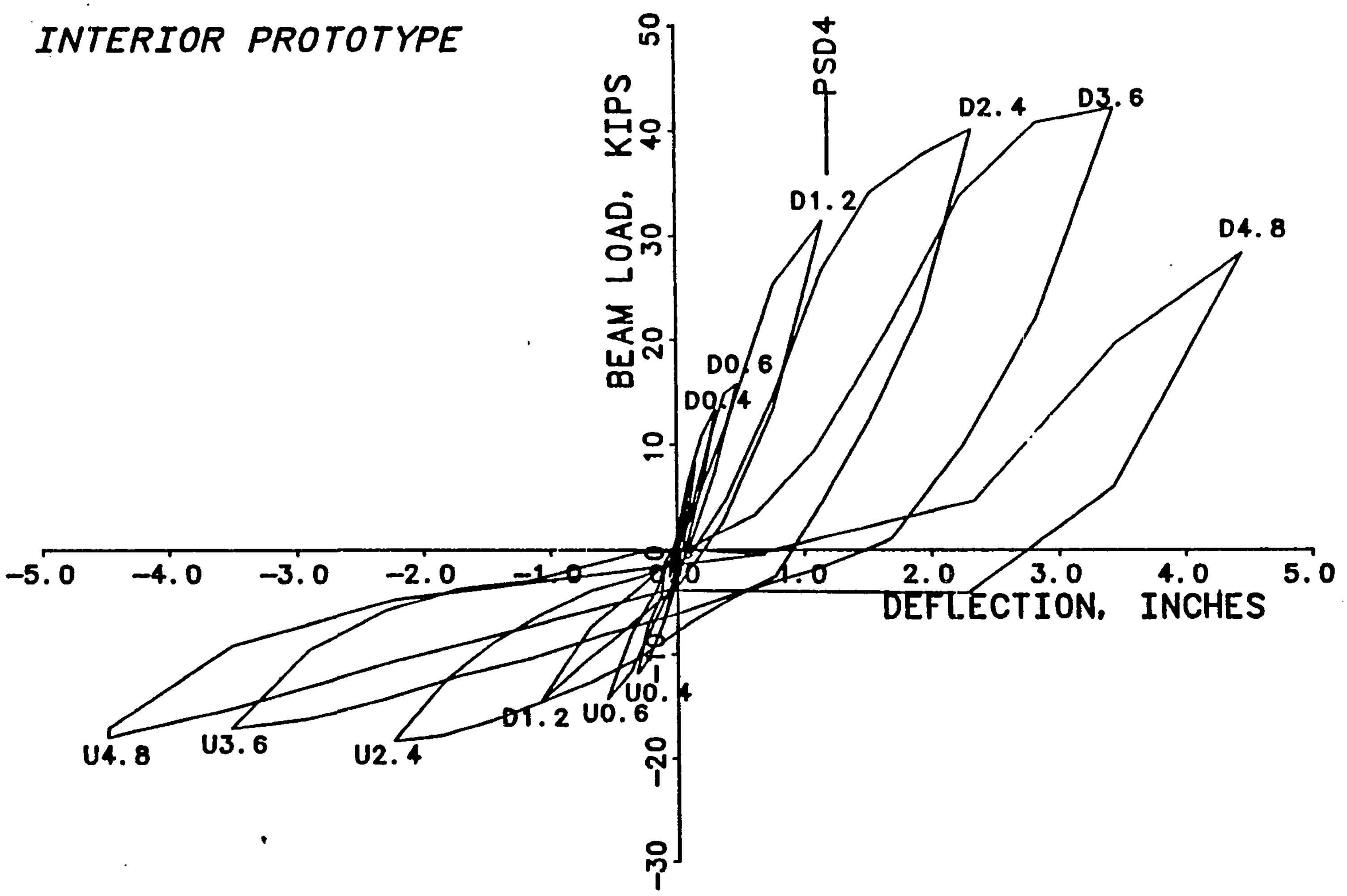

Fig. 3.2 Load versus deflection, interior prototype specimen

column face and extended about 20-25 in. from the longitudinal beam at load stage D0.4. The initial flexural cracking led to a small loss of stiffness and formation of a small hysteresis loop in the load-deflection curve, as can be seen in Fig. 3.2.

Flexural cracks extended and additional cracks formed at a deflection of 0.6 in. At D0.6, a new crack formed on the top surface of the slab, about 15 in. from the column face and extended nearly the full width of the slab (see Fig. 3.3). Previously formed cracks on the top surface of the slab at the column face propagated to the edge of the slab. Under negative moment, flexural cracking penetrated to the bottom surface of the slab. Two cracks 10-15 in. from the column face parallel to the transverse beam, extending about 24-30 in. on either side of the longitudinal beam were noted at D0.6 (see Fig. 3.4). New flexural cracks were formed at U0.6 in the longitudinal beam. A small reduction in the stiffness of the specimen at 0.6-in. deflection can be seen in Fig. 3.2.

Initial torsional cracking in the transverse beam was observed at load stage D1.2, in the form of two parallel cracks inclined at about 30° to the horizontal and within a distance of about 10 in. from the column (see Fig. 3.5). The resulting loss of torsional stiffness of the transverse beam can be seen in Fig. 3.6. Cracks were also detected on the top of the transverse beam near the column face.

A new crack about 35-40 in. from the column face was formed at the top surface of the slab. This crack extended parallel to the

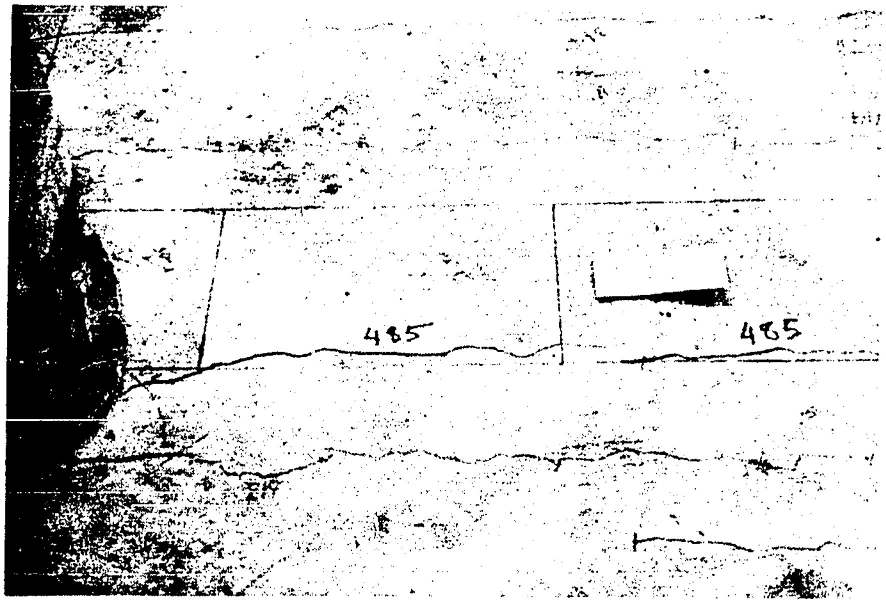

Fig. 3.3 Top slab at D0.6, interior prototype

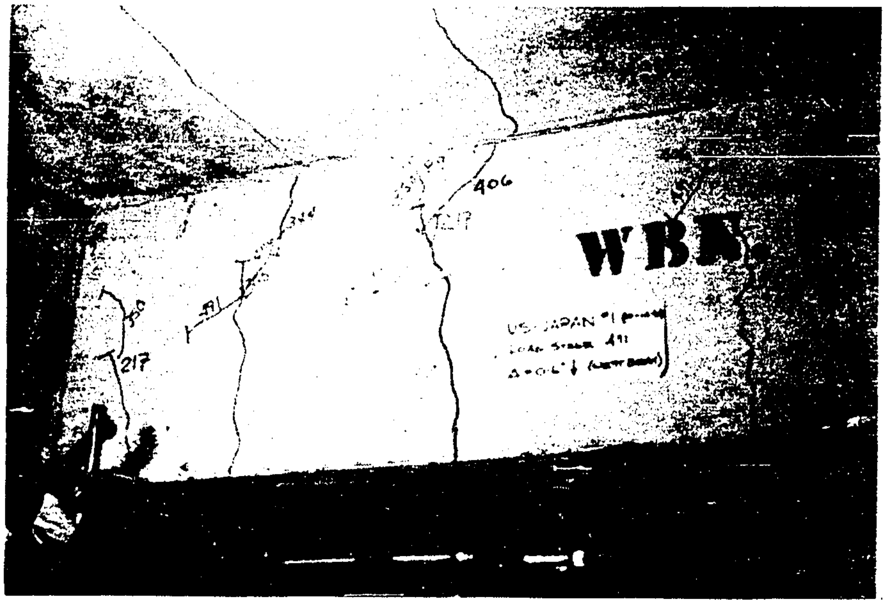
406
217
217
US-JAPAN #1
LOAD STAGE 411

Fig. 3.4 Bottom of slab and longitudinal beam at D0.6, interior prototype

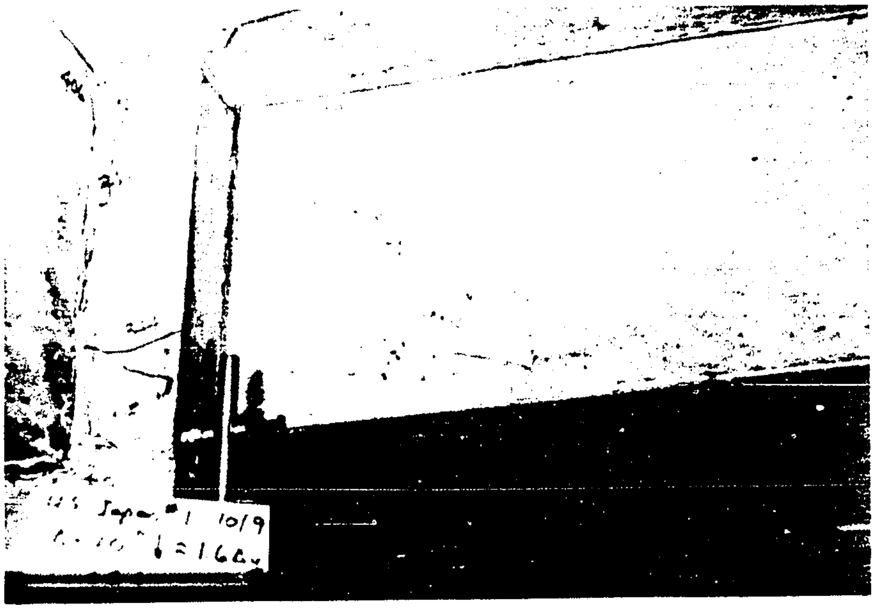

Fig. 3.5 Torsional cracks in transverse beam, interior prototype

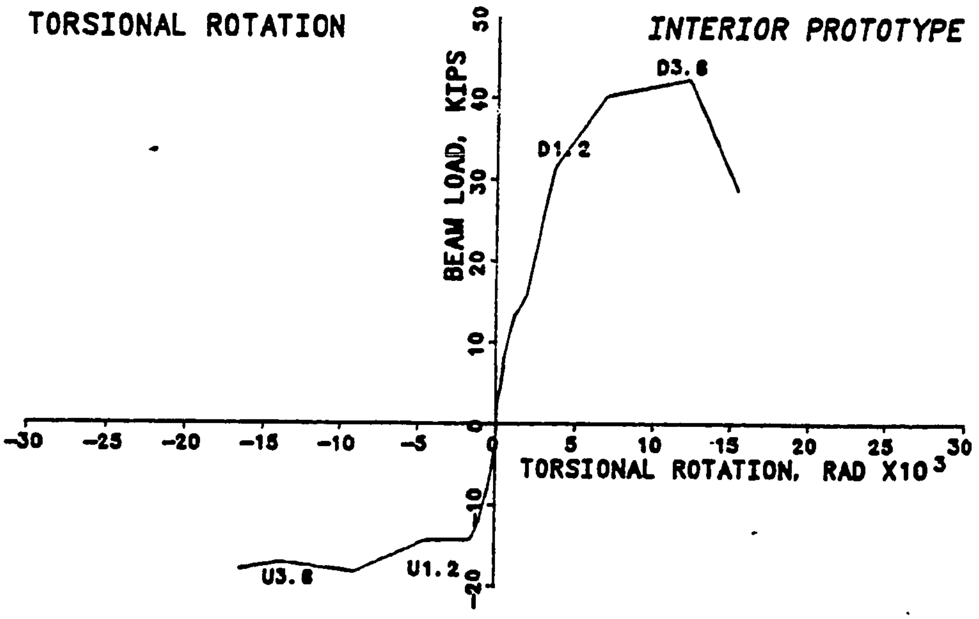

Fig. 3.6 Beam load versus torsional rotation, interior prototype

transverse beam near the longitudinal beam, as the crack extended towards the edge of the slab it turned diagonally towards the load point. This semicircular crack pattern around the load point was observed in all the tests (see Fig. 3.7). A similar semicircular crack was also formed at the bottom surface of the slab at the same load stage. These punching shear-type cracks resulted from the transfer of high shear from the loading point into the slab.

The flexural cracks on the bottom surface of the slab near the column are shown in Fig. 3.8. The top longitudinal beam steel yielded at D1.2. This resulted in a pronounced break in the load-deflection curve. Widening and propagation of flexural cracks in the longitudinal beam was observed at U1.2. At load stage U1.2 yielding of the bottom beam steel was noted. The load-deflection curve from D1.2 to U1.2 shows a considerable loss of stiffness after passing through zero load. This is likely due to the fact that cracks which opened at D1.2 were not fully closed when U1.2 was reached. The bottom steel was unable to develop sufficient tension to yield the steel in compression and to close the cracks.

Vertical cracks, located about 24 in. from the column face and extending the full depth of the transverse beam were formed on the west face at load stage D2.4 (see Fig. 3.9). Similar vertical cracks were observed in the transverse beams of all four specimens. Since such cracks were not noticed in the seven-story structure, there is a reason to believe that the cracks may have been formed in the test specimens due to the specific displacement constraints and

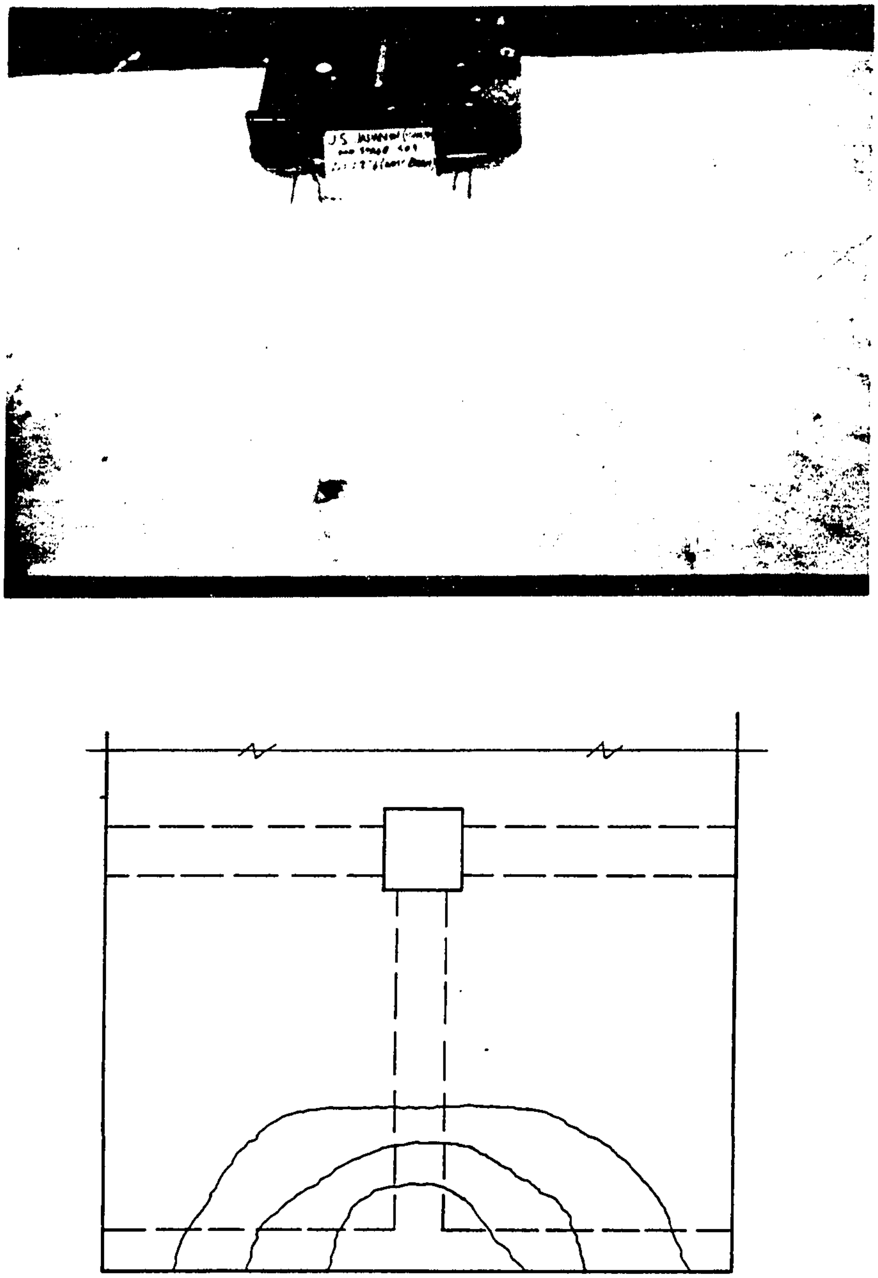

Top of the Slab

Cracking around the Load Point

Fig. 3.7 Cracks around the load point

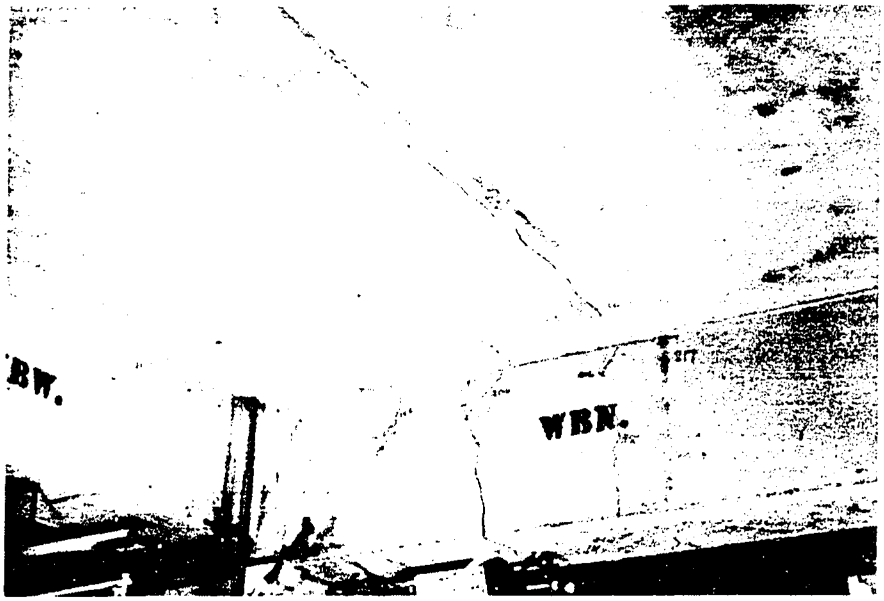

Fig. 3.8 Bottom of slab at D1.2, interior prototype

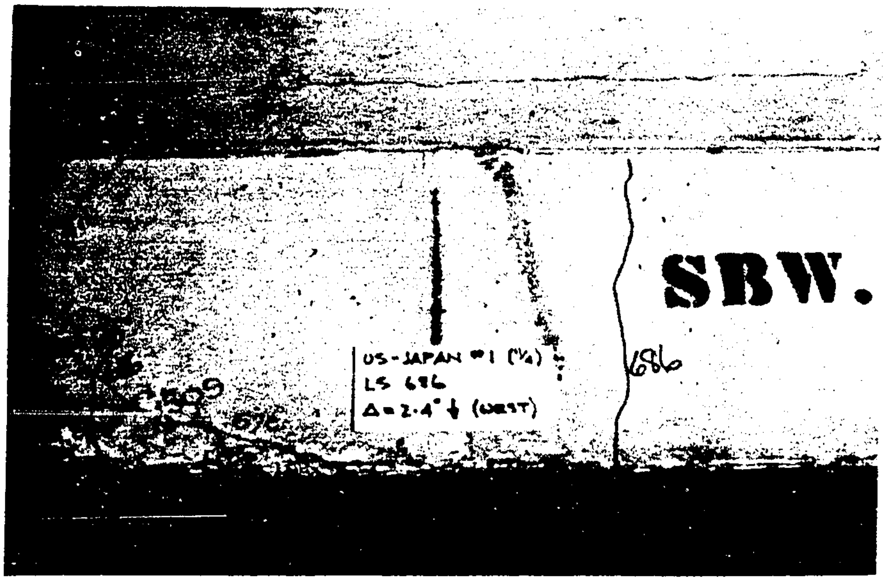
SBW.
686
US-JAPAN #1 (¼)
LS 686
Δ=2.4" ↓ (WEST)
676

Fig. 3.9 Vertical cracks in transverse beam at D2.4, interior prototype

the loading scheme. The downward deflection of the west beam results in a horizontal force being applied to the transverse beam along its length. This horizontal force is introduced into the transverse beam through the longitudinal beam and the slab. The stiffer, uncracked edges of the slab offer considerable resistance to the horizontal movement of the transverse beam, whereas severely cracked portion of the slab near the joint offers very little resistance to horizontal movement. This differential resistance along the length results in flexural bending of the transverse beam in the horizontal plane, convex towards the west, producing tension and subsequently cracking on the west face.

Severe torsional distress was observed in the transverse beam at load stage D2.4. This resulted in large torsional rotations of the transverse beam (see Fig. 3.6). No new major cracks formed in the slab, but the existing cracks widened. A view of the top of the slab at load stage D2.4 is shown in Fig. 3.10. Shear cracks formed as continuations of the bottom slab cracks and penetrated nearly 2/3 the depth of the longitudinal beam (see Fig. 3.11). Shear cracking produced pinching of the load-deflection hysteresis loop. Crushing and spalling of concrete occurred in the longitudinal beam near the column face. At load stage U2.4 a wide separation was observed between longitudinal beam and the column. Peak beam end load of 18.4 kips was recorded at U2.4 under positive bending (slab in compression).

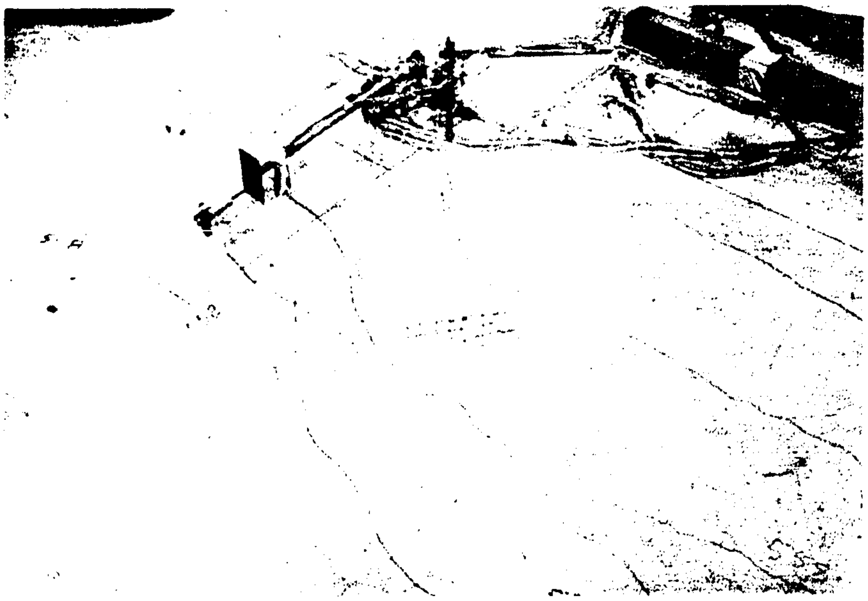

Fig. 3.10 Top of slab at D2.4, interior prototype

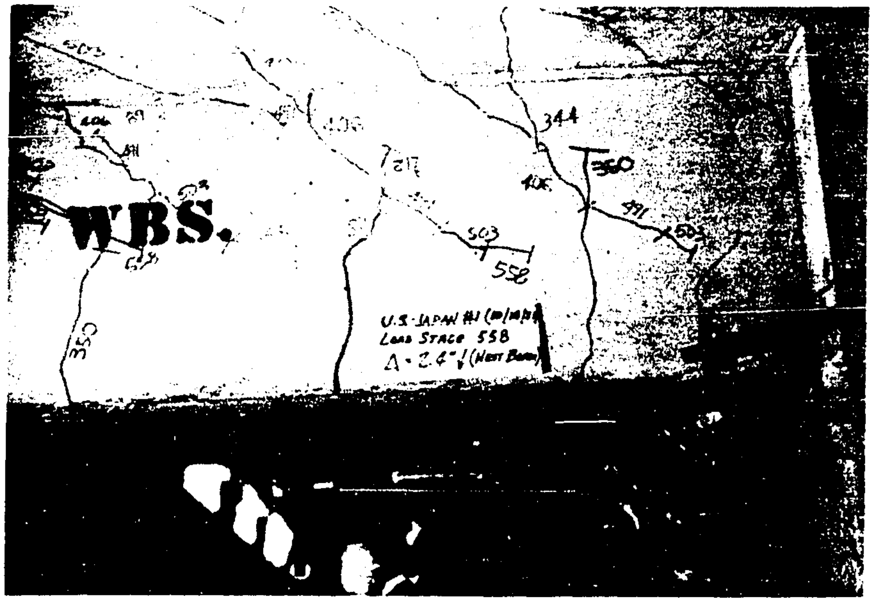
WBS.
344
360
406
503
558
350
U.S.-JAPAN #1
LOAD STAGE 558
Δ = 2.4" (WEST BEAM)

Fig. 3.11 Longitudinal beam at D2.4, interior prototype

Deflections of 3.6 in. produced little new cracking, except for additional torsional cracks near the column in the transverse beam. The previous cracks widened and extended. Crushing and spalling of concrete in the column corner between the beams and on the bottom face of the longitudinal beam was observed. Figure 3.12 shows the joint region at the end of the test. A peak beam end load of 42.2 kips was recorded at load stage D3.6 (slab in tension). In the cycle from U2.4 to D3.6, pinching near the origin of the load-deflection curve can be seen. The loss of stiffness is due to the extensive cracking and yielding of beams at deflections of 2.4 in.

Higher deflection levels caused losses in negative moment capacity, probably due to loss of bond of tensile reinforcement due to cycling. Flexural hinges were formed in the west and the east longitudinal beam as evidenced by the flexural cracking in the beam and the slab and the yielding of the longitudinal reinforcement in both the beams and the slab. The controlling failure mechanism was thus the flexural hinging of the longitudinal beams.

3.4 Exterior Prototype

The beam end load versus the beam end deflection response for the exterior prototype specimen is shown in Fig. 3.13. The behavior of the specimen was elastic up to a deflection level of 0.1 in. and no cracking was observed.

The first flexural cracks in the longitudinal beam were observed at U0.25. These vertical flexural cracks extended nearly 3/4

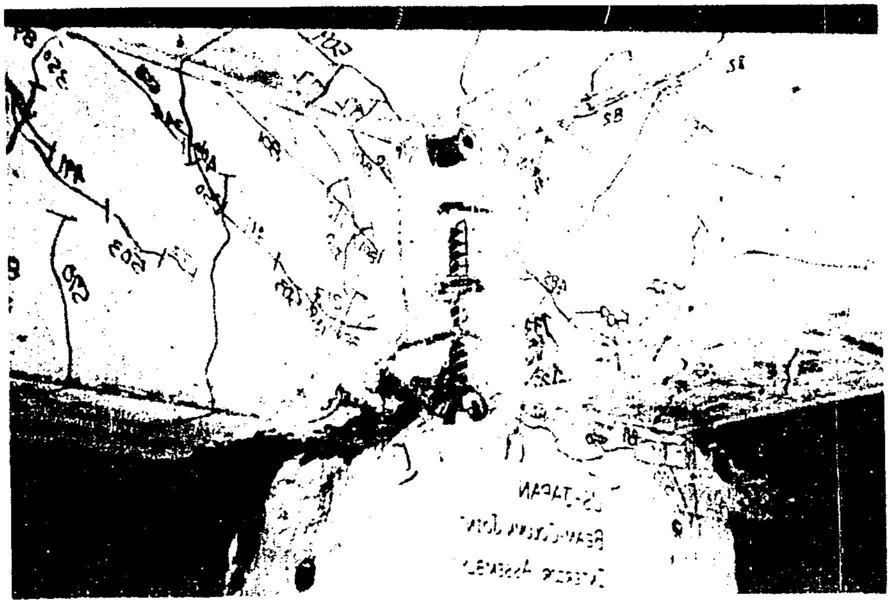

Fig. 3.12 Joint area at end of test, interior prototype

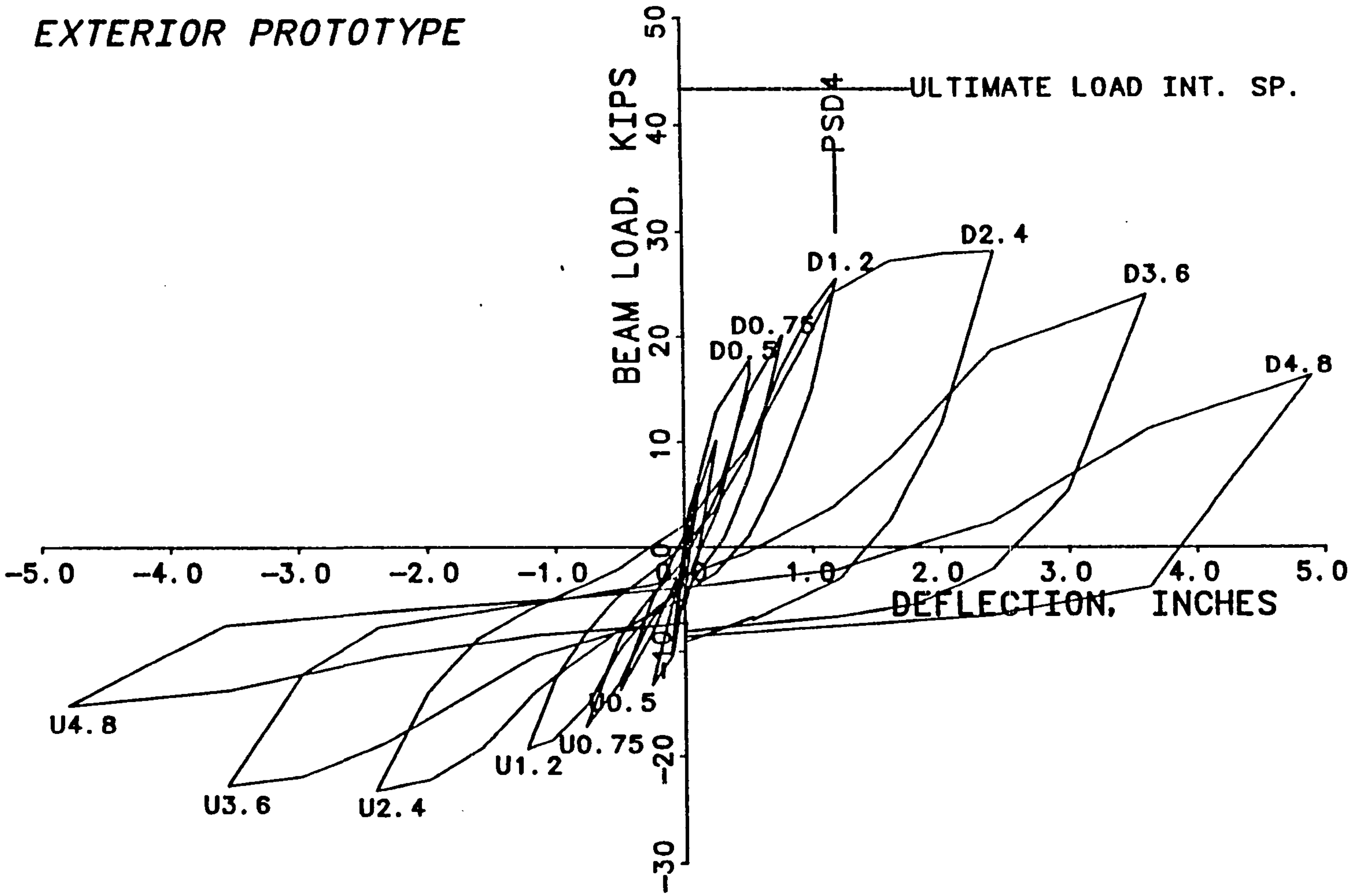

Fig. 3.13 Load versus deflection, exterior prototype

of the depth of the beam from the bottom towards the slab. A downward deflection of 0.25 in. in the west beam produced initial cracking in the transverse beam and in the slab. Slab flexural cracking extended about 50-60 in. on either side of the longitudinal beam and parallel to the transverse beam. A crack at the same location but on the bottom surface of the slab also appeared at this load stage. This crack, however, extended only about 25-30 in. on either side of the longitudinal beam The first torsional cracks were formed on the east face of the transverse beam very close to the column face. This cracking did not significantly change the stiffness of the specimen but some non-linearity was observed (see Fig. 3.13).

At the next peak cycle of 0.5 in. beam end deflection level, considerable cracking was observed. New flexural cracks appeared on the longitudinal beam. Several flexural cracks appeared on the top of the slab at D0.5 (Fig. 3.14), and extended nearly the full width of the slab. A diagonal crack was detected at the top of the slab starting at the column edge and extending away from the longitudinal beam (see Fig. 3.14). The bottom of the slab also showed new cracks which extended into the longitudinal beam as diagonal cracks inclined towards the column. Flexural cracking of the beam and the slab led to a significant reduction in stiffness (widening of the hysteresis loop), as shown in Fig. 3.13.

At load stage D0.75 torsional cracking of the transverse beam was observed (Fig. 3.15). Diagonal cracks appeared on the east face

Fig. 3.14 Top of slab at D0.5, exterior prototype

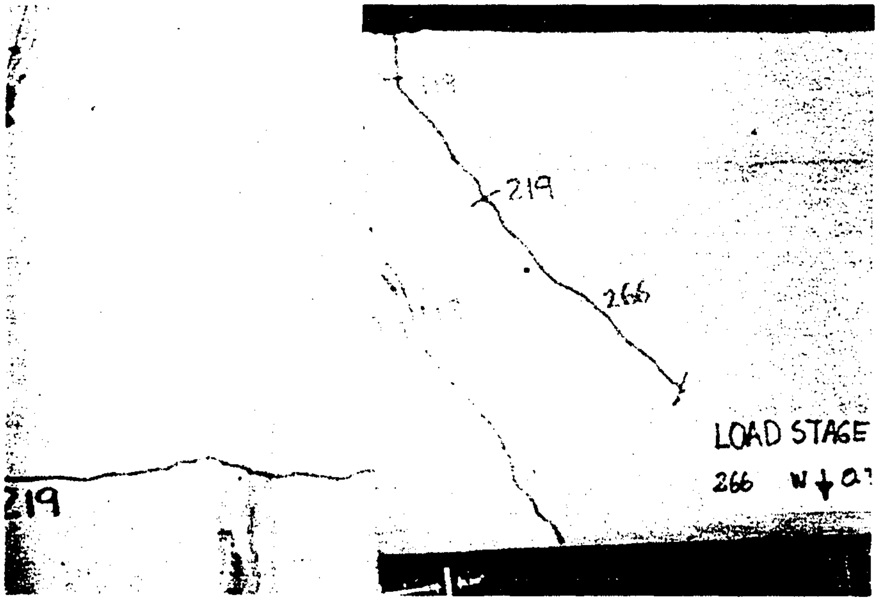
219
266
LOAD STAGE
266
219

Fig. 3.15 Torsional cracks in transverse beam at D0.75, exterior prototype

of the transverse beam about 8-10 in. from the column. These diagonal cracks were at an angle of about 30^o with the vertical. At this deflection level, vertical cracks were observed on the west face of the transverse beam, about 10-15 in. on either side of the column, extending through the full depth of the beam, (see Fig. 3.18, which shows the cracks at a later stage). This cracking of the transverse beam resulted in a reduction in stiffness of the transverse beam, seen on the load versus torsional rotation curve (Fig. 3.16). No significant new cracks were formed in the slab but the previous cracks widened. A marked stiffness deterioration was observed in the load-versus-deflection curve. The load-deflection curve also showed slight pinching of the for the first time.

Longitudinal beam bars yielded at a deflection level of about 1.2 in. The crack pattern in the longitudinal beam at U1.2 is shown in Fig. 3.17. Not all of the top longitudinal beam bars yielded at this stage. Some slip of the beam bars was detected. Although there was no new major cracking of the slab at D1.2, the existing cracks extended and widened. This led to the loss of stiffness indicated in the load-deflection curve. Torsional cracking on the transverse beam was observed as seen in Fig. 3.18.

Some hysteresis, with pinching near the origin, characterized the load-displacement curves at a deflection level of 1.2 in. The specimen reached a peak load of 28.1 kips at this deflection level under negative moment and 23.3 kips under positive moment. Anchorage controlled the response of this specimen. The ultimate negative

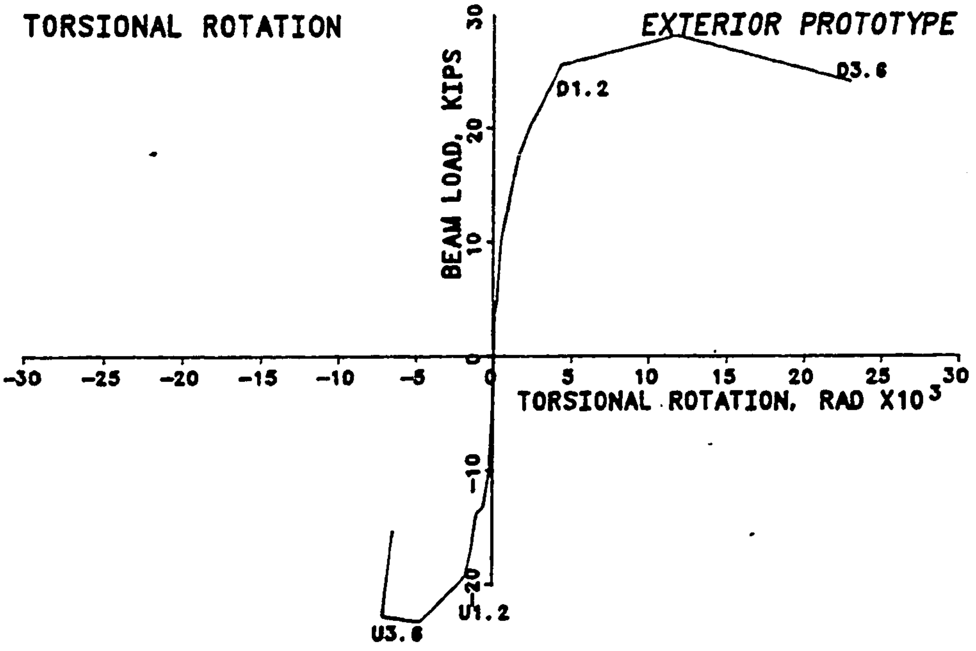

Fig. 3.16 Beam load versus torsional rotation, exterior prototype

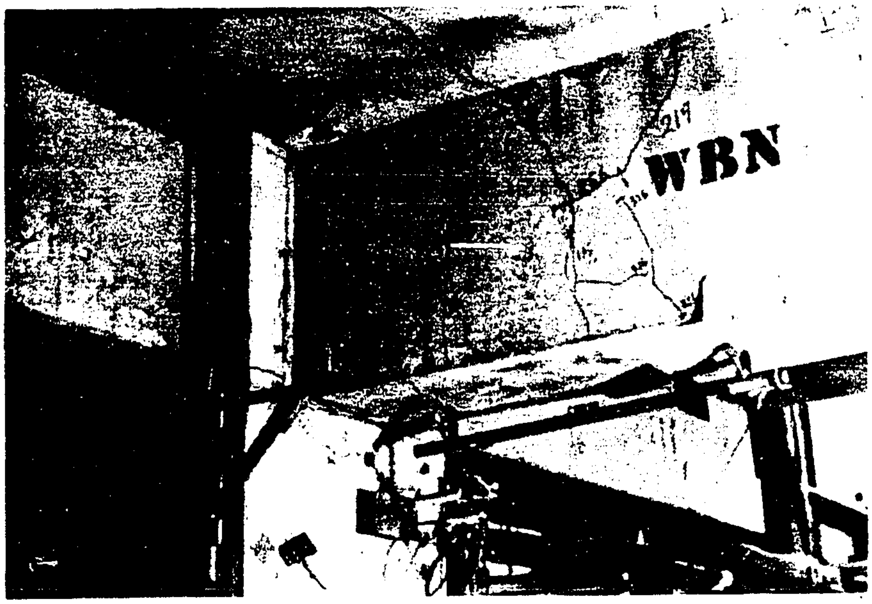

Fig. 3.17 Longitudinal beam at U1.2, exterior prototype

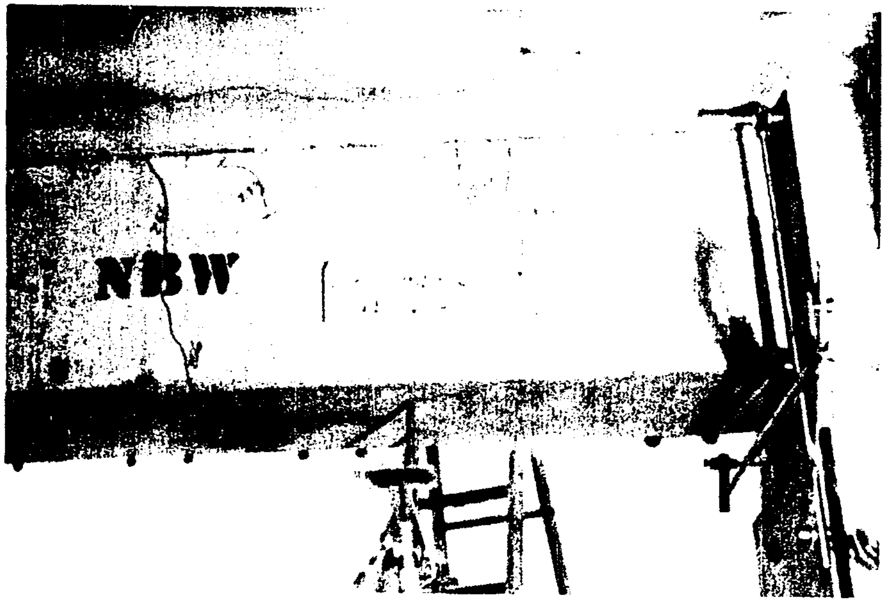

Fig. 3.18 Transverse beam at D1.2, exterior prototype

moment capacity of the exterior specimen was about 2/3 of that attained by the interior prototype (see Fig. 3.13). In Fig. 3.19, the strains in the top longitudinal beam bar are compared for the interior and exterior prototype specimens. The figure clearly indicates that the stress in the longitudinal beam bars in the exterior specimen was not increasing as deflections increased. An examination of the concrete in the joint area indicated that the cover was adequate and that good compaction of the concrete had been achieved. A plot of longitudinal beam bar slip versus the beam end deflection for the two specimens shown in Fig. 3.20 amplifies the conclusions regarding an anchorage failure.

Due to the loss of anchorage of the longitudinal beam bars, the main element transferring load at this level (D2.4) was the slab. The role of the slab was reflected by the opening of several new cracks at the top and bottom faces of the slab (see Figs. 3.21 and 3.22). Several new torsional cracks were formed, indicating the high torsion introduced into the transverse beam by the slab. Large torsional rotations were recorded as the cracks formed (see Fig. 3.16). Fairly evenly-spaced vertical cracks, extending a distance of about 3 ft on either side of the column, were present on the west face of the transverse beam. The west face was also cracked diagonally near the column. The cracks were about 30-40 deg from the vertical. Severe torsional distress was evident at this stage in the form of several closely spaced diagonal cracks on the east face of the transverse beam (Fig. 3.23). A large diagonal crack formed on

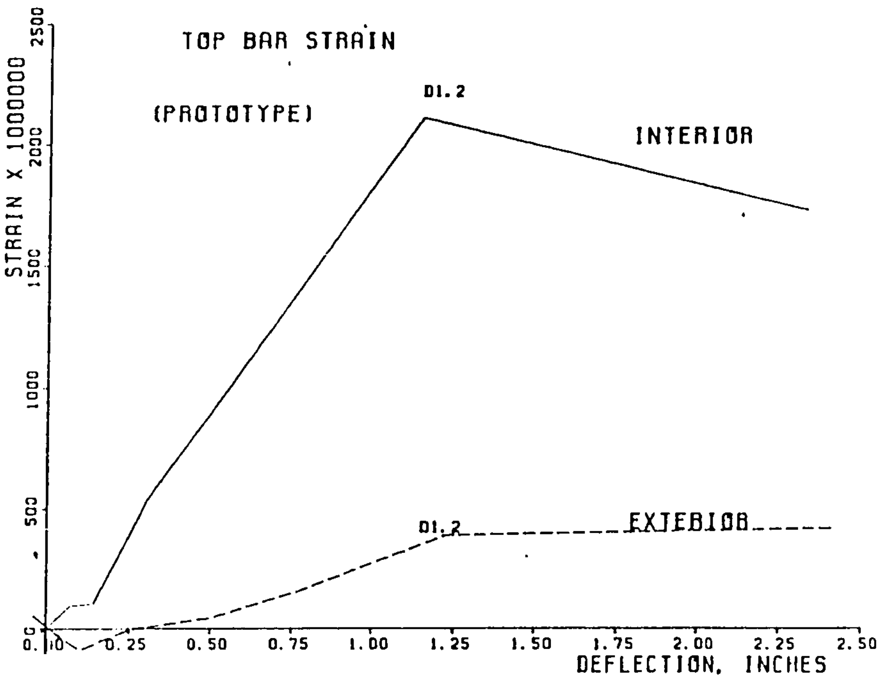

Fig. 3.19 Top longitudinal beam bar strain versus deflection, prototype specimens

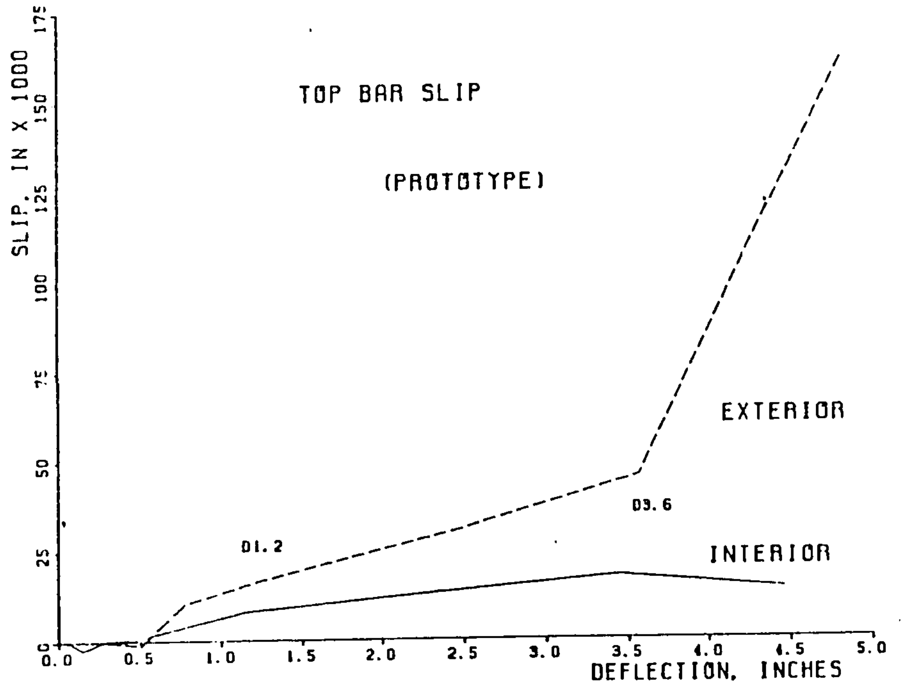

Fig. 3.20 Top longitudinal beam bar slip versus deflection, prototype specimens

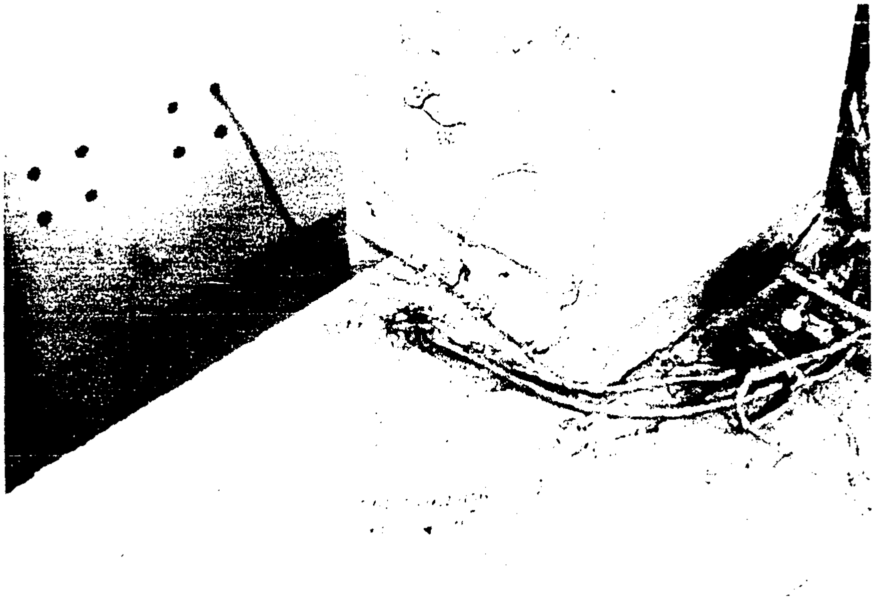

Fig. 3.21 Top of slab at D2.4, exterior prototype

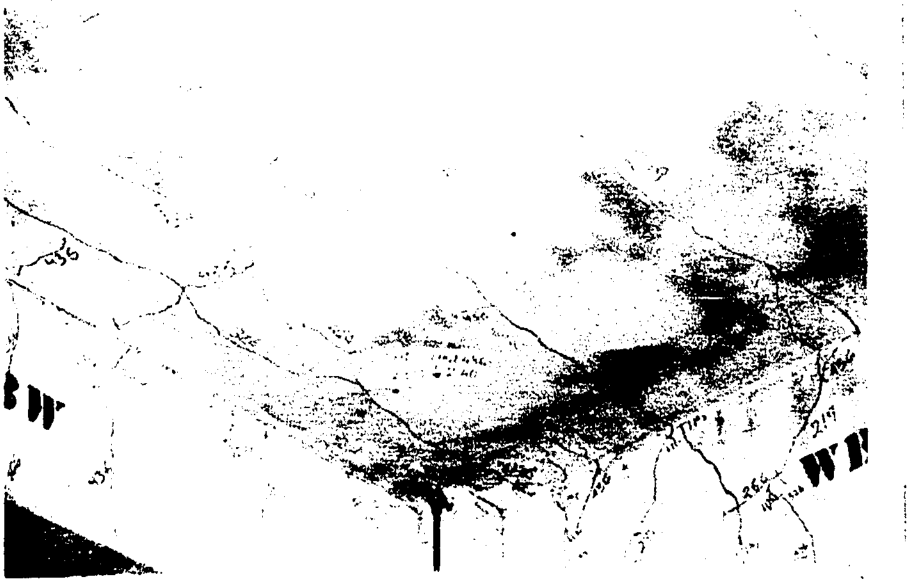

Fig. 3.22 Bottom of slab at D2.4, exterior prototype

the east face on either side of the column inclined at an angle of 30-60 deg from the vertical.

At higher deflection levels a large separation formed between the longitudinal beam and the slab. Crushing of concrete was observed at the longitudinal beam and column intersection during the upward excursion of the beam, as the concrete strains in the top fiber increased due to large imposed deformations. Concrete spalling was evident on the east face of the transverse beam, about 30-36 in. from the column face. A loss of load carrying capacity was recorded in cycles past a deflection level of 2.4 in. and severe pinching of the load deflection curve was noted as a result of the extensive torsional cracking of the transverse beam and failure of the anchorage for the longitudinal beam reinforcement.

The concrete cover at the back of the column was removed easily with a hammer at a deflection level of 3.6 in. Slip of the longitudinal beam bars could be seen when the specimen was cycled (see Fig. 3.24). The movement of the hooked bars towards the back face caused spalling and outward deformation of the transverse steel through the joint.

3.5 Modified Interior

Curves of the west beam load versus the beam end deflection at the first peak cycles are shown in Fig. 3.25. As mentioned in the discussion on the prototype interior specimen, only the west beam behavior will be discussed; the east beam behaved in a similar

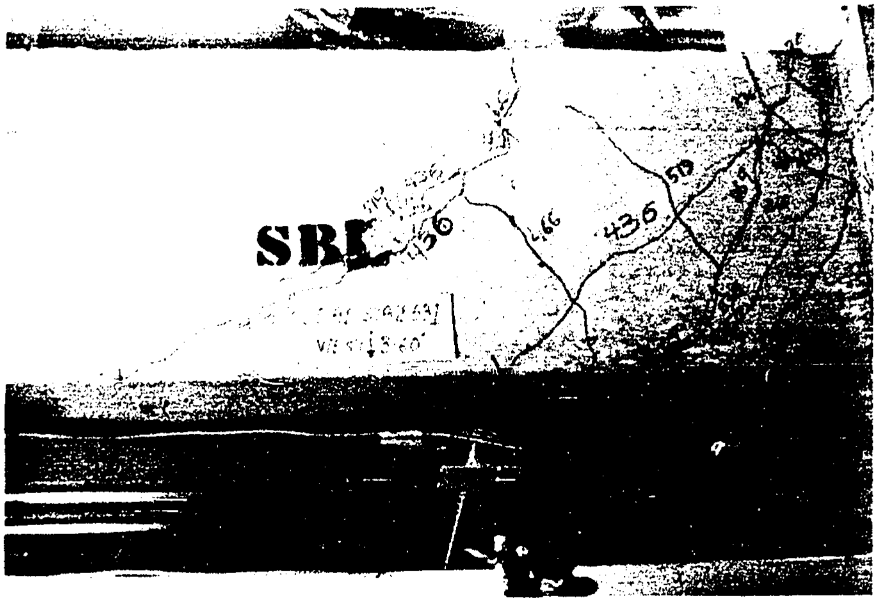
SBL
436
436
.66
50

Fig. 3.23 Transverse beam at D3.6, exterior prototype

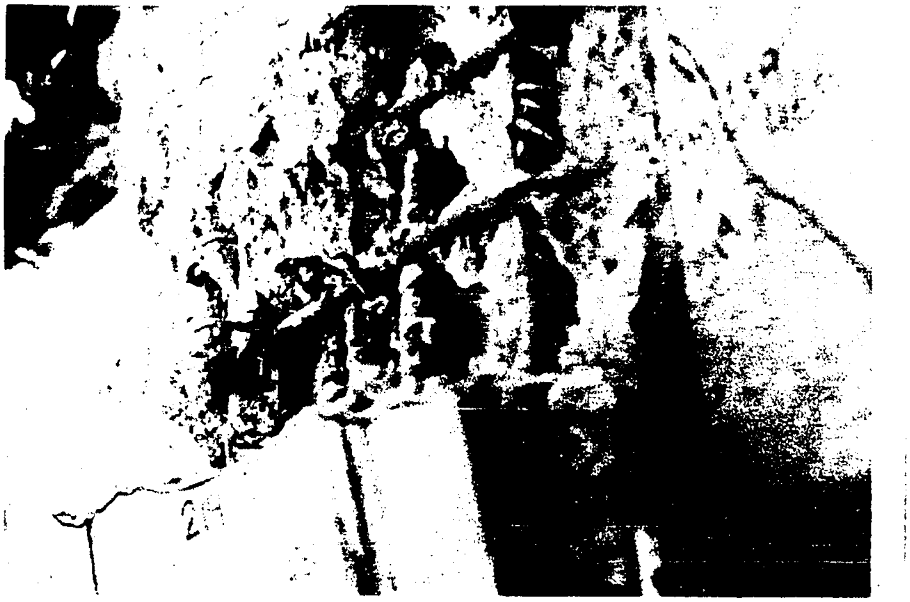

Fig. 3.24 Back of column at end of test, exterior prototype

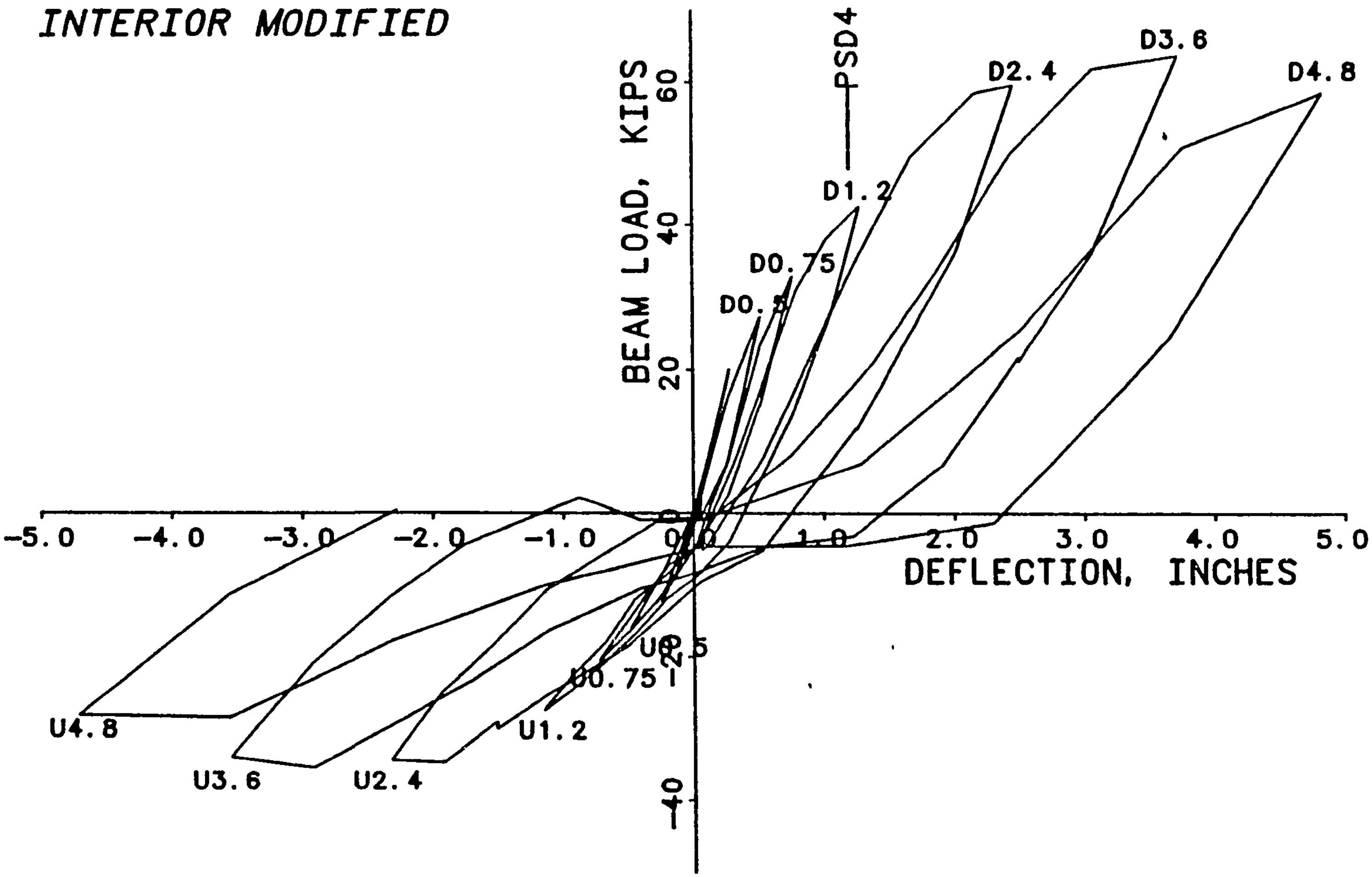

Fig. 3.25 Load versus deflection, interior modified specimen

manner. The response of the specimen was fully elastic at deflection levels less than 0.25 in.

At a deflection level of 0.5 in., flexural cracking initiated in the longitudinal beam and slab. Flexural cracks, extending about 1/2 to 3/4 of the depth of the longitudinal beam, were first formed at a load stage U0.5. These cracks were fairly uniformly distributed and occurred within a distance of 30-36 in. from the column face. Flexural cracks, extending nearly across the width of the slab and located at about 8 in. and 18 in. from the column face, formed on the top surface of the slab at load stage D0.5. The bottom surface of the slab also showed a flexural crack extending about 20-24 in. on either side of the longitudinal beam and located at about 8 in. from the column face. Very little loss in stiffness was observed at cycles up to 0.5 in. deflection.

Two short torsional cracks, about 3 to 4 in. long, formed on the west face of the transverse beam at load stage U0.75. Flexural cracks in the longitudinal beam propagated to the full depth of the beam (see Fig. 3.26). A few new flexural cracks were also formed in the longitudinal beam at U0.75. The flexural crack at the bottom of the slab propagated to half the width of the slab at D0.75 (see Fig. 3.27). A crack was formed at D0.75 on the top surface of the slab, originating about 30-36 in. from the column face and running parallel to the transverse beam near the longitudinal beam and then turning diagonally towards the load point. This crack extended to within 12 in. from the edge of the slab. A corresponding crack also formed at

Fig. 3.26 Longitudinal beam at U0.75, interior modified

Fig. 3.27 Bottom of slab at D0.75, interior modified

D0.75 on the bottom surface of the slab but not extending as far towards the edge of the slab. Shear-type cracks were a result of the transfer of large shear to the slab from the loading plate. Load-deflection response was not significantly different from that of the previous deflection level.

The deflection level of 1.2 in. was marked by yielding of the longitudinal beam bottom steel. Flexural cracking at stage U1.2 extended over a wide area in the longitudinal beam, with most of the cracks extending the full depth of the beam. Some of the flexural cracks turned away from the column, near the bottom of the beam, to form shear cracks. Diagonal cracks near the column face on the west side of the transverse beam also formed at U1.2. At load stage D1.2, new flexural cracks opened on the top surface of the slab. A few diagonal cracks on the top of the transverse beam were formed. Cracks radiating towards the loading point also formed at the top surface of the slab. The bottom surface of the slab showed new flexural cracks close to the column and semicircular cracks surrounding the loading point. The first major torsional cracking of the transverse beam occurred at this stage in the form of diagonal cracks within 10 in. from the column face. These cracks were inclined up and away from the column on the west side and down and away from the column on the east side. This resulted in large loss of torsional stiffness of the transverse beam (see Fig. 3.28). The first significant loss of stiffness occurred at 1.2-in. deflection.

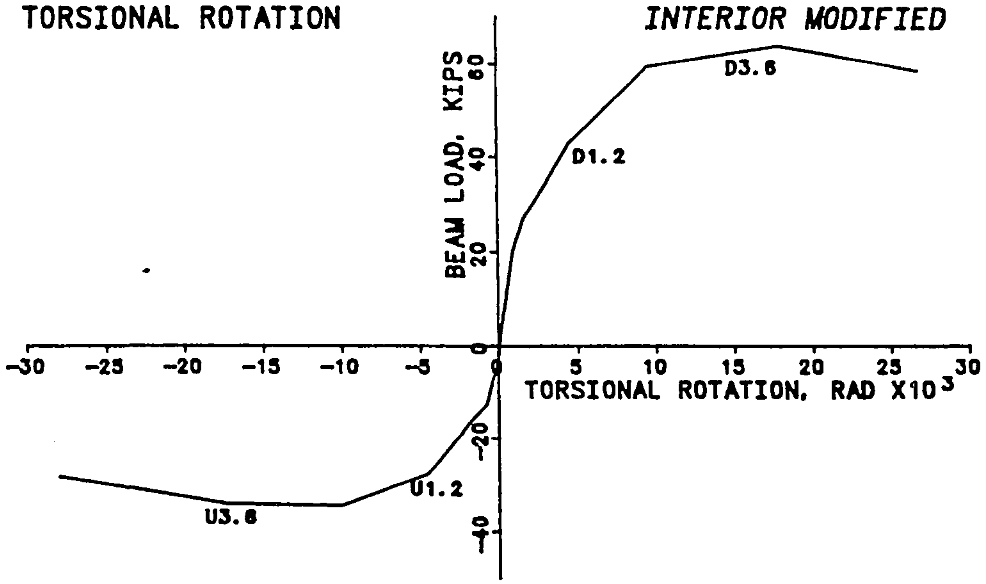

Fig. 3.28 Beam load versus torsional rotations, interior modified

The deflection level of 2.4 in. was characterized by a marked loss of stiffness in the load-deflection curve. The top longitudinal beam steel yielded at D2.4. A wide crack was formed at the top of the slab near the intersection with the column. Regularly spaced cracks formed on the top of the slab. The cracks were closely spaced near the column. The cracks away from the column turned diagonally towards the loading point. Corresponding cracks also formed on the bottom face of the slab. The diagonal cracks near the column in the transverse beam propagated the full depth of the transverse beam. Extensive cracking of the transverse beam resulted in large torsional rotations (see Fig. 3.28). A peak load of 34.3 kips was recorded at U2.4 (slab in compression).

A peak beam load of 63.7 kips was achieved at load stage D3.6 (slab in tension). Spalling and cracking of concrete at the top (U3.6) and at the bottom (D3.6) was observed at a deflection level of 3.6 in. No major new cracks formed in the slab or in the longitudinal beam, but extensive widening and propagating of existing cracks occurred at this deflection level. Vertical cracks located at about 20-25 in. from the column face appeared at D3.6 on the west face of the transverse beam. Large torsional rotations of the transverse beam indicated a severe loss of torsional stiffness. Significant pinching of the load-deflection curve occurred at this deflection level. Figures 3.29 and 3.30 show different views of the specimen in the vicinity of the joint at the end of the test.

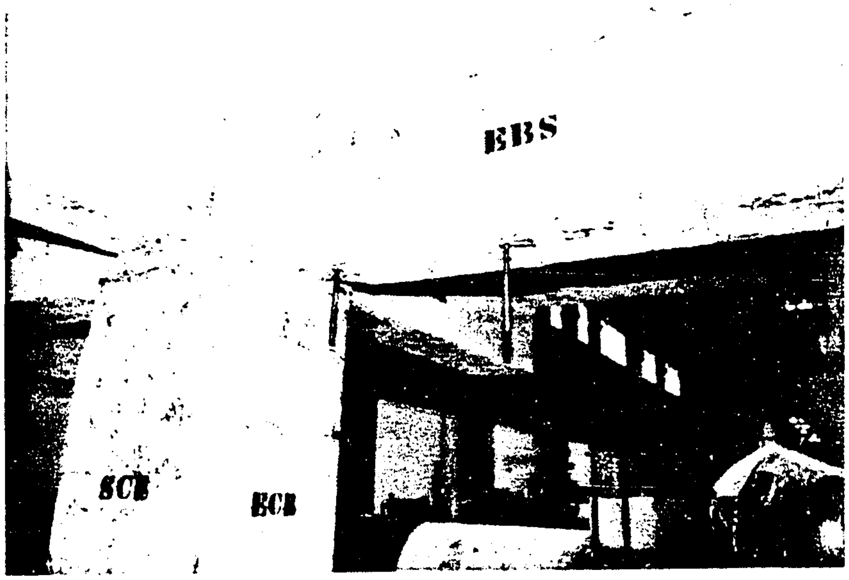

Fig. 3.29 View of beams at end of test, interior modified

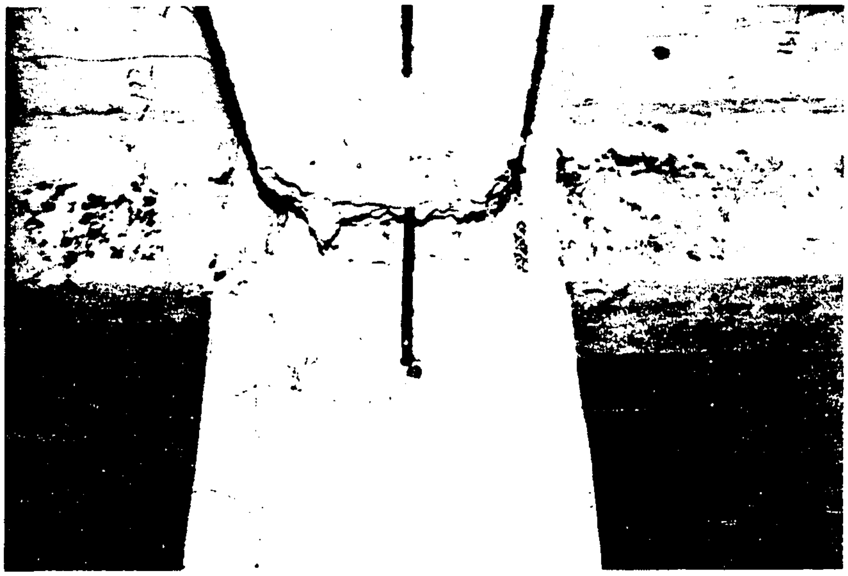

Fig. 3.30 View of joint region at end of test, interior modified

Stiffness degradation and pinching of the load-deflection curve resulted when the specimen was cycled further. A loss of load was recorded in both directions. The failure of the specimen was caused by flexural hinging of the longitudinal beam and the slab.

3.6 Modified Exterior

The west beam load versus deflection curve for the first peak cycles for the modified exterior specimen is shown in Fig. 3.31. The behavior of the specimen was elastic up to a deflection level of 0.1. in. The initial flexural cracking in the longitudinal beam was observed at deflection level U0.25. A flexural crack on the top surface of the slab, running parallel to the transverse beam, initially formed at load stage D0.25. The flexural crack in the slab extended only about 24 in. on either side of the longitudinal beam This minor cracking resulted in a very small loss in stiffness in the load-deflection curve.

Significant cracking of the longitudinal beam and the slab was first observed at a deflection level of 0.5 in. Cracks formed at the top surface of the slab at a fairly regular spacing within a distance of about 30-36 in. from the column face. These cracks, running parallel to the transverse beam, extended nearly across the full width of the slab. A flexural crack on the bottom surface of the slab also formed at D0.5. This crack continued about 3 in. down into the longitudinal beam. The longitudinal beam developed regularly spaced flexural cracks at load stage U0.5. Due to this

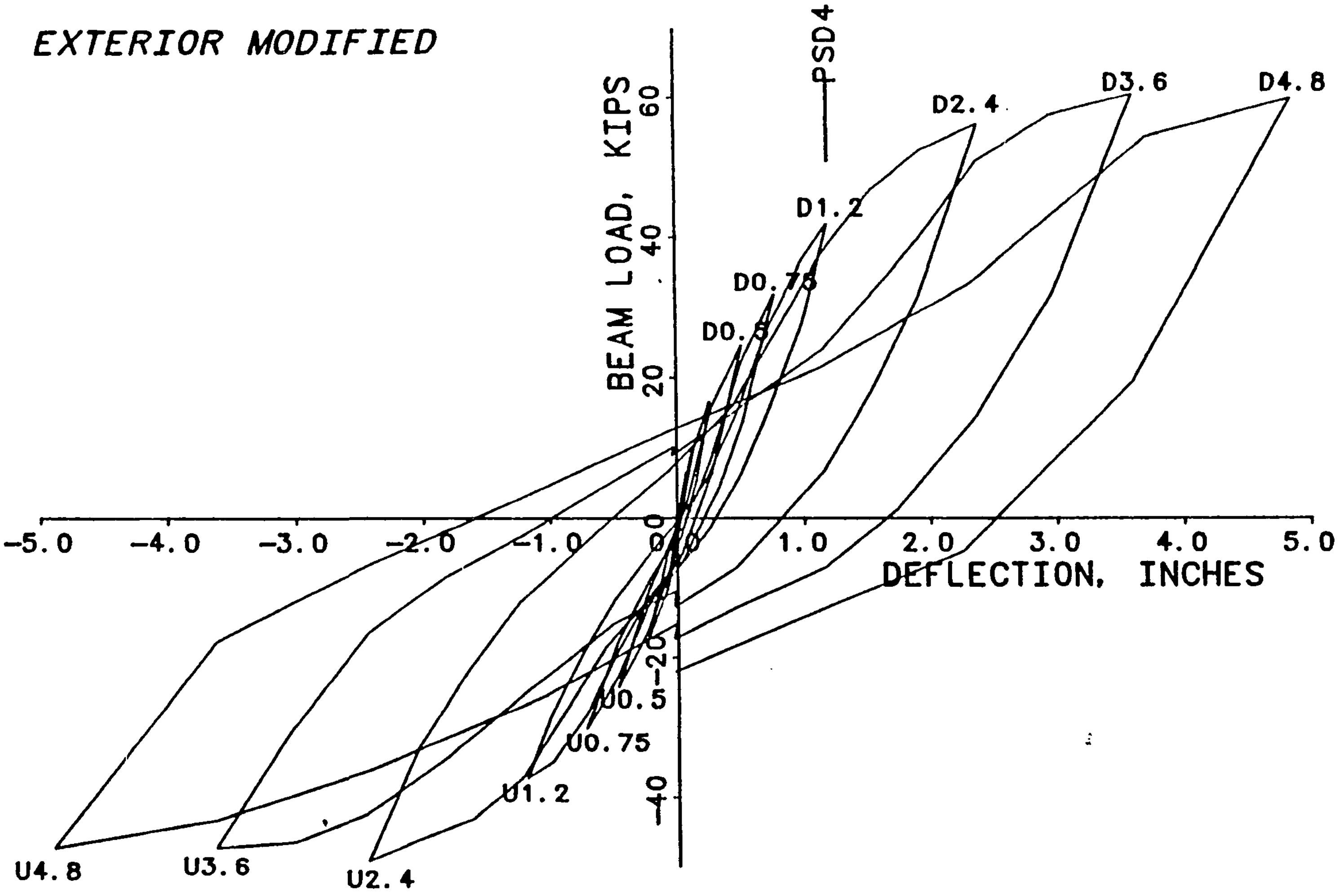

Fig. 3.31 Load versus deflection, exterior modified specimens

cracking, a small loss in stiffness was noted in the load-deflection curve.

Initial torsional cracking was observed at a deflection level of 0.75 in. From this stage onward a gradual loss in the torsional stiffness of the transverse beam was evident from the load versus torsional rotation plots (see Fig. 3.32). The diagonal cracks on the east face of the transverse beam were restricted to a zone about 6-12 in. from the column face. Cracks formed on the top of the transverse beam near its intersection with the slab. Torsional cracking was also apparent on the top of the transverse beam. The bottom surface of the slab showed cracking both in the upward and downward excursions of the longitudinal beam. At D0.75 flexural cracks formed in the bottom of the slab to a point nearly 40-50 in. from the column face.

A separation crack between the transverse beam and the slab formed at load stage U1.2. Flexural cracking at the bottom of the slab was also detected at load stage U1.2 (see Fig. 3.33). These cracks extended parallel to the transverse beam and all the way to the edge of the slab. Vertical flexural cracks, extending through the depth of the longitudinal beam, formed along the longitudinal beam for a distance about 70 in. from the column face (see Fig. 3.34). The bottom steel in the longitudinal beam yielded at load stage U1.2. Evenly spaced flexural cracks, extending to the edge of the slab, were observed at load stage D1.2 (see Fig. 3.35). Diagonal cracks also formed at the top of the transverse beam. The west face

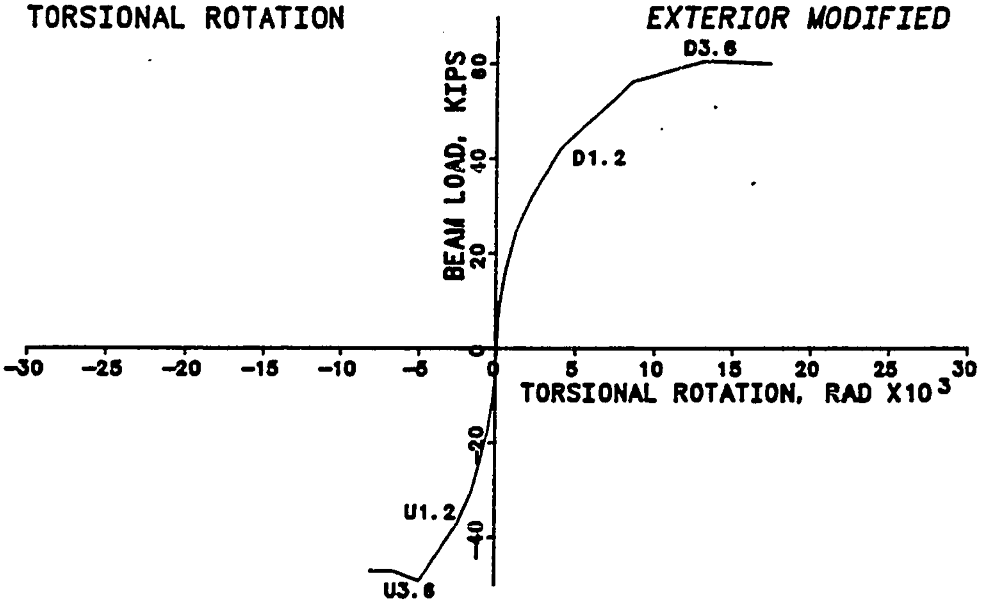

Fig. 3.32 Beam load versus torsional rotation, exterior modified

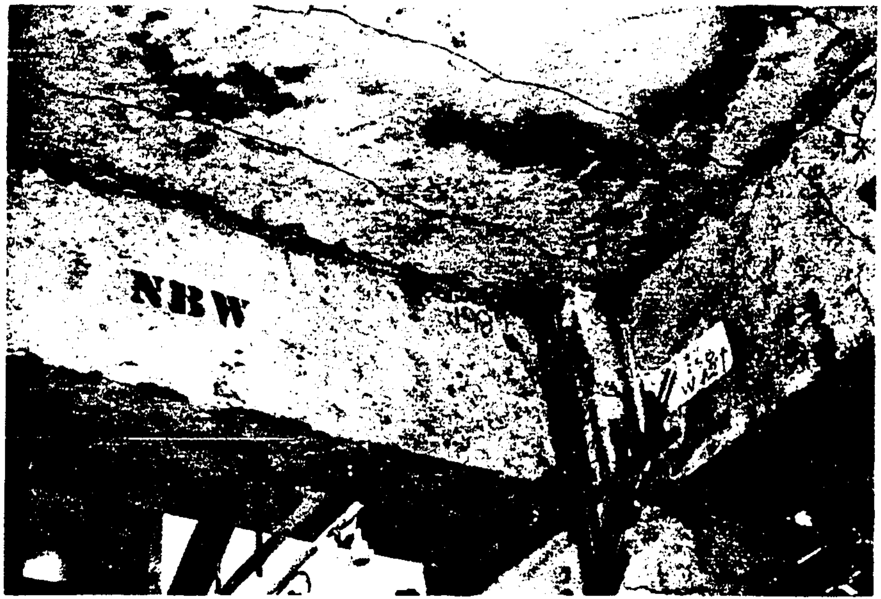

Fig. 3.33 Bottom of slab at U1.2, exterior modified

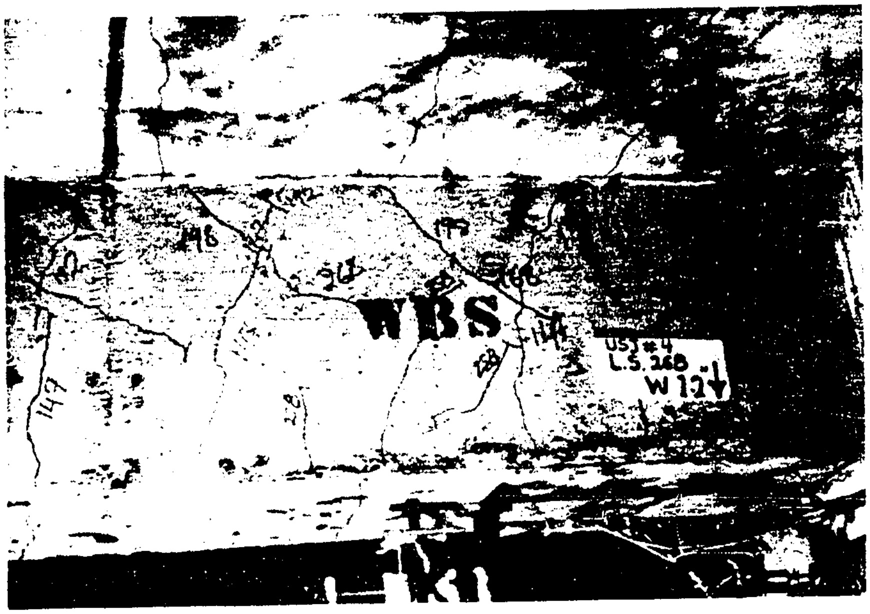
148
WBS
147
US1 #4
L.S. 268
W 1.2

Fig. 3.34 Longitudinal beam at U1.2, exterior modified

Fig. 3.35 Top of slab at D1.2, exterior modified

of the transverse beam experienced initial cracking at D1.2. Torsional cracks extending diagonally on the transverse beam near the column were detected. In addition, vertical cracks on either side of the column about 24 in. from the column face and extending through the full depth of the transverse beam formed on the west face of the transverse beam (see Fig. 3.36). Few new torsional cracks opened up on the east face of the transverse beam (see Fig. 3.37). The load-deflection curve showed a small degradation of stiffness and a significant widening of the hysteresis loop.

The excursion of the specimen to a deflection level of 2.4 in. resulted in yielding of the top longitudinal beam steel. The flexural cracks in the longitudinal beam and the slab opened up and became fairly wide. Additional torsional cracking was observed on the transverse beam in the form of diagonal cracks near the column and vertical cracks away from the column. Torsional cracking in the modified exterior specimen was not as widespread and predominant as that in the prototype exterior specimen at this deflection level. The yielding of the longitudinal beam steel and widening of the cracks led to a wide hysteresis loop at this level. Deterioration in stiffness can be observed. The torsional cracking resulted in severe loss of torsional stiffness at this stage, as can be seen in Fig. 3.32. It is important to note at this stage that no pinching of the load-deflection curve was observed at either this level or at higher deflection levels. A peak beam load of 49.4 kips was recorded at load stage U2.4 (slab in compression).

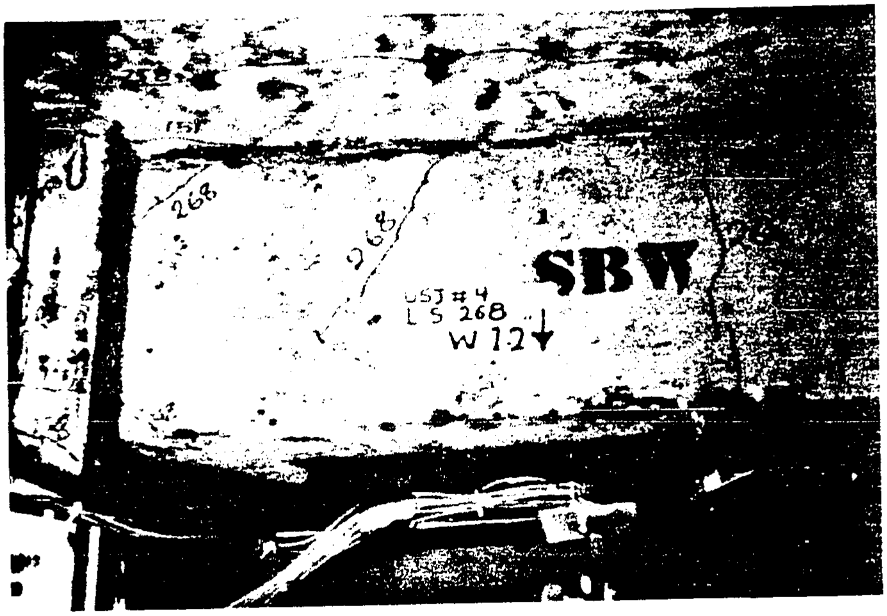
268
268
SBW
USJ #4
LS 268
W 12

Fig. 3.36 Transverse beam at D1.2, exterior modified

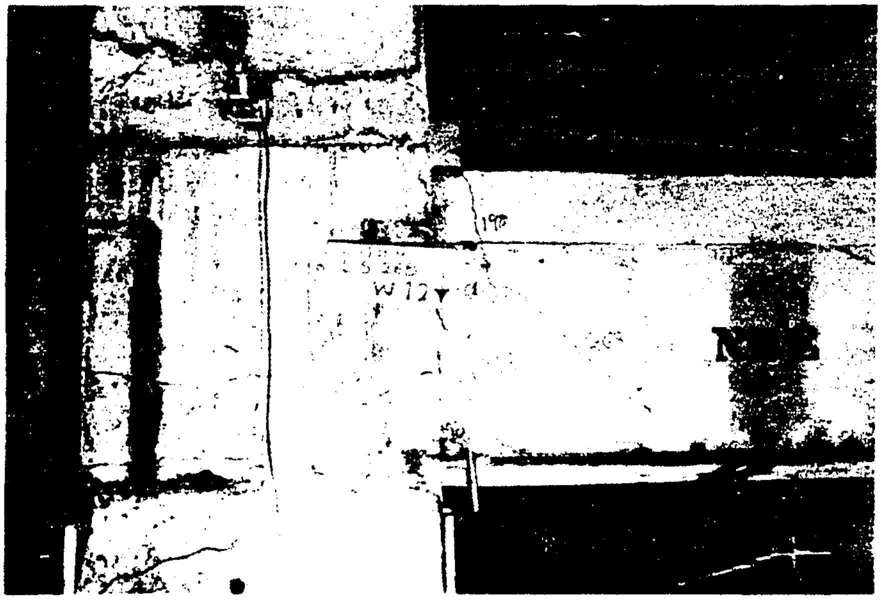

Fig. 3.37 Transverse beam east face at D1.2, exterior modified

Additional torsional cracking of the transverse beam resulted at load stage D3.6 on the east and west side and also on top of the slab (see Fig. 3.38). A peak load of 60.5 kips was recorded at load stage D3.6 (slab in tension). The load-deflection curve showed a loss in stiffness. Separation of the longitudinal beam from the column could be seen. The bottom beam bars were exposed at a deflection level of 4.8 (see Fig. 3.39) and a very small loss in load-carrying capacity was observed.

No anchorage problems were encountered as in the exterior prototype specimen. The addition of cross ties in the joint resulted in excellent performance of the longitudinal beam and the specimen in general.

3.7 General Behavior

The response of all four specimens to reversed cyclic loading was predominantly flexural. The mode of failure in the case of all but the exterior prototype specimen was flexural hinging. Inelastic behavior through beam hinging is desirable, since this provides a mechanism for energy dissipation.

All four specimens showed stiffness degradation after yielding of the longitudinal reinforcement. The load-deflection curves also showed pinching near the origin, associated with flexure and shear cracks in the beams and the bond problems through the joint. These problems, however, were encountered only at very large deflection levels, corresponding to story drifts of 3-1/2 to 5

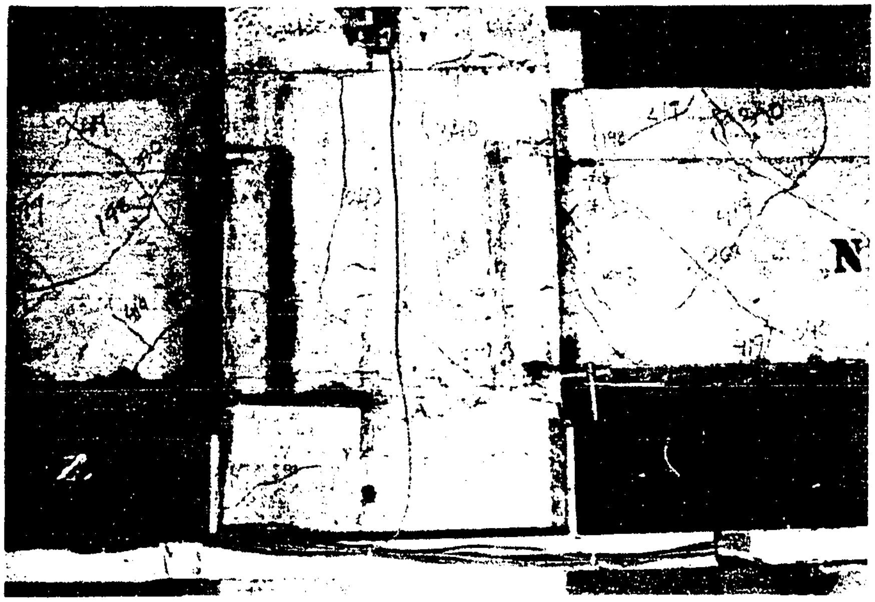

Fig. 3.38 Torsional cracking at D3.6, exterior modified

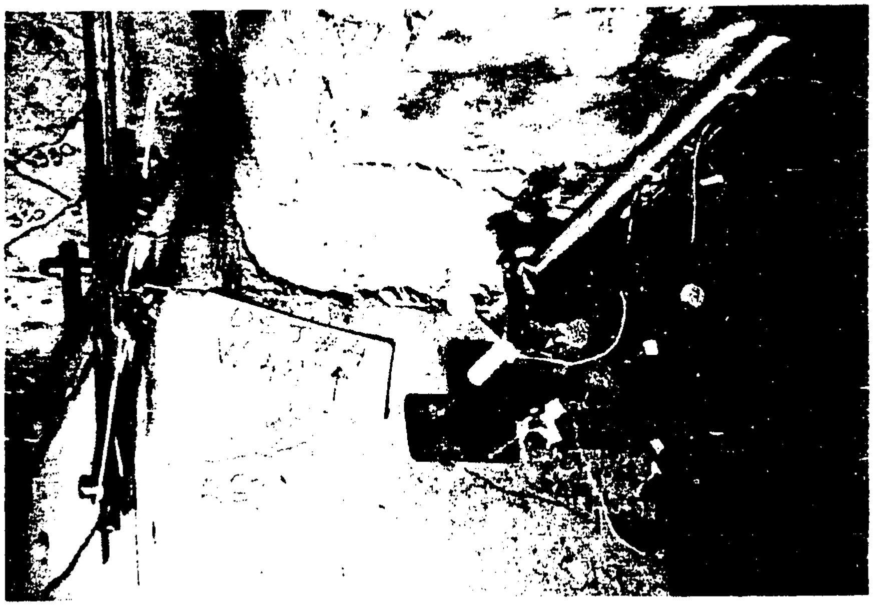

Fig. 3.39 Joint region at end of test, exterior modified

percent. The reduction in the load-carrying capacity at these high deflection levels was of the order of 20 to 25 percent of peak capacity for the prototype specimens and about 5 to 8 percent for the modified specimens.

As mentioned previously, the specimens were subjected to about four times the deflection levels of the seven-story structure. A structure generally will not be called upon to perform well at drift levels as high as 5 percent. The story drift level estimated to correspond to the maximum deflection level achieved during PSD4 is about 1.3 to 1.5 percent. The local deflection level depends on several factors besides just the overall structure drift. The behavior of the adjoining members is expected to alter the maximum local deformation requirements. The level corresponding to PSD4 is indicated on the load-deflection response of the specimens (see Figs. 3.2, 3.13, 3.25, and 3.31). The performance of all specimens up to this level was excellent, and the behavior was governed by flexure. The degradation in stiffness due to cycling was minimal. There was no indication of shear or bond distress in or near the joint,and very little evidence of serious torsional distress in the transverse beam. The columns showed minor flexural cracking at this level.

The measured and the predicted loads for negative bending are given in Table 3.1. The ultimate loads were significantly higher than those predicted using the ACI effective flange width. The problem of evaluating slab participation deserves special attention and is discussed in detail in the next chapter. The exterior

TABLE 3.1 Comparison of Observed and Computed Flexural Capacities, kip-in.

Slab in Tension	Prototype		Modified	
	Int.	Ext.	Int.	Ext.
Measured Expt. Capacity	3635	2415	5480	5205
Computed Capacity:				
Beam Only	1635	1615	3535	3625
ACI Effective Width	2485	2460	4380	4515
Full Width as Flange	4380	4340	6490	6765

prototype specimen exhibited an anchorage failure and did not show the same high strength as the other three specimens.

3.8 Anchorage

The ultimate load reached by the exterior prototype specimen under negative moment (slab in tension) was about 2/3 of that attained by the interior prototype. As explained earlier, the controlling failure mode for the prototype exterior specimen was loss of anchorage. In the modified exterior specimen, additional crossties were provided through the joint, preventing an anchorage failure in spite of increased reinforcement congestion and larger bar diameter.

The hooks from the top longitudinal bars and from the bottom longitudinal bars and the column bars formed a continuous steel "wall" at the far end of the column. The confinement provided by the column transverse reinforcement was insufficient to prevent spalling, resulting from movement of the hooked bars towards the back face of the column, thus prying off the back cover. Congestion of the hooked reinforcement and lack of sufficient transverse confinement resulted in loss of anchorage of the longitudinal steel, even though an anchorage length of 17.8 in. was available, much higher than the 10.2 in. required by ACI 318-83 Appendix A [3]. It should be mentioned here that the beam bars were carried to the far end of the column, a common U.S. practice, rather than being taken only to the center of the joint, a recommended Japanese detail. If the Japanese detail had been used, the available development length would have been only about 9.8 in.

Although the behavior of the exterior prototype joint was governed by anchorage failure, this occurred at high deflection levels. This type of anchorage failure was not observed in the seven-story structure. For deflection levels estimated to correspond to the maximum deflection level imposed in the seven story structure tests, the performance of the exterior prototype specimen was adequate, although not excellent. There could be two primary reasons why no anchorage failure was observed in the seven-story structure. First, the deformation levels actually imposed on the beams were smaller than those applied in the prototype test. Second, the continuous multibay, multistory, highly redundant structure has the ability to redistribute internal actions.

3.9 Joint Shear

Due to the large size of the columns, shear problems in the joint were not anticipated, and none of the four specimens tested showed any shear distress. Measured values of joint shear strain were about of 2.5×10^{-3} radians up to deflection levels estimated to correspond to the maximum deflection levels achieved in PSD4 (see Fig. 3.40). The steady increase in positive shear strain and decrease in negative shear strain at large deflection levels was likely due to the high shears transferred to the joint as the

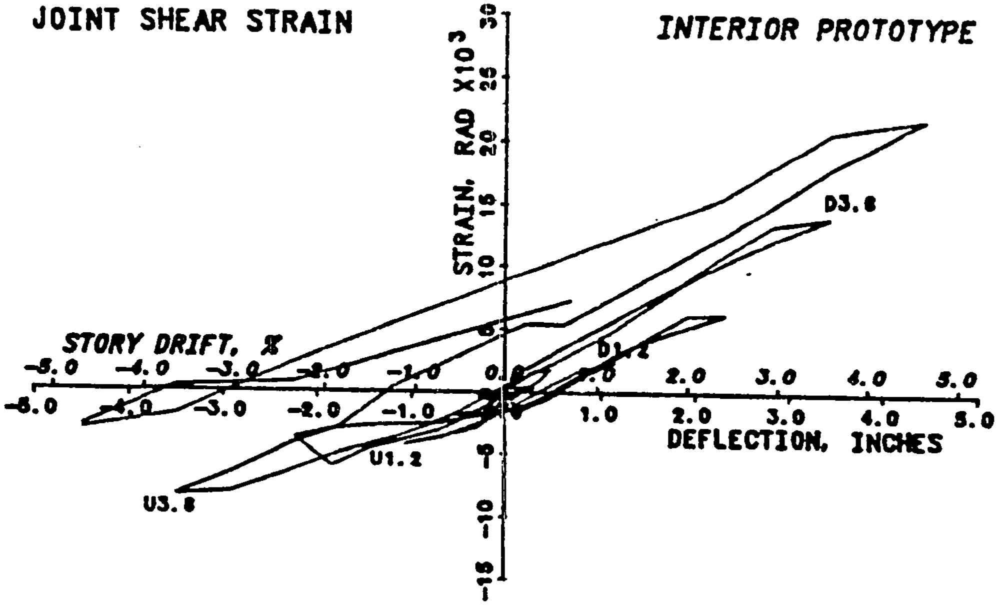

Fig. 3.40 Joint shear strain versus deflection, interior prototype

resistance of the slab increased. The orientation of the shear strain instrumentation may also have accounted for the difference in positive and negative shear strain magnitudes. The maximum shear strains were about 30 x 10^{-3} radians. The exterior modified specimen which had additional joint confinement showed much smaller shear strains (10 x 10^{-3} radians) than the other three specimens. Typical column hoop strains indicated that the hoops in the center of the joint were more severely strained than the hoops at the top and bottom of the joint. The strains were mostly in the elastic range and yielding, if at all, was observed only at very high deflection levels.

Table 3.2 shows the shear stress in the joint at a level corresponding to PSD4 and at the ultimate loads for the four specimens tested. As mentioned earlier, the higher effectiveness of the slab led to measured capacities larger than those predicted. Hence, as a conservative estimate, measured rather than computed capacities were used in computing the joint shear stress. It was also assumed that the entire moment generated by the applied load was effective in introducing shear in the joint. This assumption will lead to an overestimation of the joint shear stress. In the interior prototype specimen the maximum shear stress was about $12\sqrt{f'_c}$, whereas at a level corresponding to PSD4 it was about $8\sqrt{f'_c}$. In all cases, the values were well below the ACI Committee 352 [3](or ACI 318-83 [2]) recommended limits for shear capacity of joints. An improper

TABLE 3.2 Joint Shear Stresses

	Joint Shear Stress, psi	
Specimen	at PSD4*	Ultimate
Interior Prototype	$8.1\sqrt{f'_c}$	$11.5\sqrt{f'_c}$
Exterior Prototype	$4.8\sqrt{f'_c}$	$5.3\sqrt{f'_c}$**
Interior Modified	$14.0\sqrt{f'_c}$	$21.1\sqrt{f'_c}$
Exterior Modified	$9.0\sqrt{f'_c}$	$13.0\sqrt{f'_c}$

* Note: These values are computed from the observed experimental loads at an equivalent drift level.

** Anchorage failure.

estimate of the slab influence could lead to serious underestimation of the expected joint shear stress.

3.10 Comparisons of Crack Patterns Between Seven-Story Structure and Slab-Beam-Column Assemblages

Due to the limitations of the data from the seven-story structure, direct comparisons between test results from the seven-story structure and the component tests were not possible. However, the crack patterns between the seven-story structure and the prototype test specimens, especially regarding the slab participation, can be compared as shown in Fig. 3.41. The crack patterns between the two structures were very similar and hence it can be concluded that the participation of the slab in the test specimens closely represented participation of the slab in a real continuous structure. It should be noted, however, that the difference in the crack patterns around the exterior joints are due to the presence of the spandrel walls in the seven-story structure.

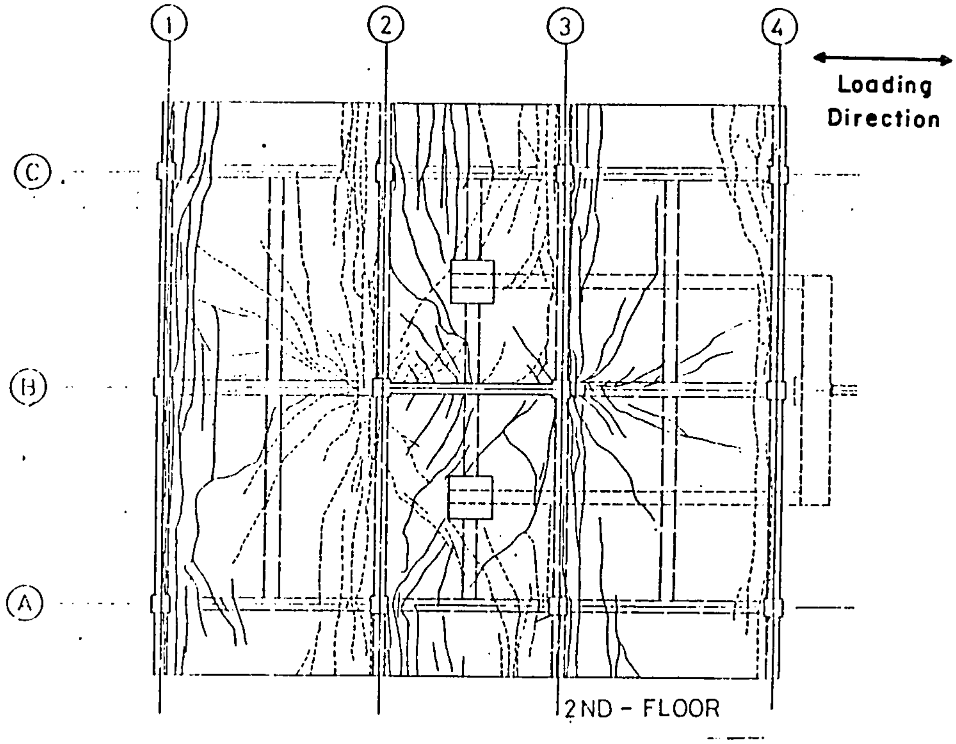
1
2
3
4
Loading Direction
C
B
A
2ND - FLOOR

seven-story structure

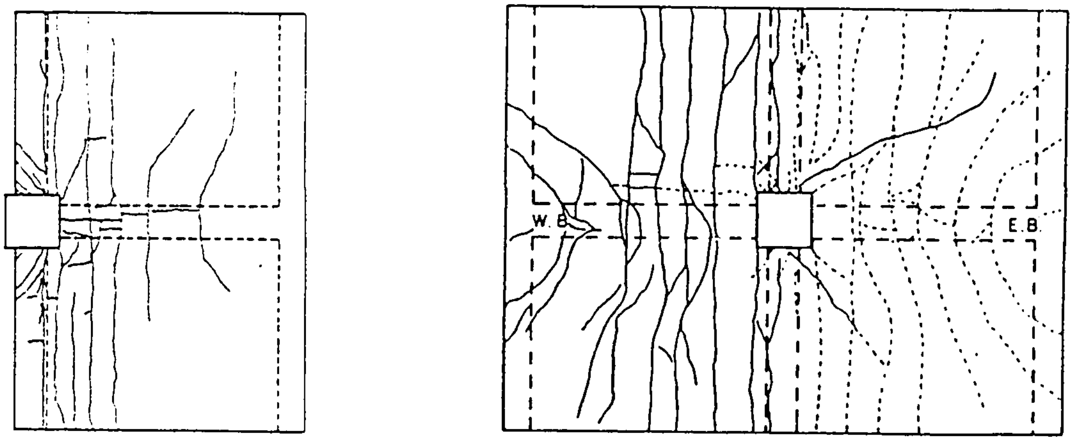

exterior prototype

interior prototype

Fig. 3.41 Comparison of crack patterns, seven-story structure versus prototype test specimens.

CHAPTER IV

INFLUENCE OF THE SLAB ON FLOOR SYSTEM STRENGTH

4.1 Introduction

In monolithic construction the beam and the slab are expected to act integrally. This interaction of the beam and the slab is accounted for in the ACI code by effective width provisions. The effective width provisions were intended to be applied for the compression flange of the T-beam. Although the code does not specifically state that these guidelines are for positive bending. There are no specific recommendations to account for the contribution of the slab when it acts as a tension flange. The need for guidelines to compute the negative bending capacity of a T-beam is thus obvious. The guidelines for determining the effective width of slab acting as a T-beam flange in the ACI 318-83 Code (clause 8.10.2) state that

> 8.10.2--Width of slab effective as a T-beam flange shall not exceed 1/4 the span length of the beam, and the effective overhanging slab width on each side of the web shall not exceed:
> (a) 8 times the slab thickness, or
> (b) 1/2 the clear distance between the web.

The current guidelines for using a part of the slab to act as a flange of the beam were intended for determining the positive moment capacities of such T-sections. The requirements of the effective width of slab acting as a flange have remained unchanged since the Report of the 1924 Joint Committee on Standard Specifications for Concrete and Reinforced Concrete [10]. The provisions are empirical but were based on tests of T-beams and elastic analysis with shear lag approach. The references on these tests are not available. In general, using the Code provisions for the flange widths to compute flexural response will give a conservative estimate of the positive moment capacity (slab in compression) of the beam.

When the beam is subjected to a negative bending moment (slab is in tension), some of the longitudinal slab steel will act with the top longitudinal steel in the beam. The current Code effective flange width specifications were not formulated to cover this case of negative bending. Since the ACI code does not specifically exclude the application of effective flange width provisions to the tension flange, these provisions were assumed to be valid even for the tension flange. The effective flange width provisions were used to calculate the beam strengths for both positive and negative bending. The measured negative moment capacities were significantly greater than estimated using ACI effective width recommendations.

It is necessary to determine accurately the contribution of the slab to the moment capacity of a beam when designing structures to resist seismic loads. Counting only the tensile capacity of the reinforcement located in of the effective flange width as specified by the ACI 318-83 Code in assessing the strength of the beam leads to an underestimation of the negative moment capacity, as can be seen from the test results. In designing for static loads, such an element overstrength would generally lead to a safer structure. However, in seismic design where deformations are imposed on the structure and the moment imposed on the column by the floor system is to be determined, underestimation of beam strength is no longer conservative. The presence of elements with strengths greater than accounted for in design may result in excessive strength and ductility demands on other elements. The behavior and the failure mechanism of the structure may differ from that desired or assumed in design. Such differences may result in potentially serious damage to the structure leading to local or general collapse conditions.

The test results relating to the contribution of the slab to the flexural capacity of the floor system will be discussed. The observed capacities will then be compared with predicted values.

4.2 Behavior of the Slab

The behavior of the floor system will be discussed in resisting both positive moment (slab in compression) and negative moment (slab in tension). The exterior prototype specimen exhibited an anchorage failure and cannot be compared on the same basis as the other three tests. The loss of bond of the longitudinal beam bars resulted in the exterior prototype specimen failing before the strength of the beam was realized. However, the general behavior of the slab system was essentially the same as in the other three specimens.

4.2.1 Crack Patterns. Typical crack patterns under negative moments are shown in Figs. 4.1 and 4.2. Flexural cracks on the top surface of the slab were observed at very early load stages during the downward excursion of the longitudinal beam (negative bending, slab in tension). These cracks extended nearly the full width of the slab even at fairly small displacements (D0.5 to D0.75). Corresponding flexural cracks on the bottom surface of the slab also opened across nearly 1/2 to 3/4 of the width of the slab. If the slab was acting independently from the beam, its bottom surface would have been in compression, and uncracked. This indicates that a substantial portion of the longitudinal slab steel was acting in tension balancing the compressive force in the web of the beam. Similar crack patterns were observed in the seven-story structure as shown in Fig. 3.41.

Under the action of positive moments the bottom surface of the slab showed flexural cracks extending from the edge of the slab towards the longitudinal beam for a distance of about 1/2 the slab width, as shown in Fig. 4.3. This would indicate that under the action of a positive moment the slab close to the beam was acting as a compressive flange but portions of the slab further away were acting as shallow flexural sections.

4.2.2 Steel Strains. The variation of the strain in a typical longitudinal beam bar with the beam end deflection is shown

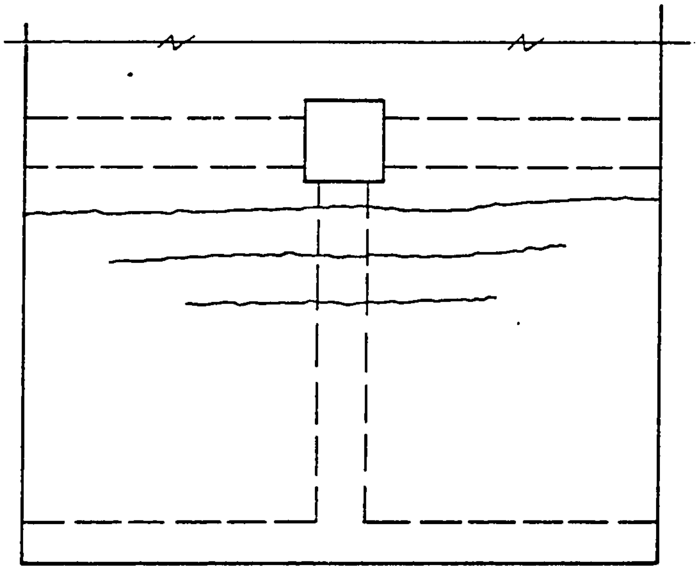
Top of the Slab

Fig. 4.1 Flexural cracks at top of slab under negative moment

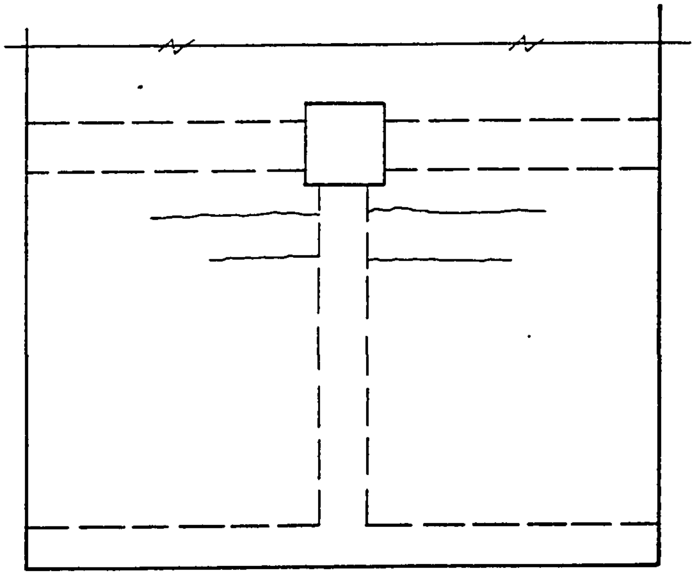
Bottom of the Slab

Fig. 4.2 Flexural cracks at bottom of slab under negative moment

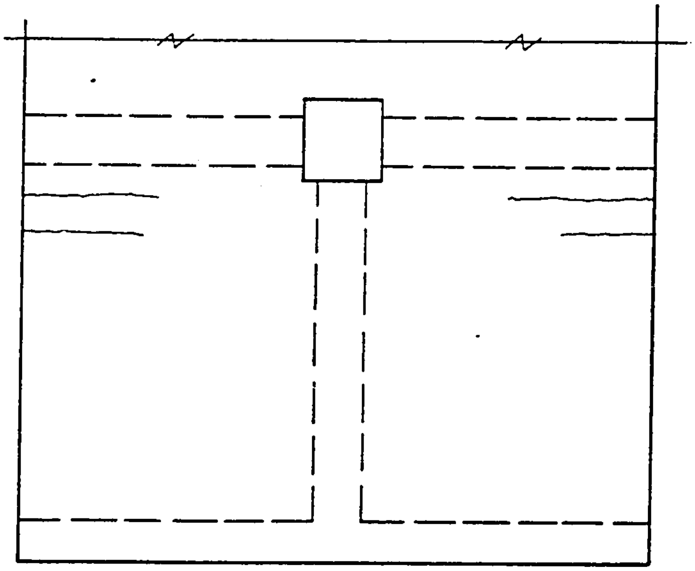

Bottom of the Slab

Fig. 4.3 Flexural cracks at bottom of slab under positive moment

in Fig. 4.4. Under negative bending moment, the top longitudinal beam bar yielded at a deflection level of 1.2 in. (D1.2). A substantial increase (about 20-25 percent) in the strength of the beam was recorded after the yielding of beam steel. This increase in the beam strength at higher deflection levels can be attributed to the strain hardening of the steel and the added participation of the slab as a flange of the T-beam. In Fig. 4.5 is shown the level of strain in two top longitudinal slab bars. One bar is close to the column (2 in., 5 cm), and the other is far from the column (58 in., 145 cm). The steel close to the longitudinal beam yields at about the same deflection level as the beam steel. At this deflection level the strain in the slab steel 58 in. from the column face is relatively small. At larger deflection levels (D3.6) the slab steel 58 in. from the column starts to show higher strains indicating a large contribution of slab steel to load resistance. Thus, it may be hypothesized that at low drift levels contribution of the slab to load resistance is small but, as deformations increase, the slab participation in resisting moments becomes much more significant.

Figures 4.6 and 4.7 shows the variation of strain in the top and bottom longitudinal slab steel, along the transverse beam, under the action of negative moment for the interior modified specimen. Slab steel strain profiles along the transverse beam for the other three specimens under negative moment are shown in Figs. 4.8 through 4.10. Under negative moment, the top steel shows higher tensile strain levels than the lower steel. At smaller deflection levels,

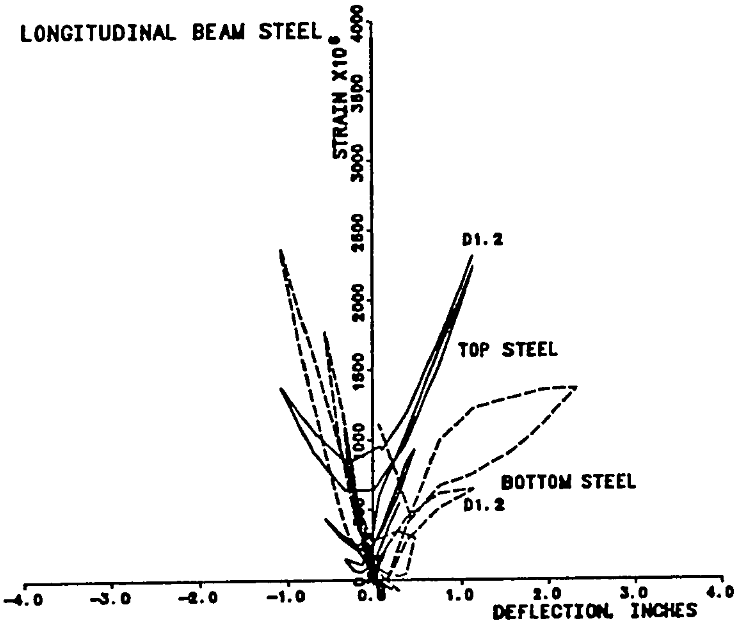

Fig. 4.4 Beam bar strains versus beam deflection,interior prototype

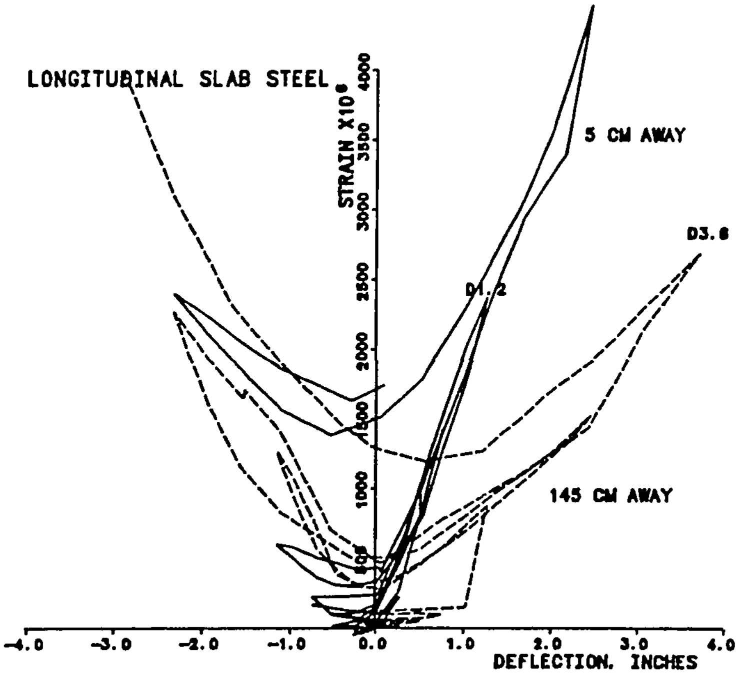

Fig. 4.5 Slab bar strain versus beam deflection, interior prototype

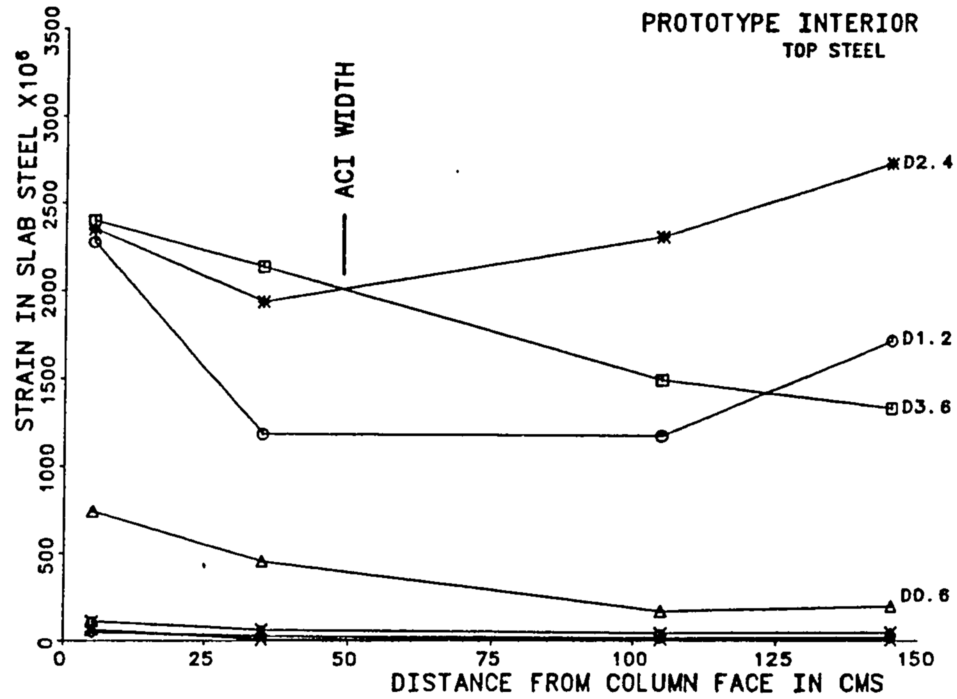

Fig. 4.6 Profiles of top slab steel strain under negative moment, interior prototype

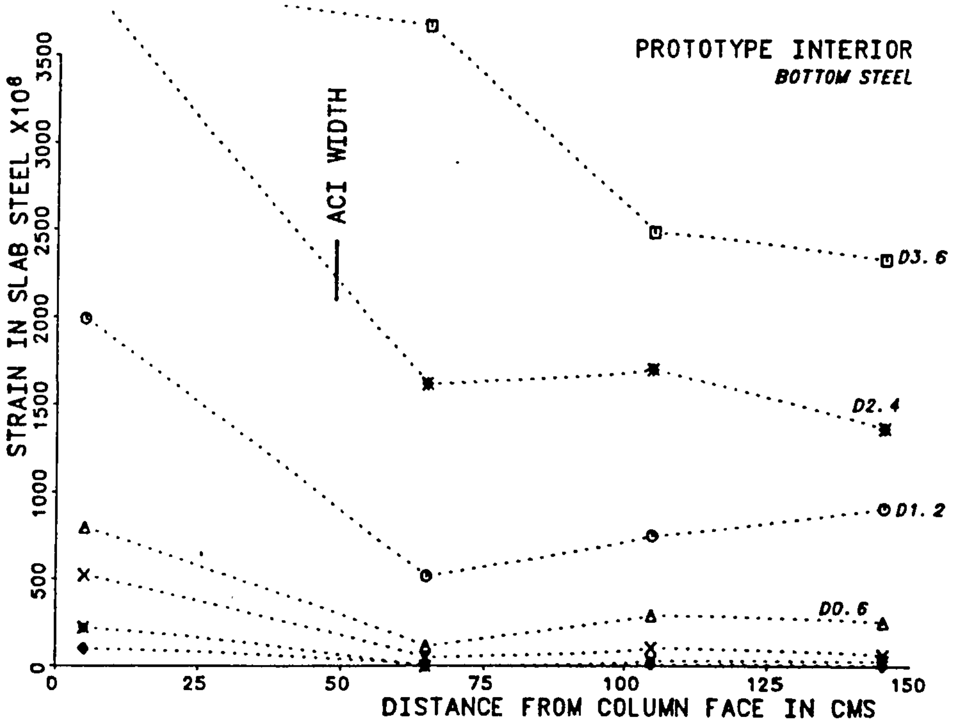

Fig. 4.7 Profiles of bottom slab steel strain under negative moment, interior prototype

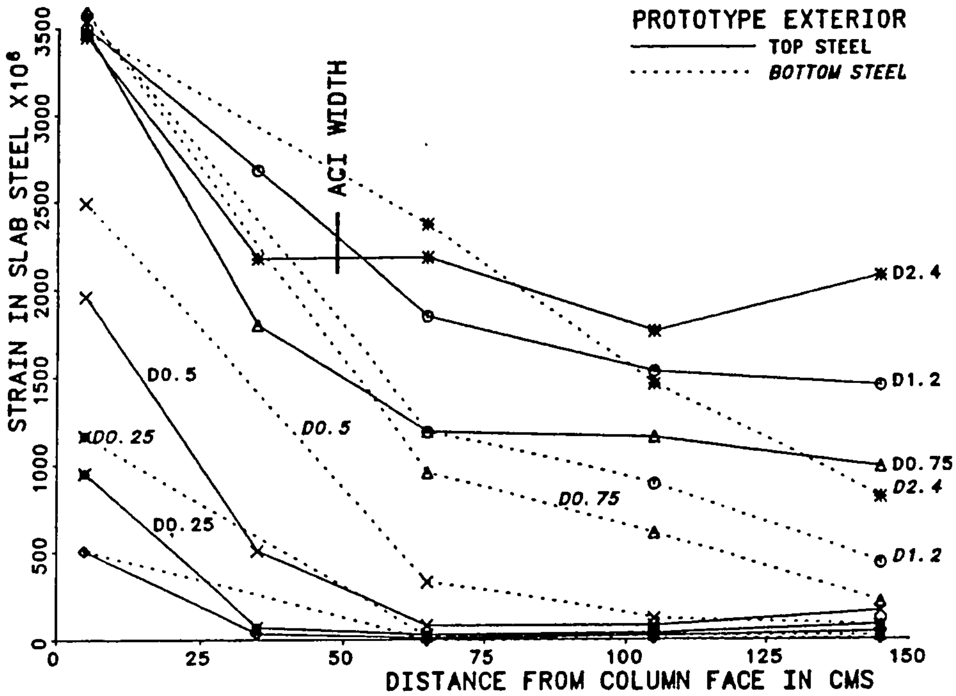

Fig. 4.8 Profiles of slab steel strains under negative moment, exterior prototype

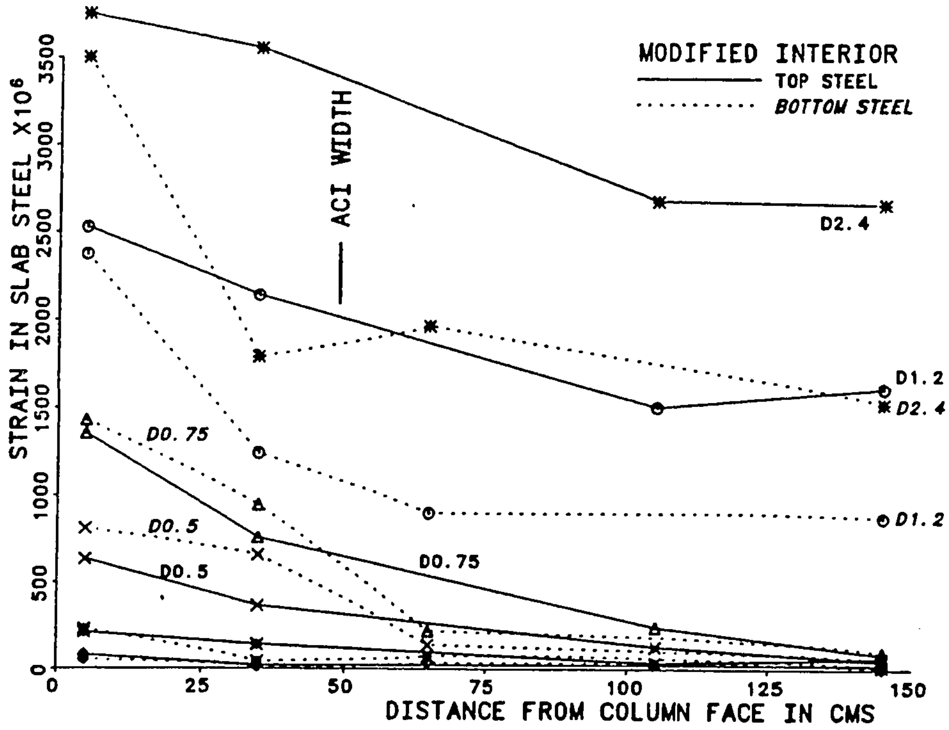

Fig. 4.9 Profiles of slab steel strains under negative moment, interior modified

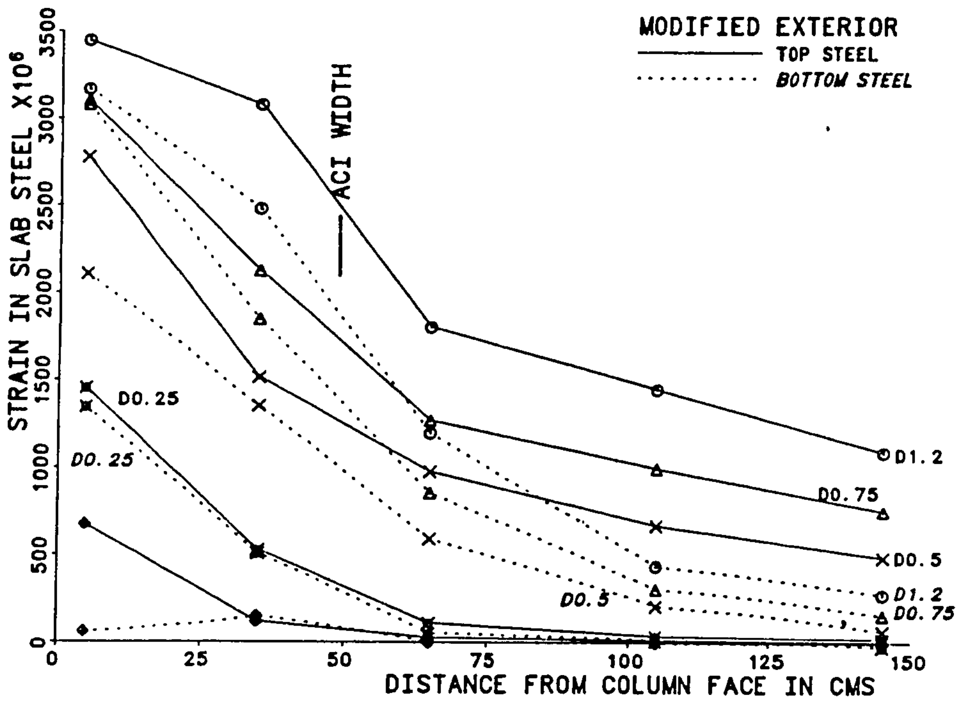

Fig. 4.10 Profiles of slab steel strain under negative moment, exterior modified

steel close to the column shows much larger strains than the steel further away. At early stages, the bottom steel close to the column shows much larger strains than the bottom steel away from the column, where strains are negligible. This would seem to indicate that at small deflection levels, the slab close to the beam was acting integrally with the beam whereas the slab away from the beam was acting as a shallow flexural section. The variation in strains could also result from the shear deformations in the flange, shear lag reducing the strains as the distance of steel increases from the web. At larger deflection levels even the bottom steel shows strains very close to yield strains. This could result from the fact that these bars experienced large strains when subjected to a positive moment in the previous load stages (see Fig. 4.13) and had large residual strains. Another explanation is that the load-resisting action of the slab changed from the shallow slab section, uncoupled or independent from the beam with a small lever arm and with compression at the bottom, to an effective flange of the longitudinal T-beam or coupled with the T-beam, with both the top and bottom slab steel acting in tension (see Fig. 4.11). It is likely that both phenomena contributed to the large bottom steel strains at large deflection levels.

The variation of strain in the top and bottom slab steel under positive moment for the interior modified specimen is shown in Fig. 4.12 and 4.13. The variation of strain for the other three specimens is shown in Figs. 4.14 and 4.16. The bottom steel shows

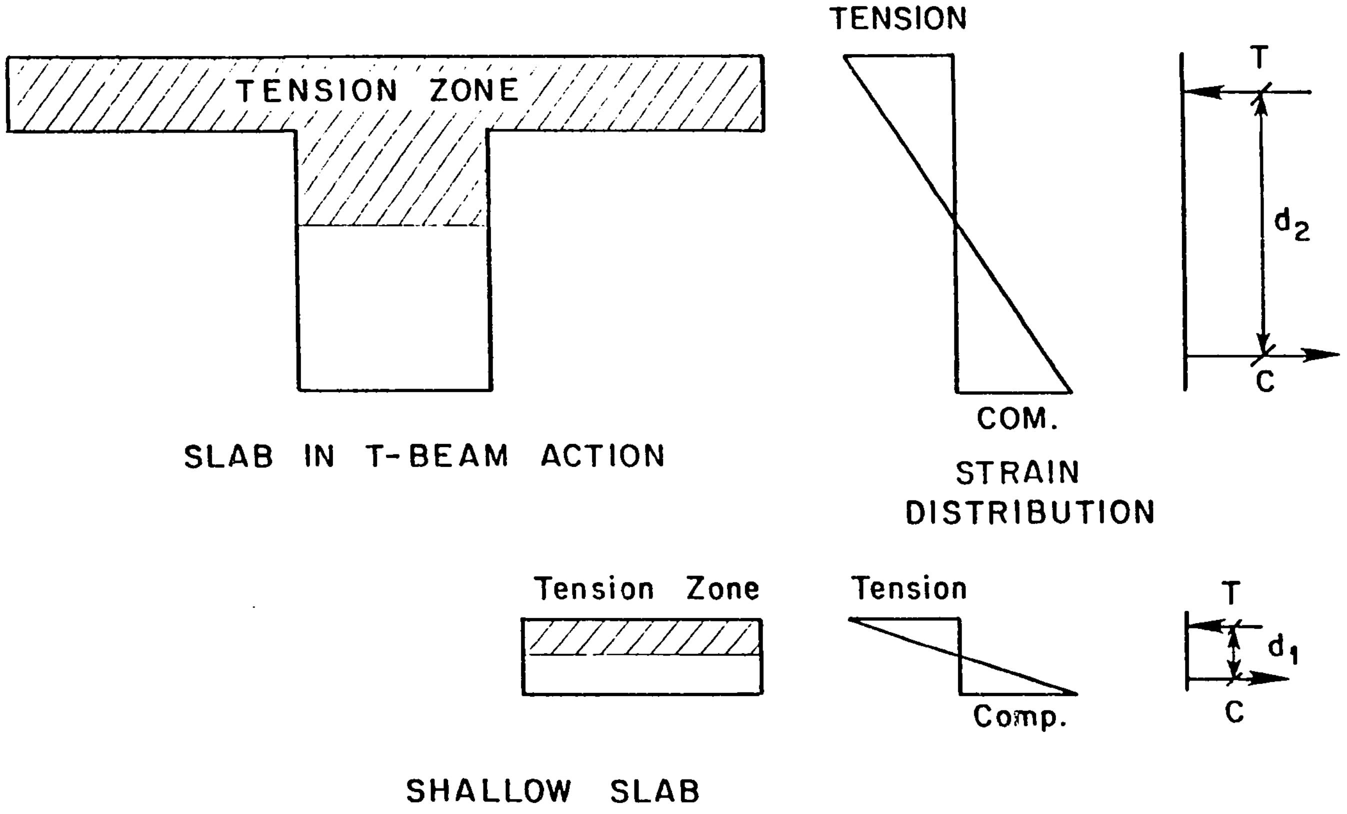
TENSION ZONE
SLAB IN T-BEAM ACTION
TENSION
COM.
STRAIN DISTRIBUTION
T
d_2
C
Tension Zone
Tension
Comp.
T
d_1
C
SHALLOW SLAB

Fig. 4.11 Flexural resistance of slab, flange of T-section, versus shallow slab section

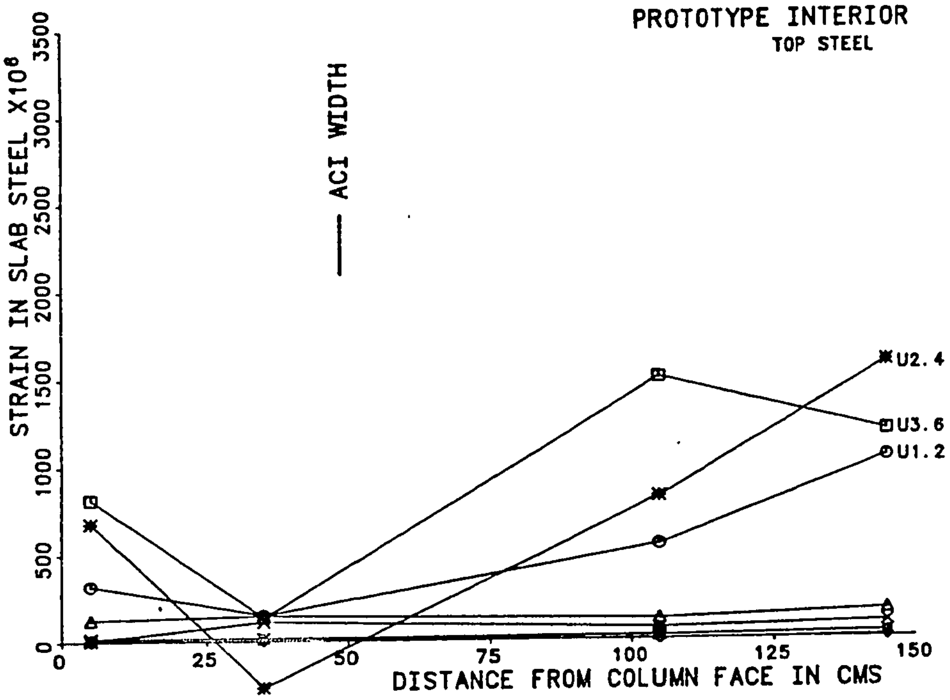

Fig. 4.12 Profiles of top slab steel strain under positive moment, interior prototype

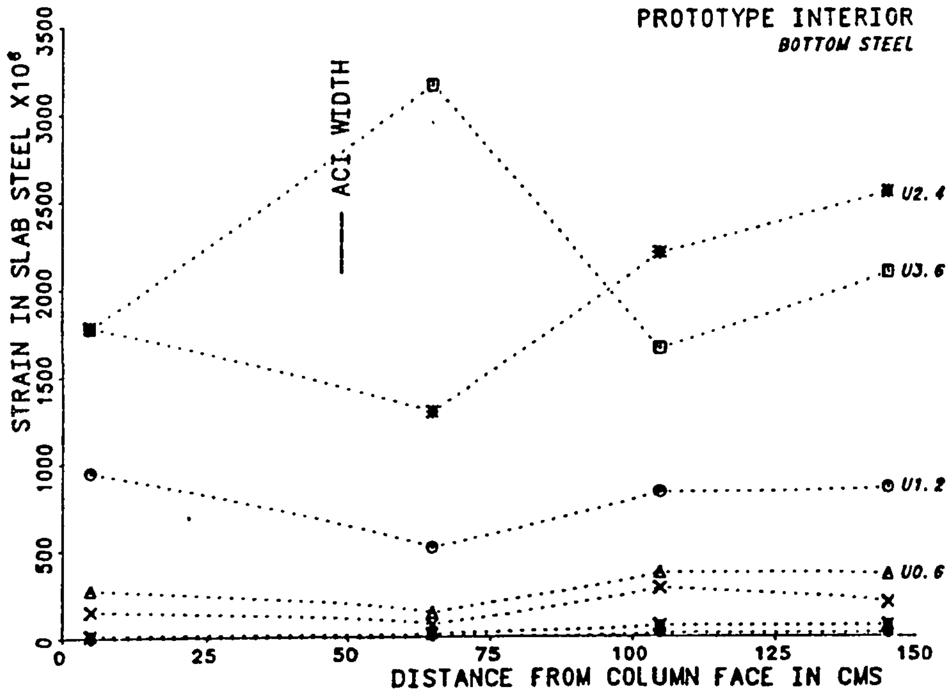

Fig. 4.13 Profiles of bottom slab steel strain under positive moment, interior prototype

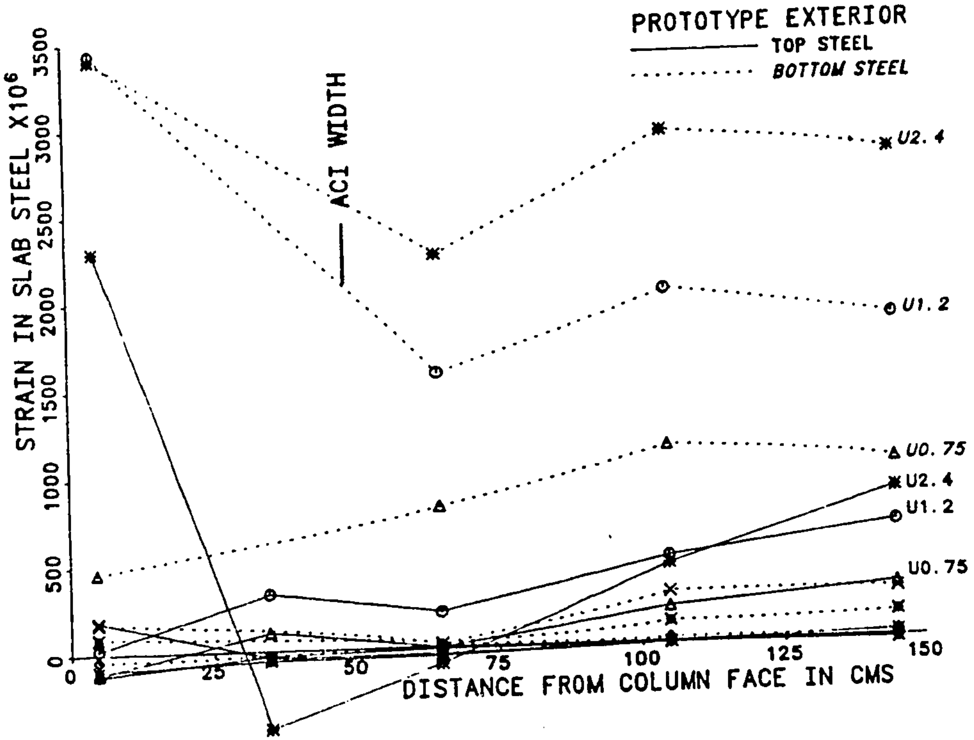

Fig. 4.14 Profiles of slab steel strain under positive moment, exterior prototype

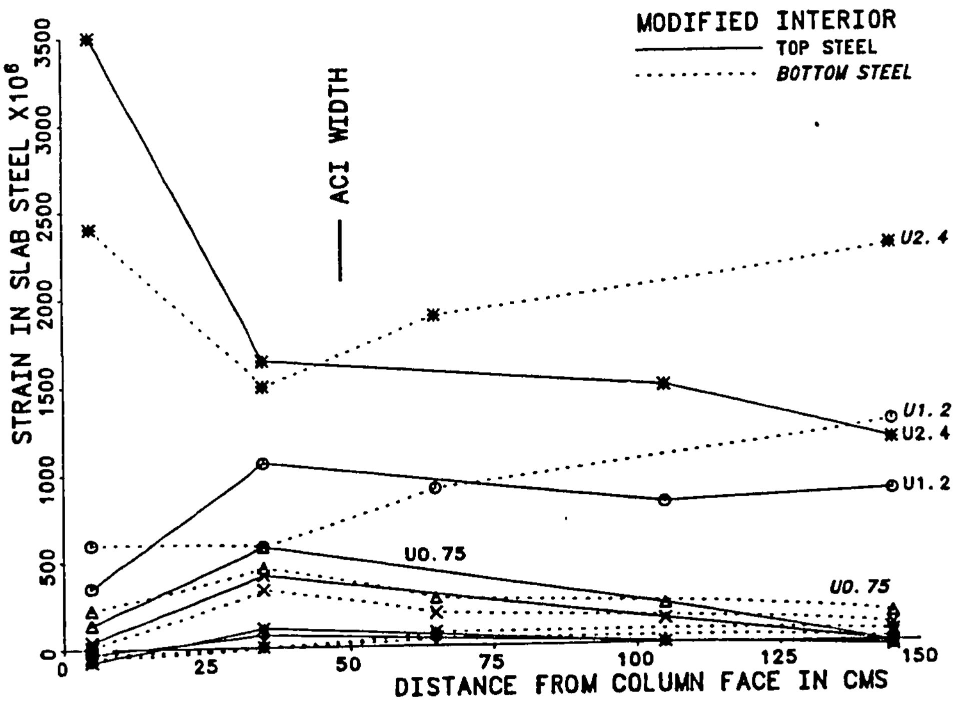

Fig. 4.15 Profiles of slab steel strain under positive moment, interior modified

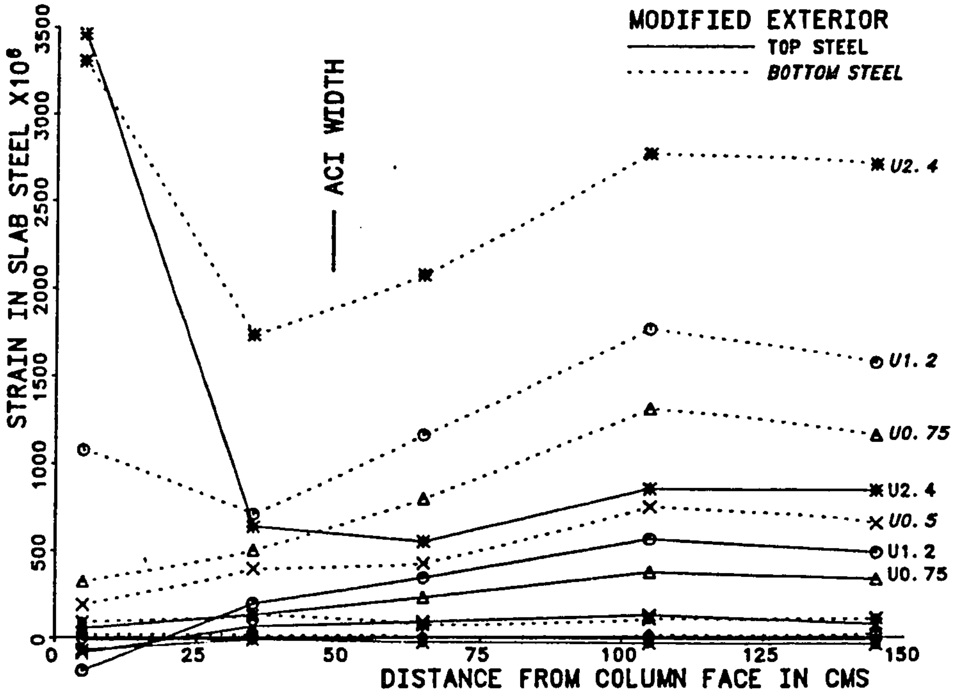

Fig. 4.16 Profiles of slab steel strain under positive moment, exterior modified

larger strains than the top steel. At large deflection levels the bottom slab steel farther from the column shows larger strains than steel close to the column because the part of the slab close to the column is acting as a compression flange of the longitudinal beam whereas the portions further away are acting independent from the beam as shallow flexural sections.

4.3 Torsional Rotations of the Transverse Beam

A typical envelope of the beam load versus torsional rotation of the transverse beam is shown in Fig. 4.17. The variation of the torsional rotation at a distance equal to the effective depth away from the column face and at the end of the beam for the exterior prototype specimen is shown. This plot was typical of the relationships between the torsional rotations at these two locations. The plot shows that the torsional rotation at these two locations is nearly the same at all deflection levels which means that relative torsional rotation between these two locations is very small. The torsional rotation is dependent on the torsion introduced into the transverse beam which in turn is an indication of the participation of the slab.

Most of the torsional distress in the transverse beam occurred very close to the column, the zone of large torque in the torque distribution diagram. After cracking, the transverse beam lost most of its torsional stiffness. The exterior prototype specimen, in which an anchorage failure occurred, showed the greatest

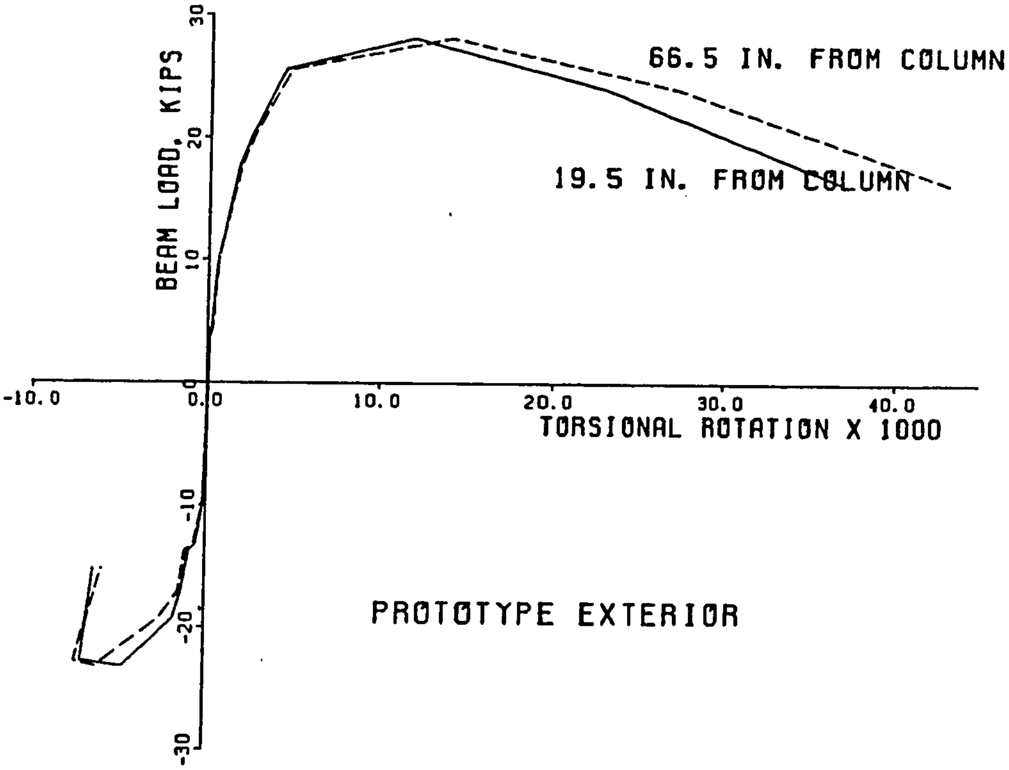

Fig. 4.17 Load versus torsional rotation along the length of transverse beam

torsional distress and provides an indication of the slab participation.

4.4 Summary

The discussion of behavior of the joint specimens indicates that there was a significant influence of the slab on the strength of the beam. The magnitude of the participation of the slab as effective tension flange width is a function of the deformation level with greater participation at larger deformations. The total flexural capacity in the direction of loading could be hypothesized to be the sum of the following two quantities: 1) the flexural strength of the longitudinal beam acting as a T-beam with a portion of the slab participating as the flange, and 2) the flexural strength of the remainder of the slab, acting as an isolated shallow flexural section. As shown in Fig. 4.11, the longitudinal slab steel within the width of the slab acting as a flange of the longitudinal beam is effective in resisting a large moment due to its larger effective depth (d2). The slab steel outside this width acts with a small lever arm (d1), thus resisting a much smaller moment. The question, then, is to determine how much of the slab participates as the tension flange of the longitudinal beam.

4.5 Comparison of Measured and Predicted Beam Slab Flexural Capacities

The measured loads are compared with the "predicted" loads in Table 4.1 for negative bending and in Table 4.2 for positive bending.

TABLE 4.1 Beam Strength-Negative Bending

	Moment in Kip-In.			
	Prototype		Modified	
	Int.	Ext.**	Int.	Ext.
Measured (Expt) Capacity*	3635	2415**	5480	5205
Computed Capacity:				
Beam only (A)*	1635	1615	3535	3625
Beam only (A) + slab (B)	2035	2015	4040	4130
ACI flange width beam (C)	2485	2460	4380	4515
ACI flange beam (C) + slab (D)	2780	2755	4760	4895
Full flange width beam (E)	4380	4340	6490	6760
Measured/Computed:				
Beam + slab	1.79	1.20	1.37	1.27
ACI beam + slab	1.32	0.88	1.15	1.06
Full width beam	0.83	0.56	0.85	0.77

* Refer to Fig. 4.18
** Anchorage failure

TABLE 4.2 Beam Strength-Positive Bending

	Moment in Kip-In.			
	Prototype		Modified	
	Int.	Ext.**	Int.	Ext.
Measured (Expt) Capacity	1580	2003	2950	4250
Computed Capacity:				
Beam only (A)*	1200	1195	2405	2465
Beam only (A) + slab (B)*	1600	1595	2910	2970
ACI flange width beam (C)*	1810	1805	3335	3480
ACI flange width beam (C) + slab (D)*	2105	2100	3715	3860
Measured/Computed:				
Beam only + slab	0.99	1.26	1.01	1.43
ACI beam + slab	0.75	0.95	0.79	1.1
Full width beam	0.71	0.90	0.73	1.04

* Refer to Fig. 4.19

** Anchorage failure

The exterior prototype specimen exhibited an anchorage failure and cannot be compared on the same basis as the other three tests. The assumptions involved in predicting the moment capacities are presented below.

Both the positive and the negative flexural capacities of the longitudinal beam were computed for three different assumed flange widths. Estimates of the flexural strength were made using only the beam rectangular section, the ACI compression flange effective width of 59 in. was also assumed valid for the tension width and the full slab width of 157.5 in. as effective flange (see Sec. 2.10.2, "Member Strengths"). It was assumed that the part of the slab not acting as the flange of the longitudinal beam reached and maintained its maximum capacity as a shallow slab until the specimen reached its maximum moment capacity. This hypothesis leads to an upperbound to the actual flexural capacity. It is apparent that the full capacity of the shallow slab section will not be reached simultaneously with the longitudinal beam. Even after the longitudinal beam has reached its ultimate capacity and initiated redistribution of internal forces, a complete redistribution resulting in all the flexural members reaching their maximum capacities may not be accomplished. But it is certainly a conservative assumption which results in overestimation of the available strength. The strength of the specimen was also computed as the sum of the capacity of the beam (with the assumed flange width) and the nominal capacity of the remaining slab.

Figure 4.18 shows the comparative strengths, computed using the actual material properties.

The measured capacities are obtained as a product of the measured beam end load and the distance between the point of application of the load and the column face. This implies that the comparisons between the measured and predicted capacities are made at the column face. Measured capacity would be slightly higher (2-3 percent) if comparison is made at the intersection of the slab with the transverse beam.

Ratios of measured capacity to that predicted using the reinforcement within the ACI effective flange width, for the case of negative bending, shows that use of ACI effective flange width results in underestimation of the strength over a range of 6 percent (exterior modified) to 32 percent (interior prototype). The assumption that the full slab width acts as a tensile flange results in a severe (18 to 30 percent) overestimation of the available strength. Thus, it appears that a greater slab width than that prescribed by ACI was effective (in these tests) as the negative flange of the T-beam at ultimate. The need for realistic guidelines to compute the negative bending moment capacity of the floor system is obvious.

Under positive bending (Table 4.2), the ratios of measured capacity to that predicted using ACI effective flange width provisions, show that the ACI estimate is fairly accurate (within 5 percent) for the exterior joint specimens, but overestimates the

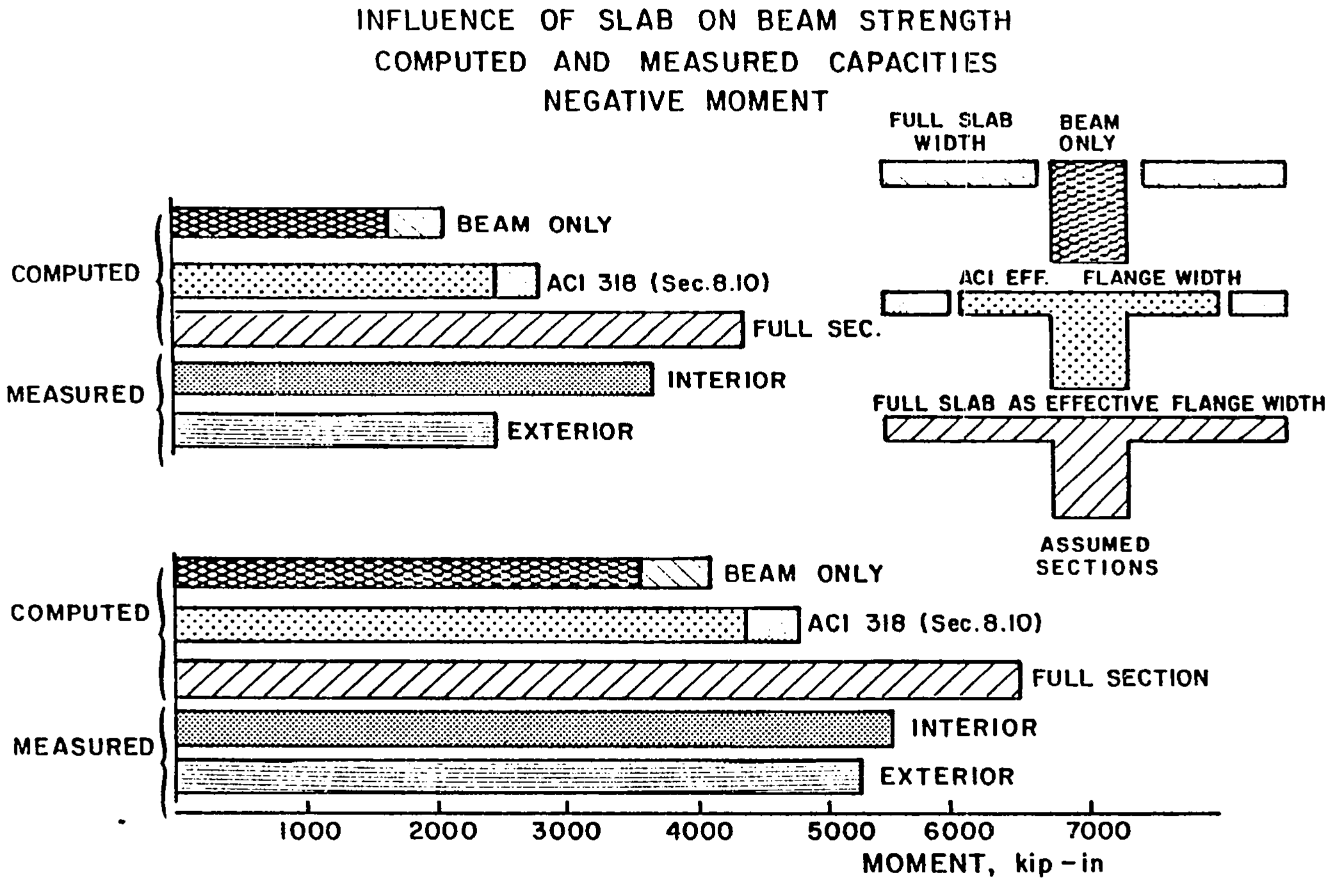

Fig. 4.18 Influence of slab on floor strength, negative moment

strength by about 25 percent (modified specimen) to 33 percent (prototype specimen) for the interior specimens. Figure 4.19 shows the comparative strengths computed using actual material properties. The beam load versus beam end deflection envelopes for the four specimens (see Fig. 4.20) show that exterior joints were much stronger in positive bending (slab in compression) than the interior joint specimens. For the interior joint, a positive moment on one side is also accompanied by a larger negative moment on the other side of the joint. The negative moment induces large tension in the the beam steel and the slab steel. Due to factors such as bond deterioration and slip of this reinforcement, the "compression steel" in the positive bending direction may actually be in tension. The strain observations for longitudinal beam and slab bars confirm this hypothesis. Tension in "compression steel" would result in a reduction of the lever arm and thus a reduction in the strength.

The increased participation of the slab is a function of deformation level. It is important to determine the slab contribution at deformations much in excess of average story drift levels as local deformation levels could exceed average story drift levels.

4.6 Relative Strength of Columns to Beams

4.6.1 Review of Current Code Procedures.

In general, the code provisions for design of frame structures in seismic zones are based on the development of plastic hinges in the beams rather than

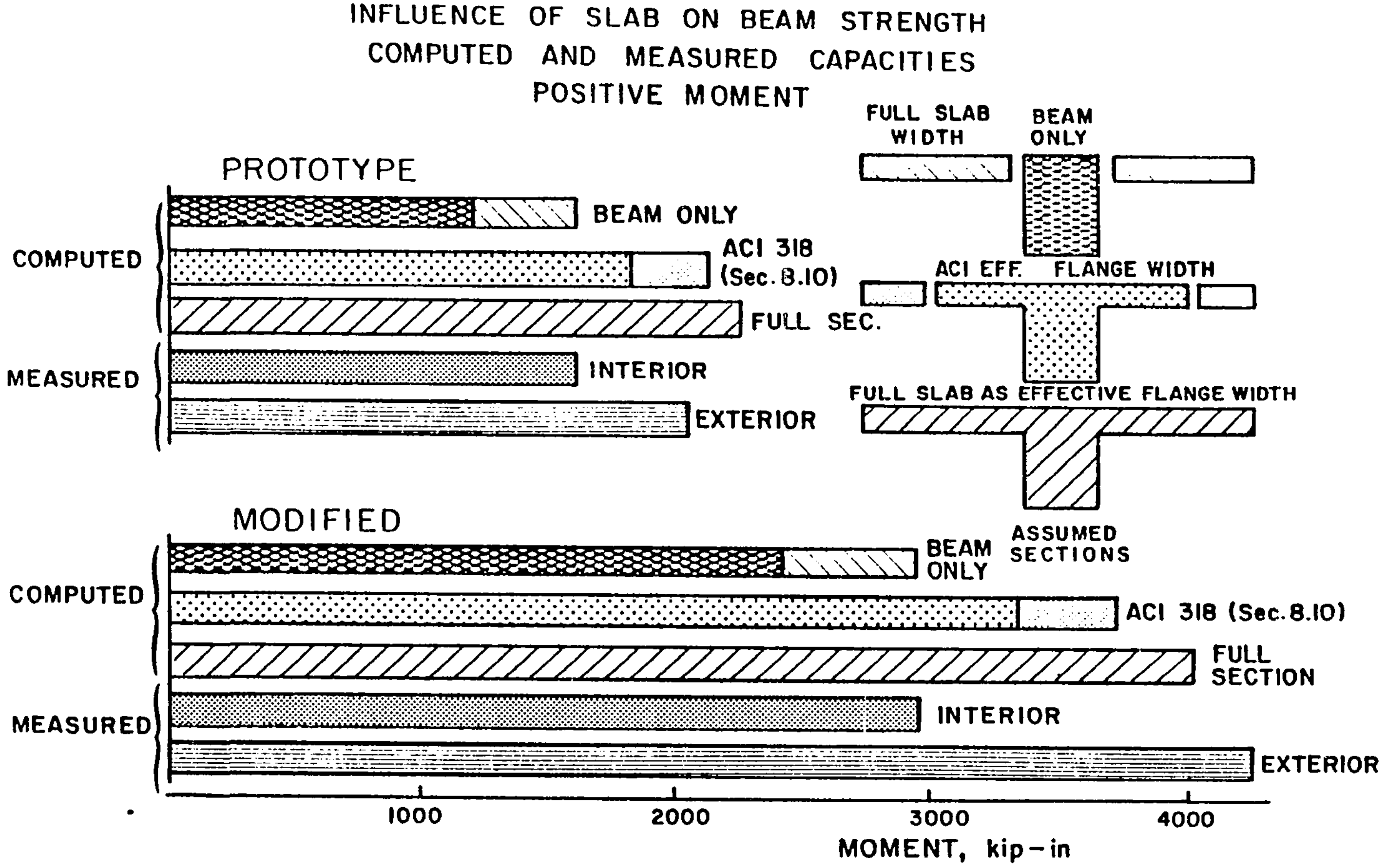

Fig. 4.19 Influence of slab on floor strength, positive moment

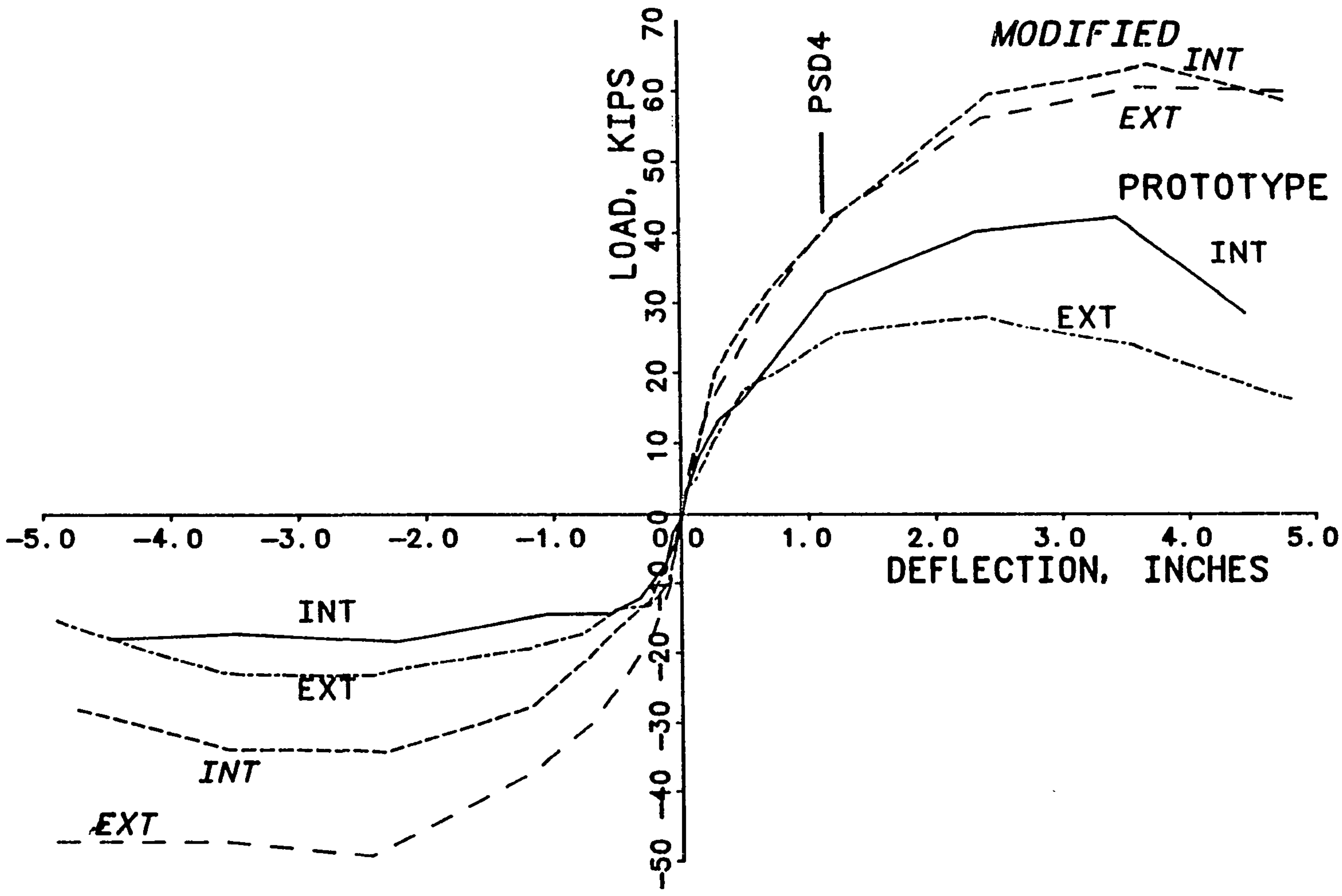

Fig. 4.20 Load versus deflection envelopes for test specimens

in the columns for two main reasons: 1) formation of column hinges permits development of a single-story sidesway mechanism involving relatively few hinges, and hence little energy dissipation, and 2) column hinging threatens the integrity of vertical load resistance mechanism of a frame structure.

In both the SEAOC [13] and the Uniform Building Code [9], this is achieved by the following clause:

> DESIGN LIMITATIONS: At any beam-column connection where $P_u/A_g \geq 0.12 f_c'$, the total ultimate moment capacity of the column at the design earthquake axial load shall be greater than the total ultimate capacity of the beams, along the principal planes at that connection.

The SEAOC commentary for the clause reads:

> The column at a joint which is providing the primary vertical support for the structure (i.e., where $P_u.A_g$ is greater than $0.12 f_c'$) is required to have a greater total ultimate moment capacity than the beams at the beam-column connection. This is to minimize the development of a single-story collapse mechanism.
>
> In comparing the ultimate capacities, it is not considered necessary to correct for different ϕ factors, differences between specified and actual steel and concrete strengths, and column strength reduction factors since these factors are assumed to be self-compensating in the overall comparison.

In the ACI Code the clause dealing with the relative column strength has been revised in the ACI 318-83 Appendix A. Clause A6.2 in ACI 318-77 [1] states:

> At all beam-column connections, the sum of moment strengths of columns at factored axial loads shall be greater than the sum of the moment strengths of flexural members along each principal

> plane at that connection, unless the sum of moment strengths of confined column cores is sufficient to resist applied factored loads.

The revised ACI 318-83 (Clause A.4.2.2) [2] version states:

> A.4.2--Minimum flexural strength of columns
>
> A.4.2.1--Flexural strength of any column proportioned to resist a factored axial compressive force exceeding ($A_g f_c'/10$) shall satisfy Section A.4.2.2 or A.4.2.3.
>
> Lateral strength and stiffness of columns not satisfying Section A.4.2.2 shall be ignored in determining the calculated strength and stiffness of the structure but shall conform to Section A.8.
>
> A.4.2.2--The flexural strengths of the columns shall satisfy Eq. (A.1)
>
> $$M_e \geq (6/5) \quad M_g \qquad (A.1)$$
>
> M_e = sum of moments, at the center of the joint, corresponding to the design flexural strength of the columns framing into that joint. Column flexural strength shall be calculated for the factored axial force, consistent with the direction of the lateral forces considered, resulting in the lowest flexural strength.
>
> M_g = sum of moments, at the center of the joint, corresponding to the design flexural strengths of the girders framing into that joint.
>
> Flexural strengths shall be summed such that the column moments oppose the beam moments. Eq. (A.1) shall be satisfied for beam moments acting in both directions in the vertical plane of the frame considered.

Unfortunately, the Code provisions will not prevent the formation of hinges in the column. The column moments for earthquake design are generally computed using the equivalent static load. Under the application of this static load points of contraflexure generally exist close to the midpoints of all but the top and bottom story columns. If the point of contraflexure in a column occurs away from the mid height, when the structure resists an earthquake, then a larger column capacity than that prescribed by clause A6.2 (ACI 318-77) is required to prevent hinging in the columns. Earthquakes generally will not act in the principal direction of a structure. Biaxial bending can result in increasing the moments introduced by the beams into the columns, resulting in column hinging. The code does not indicate how biaxial bending can be accounted for. It is beneficial to prevent formation of plastic hinges in the columns, but under certain circumstances it may not be possible to avoid plastic hinging of the columns.

The code provisions tacitly assumed that the flexural capacities of the framing beams can be accurately determined. An explanation of the relative beam-column strength clause in the commentary of the ACI 318-77 code reads:

> A.6.2 and A.6.3--It is desirable to have plastic hinges form in the beams rather than in the columns. The Code, therefore, required that the moment strengths of the columns exceed those of the beams at a connection except when special provisions are made. . . .

Unfortunately, the contribution of the slab as a part of the flexural member along the principal plane is not even mentioned in the commentary. In the revised version (ACI 318-83) of the clause, the term "flexural members" has been replaced by "girders." This still does not clarify how much of the slab should be considered as an integral part of the girder. Guidelines are needed to address the inclusion of a portion of the slab as an integral part of the T-beam. The necessity of ensuring a larger column strength is realized in the 318-83 Code by requiring that the sum of the strength of the columns be at least 20 percent higher than the sum of the strength of the girders.

The commentary to the SEAOC code considers understrength factors self-compensating with other differences in calculating the capacities of the beams and the columns. This could lead to unconservative designs if the actual materials used in the beams are stronger than their nominal strengths. When computing the shear in the joint, all three codes (ACI, SEAOC and UBC) require that the forces at the joint faces be determined by assuming that flexural tensile reinforcement is stressed to 1.25 f_y to get an upper limit on the shear stress in the joint. The fact that overstrength of flexural steel is common is also realized. It therefore seems reasonable to suggest that some kind of safety margin should be introduced in the relative beam-column strength equations and the computation of the various quantities involved in order to ensure that floor flexural strength is not underestimated.

The lack of specific guidelines to compute the flexural capacity of a T-beam with a tension flange is apparent. It is necessary to incorporate a clause in the ACI code to handle a T-beam with a tension flange.

4.6.2 Comparison of Measured and Computed Relative Column Capacities. Table 4.3 shows the ratios of the sum of the column strengths (computed) to the sum of the beam strengths (i) measured, ii) predicted using different flange width assumptions) for the interior joint specimens. This consideration is not very critical for the exterior joints as beam moments exist only on one side of the column.

The measured ratios were all greater than one. Little distress was visible in the column and the behavior of the specimens was excellent. Using only the capacity of the beam section in designing the column would have resulted in underdesigning the column. The strength ratios predicted by using the ACI effective width as a flange of the beam section for both tension and compression flanges , and without consideration of the remaining slab, are 27 percent (unconservative) higher than the observed ratios for the interior prototype, and 11 percent higher (unconservative) for the interior modified. The addition of the flexural capacity of the remaining portion of the slab to the above T-beam capacity in computing the total flexural strength in the principal plane results in a fairly close but still unconservative solution. It is, therefore, important to include the slab as a flexural member along the principal plane.

4.7 Need for Analytical Studies

Comparisons of test results with current design procedures showed that current design procedures [1,2,9,13] do not adequately

TABLE 4.3 Relative Strength of Column to Beams, Interior Specimens

	PROTOTYPE INTERIOR			MODIFIED INTERIOR		
Predicted nominal column capacity	3340 kip-in.			5260 kip-in.		
	+ Ve Moment kip-in.	- Ve Moment kip-in.	$\frac{M_c}{M_b}$	+ Ve Moment kip-in.	- Ve Moment kip-in.	$\frac{M_c}{M_b}$
Measured capacity	1580	3635	1.28	2950	5480	1.25
Computed:						
Beam only (A)	1200	1635	2.36	2405	3535	1.77
ACI effective width as flange (C)	1810	2485	1.55	3335	4380	1.36
Full width (E)	2220	4380	1.01	4025	6490	1.00
Beam only + slab (A + B)	1600	2035	1.83	2910	4040	1.51
ACI flangebeam + slab (C + D)	2105	2780	1.37	3715	4760	1.24

reflect actual behavior. It was not possible to suggest specific design procedures based on experimental data and the simple analytical approach previously described. It was therefore necessary to conduct detailed analytical studies to better understand the behavior of the slab systems. A nonlinear finite element analysis was conducted. Results from these analytical studies are presented in the next chapter.

CHAPTER V

COMPARISON OF EXPERIMENTAL AND ANALYTICAL RESULTS

5.1 Introduction

The experimental results showed that under negative moment, flexural capacities of the slab-beams of the specimens significantly exceeded the capacities estimated using either the beam section alone or the ACI effective width provisions. Under positive moment, the flexural capacity of the slab system is not very sensitive to the assumed effective width because for under-reinforced sections the flexural capacity is governed by the amount of bottom longitudinal beam steel.

Analytical studies were deemed necessary to better understand some of the experimental results, to predict the behavior of floor systems under lateral loads, and to develop design guidelines. The two-part behavior of the slab hypothesized from experimental results as the sum of 1) a certain width acting as flange of the T-beam and 2) the remaining slab acting as a shallow flexural section, needed analytical verification. Effective flange widths of beams have usually been determined elastically for compression flanges. However, the experimental results reported here showed that behavior of the test specimens was quite different in the inelastic versus elastic range. It was also observed that the level of participation of the slab was a function of the drift level.

Hence, an inelastic analysis which could closely represent the actual behavior was necessary. The analytical investigation consisted of elastic and inelastic finite element analyses of the test specimens.

Results from the analytical investigation are presented and compared with experimental results. Based on these comparisons, a method for computing the negative moment capacity of a reinforced concrete slab system is presented.

5.2 Analytical Model

5.2.1 Objectives. The primary objective of the analysis was to study the response of the slab-beam-column connection under lateral deformations. The specific objectives were:

1. to determine the interaction of the slab and the beam;
2. to determine the strength and stiffness of the beam-slab system before and after cracking; and
3. to compare analytically predicted crack patterns with those observed during testing.

5.2.2 Choice of Finite Element Program. The finite element analysis was carried out using ABAQUS, a commercial finite element package program distributed by Hibbitt, Karlsson & Sorenson, Inc. [6,7,8]. The program is capable of handling reinforced concrete modeling including cracking in the concrete, yield of reinforcement and post-cracking behavior.

It was originally proposed to use the program to determine the entire load-deflection curves for the test specimens. However, the entire curve could not be determined from the nonlinear finite element analysis. The version of the program available at the time (version 4-5-22) had limitations in handling 1) yielding of reinforcing steel, and 2) convergence at larger deflection levels (see discussion in Appendix A). Analytical results were obtained up to a beam end deflection of 0.7 in., corresponding to an average story drift of about 0.8 percent.

5.3 Geometry

The specimen was symmetric about its centerline in the direction of loading, both in terms of geometry and loading. Taking advantage of this symmetry, only one-half of the specimen had to be modeled, as shown in Fig. 5.1. Two types of elements, a three-node curved beam in space (B32) and an eight-node shell with reduced integration (S8R) were used. Both beam and shell elements had six degrees of freedom at each node. The B32 beam element allows both flexural, shearing and axial deformations, and was formulated using Timoshenko beam theory. The shell element allows flexural, shearing and in-plane axial deformations. Several integration points can be assigned on both beam and shell sections, and element stiffnesses are obtained by numerical integration.

The slab was discretized by a 3 x 6 mesh of eight-node shell elements, shown in Fig. 5.2. Since stresses were expected to vary sharply near the column, a finer grid with smaller size elements was used there. The slab was divided into three elements in the

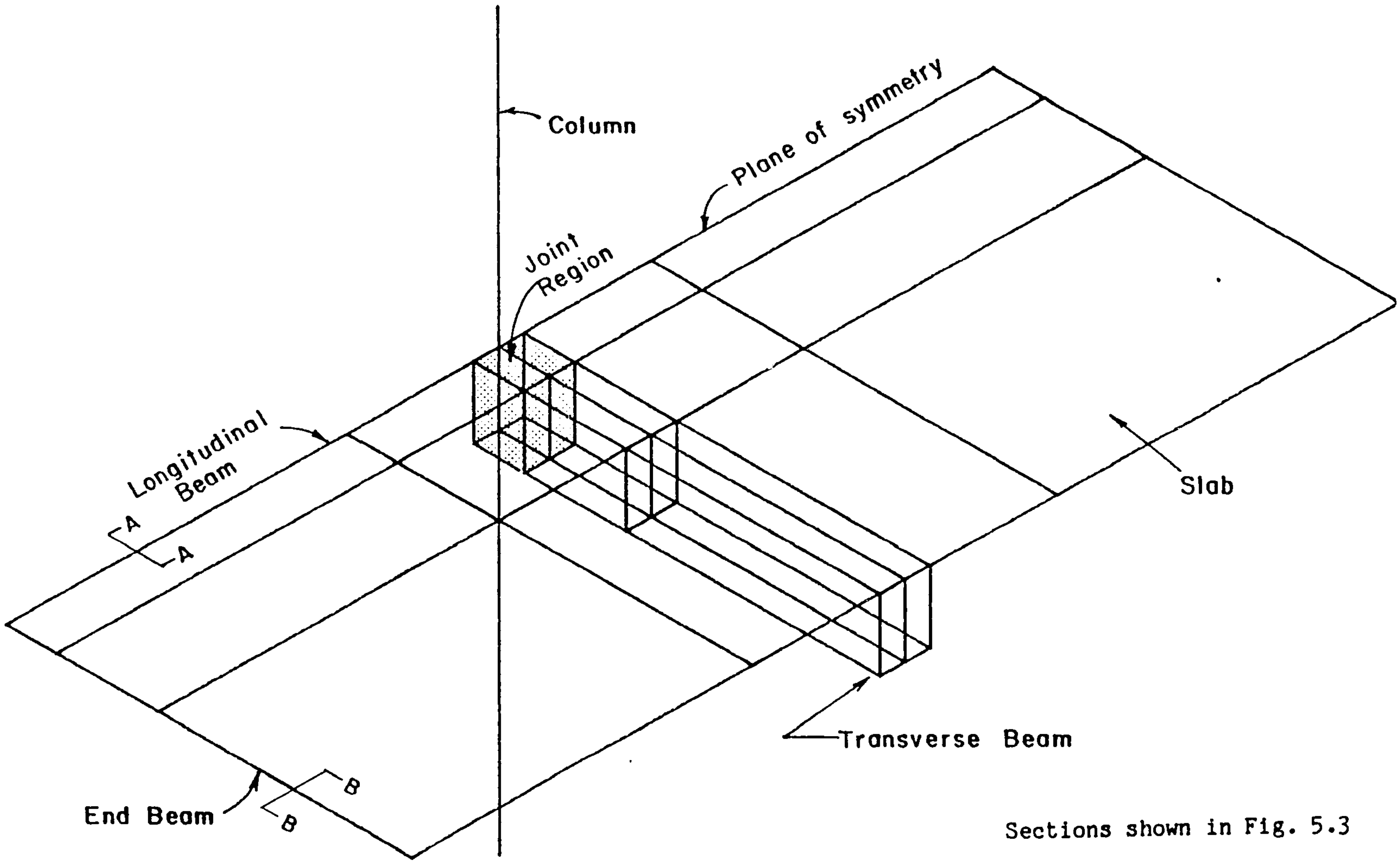
Column
Plane of symmetry
Joint Region
Longitudinal Beam
A
A
Slab
Transverse Beam
End Beam
B
B

Sections shown in Fig. 5.3

Fig. 5.1 Finite element model of test specimen

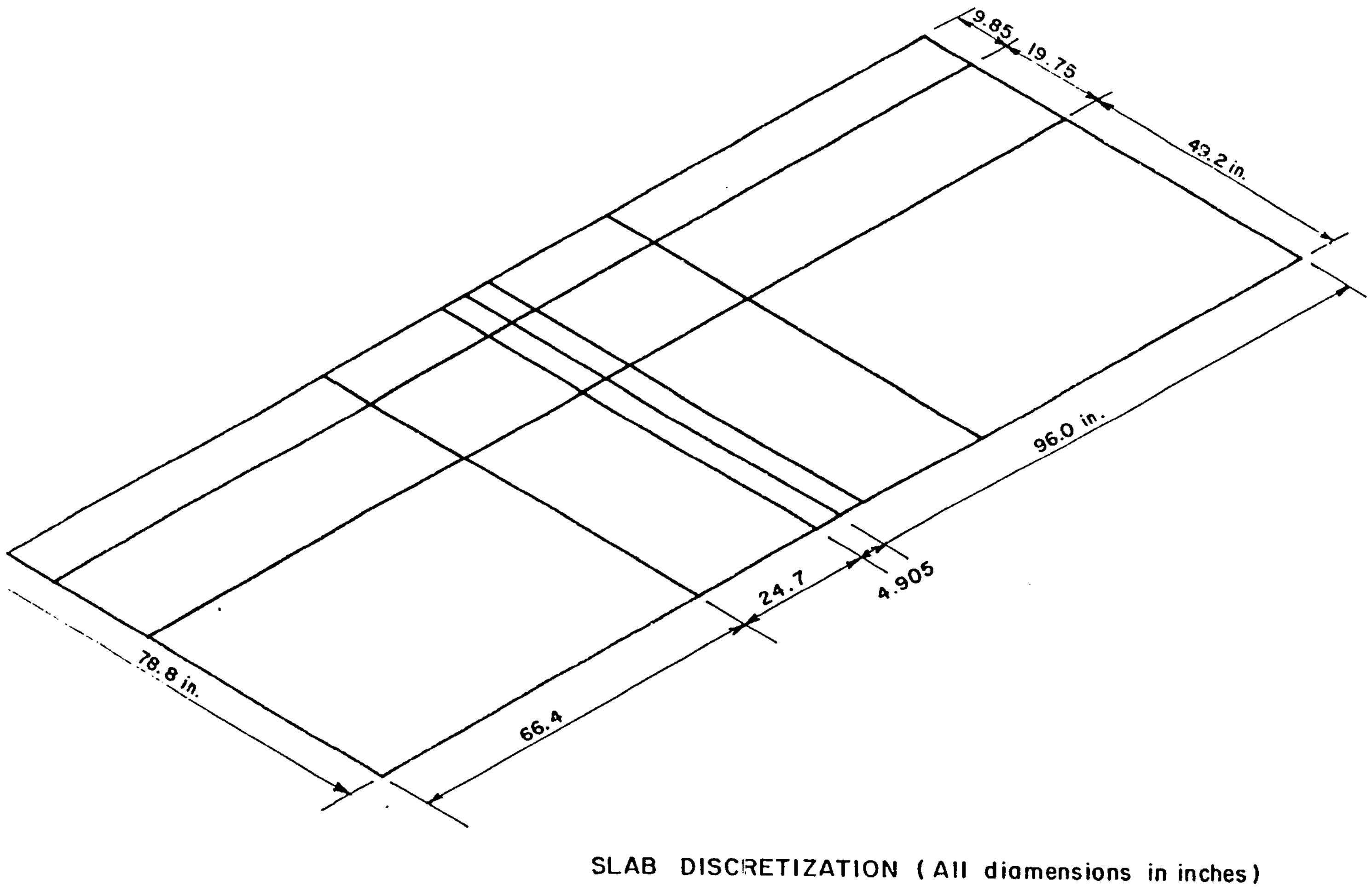
9.85
19.75
43.2 in.
96.0 in.
4.905
24.7
66.4
78.8 in.
SLAB DISCRETIZATION (All diamensions in inches)

Fig. 5.2 Slab discretization

transverse direction. The width of the first row of elements represented half the column width; the second row of elements was as wide as the depth of the longitudinal beam. Three rows of elements were used on either side of the column in the longitudinal direction. The length of the first row was nearly half the width of the transverse beam. The length of the second row was equal to the depth of the longitudinal beam. The thickness of the shell elements was equal to the slab thickness. Two layers of longitudinal and transverse slab reinforcement were specified at appropriate depths as smeared steel layers.

The longitudinal beam was modeled as a stiffener attached to the shell elements of the slab (Fig. 5.3). A rectangular beam section with width equal to half the width of the longitudinal beam (due to symmetry), and depth equal to that of the longitudinal beam was used as a stiffener. The longitudinal beam steel was specified as individual reinforcing bars in appropriate locations.

Since the beam elements warping torsion, nor of including the effects of transverse reinforcement, the transverse beam was modeled as a tube made of three vertical shell elements, connected at the top by the horizontal shell elements of the slab, and at the bottom by another set of horizontal shell elements (Fig. 5.4). The sum of the thickness of the three vertical shell elements equaled the width of the transverse beam. The thickness of the two vertical side shell elements and the bottom shell elements was determined considering the effective wall thickness for rectangular reinforced

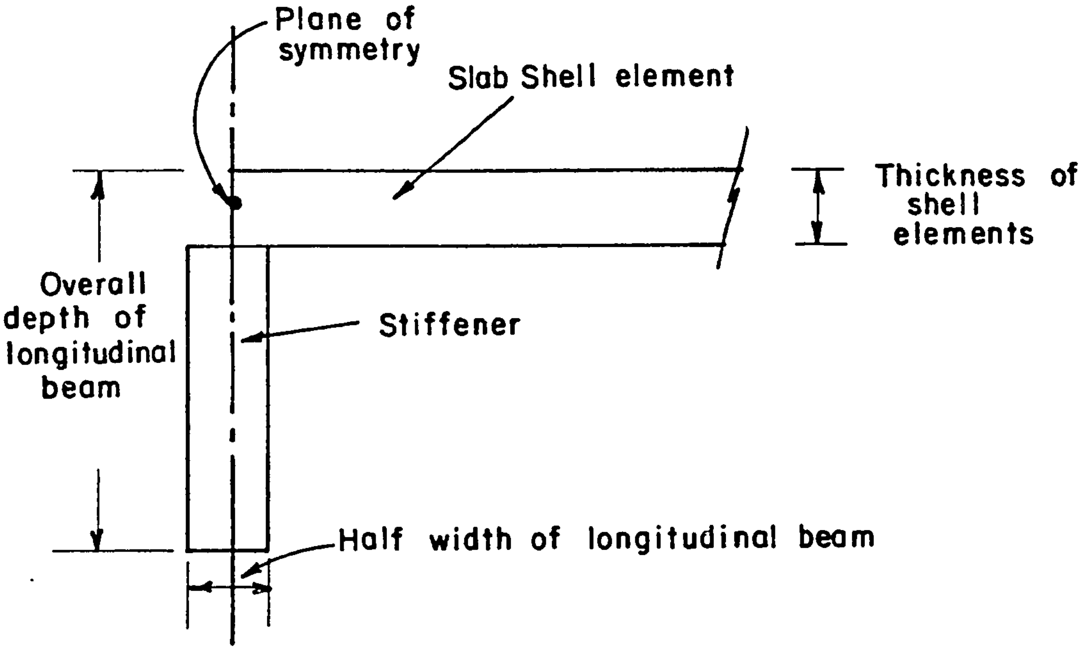
Plane of symmetry
Slab Shell element
Thickness of shell elements
Overall depth of longitudinal beam
Stiffener
Half width of longitudinal beam

SECTION OF A-A LONGITUDINAL BEAM

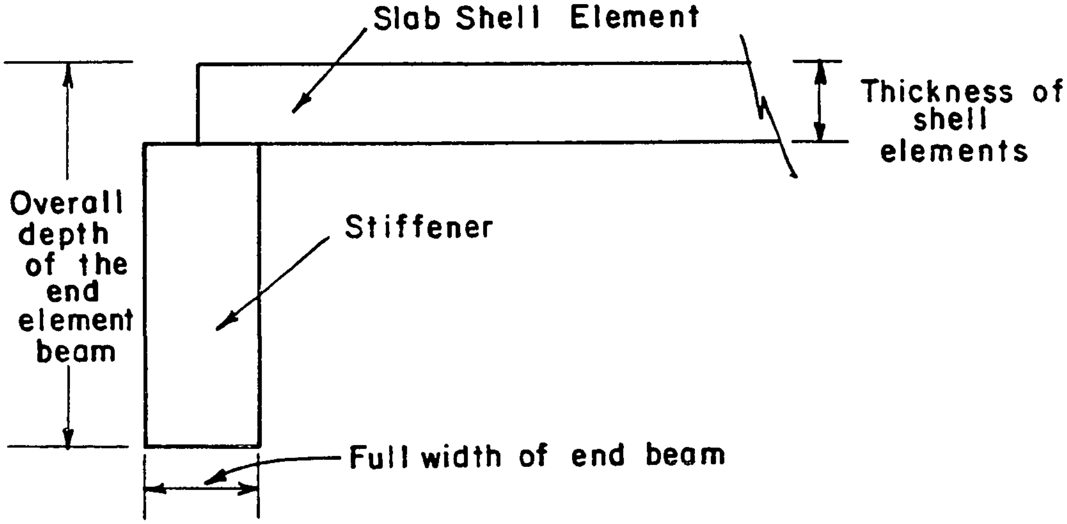
Slab Shell Element
Thickness of shell elements
Overall depth of the end element beam
Stiffener
Full width of end beam

SECTION B-B END BEAM

Sections from Fig. 5.1

Fig. 5.3 Longitudinal and end beam sections

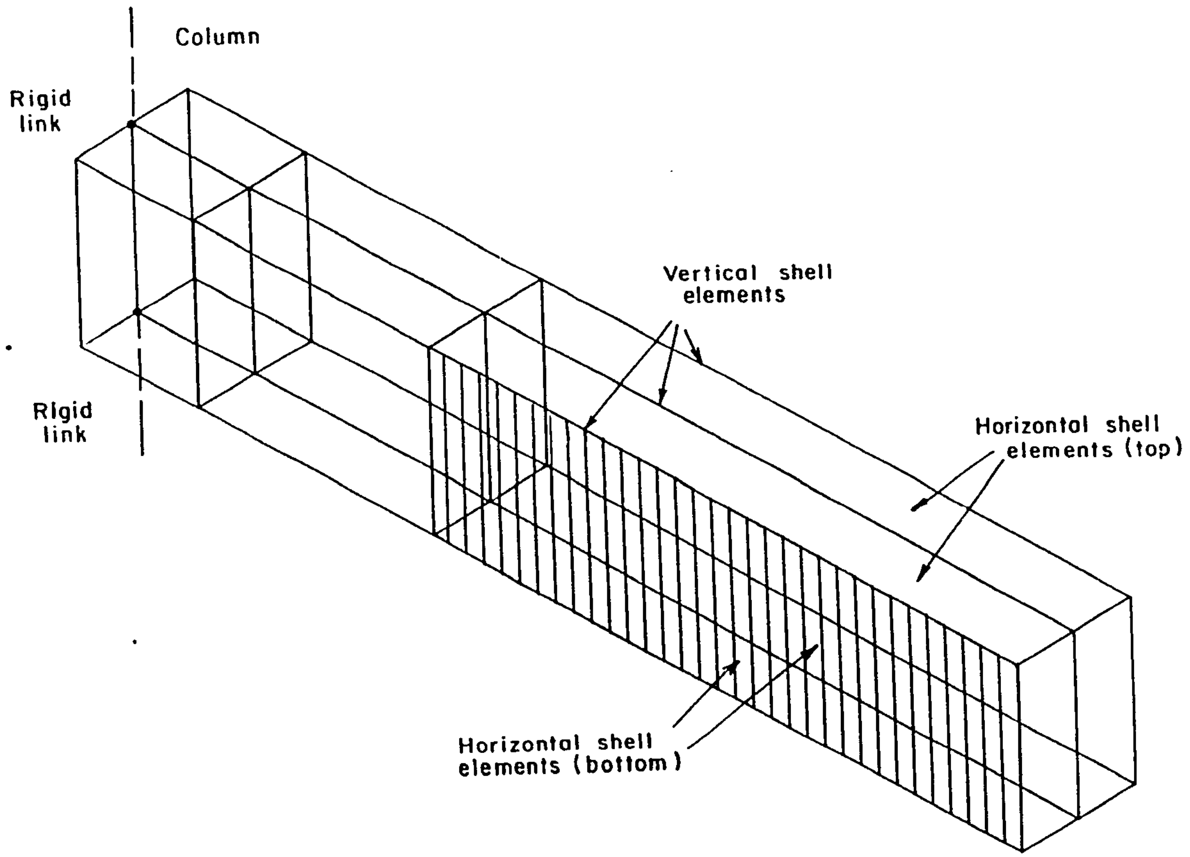
Column
Rigid link
Rigid link
Vertical shell elements
Horizontal shell elements (top)
Horizontal shell elements (bottom)

Fig. 5.4 Transverse beam discretization

concrete sections under torsion [5]. The selected thickness of the shell elements was greater than the effective wall thickness to accommodate the transverse and the longitudinal steel in the outside elements. The transverse steel and longitudinal steel in the transverse beam were both specified as smeared layers of steel.

The column was modeled using rectangular beam elements with steel specified as individual reinforcing bars. The width of the column elements in the transverse direction was half the column width (due to symmetry). The edge beams were modeled as stiffener elements on the slab similar to the longitudinal beam (Fig. 5.3).

5.3.1 Boundary Conditions. The nodes of the middle column element were connected to the shell elements at the top and bottom by a rigid link to impose identical displacements and rotations. All three translational degrees of freedom were constrained at the base of the column. Similar restraint was provided at the top of the column, with the exception that vertical translation was permitted. In addition to these constraints, all nodes on the plane of symmetry were constrained against out of plane displacement and rotations about axes lying in that plane. These boundary conditions are shown in Fig. 5.5.

5.3.2 Material Model. A single reinforced concrete model was used for all but the shell elements lying in the joint region. The slab and transverse beam elements lying within the joint region were modeled with an elastic material having the initial stiffness of

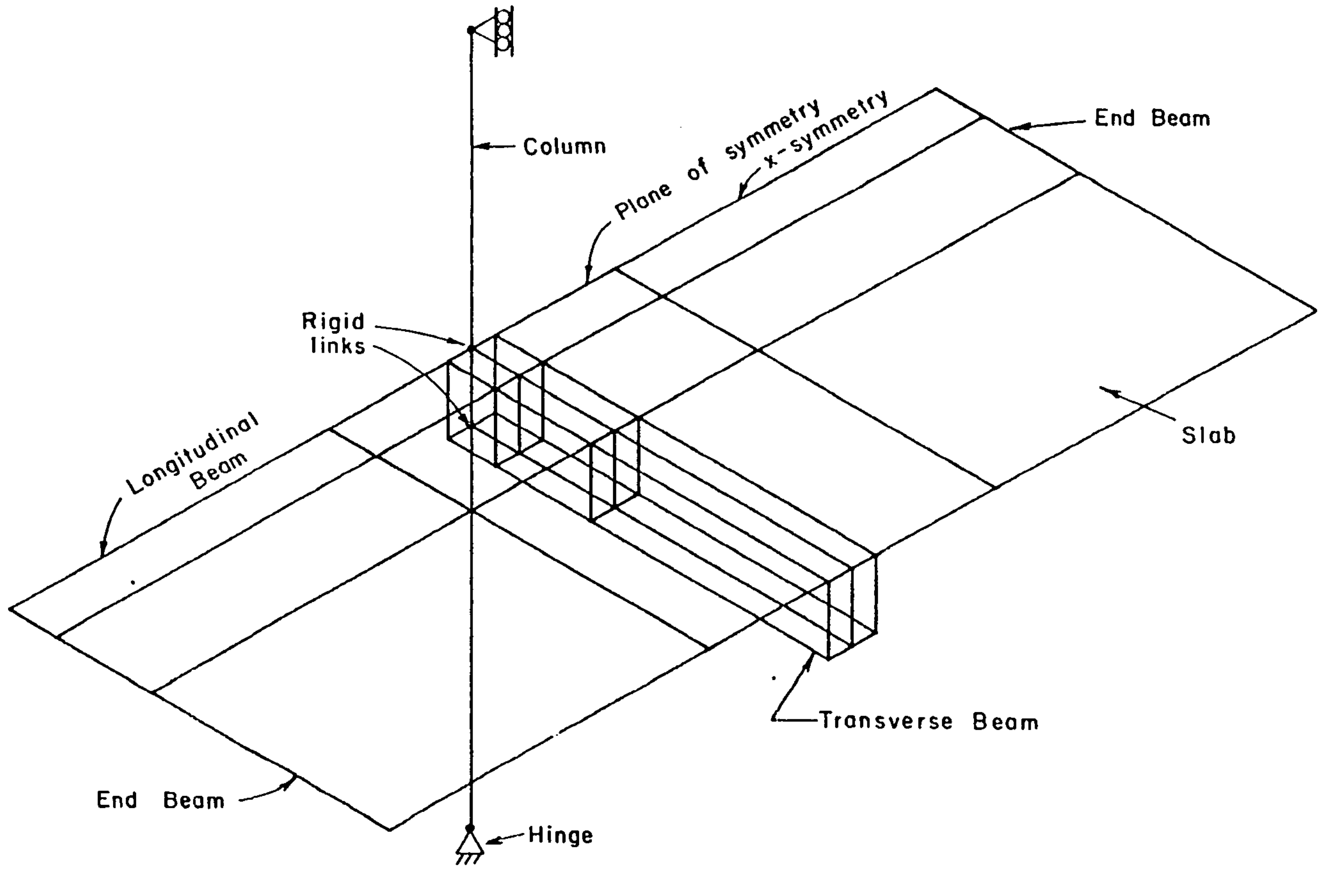
Column
Plane of symmetry
x-symmetry
End Beam
Rigid
links
Longitudinal
Beam
Slab
Transverse Beam
End Beam
Hinge

Fig. 5.5 Boundary conditions for the finite element model

concrete. It was assumed that there was no cracking in the joint region. However, the column and the longitudinal beam elements in the joint region were modeled as reinforced concrete.

A nonlinear plain concrete material model was used for beam and shell elements. Location, size and spacing of the reinforcement were specified separately. The two materials, concrete and reinforcing steel, were assumed to have compatible displacements but their stresses were calculated separately, controlled by their own material models. The concrete behavior following tensile cracking was modeled by the "tension-stiffening" technique [8].

The concrete constitutive relationship is defined by an extension of the strain-hardening plasticity theory of Chen and Chen (Fig. 5.6) [4]. In this approach, an initial yield surface is defined as the limiting surface for elastic behavior. When the material is strained beyond the elastic limit surface, a subsequent new discontinuity surface, called the loading surface, is developed. The two-part loading surface expands isotropically in space with additional plastic strain until a failure surface is reached. Further concrete response is dependent on which part of the surface is reached. If the parabolic surface in the compressive region is reached, then concrete is assumed to crush instantaneously and lose all its strength. If the hyperbolic surface in the remaining region is reached, concrete is assumed to crack orthogonal to the largest principal strain. After cracking, the plain concrete loses all its strength but the concrete/reinforcing steel composite loses its

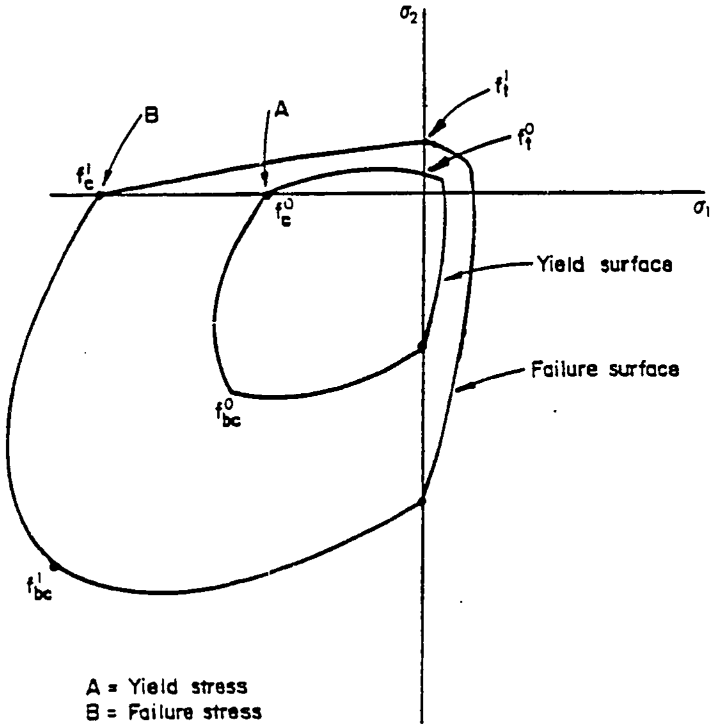
σ_2
f_t'
f_t^0
B
A
f_c'
f_c^0
σ_1
Yield surface
Failure surface
f_{bc}^0
f_{bc}'
A = Yield stress
B = Failure stress

Fig. 5.6 Concrete constitutive relationship

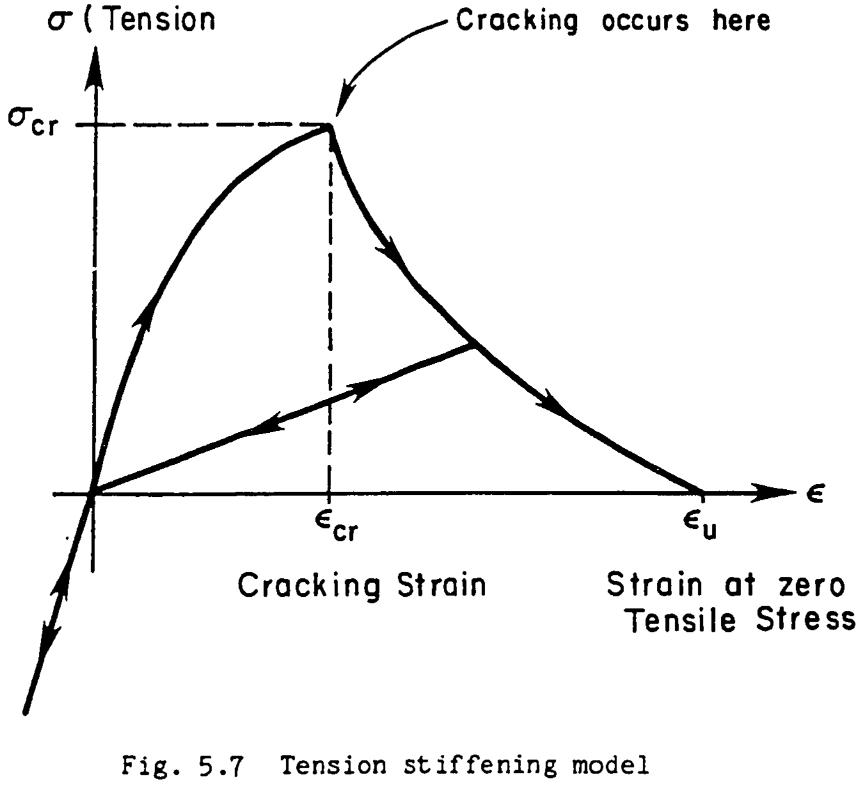
σ (Tension
Cracking occurs here
σ_{cr}
ϵ
ϵ_{cr}
ϵ_u
Cracking Strain
Strain at zero Tensile Stress

Fig. 5.7 Tension stiffening model

strength gradually. This effect is modeled by artificially changing the assumed plain concrete behavior to a gradual, instead of sudden, loss of strength beyond the failure strength using tension stiffening, as illustrated in Fig. 5.7. The uniaxial compression stress-strain curve specified for concrete is shown in Fig. 5.8. An elasto-plastic stress-strain model was assumed for the reinforcement, as shown in Fig. 5.9. Actual material strengths were used for specifying concrete and steel material models.

5.4 Elastic Finite Element Analysis

It was observed that at very small deflections, before the onset of flexural cracking, the behavior of the test specimens was essentially elastic. An elastic finite element analysis was therefore conducted using elastic, homogeneous and isotropic material properties for all elements. The modulus of elasticity of concrete, calculated according to the ACI Code [2], was specified for material properties. The primary objective of the elastic analysis was to verify the geometric model by comparing its response with that of test specimens in the elastic range.

The ACI effective width provisions are based on elastic analysis of positive moment T-sections (where the slab is in compression) by theory of elasticity. Hence, results from the elastic finite elements are compared with the theory of elasticity derivation. Of specific interest is the stress distribution in the slab under negative moment.

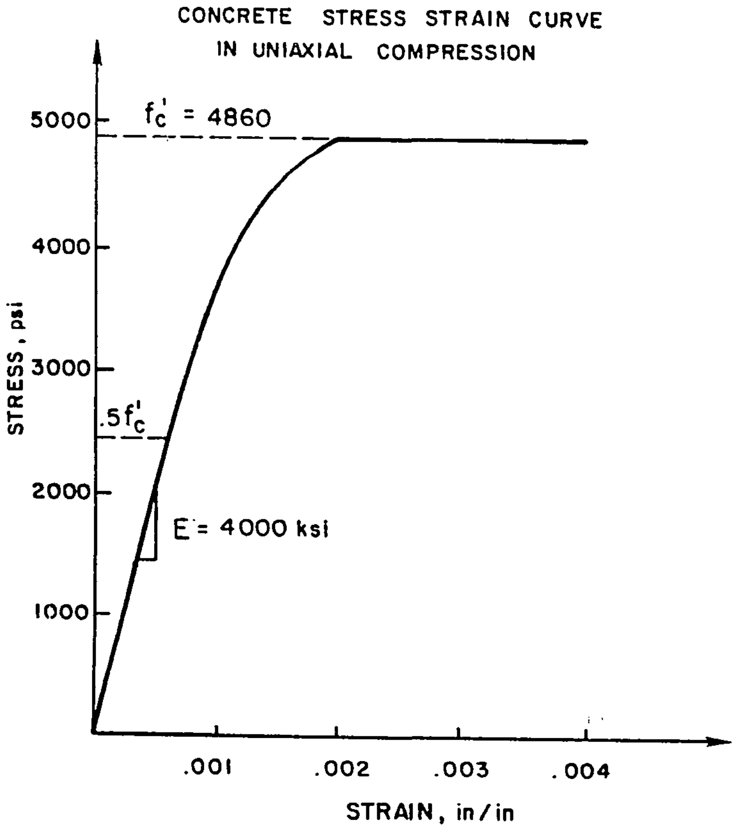

Fig. 5.8 Specified concrete stress-strain relationship

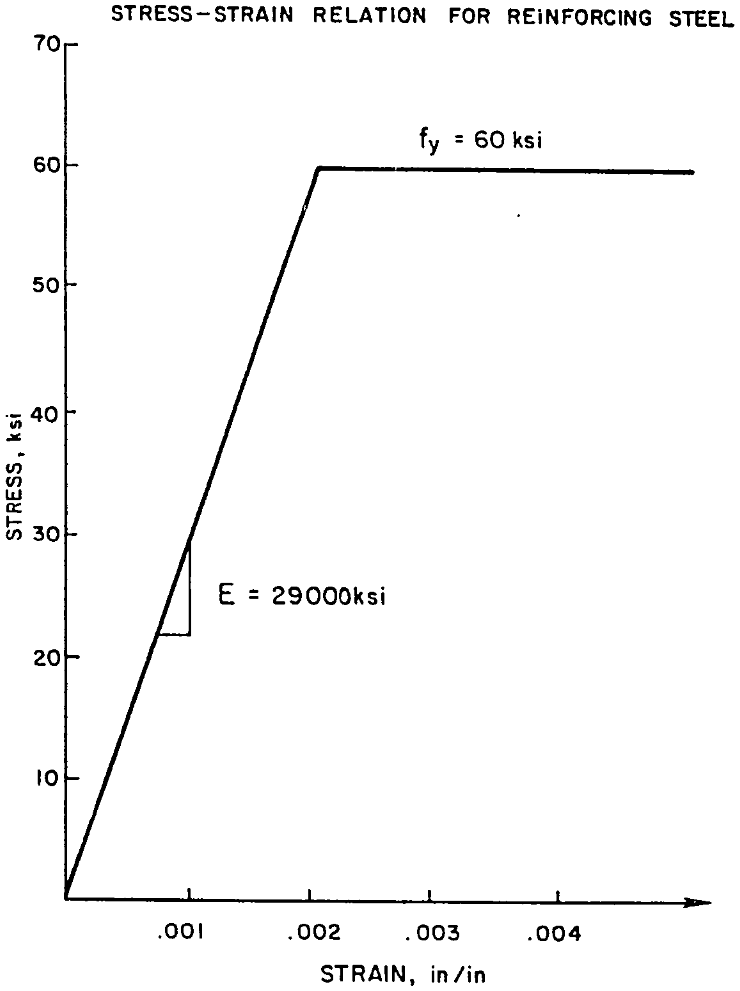

Fig. 5.9 Specified reinforcing steel stress-strain relationship

5.4.1 Elastic Stiffness. The load-deflection behavior predicted by the linear finite element model is compared with the observed load-deflection response of test specimens in Fig. 5.10 for interior specimens and Fig. 5.11 for exterior specimens. Since modified and prototype specimens differed only in the amount of steel reinforcement in beams and columns, their initial elastic response was similar.

The analytical results compare well with the experimental observations. The response of the test specimens was the same under both positive and negative bending in the very early elastic stage. Hence, only negative bending is compared. Elastic analysis overestimated the stiffness of the specimens under negative moment (tension at the top of the slab) by about 20 percent. This overestimation is believed to be due to the following factors: 1) initial shrinkage and temperature cracks in the test specimens reduced the stiffness, but were not reflected in the analytical model;. 2) concrete properties could have varied from the idealized stress-strain curve; and 3) analytical response was computed for monotonic loading, whereas the actual specimens were subjected to cyclic load reversals. Thus, the accuracy of the analytical model is reasonably good, and the validity of the geometric model was verified.

5.4.2 Interior versus Exterior Specimens. Analytically predicted load-deflection curves indicate that exterior specimens are stiffer than interior specimens. Similarly, experimental results indicate that the exterior specimens are initially stiffer than the

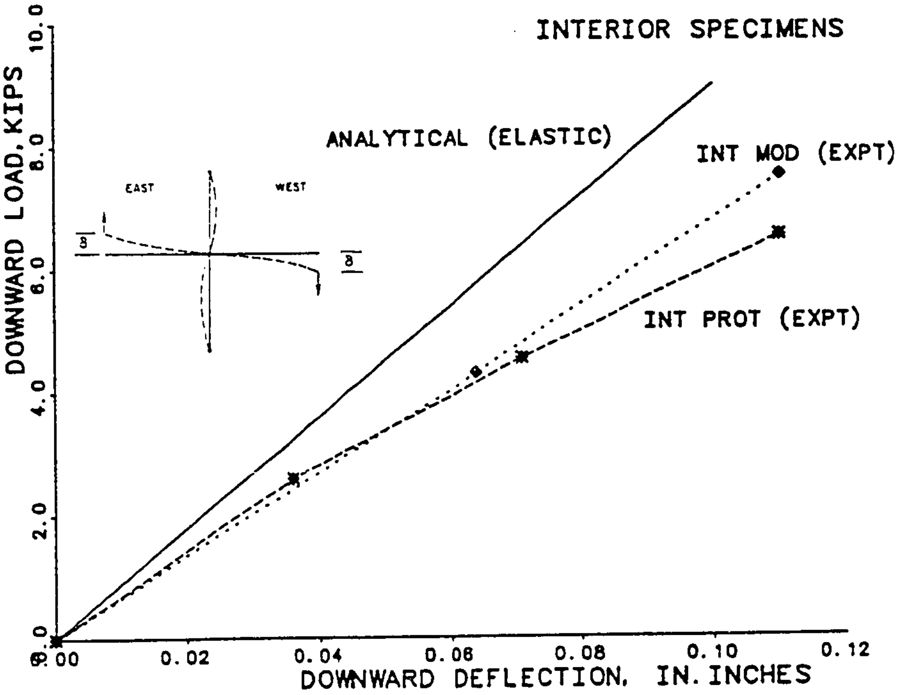

Fig. 5.10 Comparison of load-deflection behavior, interior specimens

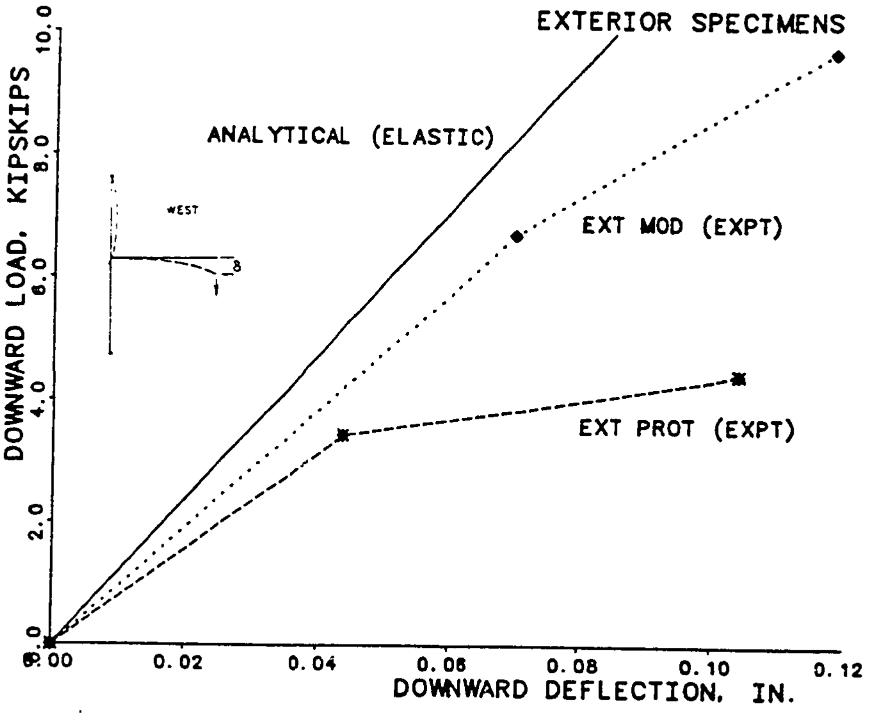

Fig. 5.11 Comparison of load-deflection behavior, exterior specimens

interior specimens, when beam end load versus beam end deflection curves are compared. This apparent difference in the stiffnesses of interior and exterior specimens, in spite of both having the same cross sectional properties and reinforcement ratios, is due to the nature of the boundary and loading conditions. Both the beams of the interior specimen were loaded simultaneously , whereas the exterior specimens had only one loaded beam. For the interior specimens, load on one beam also causes the other beam to displace, and a smaller load is then required on that other beam to achieve a given displacement. This reduces the apparent stiffness of the interior specimens compared to the exterior specimens when load versus deflection curves are compared.

5.4.3 Distribution of Torsion Along Transverse Beam.

Variation of torsion along the transverse beam is of interest in understanding the behavior of the slab system. The variation of normalized torsion (torque/total moment %) along the transverse beam obtained from elastic finite analysis is shown in Fig. 5.12, for the interior and exterior specimens, and is nearly parabolic.

Based on the maximum tensile stress in the transverse beam reaching concrete cracking stress, the cracking torsion was estimated at 190 kip-in. using the elastic finite element analysis. This compared well with the value of 206 kip-in. predicted as suggested by Collins [5], and verifies the adequacy of the discretization used for modeling the transverse beam.

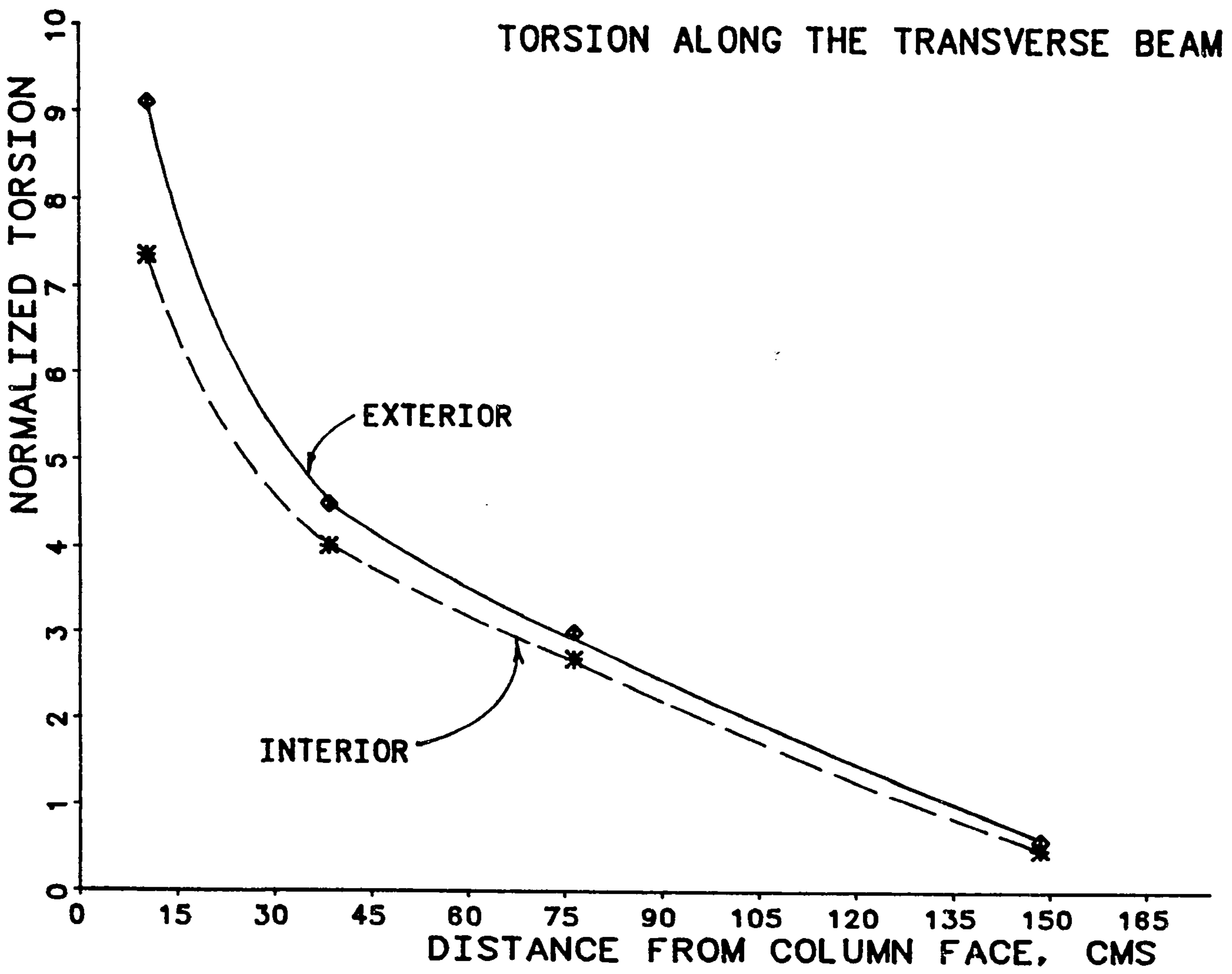

Fig. 5.12 Comparison of normalized torsion, interior vs. exterior specimens

For a given externally applied moment, about 25 percent more torsion is introduced into the transverse beam of the exterior specimens, than that of the interior specimens (see Table 5.1). In the interior specimen, some of the moment on one side of the transverse beam is transferred to the other side by membrane forces in the continuous slab without introducing torsion into the transverse beam. In exterior specimens, the external moment has to be transferred to the column from one side only, and so more torsion is introduced into the transverse beam. Thus, even though the moment induced by the longitudinal beam may be smaller for an exterior joint than for an interior joint, the torsion induced in the transverse beam of the exterior joint may still be large.

5.4.4 Effective Width of T-Beams, Elastic Range. As illustrated in Fig. 5.13, the classical effective width concept for T-beams is derived from closed-form solutions of the stress distribution in a thin, infinitely wide flange connected to a deep web. Stresses in the flange are assumed not to vary with depth. Elementary theory of bending assumes that plane sections remain plane, that bending stresses are proportional to the distance from the neutral axis, and that stresses are uniform across the width of the section at any depth. The existence of shear flow in the T-beam flanges implies shearing deformations in the beam flanges. Due to these shearing deformations, parts of the flanges far from the web are subjected to reduced bending stresses. The section is thus weaker than would be indicated by elementary bending theory, assuming uni-

TABLE 5.1 Distribution of Elastic Torsion

Location	Distance from Column Face, in.	Interior Specimen Torsion, kip-in.	Interior Specimen % of Total Moment	Exterior Specimen Torsion, kip-in.	Exterior Specimen % of Total Moment
1	10.6	635	7.3	516	9.1
2	38.6	347	2.9	254	4.5
3	76.6	234	2.7	172	3.0
4	148.7	40	0.5	31	0.6

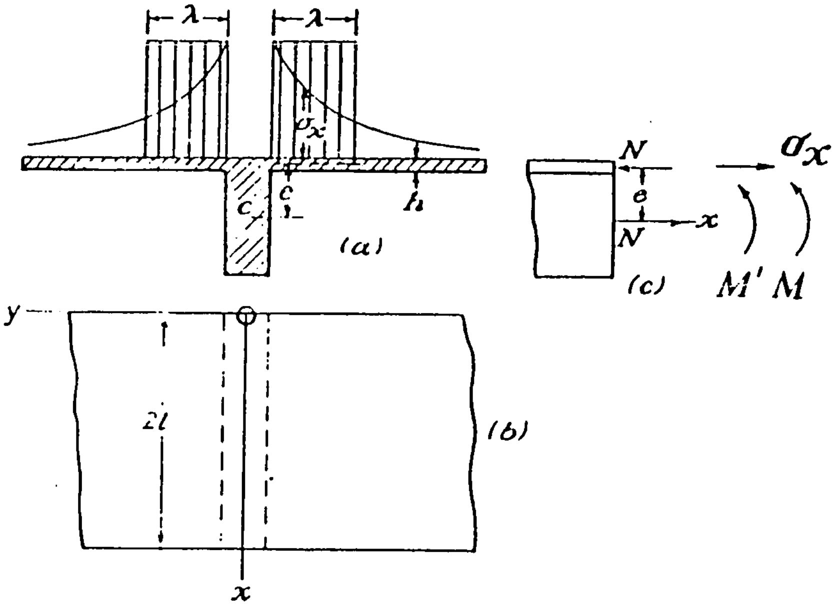
λ
λ
σ_x
c
c_1
h
(a)
y
2l
x
(b)
N
e
N
x
(c)
σ_x
M'
M

Fig. 5.13 Effective width of T-beam, theory of elasticity

form stress distribution across the width. The effective width concept assumes that if the actual width of the flanges is replaced by a certain reduced width then elementary bending theory can be applied to this effective beam cross-section, to correctly predict the flexural behavior of the entire slab-beam system.

This reduced width, commonly called the effective width, is derived considering the flange to be infinitely wide and very thin compared to the beam, so that the bending of the flange as a thin plate can be neglected. During bending of the beam, forces are transmitted to the flange in its middle plane only. According to the effective width concept, increases in flange width beyond the effective width will not result in increased moment capacity.

ACI effective width provisions are based on this concept. According to the ACI provisions, the contribution of that portion of the slab lying outside the effective width is implicitly included when strength and stiffness of this reduced cross section is determined by simple bending theory.

Results from the elastic finite element analysis show that the above assumptions are unrealistic for reinforced concrete sections with normal proportions, in which the slab is not very thin compared to the depth of the beam. The stress distribution across the depth and the width of the flange from the elastic finite element analysis is shown in Fig. 5.14. Qualitative stress distributions from the theory of elasticity and from the elastic finite element analysis are compared in Fig. 5.15. Results from the finite element

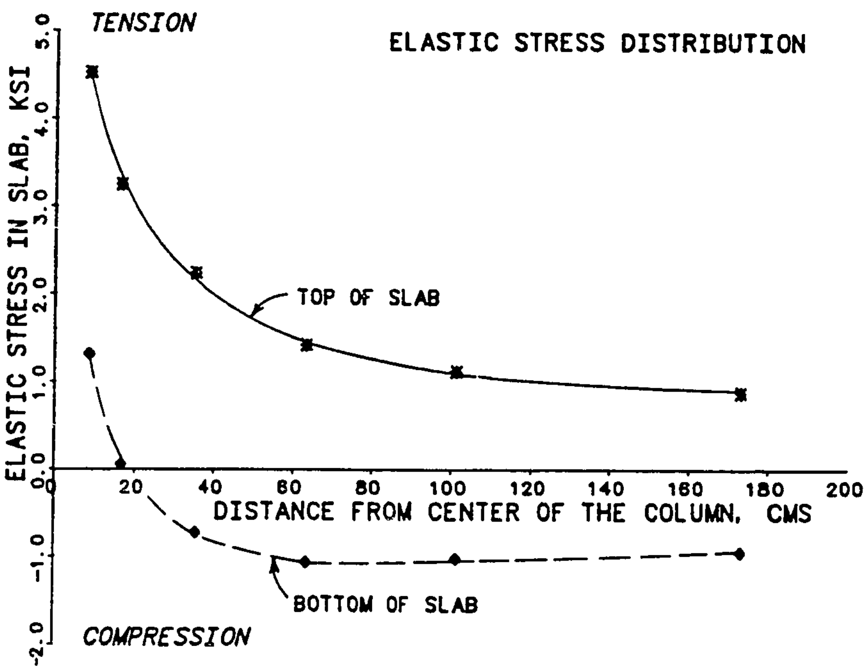

Fig. 5.14 Stress distribution along the slab, elastic analysis

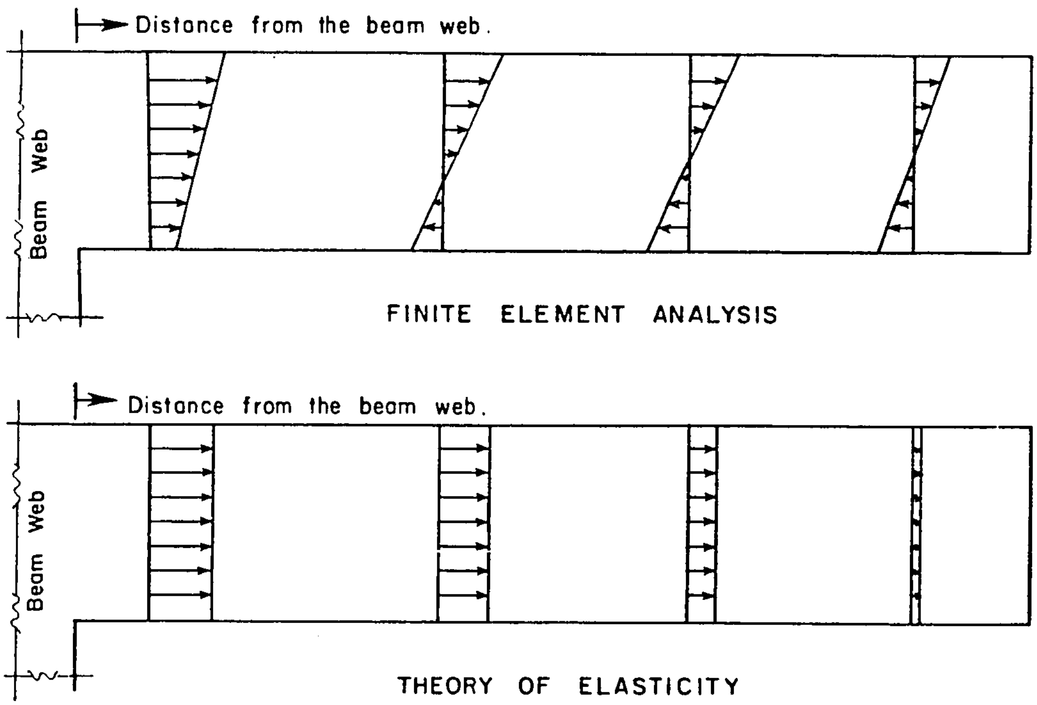
Distance from the beam web.
Beam Web
FINITE ELEMENT ANALYSIS
Distance from the beam web.
Beam Web
THEORY OF ELASTICITY

Fig. 5.15 Comparison of slab stress variation, finite element analysis theory of elasticity

analysis indicate that far from the web, the slab continues to participate by bending as a thin plate. The calculated location of the neutral axis across the entire width of the T-beam is shown in Fig. 5.16. The ACI effective width is also indicated in these figures. Contrary to the effective width concept, while a portion of the slab does act as a flange of the beam, the rest of the slab acts as a shallow flexural section. The reduction in effectiveness of the flange is due primarily to the variation in the position of the neutral axis across the width, not to shearing deformations in the flange.

5.5 Comparison of Crack Patterns

The behavior of the specimen changes at the onset of cracking. The nonlinear finite element program was able to handle cracking of concrete, and to determine approximate locations and orientations of cracks. These predicted crack patterns are compared with observed experimental results for the interior prototype specimen. Only those crack patterns significant to negative bending of the slab system are discussed. For this statically determinate specimen, concrete tensile stresses are determiend by the applied loads. Crack initiations and extensions are therefore compared at similar load levels, rather than at similar deflections. General locations and orientations of cracks from the nonlinear finite element analysis compared well with observed cracking. Predicted

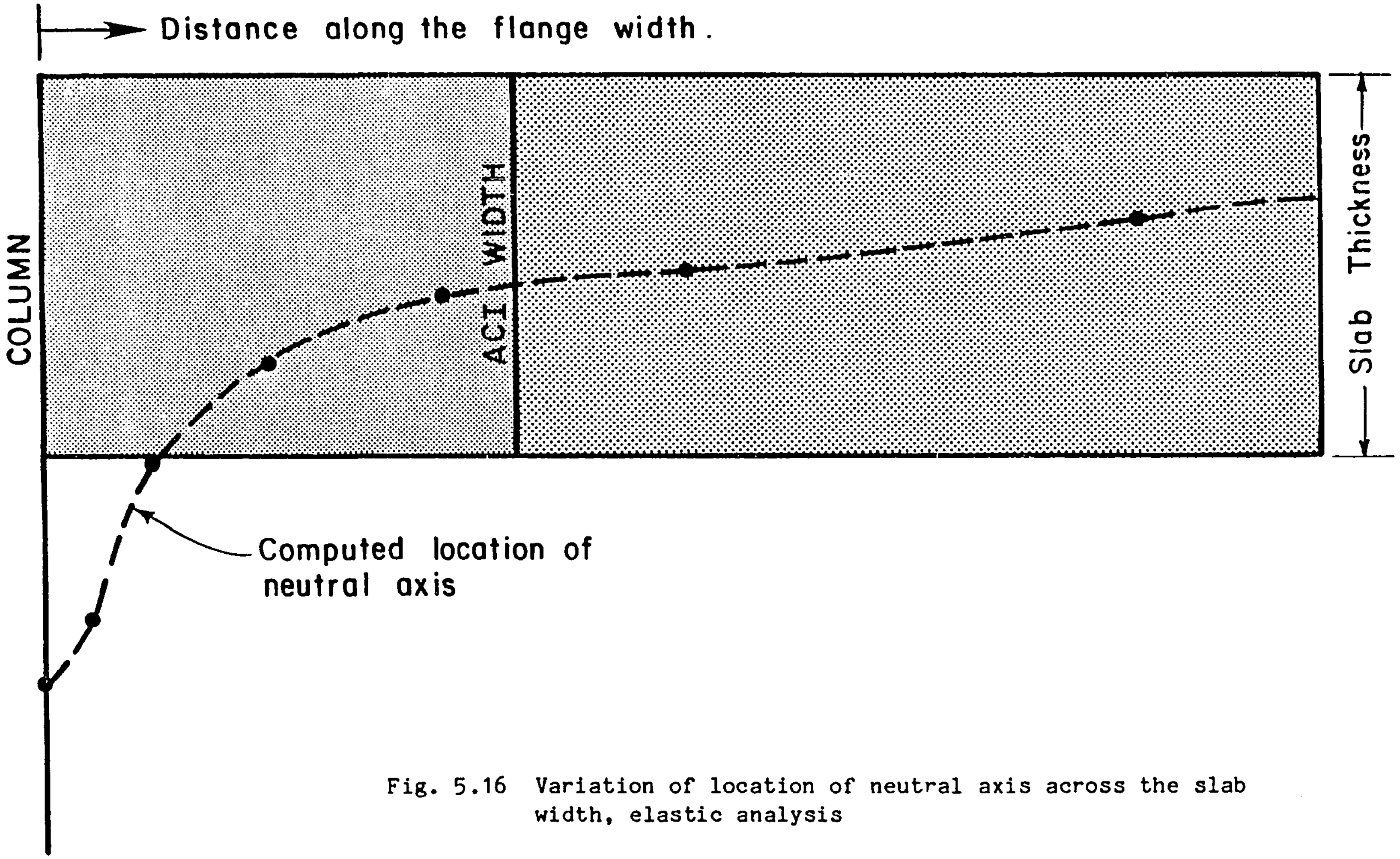
Distance along the flange width.
COLUMN
ACI WIDTH
Slab Thickness
Computed location of neutral axis

Fig. 5.16 Variation of location of neutral axis across the slab width, elastic analysis

crack extensions agreed well with crack propagation observed during experiments.

Initial flexural cracks were observed in the slab at a beam end load of 13 kips and were formed parallel to the transverse beam and extended about 20-25 in. from the longitudinal beam. Analytical studies indicated that the top of the beam cracked initially at a load of 10 kips, and that at 17 kips, cracks extended about 20-24 in. from the longitudinal beam. During testing, the cracks had extended the full width of the slab at a load of 15 kips. Complete propagation of the flexural cracks across the slab was analytically predicted at a load of 19.5 kips.

During testing, flexural cracks were observed on the bottom of the slab at a load of 16 kips and extended nearly 25 in. from the longitudinal beam. Analyses predicted initial cracking of the bottom surface at a load of 20 kips, and the extension of these cracks to about 20-25 in. at a load of 22 kips.

Under negative moment, the cracking load was estimated to be 17 kips whereas the observed cracking load was 13 kips. Crack propagation was thus adequately predicted by the analytical model.

5.6 Nonlinear Finite Element Analysis

5.6.1 Stiffness. The load-deflection response from nonlinear finite element analysis is compared in Fig. 5.17 with the observed load-deflection relationship for the interior prototype specimen. Load-deflection response was determined up to a beam end

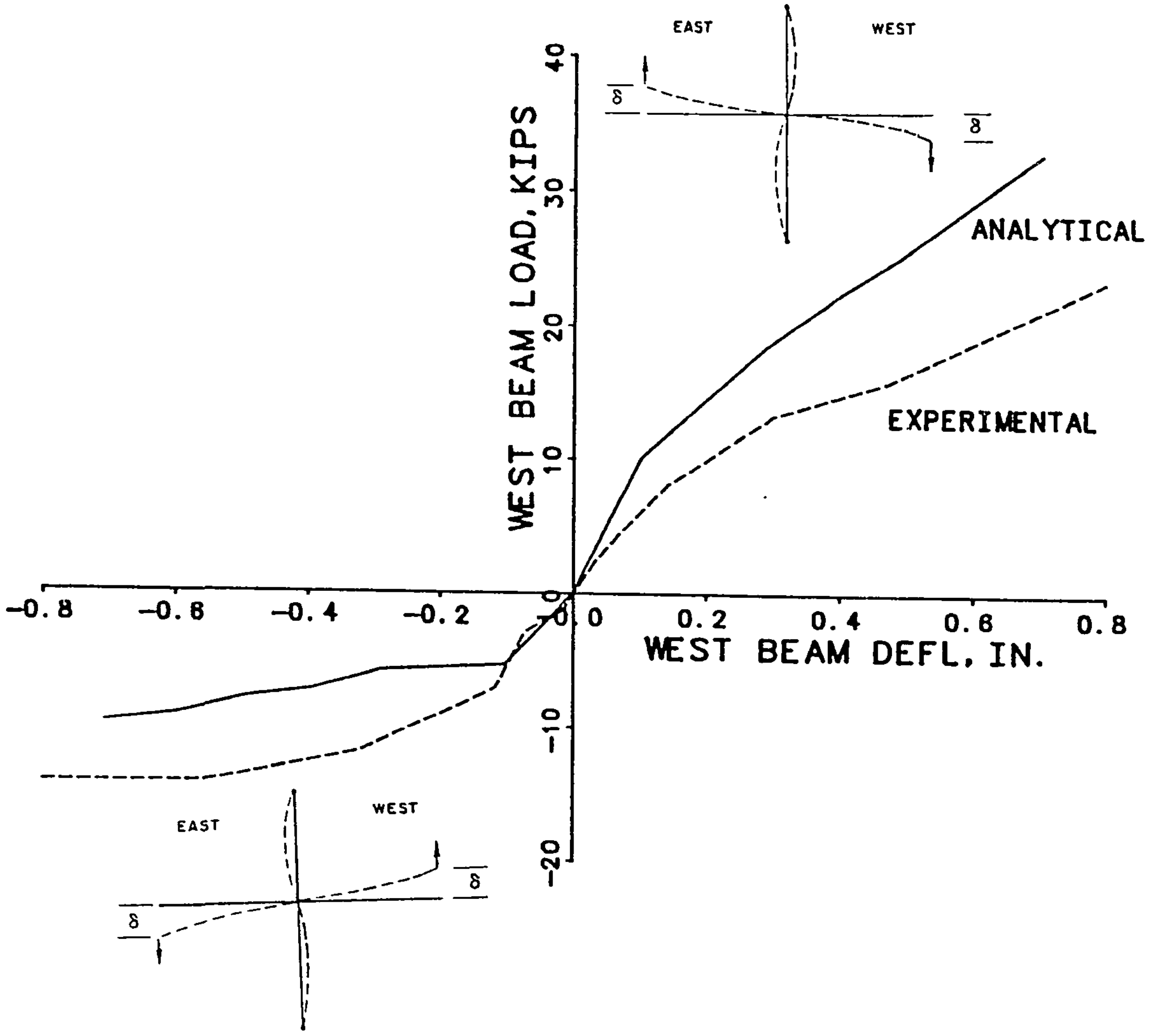

Fig. 5.17 Comparison of load-deflection behavior, interior prototype specimen

deflection of 0.7 in. As mentioned earlier, the entire load-deflection curve could not be determined analytically due to limitations of version 4-5-22 of the computer program in handling 1) yielding of reinforcing steel, 2) convergence at larger deflection levels (see discussion in Appendix A), and 3) running out of time.

The experimental load-deflection response shown in Fig. 5.17 is the envelope of the measured load versus deflection curves for the west beam of the interior prototype specimen. Downward displacement of the west beam, introducing a negative moment there, is shown in positive sense. For an interior specimen, the east and west ends of the longitudinal beam were subjected to equal and opposite displacements. Thus, a positive beam end deflection at the west beam was accompanied by a negative beam end deflection at the east beam. Response of the east beam is not shown in the figure. It was observed that cyclic loading caused minimal stiffness degradation of the longitudinal beams from one cycle to the next at such small (0.7 in.) deflections. Thus, the east beam load-deflection envelope was essentially the same as that for the west beam. Since load-deflection response from nonlinear finite element analyses was computed assuming monotonic loads, analytical load-deflection curves are identical for the east and west ends. Hence, the load-deflection plot of Fig. 5.17 could be viewed either as a load-deflection curve for the west beam from a maximum negative deflection to a maximum positive deflection, or as the positive load-deflection curve for the west beam with accompanying negative load versus deflection curve for the east beam. This is approximately true of the experimental curve as well, since it was observed that the west and east beam load-deflection envelopes were very similar.

Compared with experimental results, at beam end deflections of 0.7 in., the analytical model overestimates the secant stiffness under negative moment by about 30 percent, and underestimates the stiffness under positive moment by about 35 percent. Analytical estimates of total moment introduced into the column compare very well with observed behavior, as shown in Fig. 5.18. The total moment is the sum of the moments imposed on the column by the east and west beams.

The overestimation of stiffness under negative moment can be largely attributed to the stress-strain curve specified in the tension-stiffening range. A linear stress-strain relationship was specified for the post cracking region (see Fig. 5.19). Generally, the initial drop in concrete tensile stress after cracking would be considerably greater than that implied by a linear curve, (and a more realistic stress-strain relationship for post cracked concrete is also shown in Fig. 5.19). Thus, the strength of cracked concrete was overestimated and resulted in an increase in computed flexural strength under negative moment. Under negative moment, a large area of concrete reaches strains in this region of the tensile stress-strain curve (slab in tension), and the tensile contribution of cracked concrete to moment capacity is significant. The stiffness of the slab system under positive moment is rather small compared to

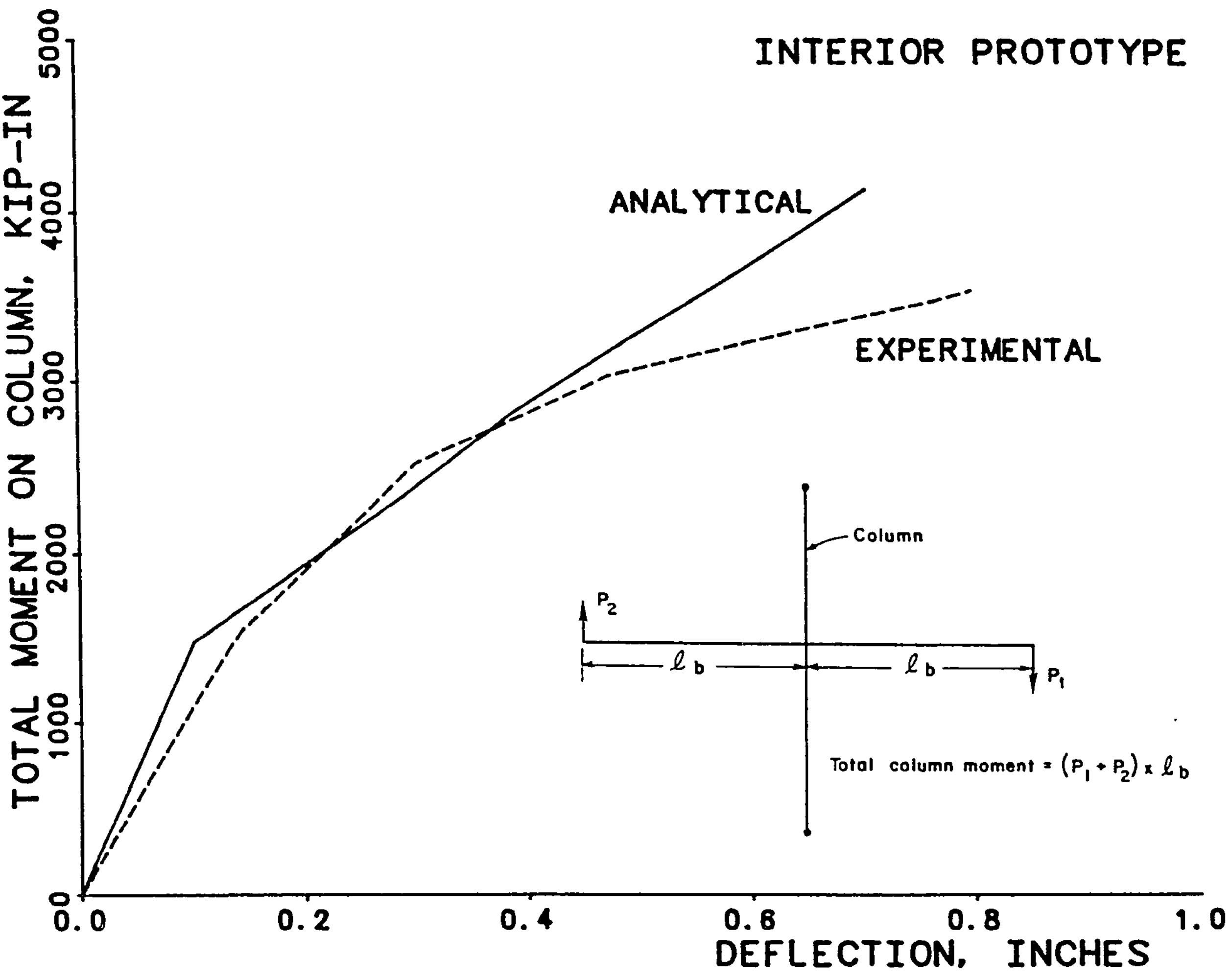

Fig. 5.18 Comparison of total column moment, interior prototype specimen

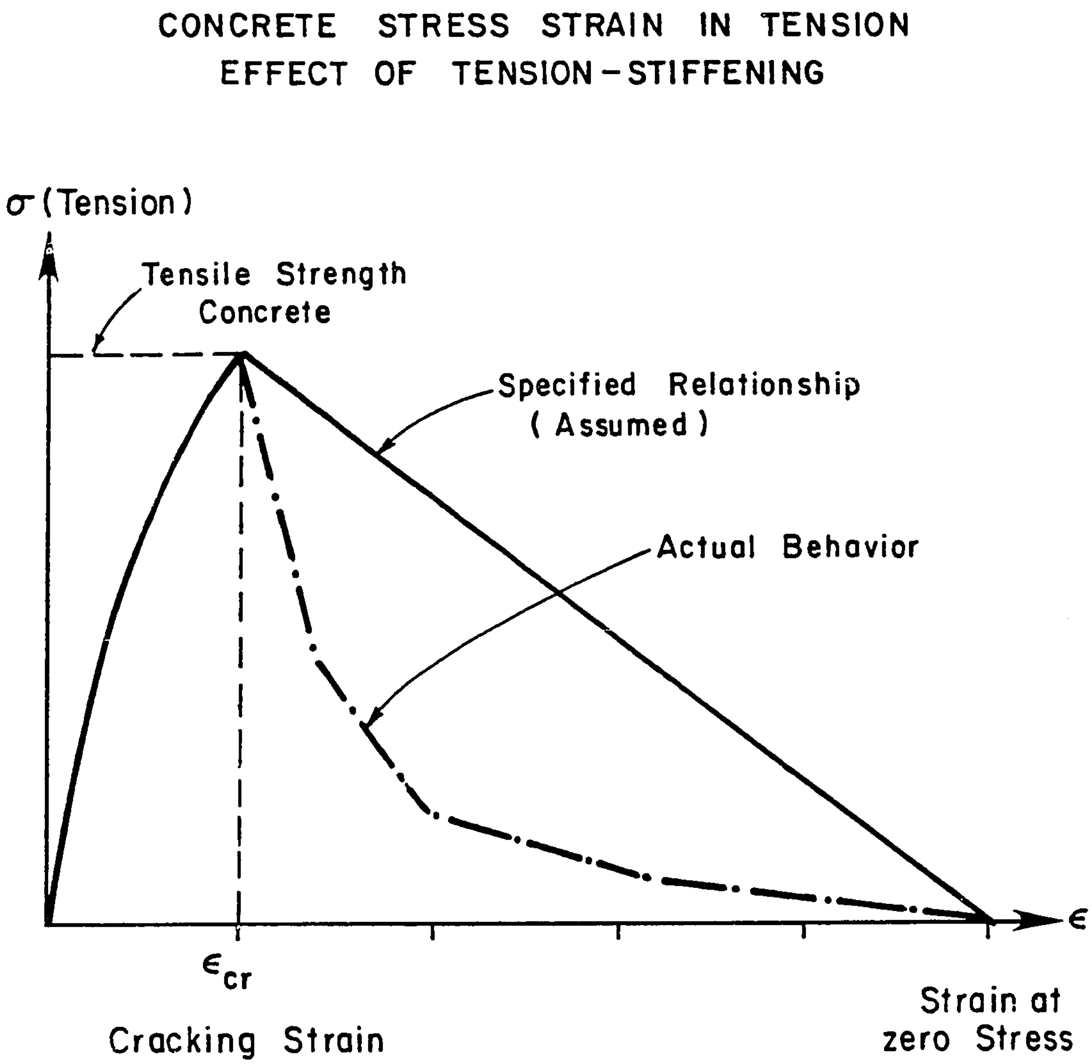
CONCRETE STRESS STRAIN IN TENSION
EFFECT OF TENSION-STIFFENING
σ (Tension)
Tensile Strength Concrete
Specified Relationship (Assumed)
Actual Behavior
ϵ
ϵ_{cr}
Cracking Strain
Strain at zero Stress

Fig. 5.19 Specified versus actual tension stiffening relationship

stiffness under negative moment. Overestimation of the stiffness under negative moment introduces a larger moment in the column from that end and produce a greater upward displacement at the other end. A smaller load is then needed on the end deflected upward to produce identical deflections at both ends.

Overestimation of the tensile strength of cracked concrete resulted in overestimating the negative moment corresponding to a given downward beam end displacement. This in turn resulted in underestimating the positive moment corresponding to given upward displacement of the other beam. However, the predicted and observed load-deflection curves are very similar in shape. The changes in stiffness with increasing deflection levels agree well with experimentally observed response. Errors are believed to be due to the way in which tension stiffening was modeled. Except for overestimating the tensile strength of cracked concrete, the analytical model closely predicted the observed response.

5.6.2 Effective Width of T-Beams, Inelastic Range. As discussed earlier, the effective width of a T-beam based on elastic finite element analysis was very different from the effective width suggested by ACI Code provisions and derived from theory of elasticity for both positive and negative bending. Both observed and analytical results showed that the slab behaves very differently in the inelastic range. Behavior of the slab system from nonlinear finite element analysis is discussed and compared with experimental results.

The variation of longitudinal slab steel stresses across the transverse beam as predicted by nonlinear finite element analysis is shown in Fig. 5.20. These stress profiles are very similar to longitudinal slab steel strain profiles from experimental observations (see Figs. 4.6 through 4.10 and 4.12 through 4.16). In Figure 5.21 slab steel stress profiles from analytical results are compared with those from experiments, at similar loads. These figures show similar distributions of stresses across the width of the slab. An exact match between experimental and analytical steel stresses is not expected, since experimental values of strain are dependent on the location of the cracks and are measured at particular points, whereas analytical results give average values of stresses over a larger area of slab.

Figure 5.22 shows the profiles of the location of the neutral axis at various deflection levels predicted by the nonlinear finite element analysis. These neutral axis locations were computed assuming a linear strain distribution over the depth at each location. The change of neutral axis location with increased deflections and increased cracking across the slab is apparent. At increased deflection levels, the neutral axis moves further down from the top surface of the slab, resulting in increased internal lever arm. At a beam end deflection of 0.7 in., the entire slab is in tension. As deflections increase, stress distribution across the slab becomes more uniform. Unfortunately, response at larger deflection levels was not obtained by finite element analysis, since

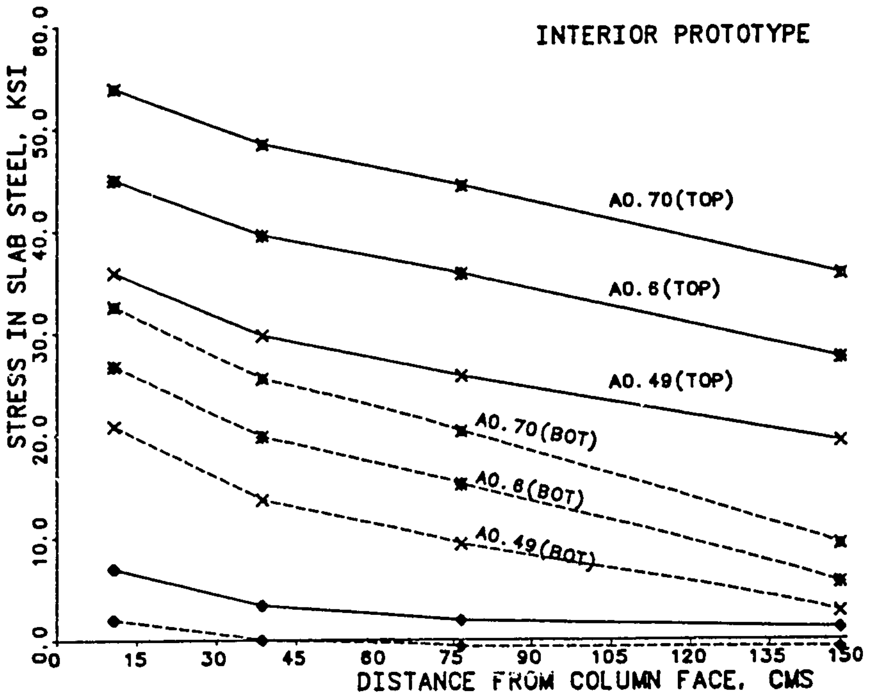

Fig. 5.20 Slab steel stress profiles from nonlinear analysis

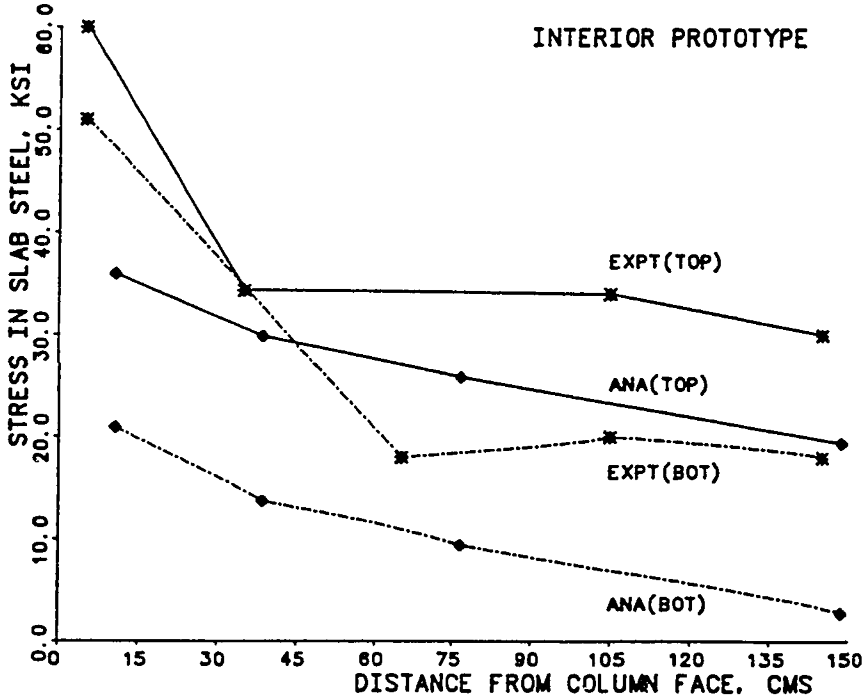

Fig. 5.21 Comparison of slab steel stress profiles, analytical vs. experimental

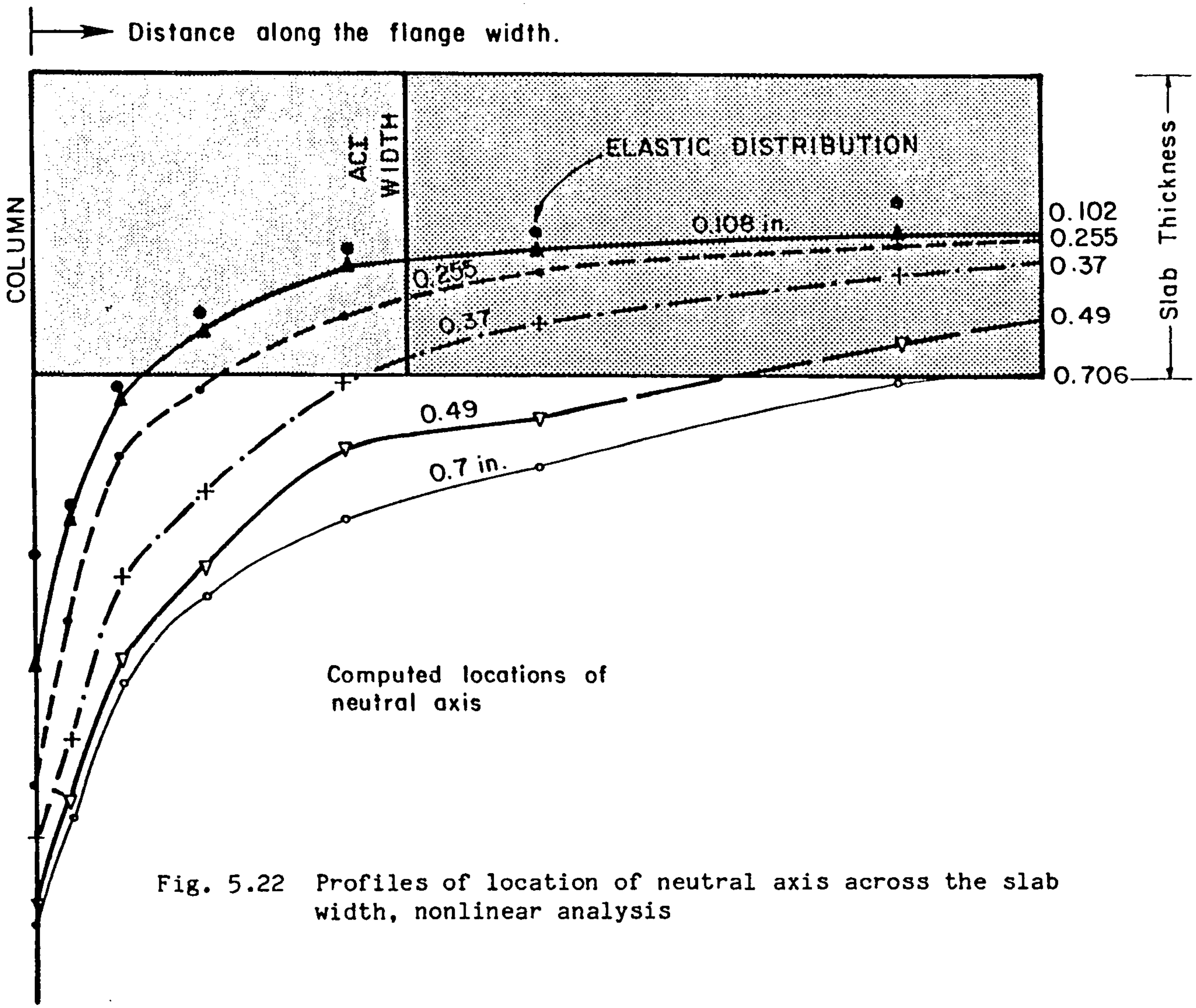

Fig. 5.22 Profiles of location of neutral axis across the slab width, nonlinear analysis

the original version of the finite element analysis program did not permit yielding of reinforcement. However, available results imply that as slab reinforcement starts to yield, the distribution of stress in the steel across the slab section would be fairly uniform since increased deflection would increase strains so that yielding would progress across the slab width. Experimental results showed that most of the slab steel did yield at large deflections.

The variation of the position of the neutral axis across the width of the slab indicates that even though steel far from the beam was stressed to a level comparable with the beam steel it was not as effective as the beam steel in resisting moment. The fundamental difference between the basis for ACI effective width provisions and the actual behavior is thus apparent. ACI provisions, based on the shear lag concept, imply that slab effectiveness far from the web is reduced because the stress distribution across the slab is not uniform, with the stress in the slab decreasing with increasing distance from the web of the T-beam. Analytical results show that stress across the slab is actually fairly uniform, but that the slab farther away from the web does not behave as would be expected by simple flexural theory because the neutral axis location changes with its distance from the web.

If a reduced effective width is used in conjunction with simple bending theory for computing flexural capacity of the slab system, the justification should not be that stresses vary across the flange but rather that plane sections do not remain plane during bending.

5.7 Development of Design Guidelines

There are three distinct stages in the behavior of the slab systems: the initial elastic uncracked stage; post-cracking, pre-yielding stage; and the post-yielding stage. Cracking occurs at fairly small drift levels,about 0.05-0.1 percent. Yielding of flexural reinforcement occurs at story drifts of about 1.0-1.5 percent.

The stiffness of the slab system at service loads must be accurately estimated in order to compute serviceability deflections. The flexural capacity of the slab system must be accurately estimated for capacity design of earthquake resistant structures. Current ACI provisions for these two stages are discussed, and guidelines are suggested for design based on the available experimental and analytical data.

5.7.1 ACI Provisions for Effective Width. The ACI provisions imply that the effect of the entire beam-slab system in resisting flexure can be determined using simple bending theory, considering a particular width of the slab to act as a flange of the T-beam section. This implies that the participation of the entire slab can be accounted for using a T-beam section having this effective width, and that when this T-beam section is evaluated using simple bending theory the stiffness and strength of the entire slab-beam system are correctly assessed. using simple bending theory. The ACI provisions are compared with available results to help the designer understand the limitations of the ACI approach.

5.7.2 Stiffness. Analytical and experimental results showed that all of the longitudinal slab steel participated in resisting the applied deformations, even at story drifts corresponding to the serviceability range. It was shown that the slab steel far from the web was not as effective as would be suggested by simple bending theory (plane sections remaining plane) because the distance of the neutral axis from the slab steel changed with its distance from the web. Thus, if an idealized beam section is to be analyzed by simple bending theory to reflect the observed behavior of the slab system, the effect of all of the slab steel has to be included in analyzing the idealized section.

In Figs. 5.23 through 5.28, the observed load-deflection response of the interior test specimens under both negative and positive moment is compared with predicted stiffness using three different beam sections: 1) the ACI effective width; 2) the entire slab width acting as a flange; and 3) an idealized beam section which includes the effect of all the slab steel. The idealized beam section is defined as a section with the geometric properties of the ACI section, but with an amount of slab steel equal to the sum of the area of the slab steel in the ACI effective width, plus half of the area of the slab steel lying outside the ACI section. This factor of one-half reflects the reduced participation of steel far from the web, and is discussed further in the next section (see Fig. 5.30).

Using simple bending theory, the cracked stiffnesses of the beam sections were used to predict the load-deflection behavior. The column stiffness was estimated using two limiting cases: 1) gross moment of inertia; and 2) cracked, transformed moment of inertia.

For postive bending of the slab system (Figs. 5.23 through 5.25), the stiffness for these three different beam sections did not change much. The stiffness of the structure was more sensitive to the assumed behavior of the column (uncracked or cracked) than to the assumed behavior (ACI, idealized or full slab width) of the beam section. In the serviceability range, however, all computed stiffnesses considerably underestimated the measured stiffness of the test specimens.

For negative bending of the slab the assumed beam section had a significant effect on the predicted stiffness of the test structures (see Figs. 5.26 through 5.28). The variation in the predicted stiffness values was greater for the interior prototype specimen, in which the ratio of the area of slab steel to the area of beam steel was 1.96, than for the modified specimens, in which the ratio of the area of slab steel to the area of beam steel was 1.17. Even for negative bending, the sensitivity of the stiffness to the assumed behavior of the column, cracked or uncracked, was greater than the sensitivity of the stiffness to the assumed beam section. In the serviceability range, however, assuming an ACI T-beam section

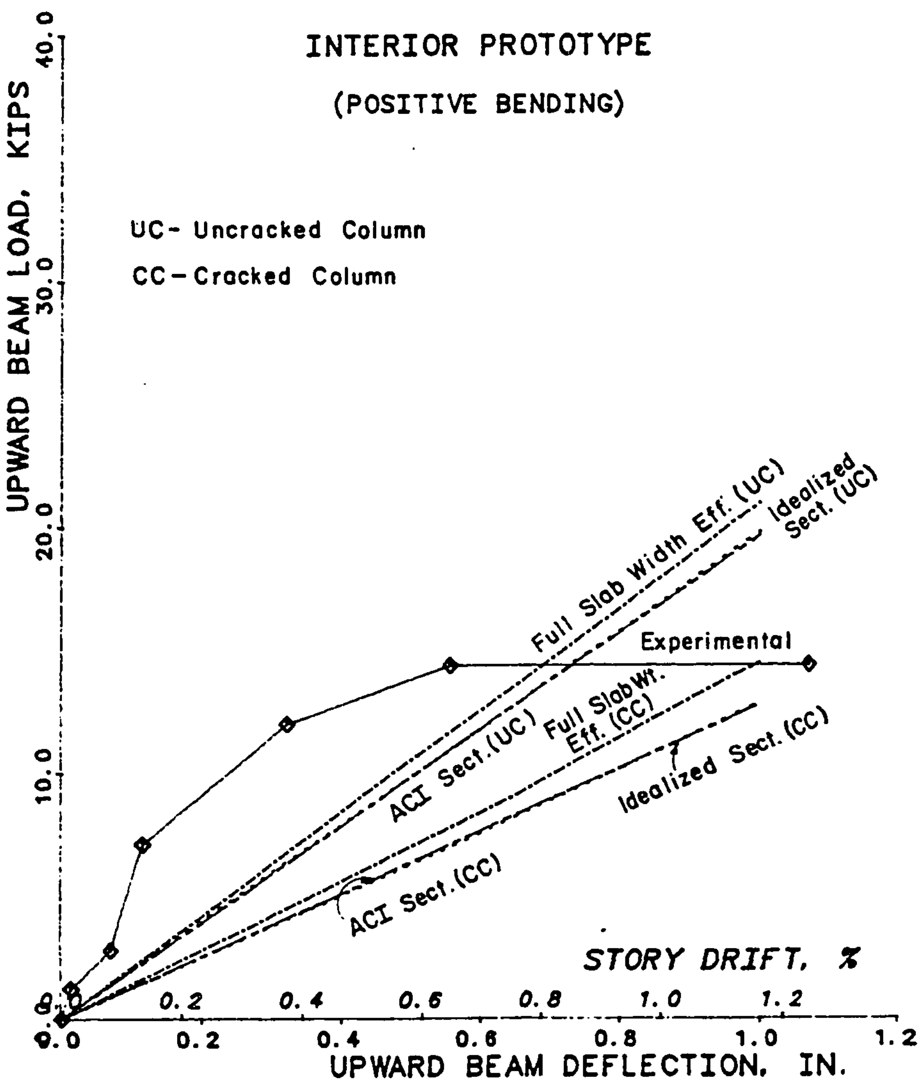

Fig. 5.23 Comparison of load-deflection relationship under positive moment, interior prototype

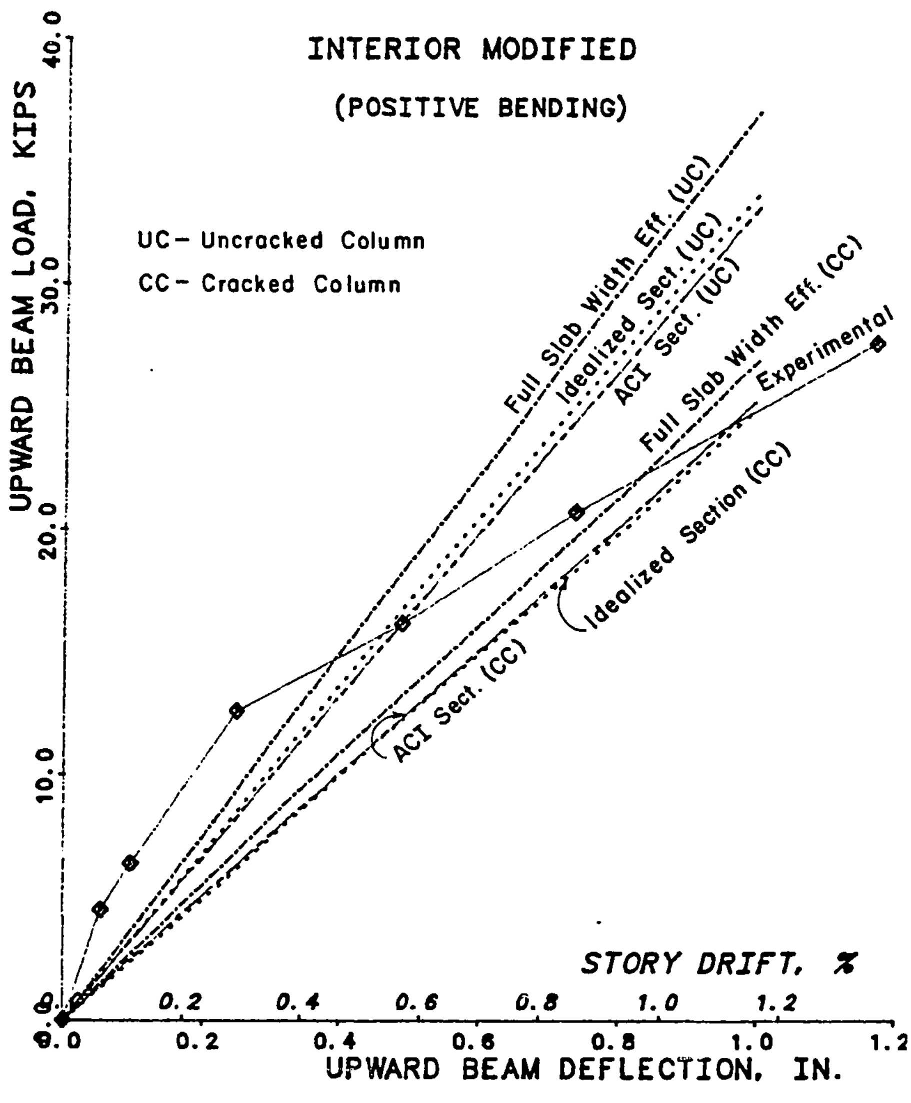

Fig. 5.24 Comparison of load-deflection relationship under positive moment, interior modified

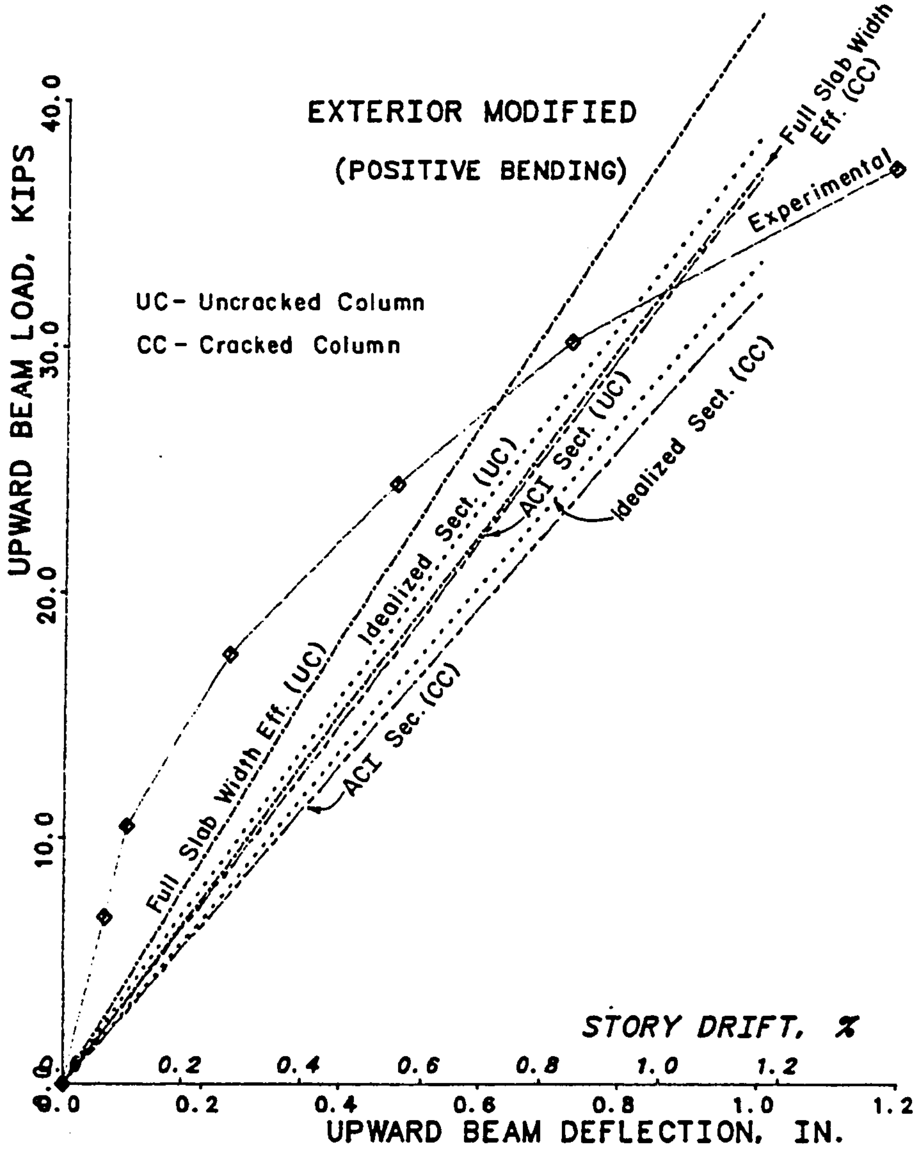

Fig. 5.25 Comparison of load-deflection relationship under positive moment, exterior modified

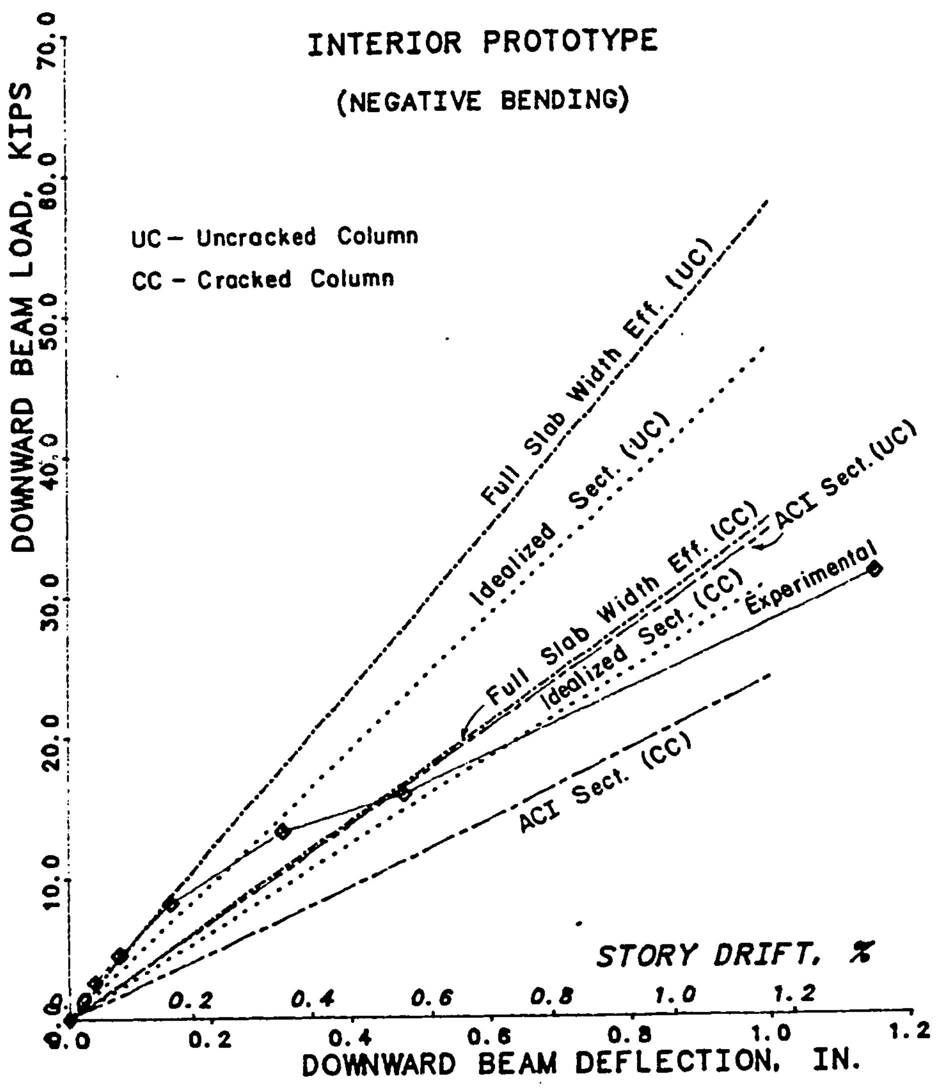

Fig. 5.26 Comparison of load-deflection relationship under negative moment, interior prototype

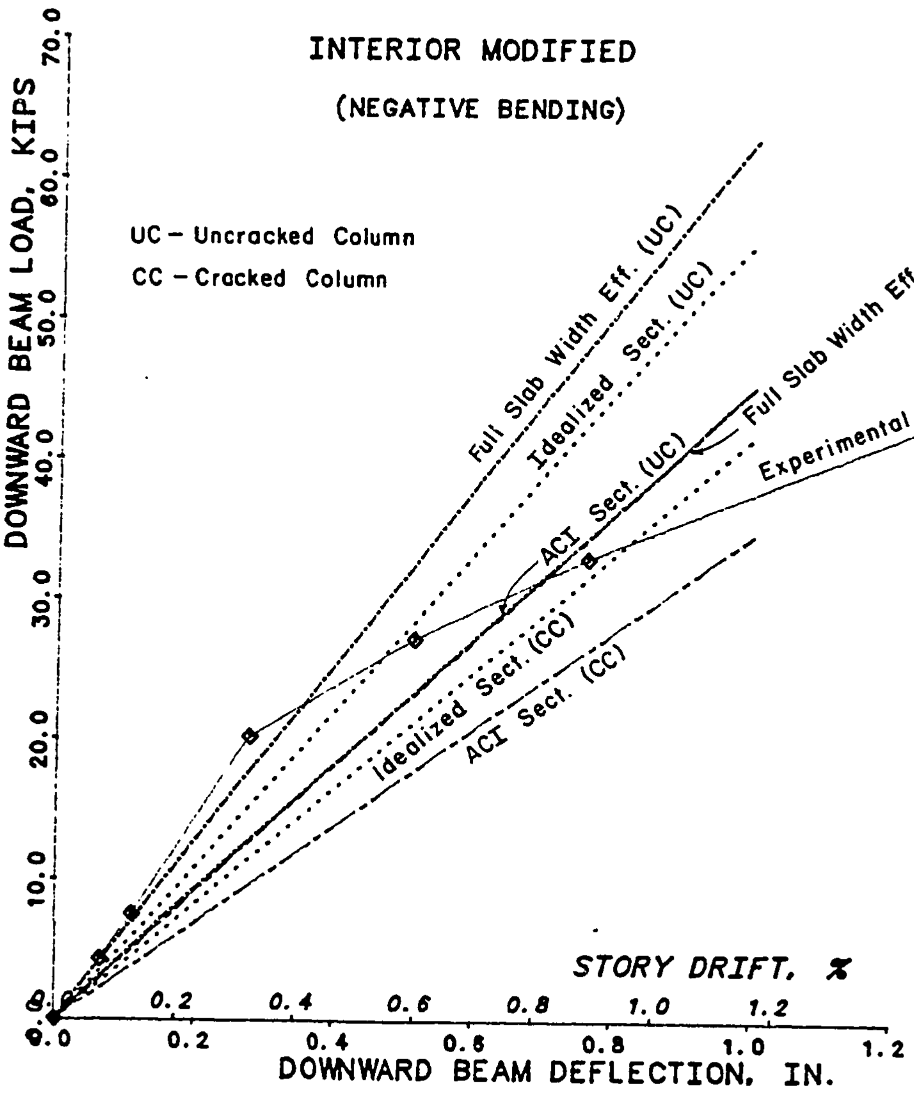

Fig. 5.27 Comparison of load-deflection relationship under negative moment, interior modified

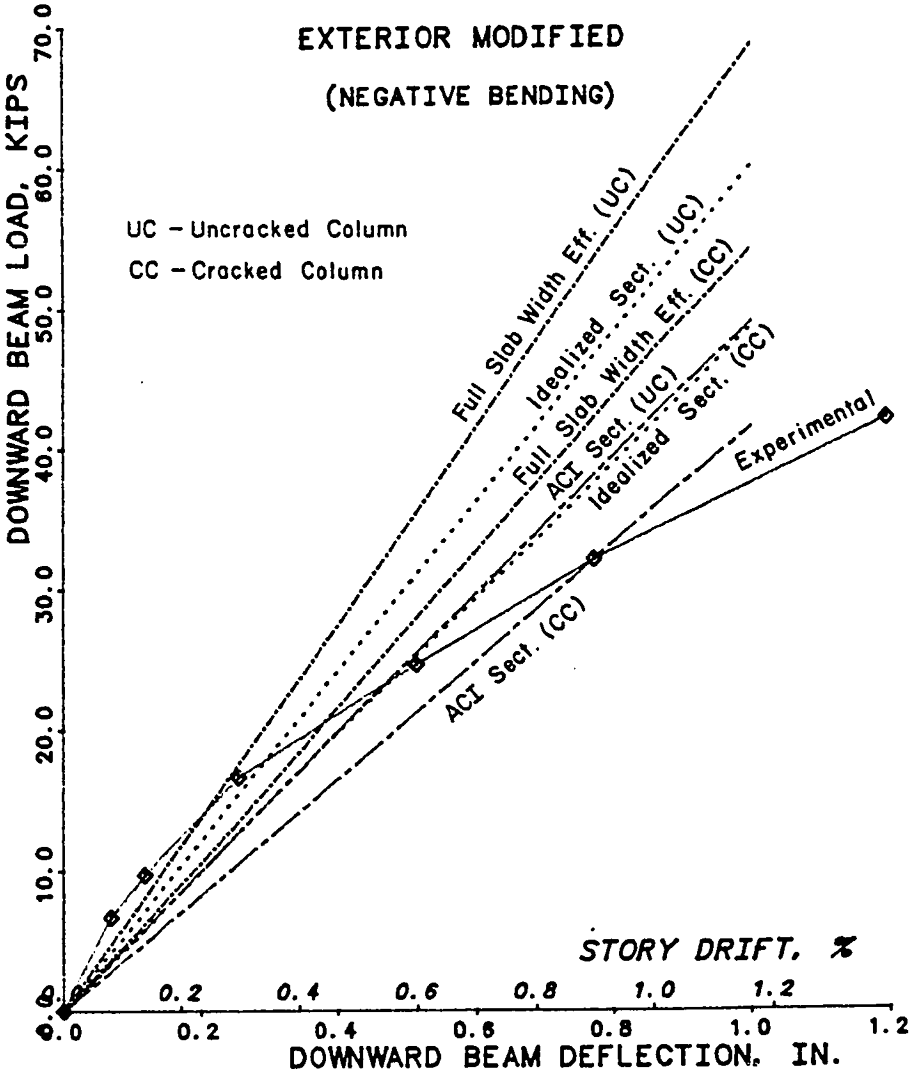

Fig. 5.28 Comparison of load-deflection relationship under negative moment, exterior modified

resulted in underestimating the observed stiffness irrespective of the assumed behavior of the column.

Used in conjunction with a cracked column section, the ACI beam section gave a lower bound to the actual stiffness. An upper bound on the stiffness was obtained using an uncracked column stiffness and a beam section whose effective flange width was equal to the full slab width.

5.7.3 Estimation of Strength. As discussed earlier in Chapter IV, it is necessary, when designing structures to resist seismic load, to determine accurately the contribution of the slab to the moment capacity of a beam. As can be seen from the test results, the use of effective flange width from ACI 318-83 in assessing the strength of the beam leads to an underestimation of the negative moment capacity. The positive moment capacity was not very sensitive to the assumptions made for the flexural section of the slab system since positive moment capacity is controlled by the bottom steel in the longitudinal beam for underreinforced sectons. As mentioned earlier, it is necessary to develop rational guidelines for estimating the slab contributions to the negative moment capacity of the beam. An approach using on both analytical and observed results was developed to assess the contribution of the slab to strength.

All four test specimens were underreinforced sections, even when the entire slab width was assumed to act as an effective flange of the T-beam. All moment capacities were estimated using the actual, rather than nominal, material strengths of concrete and reinforcing steel.

5.7.4 Idealized Model Based on Varying Neutral Axis Position. Experimental results show that under negative moment, all the longitudinal slab reinforcement had yielded at peak capacity. Nonlinear finite element analysis in the post-cracking, pre-yielding stage of the resonse showed that the location of neutral axis varies across the width of the slab, and that the closer the slab section is to the web, the farther the neutral axis is from the centroid of slab steel. The distance of the centroid of the slab steel from the neutral axis is also a function of deflection level.

The effectiveness of slab steel decreases as its distance from the web increases, due to the reduction in its distance from the neutral axis. Hence, when simple bending theory is used to predict the moment capacity of the section, considering the entire slab as a flange of the T-section, both the effective internal lever arm and the flexural capacity of the section are overestimated. Although the stress distribution across the section is fairly uniform, the location of the neutral axis across the slab changes during bending of a reinforced concrete beam with a very wide flange. The approach used by ACI to determine effective width is based on the shear lag concept, i.e., the stress distribution across a wide flange is nonuniform, with stresses decreasing with distance from the web near peak capacity. Contrary to the shear lag approach, near peak capacity, the steel stresses are uniformly equal to the yield stress.

Although the stress in reinforcing steel across the width is uniform near peak strength, the steel far away from the web is not as effective as the steel closer to the web because of its reduced distance from the neutral axis. Experimental results showed that when the entire slab was used as an effective width, simple bending theory overestimated of available negative flexural capacity by 15 to 23 percent. Use of ACI effective width provisions to compute flexural capacity underestimates the capacity by 14 to 47 percent, as they ignore any contribution from steel lying outside of the effective flange width is ignored. The underestimation is severe when the ratio of the area of slab steel outside the flange width to the area of slab plus beam steel inside the ACI T-section is high, as in the case of the prototype specimens. Thus, a reasonable procedure to compute negative flexural capacity should include all of the slab steel with due qualification for its distance from the web of the section.

The reduced effectiveness of slab steel far from the web can be accounted for in computing moment capacity by reducing the internal lever arm associated with this steel (Fig. 5.29). ACI effective width can be used to qualify the slab steel as being "close" or "far" from the web. The internal lever arm for slab steel "far" from the web can be assumed to be some fraction of the internal lever arm for the ACI T-beam section, and its contribution to the moment capacity of the section can then be computed by simple bending theory. A fraction between 22 and 39 percent gives results which

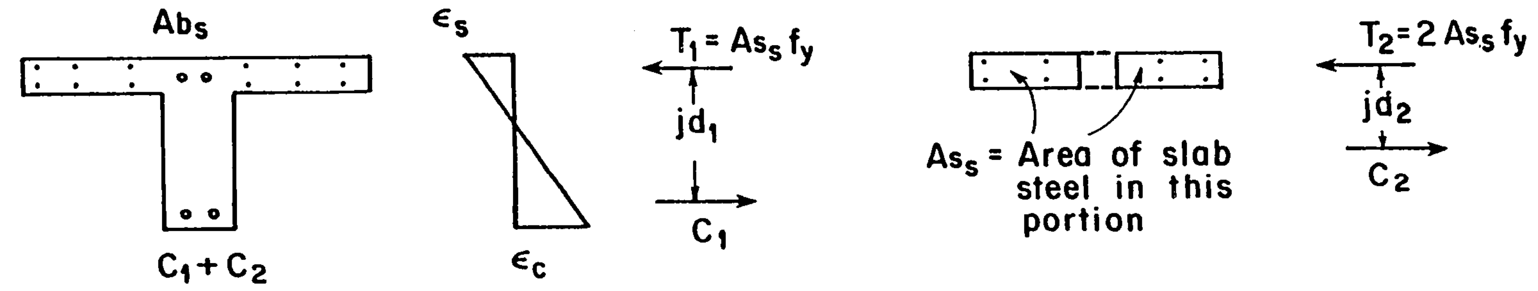

Abs
C1+C2
εs
εc
T1 = Ass fy
jd1
C1
Ass = Area of slab steel in this portion
T2 = 2 Ass fy
jd2
C2

ACI eff. flange width

$T_1 = Ab_s \, f_y$

$T = 2 \, As_s \, f_y$

$jd_2 = jd_1/2$

$$\text{Total moment capacity} = T_1 \, jd_1 + T_2 \, jd_2$$

$$= T_1 \, jd_1 + T_2 \, jd_1/2$$

Ab_s = area of tension steel in ACI section

Fig. 5.29 Idealized model based on varying neutral axis location

equal measured strengths (see Table 5.2). As a conservative estimate a value of 0.5 will slightly overestimate the strength. Results from such calculations for the four specimens are shown in Table 5.2.

5.7.5 Simplified Design Idealization. Although this approach reflects the observed behavior of the specimen, it could lead to difficulties in determining moment-curvature relationships and in satisfying equilibrium and compatibility for the section. Difficulties could also be encountered in determining the amount of balanced steel for the section. Hence, an alternative approach which produces similar results but avoids some of the difficulties mentioned is suggested.

In this approach, an idealized T-section is used to determine the response of the slab-beam system (see Fig. 5.30). A section having ACI effective width is determined. The reduced effectiveness of the slab steel lying "far" from the web, in the zone from the mid-panel to the edge of the T-section, is incorporated into this ideal section by adding half the area of the "far" slab steel into the ACI section. The capacity of this idealized section can now be determined using simple bending theory. The negative moment capacity computed using this idealized section would be slightly smaller than that obtained from the previous approach, because this additional steel will result in a slightly smaller internal lever arm. Results based on analysis of this idealized section are compared with the experimental results in Table 5.3. The estimated strengths are within 8 percent of observed values.

TABLE 5.2 Computations for Negative Moment Capacities

	Interior Prototype	Interior Modified	Exterior Modified
Experimental moment, kip-in.	3635	5480	5205
Moment capacity, ACI section, kip-in.	2485	4380	4515
Yield strength of steel, ksi	60	75	75
Area of tension steel in ACI section (beam + slab), sq. in.	2.2	3.88	3.88
Average lever arm, in.	18.8	15.1	15.5
Area of slab steel outside ACI section	2.64	2.64	2.64
% of lever arm for outside slab steel from experimental results	38.6	36.8	22.4
Total moment capacity assuming 50% lever arm	3975	5875	6050
Predicted/experimental moment capacities	1.09	1.07	1.16

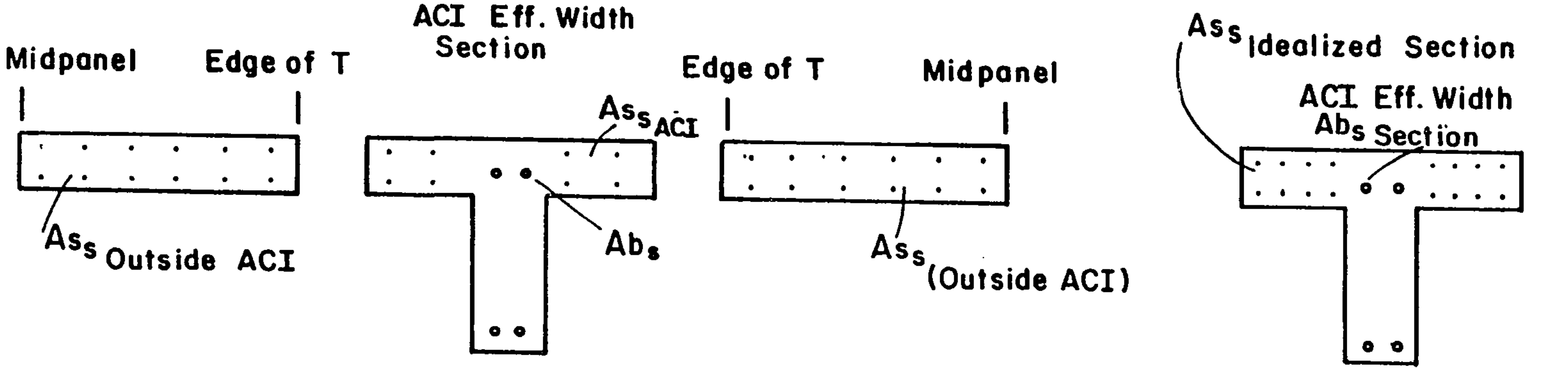
Midpanel
Edge of T
As_{s} Outside ACI
ACI Eff. Width Section
$As_{s_{ACI}}$
Ab_{s}
Edge of T
Midpanel
As_{s}(Outside ACI)
As_{s} Idealized Section
ACI Eff. Width Section
Ab_{s}

REAL SECTION

IDEALIZED SECTION

Total area of slab steel =

$$As_{s_{ACI}} + As_{s_{\text{Outside ACI left side}}} + As_{s_{\text{Outside ACI right side}}}$$

$$As_{s_{\text{Idealized Section}}} =$$

$$2As_{s_{\text{Outside ACI}}}/2.0 + As_{s_{ACI}}$$

Fig. 5.30 Proposed idealized section

TABLE 5.3 Moment Capacity Using Effective Beam

	Interior Prototype	Interior Modified	Exterior Modified
Experimental capacity, kip-in.	3635	5480	5205
Capacity of idealized section, kip-in.	3485	5490	5630
Predicted/experimental	0.96	1.00	1.08

5.8 Further Research Needs

The proposed model was calibrated using the data available from tests described herein. The amount of data available for calibration is fairly small. Further research needs to be undertaken to examine the effect of several variables such as beam depth, slab thickness, percentages of slab and beam reinforcing steel, transverse slab spans and torsional capacity of the transverse beam. Analytical investigations using the nonlinear finite element program (ABAQUS) should be undertaken to conduct parametric studies of the above variables. Experimental programs can then be designed to verify the influence of the significant parameters.

Several investigations are currently underway [17] to determine participation of the slab in flexural strength under negative moment. These studies were not available at the time was conducted and hence it was not possible to evaluate them in this report. However, initial review of this recently reported work indicated that the major thrust was to determine the amount of slab participation required to explain the strength observed in the seven-story structure. No extensive analytical effort to determine the mechanism of flexural resistance was involved.

CHAPTER VI

SUMMARY AND CONCLUSIONS

6.1 Summary

The behavior of reinforced concrete slab-beam-column connections under deformations simulating lateral load effects was investigated. Both experimental and analytical studies were conducted in this research.

6.1.1 Experimental Program. An experimental study of the behavior of reinforced concrete slab-beam-column connections was conducted as a part of the U.S-Japan Cooperative program on large-scale testing, established to improve the design of seismic resistant structures. A series of tests on a full scale seven story reinforced concrete structure was carried out in Japan. Supporting tests performed in both the U.S. and Japan included component beam-column-slab assemblies, scale models of full scale structure, or portions of the structure, and shake table models. The primary objective of the cooperative program was to compare the results of the suporting tests with the results from the tests on the seven story structure. Unfortunately, difficulties in data transfer from the Japanese tests and problems with scheduling did not permit direct comparison of test results in this report. However, one type of test results which were readily available from the seven-story structure, crack patterns, were compared. Since the data from the seven-story structure is now available in a more accessible format, correlation studies are currently under way as a continuation of this project.

Four full scale slab beam column assemblies were tested in the Ferguson Structural Engineering Laboratory at The University of Texas at Austin as a part of the U.S.-Japan program. The first two specimens (referred to as Prototype Interior and Prototype Exterior) were essentially identical to the slab-beam-column joints in the second story of the full-scale, seven story structure tested in Japan in terms of both geometry and reinforcing details. The remaining two specimens (referred to as Modified Interior and Modified Exterior), had increased the longitudinal reinforcement in the beams and columns, to provide a variation in the ratio of beam-to-slab strength. The four specimens were tested under reversed cyclic loading patterns with increasing levels of maximum displacement.

The response of all four specimens was excellent up to average story drifts of about 1.5 percent. The behavior of all four specimens was governed by flexure up to story drift levels of 2.5 percent. All except the exterior prototype specimen failed by flexural hinging of the longitudinal beam and the slab, a desirable failure mode providing a stable energy dissipation mechanism. The controlling mode of failure for the prototype exterior specimen was anchorage failure when the hooks of the longitudinal beam bars pried off the cover from the rear of the connection. An improved confinement detail, consisting of additional cross-ties in the joint region, resulted in improved performance of the modified exterior specimen. Due to the large size of the columns, joint shear problems were neither anticipated nor encountered.

The influence of the slab on the strength of the floor system under imposed deformations was significantly greater than would be anticipated if existing ACI Code effective width provisions for compression flanges were applied to the tension flange calculations. The participation of the slab as a flange for the beam section increases the flexural capacity of the floor elements. Evaluation of test results indicated that current design procedures do not adequately reflect actual behavior. Based on experimental results alone, it was not possible to develop specific design guidelines. Therefore, an analytical investigation was conducted to better understand the behavior of the slab systems under lateral loads.

6.1.2 Analytical Studies. Experimental results showed that the behavior of the slab changed significantly from the elastic to the inelastic range. Since the slab behaved inelastically in both the serviceability and the ultimate limit states, a finite element program (ABAQUS) which was able to reflect cracking of concrete and nonlinear behavior of reinforced concrete was selected.

The slab was discretized using eight-node shell elements. The longitudinal and end beams were modeled as stiffeners attached to the shell elements of the slab. The column was modeled using three-node beam elements. Since the beam elements are neither capable of handling warping torsion, nor of considering transverse reinforcement, the transverse beam was modeled as a tube made of shell elements. A single reinforced concrete material model was used for all but the shell elements lying in the joint region. Since the joint was expected to remain elastic during most of the response, it was modeled as an elastic material having an initial stiffness of plain concrete. The finite element analysis was used to predict the load-deflection response under monotonic loads up to a beam end deflection of 0.7 in.

6.1.3 Behavior of Slab Systems. The fundamental difficulty in analyzing a floor system with beams is in determining the distribution of moment between the slab and the beams. In converting a real three-dimensional structure to a two-dimensional structure, widths must be assigned to the columns, the beams, and the slab. The determination of the path of moment transfer becomes complex even for an elastic material. For reinforced concrete the problem is aggravated due to the nonlinear response of the material.

The usual approach to analyze a three-dimensional slab structure under lateral loads is to convert it to an equivalent two-dimensional structure using the concept of effective width. The actual flange width is replaced by a certain reduced width, and elementary bending theory is applied to this effective beam cross section to predict the behavior of the entire slab system. The ACI effective width is based on the shear lag concept, in which the nonuniformity of the stress distribution across the width of the flange (stresses becoming smaller at greater distances from the web) is considered responsible for the reduced effectiveness of the slab far from the web.

6.1.4 Proposed Idealized Cross Section for Slab Systems.

Both analytical and experimental results suggested that the behavior of the slab system was not as assumed in the ACI Code effective width provisions. Analytical results from nonlinear finite element analysis showed that the reduced participation of the flange far from the web was not due to nonuniform stress distribution across the width, but rather due to the change in the location of the neutral axis across the width of the section.

It was observed experimentally as well as analytically that all of the slab steel participates in resisting flexure at all stages of the response of the structure. Using the ACI effective flange width provisions (which were intended to be applied to positive bending only) for negative bending results in the steel lying outside the effective width not being accounted for in determination of section behavior. In the proposed model all of the slab steel is accounted for, but with some modifications. The changing position of the neutral axis is accounted for by associating the steel far from the web with a smaller internal lever arm. A modified beam cross section is determined, having the same width as suggested by the current ACI provisions. The influence of slab steel lying outside the ACI section can then be incorporated by adding the area of this slab steel, multiplied by 0.5 (to reflect its reduced effectiveness) to the area of slab steel inside the slab section. The percentage of slab steel (50%) was arrived at by calibrating the response of this idealized section against the flexural capacities observed in the tests.

The model has advantages over the current design procedure in that it accounts for the influence of all of the slab steel, and more correctly reflects the true nature of slab participation. The section can be analyzed using simple bending theory to determine moment-curvature response of the slab system. Because the total amount of effective steel is known, failure mode can be estimated as tensile, for an under-reinforced section, or as compressive failure for an over-reinforced section. The method also has appeal in that only a very minor modification has to be made to the current design procedures.

There is need for further research to calibrate this 50% factor, since the calibration was based on a small amount of data (three tests). The finite element program (ABAQUS) used here could be used to study the effect of several parameters such as beam depth, slab thickness, reinforcement ratios, transverse slab spans and torsional capacity of transverse members. Experimental studies should be conducted to verify the results of the analytical studies.

6.1.5 Comparison of Stiffnesses. Experimental results were compared with current ACI design procedures, in which the influence of the slab system is incorporated by the ACI effective width, and with results using the idealized section (added steel). Comparisons of stiffness indicate that both the ACI section and the idealized section result in underestimating the actual stiffness. The predicted overall stiffness of the structure was more sensitive to the assumptions made in determining the stiffness of the column, than to the assumptions made for the stiffness of the beam-slab system. Irrespective of the assumed section of the beam-slab system, as long as a cracked ACI or idealized section was used, a lower bound to the actual overall stiffness of the structure was obtained. In the serviceability range, where it is essential to predict the deflections of the structure, the use of either the cracked ACI section or the cracked idealized section would result in a conservative design solution, in that deflections would be overestimated.

6.1.6 Comparison of Strengths. The use of the effective flange width from ACI 318-83 in assessing the strength of the slab system resulted in severe underestimation of the negative moment capacity observed from experimental results. The percentage of underestimation of the negative capacity varied directly as the ratio of the area of the slab steel outside the ACI section, to the area of the slab steel and tensile beam steel in the ACI section. Since most of the slab steel at the supports of a typical slab-beam system would be outside the ACI section (in the middle strip), this error in estimating flexural capacity is very significant. The use of an idealized section in assessing the negative moment capacity resulted in close estimates of the flexural capacity of the slab system. The positive moment capacity was not very sensitive to the assumption made for the flexural section of the slab system, since positive moment capacity is controlled by the bottom steel in the longitudinal beam for underreinforced sections. The use of either the ACI section or the idealized section resulted in an overestimate of the positive moment capacity.

In seismic design, where lateral deformations are imposed on the structure and the moment imposed by the slab system on the column is to be determined, underestimating the slab system strength may be unconservative. The presence of elements with flexural strength greater than that accounted for in design may result in excessive strength and ductility demands on both those and other elements. The behavior and the failure mechanism of the structure may differ from that desired or assumed in design. Such differences result in potentially serious damage to the structure, leading to local or general collapse conditions. The use of the idealized section results in fairly accurate estimates of the flexural strengths of the slab systems. Accurate estimation of the strength slab system used in conjunction with other safety provisions will result in conservative design solution for structures resisting seismic loads.

6.2 Conclusions

6.2.1 Performance of the Test Specimens.

One of the objectives of this experimental program was to conduct a detailed examination of the isolated joint specimens to compare their response with the response of the beam column joints in the seven-story structure. The joints in the seven-story structure were subjected to story drifts estimated to be about 1.5%. No shear distress was evident in the slab-beam-column joint region in the seven-story structure. Performance of the isolated test specimens was evaluated with respect to the performance of the beam column joints in the seven-story structure at comparable deformation levels.

1. The behavior of the four specimens under reversed cyclic loads was excellent up to story drift levels of about 1.5% which were estimated to correspond to the maximum deflection level imposed on the seven-story structure. There was no loss in flexural strength of the specimens after cycling at this deflection level. The behavior of all four specimens up to this drift level was governed by flexure.
2. No shear distress was observed in the joint region during any stage of testing. The large columns resulted in low shear stresses in the joint (average joint shear stress was $4.9\sqrt{f'_c}$ to $14\sqrt{f'_c}$).
3. At drift levels of 4 to 5% (much higher than the maximum drift levels experienced by the seven-story structure), anchorage failure occurred in the exterior prototype specimen. This resulted in the capacity of the exterior prototype specimen reaching only 2/3 capacity of the same section in the interior prototype specimen. An improved confinement detail (transverse cross ties) in the modified exterior

joint greatly improved its performance, and the strength was now the same as that of the interior modified specimen.

4. Torsional distress was observed in all four tests at large deflection levels in the transverse beam near the column face. The anchorage failure in the exterior prototype specimen led to more severe torsional cracking in the spandrel beam than in the other three specimens.

6.2.2 Influence of Slab on the Behavior of the Floor System.

Although no problems associated with beam column joints were encountered in the test specimens, this experimental program presented an excellent opportunity to study the influence of the slab on the flexural strength of the floor system. The critical question was to determine the slab participation under the action of a negative moment. An approach based on the ACI effective flange widths was used to evaluate the slab contribution to the flexural capacity of the floor system. The ACI effective flange widths were intended to apply to the case of compression flanges, but do not specifically exclude the application to tension flanges. There is a need to develop design guidelines to determine the contribution of the slab under negative bending of the floor system. Underestimation of the floor system flexural strength could result in underestimating the flexural requirements for the column. The evaluation of slab participation is needed to determine the (1) stiffness and (2) the strength of the floor system.

The influence of the slab on the behavior of the floor system can be summarized as follows:

1. Experimental and analytical results showed that the influence of the slab on the flexural strength of the floor system under imposed deformations was considerably greater than would be anticipated by applying the ACI effective width provisions to the case of negative bending.
2. Experimental results showed that the use of the cracked section for the floor system, irrespective of the assumed effective section, underestimated the stiffness of the slab system in the serviceability range and would result in a conservative estimate of the deflections under lateral loads. The stiffness of the test specimens was more sensitive to the use of cracked or uncracked section rather than to the assumed effective widths.
3. Based on analytical and experimental data (three tests) a model was developed to estimate the negative flexural capacity of a floor system. An idealized beam cross section, having the same width as suggested by current ACI provisions, is proposed. The influence of the slab steel lying btween the T-section and the mid-panel is incorporated by adding half (50%) of the area of this slab steel to the area of the tensile steel inside the ACI T-section. However, the 50% factor needs to be further calibrated to

validate its applicability to a variety of sections. Both analytical and experimental work is needed to assess the effects of variables such as slab depth, beam depth, reinforcement ratios, transverse slab spans, and torsional strength of transverse beams.

A P P E N D I X   A

PROBLEMS ENCOUNTERED DURING ANALYTICAL STUDY

It was deemed necessary to analyze the test structure using a finite element procedure which would predict its behavior. A program able to model the structural behavior of various components (slab, longitudinal beam, transverse beam, column) the test specimens was required. Nonlinear material properties of concrete and reinforcement had to be realistically modeled.

Based on the available literature, a commercial finite element package ABAQUS [6,7,8] was selected. The User's and Theory manuals for ABAQUS indicated that this program had a wide range of capabilities. Geometric modeling could be achieved with a variety of finite elements; beam elements, shell elements, 3-D elements, etc. Any combination of these elements could be interconnected by transition elements and used to model the structure. Nonlinear material properties could be input for all the elements. A special concrete material model was included in the program. Finally, ABAQUS was available on the Dual Cyber computer system of The University of Texas at Austin.

Several problems were encountered when using the program. Initially, it was discovered that the manuals available were for the latest version of the program, whereas the version (4-5-22) on the UT system was a couple of years outdated. Hence, some of the features in the manual were not available in the old version.

Initial problems included the fact that automating internal numbering for element numbers to reduce the front width for the frontal solver was not implemented in the program, contrary to the impression created by the User's Manual. A lot of effort was required to arrive at this conclusion since it would not be determined easily from the output. This problem was solved by manually numbering the elements to have a minimum frontal size.

In the nonlinear solution algorithm, convergence was checked after the fourth cycle in each increment. If linear convergence was not achieved, then the step size was decreased. Since linear convergence is generally not possible in reinforced concrete analysis problems, the resulting step sizes determined by the solution algorithm were very small. This led to very slow progress along the load-deflection path. The User's Manual suggested that a "submax" parameter could be specified to ensure that convergence would not be checked until a specified number of iterations had been performed. Use of this "submax" parameter was recommended by the Examples Manual for reinforced concrete members. The available ABAQUS version could not use the submax parameter. This was more of an inconvenience than a serious drawback.

The most significant problem encountered with the original version used was the inability of the program algorithm to trace the response of reinforced concrete sections after the yield of reinforcing steel. This was discovered after consultations with the developers of ABAQUS when analytical results from analysis did not appear to be reasponable near the point when yielding was expected.

At this juncture it was decided to acquire the latest version of ABAQUS, which would presumably not have the various problems discussed above. A new version of the program was obtained from the developers and installed at The University of Texas computer. However, several problems were also encountered with this new version of the program. Some of the output options in the User's Manual could not be executed.

Most serious however, was the continued inability of the program to compute reasonable stresses in the reinforcing steel in the shell elements. Various solutions to rectify this situation were suggested by the developers but these did not result in successful execution. It was then decided that results could not be obtained from the new version in a reasonable amount of time. Time restrictions did not make further debugging feasible. A decision was made to work with the results obtained from the old version as these results seemed reliable until yielding of reinforcement was encountered.

All the above problems with the new version of ABAQUS were finally resolved. The author regrets that time constraints did not permit the full incorporation of the latest version of ABAQUS into this dissertation. Continued use of ABAQUS and other similar programs is a worthy topic for future research and can help in understanding of the observed behavior of complex reinforced concrete test specimens.

REFERENCES

1. ACI Committee 318, "Building Code Requirements for Reinforced Concrete (ACI 318-77)," American Concrete Institute, Detroit, 1977.

2. ACI Committee 318, "Building Code Requirements for Reinforced Concrete (ACI 318-83)," American Concrete Institute, Detroit, 1983.

3. ACI-ASCE Joint Committee 352, "Recommendations for Design of Beam-Column Joints in Monolithic Reinforced Concrete Structures," Journal of the American Concrete Institute, Proceedings, Vol. 73, No. 7, July 1976.

4. Chen, A.C.T., and Chen, W.F., "Constitutive Relations for Concrete," Journal of the Engineering Mechanics Division, ASCE, Vol. 101, No. EM4, August 1975, pp. 465-481.

5. Collins, Michael P., and Mitchell, Dennis, "Shear and Torsion Design of Prestressed and Non-Prestressed Concrete Beams," PCI Journal, Proceedings, Vol. 25, No. 5, September/October 1980, pp. 32-100.

6. Hibbit, Karlsson, and Sorenson, Inc., "ABAQUS User's Manual," Version 4, July 1982.

7. Hibbit, Karlsson, and Sorenson, Inc., "ABAQUS Theory Manual," Version 4, July 1982.

8. Hibbit, Karlsson, and Sorenson, Inc., "ABAQUS Example Problems Manual," Version 4, July 1982.

9. International Conference of Building Officials, "Uniform Building Code," 1982 Edition.

10. The Joint Committee on Standard Specifications for Concrete, "Report of the Joint Committee on Standard Specifications for Concrete and Reinforced Concrete," Proceedings, ACI, Vol. 21, 1982, pp. 329-413.

11. Mitchell, Dennis, and Collins, Michael P., "Diagonal Compression Field Theory—A Rational Model for Structural Concrete in Pure Torsion," ACI Journal, Proceedings, Vol. 71, No. 8, August 1974, pp. 398-408.

12. Okamoto, S., Nakata, S., Kitagawa, Y., Yoshimura, M., and Kamimosono, T., "A Progress Report on the Full-Scale Seismic Experiment of a Seven-Story Reinforced Concrete Building—Part of the U.S.-Japan Cooperative Program," B.R.I. Research Paper No. 94, Building Research Institute, Ministry of Construction, Japan, March 1982, 92pp.

13. Seismology Committee, Structural Engineers Association of California, San Francisco, California, 1975.

14. Timoshenko, S.P., and Goodier, J.N., Theory of Elasticity, Third Edition, McGraw-Hill, New York, 1970.

15. U.S.-Japan Planning Group, "Recommendations for a U.S.-Japan Cooperative Research Program Utilizing Large-Scale Testing Facilities," Report No. UCB/EERC-79-26, September 1979.

16. Yoshimura, M., and Tsubosaki, M., "U.S.-Japan Cooperative Research on R/C Full-Scale Building Test (Part 6: Ultimate Moment-Resisting Capacity)," Eighth World Conference on Earthquake Engineering, San Francisco, 1984.

17. Vanderbilt, Daniel M., and Corley, Gene W., "Frame Analysis of Concrete Buildings," Concrete International: Design and Construction, Vol. 5, No. 12.

VITA

Milind Ramchandra Joglekar was born on August 20, 1956, in Poona, India, to Suniti Ramchandra and Ramchandra Vasudeo Joglekar. After completing his high school education at Loyola High School, Poona, in 1972, he entered Fergusson College, Poona. In June 1974 he entered the College of Engineering, Poona, and was awarded the degree of Bachelor of Engineering with major in Civil Engineering in August 1978. In September 1978 he entered the Graduate School at the University of Toronto, Canada, and was awarded the degree of Master of Applied Science in Structural Engineering in December 1980. In January 1981 he entered The Graduate School of The University of Texas at Austin to pursue his doctoral studies. On January 20, 1984, he married Mrinal Gajanan Bhide.

Permanent address: 1226/4 Shivajinagar
Pune 411 004
INDIA

This dissertation was typed by Patricia Henderson.